CHEMERIN SIGNALLING IN ADIPOSE TISSUE AND INTESTINAL HOMEOSTASIS

by

Helen Jane Dranse

Submitted in partial fulfilment of the requirements
for the degree of Doctor of Philosophy

at

Dalhousie University
Halifax, Nova Scotia
January 2016

TABLE OF CONTENTS

LIST OF TABLES

LIST OF FIGURES

ABSTRACT

Chemerin is an adipokine and potent chemoattractant for cells expressing chemokine-like receptor 1 (CMKLR1) which plays important roles in metabolism and immunity. Chemerin is secreted as inactive prochemerin and undergoes extracellular processing to generate a variety of isoforms that range in bioactivity. Clinical studies have demonstrated that chemerin levels are positively associated with obesity and inflammatory disorders. However, the role of chemerin signalling in adipose tissue, and how elevated chemerin levels affect inflammatory disease progression, are poorly understood. In this thesis, I describe the development of techniques to modulate levels of chemerin signalling. I then investigate the role of chemerin signalling in three physiological contexts: mature adipocytes, pathogenesis of colitis, and intestinal microbiome composition.

Using a microarray-based approach, I identified matrix metalloproteinase (MMP)3 and several chemokines as novel targets of chemerin signalling in adipocytes. Decreased chemerin levels resulted in increased MMP activity and macrophage migration towards adipocyte-conditioned media, via an NFkB-dependent mechanism. This suggests that elevated chemerin levels with obesity influence adipose tissue remodelling. Importantly, these effects were mediated through a unique adipocyte-processed chemerin isoform.

I next demonstrated that local expression, secretion, and processing of chemerin were positively associated with colonic inflammation in a colitis model. CMKLR1 knockout (KO) mice developed signs of clinical illness more slowly than wildtype, but ultimately developed similar levels of inflammation. Intraperitoneal injection of bioactive chemerin had no effect on colitis severity, suggesting that local chemerin levels have a greater impact on the pathogenesis of colitis.

Finally, I investigated differences in intestinal microbiome composition between wildtype, chemerin KO, and CMKLR1 KO mice. Significant differences in *Akkermansia* and *Prevotella* abundance were observed in the absence of CMKLR1. These bacterial populations are known to correlate with adiposity and glucose homeostasis, indicating that chemerin signalling might influence metabolic processes through modulation of microbiome composition.

Considered altogether, this work demonstrates that local chemerin signalling and processing plays autocrine/paracrine roles in adipose tissue and intestinal homeostasis. Additionally, chemerin represents a novel biomarker in colon inflammation. Modulation of local, context-specific chemerin signalling therefore represents a potential therapeutic target for the treatment of metabolic and inflammatory processes.

LIST OF ABBREVIATIONS USED

α-NETA	2-(α-naphthoyl) ethyltrimethylammonium iodide
AP2	adipocyte protein 2
ß-gal	beta-galactosidase
BMI	body mass index
BSA	bovine serum albumin
BZ	Brian Zabel colony
CCL	chemokine (C-C) motif ligand
CCRL2	C-C chemokine receptor-like 2
CD	Crohn's disease
CS	Christopher Sinal colony
CMKLR1	chemokine-like receptor 1
CMV	cytomegalovirus
CVD	cardiovascular disease
DC	dendritic cells
DEXA	dual-energy X-ray absorptiometry
DMSO	dimethyl sulfoxide
DSS	dextran sodium sulphate
DTT	dithiothreitol
ECM	extracellular matrix
EDTA	ethylenediaminetetraacetic acid
EF1α	elongation factor-1 alpha
ELISA	enzyme-linked immunosorbent assay
ERK	extracellular signal-regulated kinase
GFP	green fluorescent protein
GI	gastrointestinal
GPCR	G protein coupled receptor
GPR1	G protein-coupled receptor 1
HEK	human embryonic kidney
HET	heterozygous
HFD	high-fat diet
HTLA	HEK cells stably transfected with a transcriptional transactivator-dependent luciferase reporter and an arrestin-2-TEV fusion gene
IBD	inflammatory bowel disease
IKKß	inhibitor of nuclear factor kappa-B kinase subunit beta
IFN	Interferon
IL	Interleukin
IPTG	isopropyl ß-D-1-thiogalactopyranoside
IRS	insulin receptor substrate
ITR	inverted terminal repeat
KO	knockout
LC-MS/MS	liquid chromatography-tandem mass spectrometry
LPS	lipopolysaccharide
MetS	metabolic syndrome
MMP	matrix metalloproteinase

MRM	multiple reaction monitoring
MSC	mesenchymal stem cell
NFkB	nuclear factor kappa-B
NK	natural killer
OTU	operational taxonomic unit
PB	piggyBac
PBS	phosphate-buffered saline
PCoA	Principal coordinates analysis
PCOS	polycystic ovary syndrome
PCR	polymerase chain reaction
PEI	polyethylenimine
PFA	paraformaldehyde
PGK	phosphoglycerate kinase
PPAR	peroxisome proliferator-activated receptor
PPIA	peptidylprolyl isomerase A
qPCR	quantitative polymerase chain reaction
Reck	reversion-inducing-cysteine-rich protein with Kazal motifs
RT	room temperature
Saa	serum amyloid A
SCFA	short chain fatty acid
SDS-PAGE	sodium dodecyl sulfate polyacrylamide gel electrophoresis
SEM	standard error of the mean
SRF-RE	serum response factor response element
SV40	simian virus 40
SVF	stromal vascular fraction
T2D	type 2 diabetes
TIMP	tissue inhibitor of metalloproteinase
TK	thymidine kinase
TNF	tumor necrosis factor
UC	ulcerative colitis
VAPAHCS	Veterans Affiars Palo Alto Health Care System
WAT	white adipose tissue
WT	wildtype

ACKNOWLEDGEMENTS

I would like to express my greatest appreciation to my supervisor and mentor, Dr. Chris Sinal, who has provided me with amazing guidance, support, and encouragement over the past 5 years. Chris, I have tremendous respect for the way that you approach both science and life, and I value your ability to always put my worries in perspective. I consider myself a very different person, scientist, and PCR machine-fixer, from when I first started in the lab, and you are a primary reason for that. Thank you for helping me to pursue my interests, develop as a scientist, and prepare me for the next step in my career.

I would also like to thank all of the current and past members of the Sinal lab, for the fun times in (and outside) the lab. Jillian Rourke, Nichole McMullen, Matthew Ernst, Lori MacNeil, Heather Blundon, and Muruganandan Shanmugan: thank you for the years of support, friendship, great memories, and scars from rolling down Citadel Hill!

I am also very grateful to my supervisory committee members, Drs. Eileen Denovan-Wright and Kishore Pasumarthi, for their guidance and insight throughout my training. In addition, a big thank you to all of the collaborators that have patiently answered all of my questions over the years, including Drs. Andy Stadnyk, Umang Jain, Hana James, Alejandro Cohen, Jim Fawcett, André Comeau, Morgan Langille, and Brian Zabel. Special thanks to all of the faculty, staff, and students in the department of Pharmacology, who have provided such a supportive environment and made it a pleasure to be a member of the department.

Finally, to my family: Andrew, thank you for always being a message away when I needed help with my computer or procrastinating (mostly the latter). Mum and Dad: from my very first science project ("flour in a cake - how well will it bake") to building launchers and red ants, thank you for inspiring me to work hard and try my best, teaching me the value of perseverance, and for always supporting and encouraging me. Lastly, to my husband Jeremy: I am incredibly lucky to have had you on my side throughout this degree; someone that understands the ups-and-downs of science and that wants to talk about experiments over dinner. Thank you for being my "thesis coach", and thank you for being so patient while you waited for me to finally finish…

CHAPTER 1: INTRODUCTION

Copyright statement

Portions of this chapter have been previously published (Rourke JL*, Dranse HJ*, Sinal CJ. (2013). Towards an integrative approach to understanding the role of chemerin in human health and disease. Obesity Reviews 14: 245-262). The manuscript has been updated to include recent updates in the field and modified to meet formatting requirements. Re-use is permitted with copyright permission (Appendix A).
**authors contributed equally*

Contribution statement

The review manuscript used as the basis for portions of this chapter was written in equal partnership with Dr. Jillian Rourke with guidance from Dr. Christopher Sinal.

Overview

Chemerin is an adipocyte-secreted protein with autocrine/paracrine roles on adipose development and function as well as endocrine roles in metabolism and immunity. Following prochemerin secretion, protease-mediated generation of different chemerin isoforms with a range of biological activities is a key regulatory mechanism controlling local, context-specific chemerin bioactivity. Together, experimental and clinical data indicate that localized and/or circulating chemerin expression and activation are elevated in numerous metabolic and inflammatory diseases including obesity, type 2 diabetes, metabolic syndrome, cardiovascular disease, psoriasis, and inflammatory bowel disease. These elevations are positively correlated with deleterious changes in glucose, lipid, and cytokine homeostasis, and may serve as a link between obesity, inflammation, and other disorders. This chapter highlights the current state of knowledge regarding chemerin expression, processing, biological function, and relevance to human disease, particularly with respect to inflammation, adipose tissue development, and obesity-associated diseases.

Chemerin discovery and characterization

Chemerin, also known as tazarotene-induced gene 2 (TIG2), or retinoic acid receptor responder 2 (RARRES2), was originally identified as a gene up-regulated in psoriatic skin by the synthetic retinoid tazarotene (Nagpal et al. 1997). Chemerin is structurally related to the cathelicidin and cystatin family of proteins and was re-discovered in 2003 following reverse pharmacology screening of orphan G protein coupled receptors (GPCRs) as the natural ligand for chemokine-like receptor 1 (CMKLR1) (Meder et al. 2003; Wittamer et al. 2003). In these studies, chemerin was isolated from human inflammatory fluids and shown to act as a potent chemoattractant for cells that express CMKLR1. Four years later, chemerin was identified as a novel adipokine, or adipocyte-secreted signalling molecule (Bozaoglu et al. 2007; Goralski et al. 2007). To date, chemerin has largely been characterized within these two different functional contexts and has been established to play important roles in the development of a variety of inflammatory and metabolic disorders.

Regulation of chemerin activity

Chemerin signalling is tightly regulated through a number of mechanisms including expression, secretion, processing, and signalling events. The precise coordination of these regulatory mechanisms is essential for establishing chemerin levels, localization, and ultimately, activity.

Expression and secretion

Chemerin is expressed at the highest levels in placenta, liver, and white adipose tissue (WAT), and to a lesser extent in many other tissues such as lung, brown adipose tissue, heart, ovary, kidney, skeletal muscle, and pancreas (Bozaoglu et al. 2007; Goralski et al. 2007; Issa et al. 2012; Takahashi et al. 2011). Within WAT, chemerin expression is enriched in adipocytes as compared to the stromal vascular fraction (Bozaoglu et al. 2007; Goralski et al. 2007) and, in addition to the liver, WAT is believed to be the main source of circulating chemerin. Similar to other adipokines such as leptin and adiponectin, serum levels of chemerin in mice oscillate in a diurnal-like fashion with peak and trough periods, corresponding to the day-night cycle (Parlee et al. 2010);

however, in humans these oscillations may be minimal (Chamberland et al. 2013; Tan et al. 2009). In healthy, lean populations, the concentration of total circulating chemerin ranges from 90 to 200 ng/mL in both serum and plasma (Bozaoglu et al. 2009; Chakaroun et al. 2012; Dong et al. 2011). In general, females and older adults have higher circulating chemerin than males and younger adults, respectively (Bozaoglu et al. 2007; Bozaoglu et al. 2009; Lehrke et al. 2009; Stejskal et al. 2008), although not all studies have reported these trends (Huang et al. 2012; Weigert et al. 2010a; Yamamoto et al. 2010; Yang et al. 2010).

Chemerin expression is regulated by a number of factors, including activation of nuclear receptors, growth factors, and cytokines (for review, see (Zabel et al. 2014)). With respect to nuclear receptors, chemerin was first identified as a retinoid-responsive gene in skin (Nagpal et al. 1997) and subsequent studies demonstrated that retinoic acid up-regulates chemerin expression in epithelial and endothelial cells (Gonzalvo-Feo et al. 2014; Maheshwari et al. 2009). The glucocorticoid-derivative dexamethasone and 1,25 dihydroxyvitamin D3 have also been shown to up-regulate chemerin expression in the ST2 stromal cell line (Adams 1999). Furthermore, chemerin has been identified as a direct peroxisome proliferator-activated gamma (PPARγ) and farnesoid X receptor (FXR) target gene in adipocytes and hepatocytes, respectively (Deng et al. 2013; Muruganandan et al. 2011). In addition to these nuclear receptors, free fatty acids (FFA) and a number of pro-inflammatory stimuli, including tumor necrosis factor (TNF)α, lipopolysaccharide (LPS), interferon (IFN)γ and interleukin (IL)-1ß, have been shown to up-regulate chemerin expression in adipocytes and synoviocytes (Bauer et al. 2011; Herova et al. 2014; Kaneko et al. 2011; Kralisch et al. 2009; Parlee et al. 2010). Additionally, gonadotropin and follicle-stimulating hormone have been shown to decrease chemerin expression in granulosa cells (Wang et al. 2013b). Regulation of chemerin expression is often cell type-specific, indicating local control of chemerin levels (Gonzalvo-Feo et al. 2014; Herova et al. 2014).

Chemerin is initially synthesized as preprochemerin, a 163 amino acid (aa) protein with an N-terminal signal sequence (20 aa) that is cleaved prior to secretion of the inactive 18-kDa precursor, prochemerin (Chem-163) (Wittamer et al. 2003). The majority of circulating chemerin is believed to exist in the relatively inactive prochemerin

form and requires proteolytic processing to bioactive chemerin isoforms in order to exert local biological actions.

Processing

Following secretion, prochemerin can be processed by a variety of extracellular proteases of the coagulation, fibrinolytic, and inflammatory cascades, which are differentially expressed in a wide range of tissues and cell populations. These enzymes, through cleavage at distinct sites in the C-terminus, convert prochemerin into a number of bioactive isoforms that vary in length and biological activity (Table 1.1). For example, the removal of six amino acids results in Chem-157, which exhibits the highest activity (approximately 100-fold higher than prochemerin (Wittamer et al. 2003)), while Chem-156 has slightly less activity, Chem-155 and -158 low activity, and Chem-152 and -154 are relatively inactive (Du et al. 2009; Meder et al. 2003; Wittamer et al. 2003; Yamaguchi et al. 2011; Zabel et al. 2005a; Zhao et al. 2011). Importantly, some proteases are able to process prochemerin at more than one cleavage site (e.g. elastase, tryptase (Zabel et al. 2005a)) and various chemerin isoforms may also be further processed. For example, carboxypeptidases B and N process relatively low active chemerin isoforms into more active forms (Du et al. 2009), while other proteases such as proteinase 3 (PR3) or mast cell chymase are able to process pro- or bioactive chemerin, respectively, into relatively inactive forms (Guillabert et al. 2008). This multi-step processing of chemerin provides a mechanism for local and systemic chemerin activation as well as inactivation, both directly and by limiting available precursors. Furthermore, chem-155, which has low bioactivity, might act as a weak antagonist in the presence of highly active chemerin isoforms (Yamaguchi et al. 2011), suggesting that the ratio between active and inactive isoforms is an important determinant of chemerin bioactivity. It is important to note that the majority of studies report chemerin bioactivity relative to one particular function or signalling pathway, and thus it remains unclear whether individual chemerin isoforms have differential bioactivity on multiple pathways or functions.

The bulk of knowledge regarding chemerin processing and bioactivity derives from *ex vivo* studies; however, several endogenous chemerin isoforms have also been

isolated from human samples. Differential patterns of chemerin isoform production in human blood (Chem-155, 157, 158), ascites (Chem-157), synovial fluid (Chem-158), cerebrospinal fluid (Chem-158), and hemofiltrate (Chem-154) indicate that complex prochemerin processing occurs *in vivo* (Meder et al. 2003; Wittamer et al. 2003; Yamaguchi et al. 2011; Zabel et al. 2005a; Zhao et al. 2011) (Table 1.2). At present, all proteases that modulate chemerin activity do so through processing of the C-terminus, illustrating the importance of this region of the protein for chemerin bioactivity. Cleavage of prochemerin to Chem-156 by kallikrein 7 results in a structural rearrangement that is believed to increase affinity for chemerin at CMKLR1 (Schultz et al. 2013), suggesting that C-terminal processing impacts the tertiary/quaternary structure of chemerin. However, very little information is available on the functional relevance of particular amino acids or amino acid motifs within the remainder of the protein. Thus, further characterization of chemerin isoform generation is necessary in order to fully understand local chemerin bioactivity and the biological functions of chemerin.

Chemerin receptors

Chemerin was initially described as the natural ligand and chemotactic signal for cells expressing the G protein-coupled receptor (GPCR) chemokine-like receptor 1 (CMKLR1) (Meder et al. 2003; Wittamer et al. 2003). Chemerin has also been shown to bind and activate another GPCR, G protein-coupled receptor 1 (GPR1), with similar affinity to CMKLR1 (Barnea et al. 2008; Rourke et al. 2015). However, the majority of the known biological (signalling) activities of chemerin have been ascribed to activation of CMKLR1. Thus, an important area of future research is to delineate the contribution of CMKLR1 and GPR1 in mediating the biological actions of chemerin, and whether the receptors have complementary and/or distinct roles. In addition to CMKLR1 and GPR1, chemerin is a ligand for a third receptor, chemokine (CC motif) receptor-like 2 (CCRL2), which has phylogenetic homology with members of the CC chemokine receptor subfamily. CCRL2-bound chemerin is not internalized and it is not believed to be a signalling receptor (Zabel et al. 2008). Rather, CCRL2 is been shown to focus chemerin localization *in vivo*, increasing local chemerin concentrations, presenting it to nearby

cells and thereby contributing to CMKLR1 and potentially GPR1-mediated processes (Gonzalvo-Feo et al. 2014; Zabel et al. 2008).

The three chemerin receptors have both overlapping and distinct tissue distributions. CMKLR1 is expressed at high levels in leukocyte populations, particularly macrophages and dendritic cells (DCs), adipose, bone, lung, brain, heart, and placenta (Goralski et al. 2007; Wittamer et al. 2003). Similar to CMKLR1, GPR1 is expressed in adipose tissue; however, GPR1 is also expressed in the central nervous system (CNS) and skeletal muscle, and has limited expression in leukocytes (Regard et al. 2008; Rourke et al. 2014). Additionally, unlike chemerin and CMKLR1, GPR1 expression predominates in the non-adipocyte stromal vascular fraction of adipose tissue (Rourke et al. 2014). CCRL2 is largely absent in adipose tissue, but is detected in lung, heart, spleen, and leukocytes (Zabel et al. 2008). This diversity in receptor localization may contribute to both common and independent signalling mechanisms for bioactive chemerin and consequent biological functions. Furthermore, CMKLR1 has been shown to form homomers as well as heteromers with the chemokine receptors CCR7 and CXCR4 (de Poorter et al. 2013), which might result in additional biological consequences *in vivo*.

Chemerin signalling

Very little is known regarding the signal transduction pathways coupled to CMKLR1 and GPR1 activation. Early studies demonstrated that CMKLR1 activation resulted in intracellular calcium release and a reduction in cAMP accumulation. These effects were inhibited by pertussis toxin treatment, demonstrating the involvement of a G_i family member (Wittamer et al. 2003). Chemerin treatment of various cell types, including Chinese hamster ovary (CHO), primary human adipocytes, primary human chondrocytes, vascular smooth muscle cells, and rat cardiomyocytes, has been reported to promote extracellular regulated kinase (ERK)1/2 phosphorylation (Berg et al. 2010; Goralski et al. 2007; Kaneko et al. 2011; Kaur et al. 2010; Kunimoto et al. 2015; Roh et al. 2007; Wittamer et al. 2003; Zhang et al. 2014c). Notably, some studies report that in human adipocytes and endothelial cells, chemerin treatment at low doses stimulates ERK1/2 phosphorylation, but not at higher doses (Goralski et al. 2007; Kaur et al. 2010), indicating that inhibition of signalling or desensitization may occur at higher

concentrations. Chemerin has also been reported to influence several other signalling cascades in both mouse and human cells, including ß-arrestin recruitment, p38 mitogen-activated protein kinase phosphorylation, Akt phosphorylation, phosphoinositide 3-kinase signalling, Nox signalling, and activation of serum response factor (SRF) through a RhoA/ROCK-dependent pathway (Barnea et al. 2008; Berg et al. 2010; Hart and Greaves 2010; Kaneko et al. 2011; Kaur et al. 2010; Kumar et al. 2014; Neves et al. 2015; Rourke et al. 2015; Wang et al. 2015; Yamawaki et al. 2012; Zhang et al. 2014c). Additionally, a recent study demonstrated that chemerin treatment stimulated vesicle exocytosis in mesenchymal stem cells (MSCs) by triggering calcium oscillations, suggesting that chemerin may exert paracrine effects via regulation of exocytosis (Kumar et al. 2015).

In addition to full-length chemerin, several small peptides derived from the C-terminal sequence of chemerin have been shown to activate signalling via CMKLR1 and/or GPR1. A chemerin nonapeptide (hChe9; aa 149-157) and a more stable analog (Dys10) have been shown to induce intracellular calcium mobilization, recruit ß-arrestin to CMKLR1 and GPR1, and activate SRF by a RhoA/ROCK-dependent pathway (Barnea et al. 2008; Rourke et al. 2015; Shimamura et al. 2009; Wittamer et al. 2004; Zhou et al. 2014). Additionally, some groups have reported biological effects of chem-15 and chem-19 peptides (Cash et al. 2014; Cash et al. 2013; Cash et al. 2010; Cash et al. 2008; Wargent et al. 2015) and a chem-20 peptide has been shown to induce CMKLR1 internalization and trigger cAMP production (Li et al. 2014). However, other groups have failed to report similar effects (Hart and Greaves 2010; Luangsay et al. 2009; Pohl et al. 2015; Zabel et al. 2014), suggesting that the efficacy of these peptides requires validation by independent groups. Considered altogether, further elucidation of the signalling pathways associated with chemerin activity will require targeted focus on chemerin receptors. Specifically, future studies should examine overlapping and differential CMKLR1/GPR1 signalling pathways, unique pathway activation by chemerin isoforms, synthetic peptides, and the relative contribution of these signalling mechanisms to specific biological actions elicited by chemerin.

Role of chemerin in inflammation

Chemerin was initially isolated from human inflammatory fluids secondary to ovarian or liver neoplasms and arthritic synovial fluids, and subsequently identified to function as a chemoattractant for CMKLR1-expressing leukocytes (Wittamer et al. 2003). Consequently, a large number of studies have investigated the role of chemerin signalling in the development and resolution of inflammation, and the contribution of chemerin signalling to the pathogenesis of a variety of inflammatory diseases.

Systemic elevations in chemerin levels with chronic inflammation

Circulating chemerin levels are elevated in numerous diseases associated with chronic inflammation. For example, serum chemerin levels are significantly elevated in patients with Crohn's disease, ulcerative colitis (Weigert et al. 2010b), colorectal and gastric cancers (Erdogan et al. 2015; Zhang et al. 2014a), chronic kidney disease (Pfau et al. 2010; Rutkowski et al. 2012; Yamamoto et al. 2010), chronic pancreatitis (Adrych et al. 2012), pre-eclampsia (Stepan et al. 2011), polycystic ovary syndrome (Tan et al. 2009), chronic obstructive pulmonary disease (Boyuk et al. 2014), and liver disease (Kukla et al. 2010b; Sell et al. 2010; Yilmaz et al. 2011a; Yilmaz et al. 2011b). This increase in circulating chemerin levels is positively correlated with circulating inflammatory markers such as C-reactive protein (CRP) (Feng et al. 2012; Landgraf et al. 2012; Lehrke et al. 2009; Tonjes et al. 2010), IL-6, and TNFα, as well as the pro-inflammatory adipokines leptin and resistin (Landgraf et al. 2012; Lehrke et al. 2009; Pfau et al. 2010; Sell et al. 2010; Weigert et al. 2010a). Furthermore, circulating chemerin levels often correlate with disease activity or severity (Aksan et al. 2014; Ha et al. 2014). Unfortunately, the correlative nature of these studies offers little insight into the mechanisms or impact of these associations as the origin, bioactivity, and/or site of action of the circulating chemerin remains unclear. However, consistent with the observed elevation in circulating chemerin, *in vitro* studies demonstrate enhanced secretion of pro-inflammatory cytokines such as IL-6, IL-8, TNFα, CCL2, and IL-1ß with chemerin treatment in cultured human chondrocytes and synoviocytes (Berg et al. 2010; Herova et al. 2014; Kaneko et al. 2011). Likewise, TNFα treatment increases chemerin secretion in cultured human intestinal epithelial cells, murine adipocytes, and

murine serum (De Palma et al. 2011; Maheshwari et al. 2009; Parlee et al. 2010). As such, chemerin produced in response to inflammation may actively contribute to the inflammatory response by altering the expression and secretion of inflammatory mediators, potentially creating a positive feedback loop for sustained chronic inflammation.

Local elevations in chemerin levels and activity with inflammation

Consistent with a role for chemerin in the modulation of local inflammatory responses, chemerin levels are often elevated in diseased tissues in both mice and humans, such as psoriasis, cancer, arthritis, lupus, and multiple sclerosis (Albanesi et al. 2010; Albanesi et al. 2009; Lande et al. 2008; Maheshwari et al. 2009; Monnier et al. 2012; Pachynski et al. 2012; Vermi et al. 2009; Vermi et al. 2005; Wittamer et al. 2003; Zabel et al. 2008). Additionally, local chemerin levels have been shown to correlate with the severity of inflammation in disorders such as ulcerative colitis (Lin et al. 2014). It is important to note that increased chemerin expression and bioactivation is often unique to the localized region of inflamed tissue and may or may not correspond to a similar change in circulating chemerin levels. For example, human studies show that chemerin levels are elevated in peritoneal fluid from patients with endometriosis, without a significant difference in circulating chemerin levels compared to healthy controls (Jin et al. 2015). Similarly, localized synovial fluid chemerin concentrations are elevated up to two-fold in the inflammatory milieu of rheumatoid arthritis, osteoarthritis (OA), and psoriatic arthritis, (Eisinger et al. 2012; Huang et al. 2012; Kaneko et al. 2011; Wittamer et al. 2003). However, despite the observed increase in synovial fluid chemerin with OA severity, serum chemerin levels remain unchanged (Huang et al. 2012). Moreover, within diseased joints the ratio of cleaved to total chemerin is dramatically increased and is often associated with unique isoform profiles that differ considerably from the distribution of isoforms in circulation (Zhao et al. 2011). Consistent with localized chemerin isoform production at sites of active tissue injury or inflammation, neutrophil release of chemerin-activating proteases, blood coagulation, and human pathogen-derived proteases may contribute to the increased chemerin activity (Kulig et al. 2007; Wittamer et al. 2005; Zabel et al. 2005a). However, the tissue source or cell type that contributes to

the increase in chemerin levels is largely unknown. Taken together, these studies demonstrate that total circulating chemerin levels may not necessarily reflect the extent of changes occurring in the disease state, whereas the localized expression and activation of chemerin is an important determinant of the influence of chemerin signalling on inflammatory responses.

Chemerin exhibits pro-inflammatory activities

In addition to increasing the expression and secretion of pro-inflammatory mediators, elevation of chemerin levels within inflamed or diseased tissues may contribute directly to inflammation through the modulation of immune cell recruitment. Chemerin has been shown to promote chemotaxis of CMKLR1-expressing leukocyte populations such as human macrophages, immature DCs, and natural killer (NK) cells to localized sites of inflammation, tissue damage, or bleeding, suggesting a pro-inflammatory role (Albanesi et al. 2010; Albanesi et al. 2009; Gonzalvo-Feo et al. 2014; Lande et al. 2008; Maheshwari et al. 2009; Monnier et al. 2012; Pachynski et al. 2012; Vermi et al. 2009; Vermi et al. 2005; Wittamer et al. 2003; Zabel et al. 2008). A recent study also identified a role for chemerin/GPR1 signalling in the chemotaxis of gastric cancer cells (Rourke et al. 2015; Wang et al. 2014). In addition, chemerin promotes the adhesion of murine macrophages and L1.2 CMKLR1-expressing lymphoid cells to extracellular matrix proteins and endothelial cells, supporting a role in both the recruitment and retention of leukocytes at sites of infiltration (Hart and Greaves 2010; Monnier et al. 2012).

Animal models have demonstrated a requirement for chemerin signalling in the development of optimal tissue swelling and leukocyte infiltration in various mouse inflammation models such as IgE-mediated anaphylaxis and LPS-induced pulmonary inflammation (Monnier et al. 2012; Parolini et al. 2007; Zabel et al. 2008). Similarly, CNS inflammation is reduced in the absence of CMKLR1 expression in mouse experimental autoimmune encephalomyelitis (EAE), a model of autoimmune demyelinating disease (Graham et al. 2009). Consistent with this, treatment of mice with α-NETA, a small molecule inhibitor of CMKLR1, delays the onset of EAE and results in reduced mononuclear cell infiltrate within the CNS (Graham et al. 2014). Additionally,

recent studies demonstrated that chemerin is expressed and functional on M1, but not M2, macrophages (Herova et al. 2015), and that exogenous administration of chemerin in an animal model of colitis exacerbates the severity of disease by suppressing the M2 macrophage response (Lin et al. 2014). Thus, clinical and experimental data support a role for chemerin in the recruitment of inflammatory cells and the promotion of local inflammatory processes.

Chemerin exhibits anti-inflammatory activities

Conversely, a number of studies have supported an anti-inflammatory role for chemerin signalling. Several animal studies have demonstrated that inhibition of endogenous chemerin activity or a loss of CMKLR1 expression exacerbated inflammation and decreased leukocyte infiltration in various inflammation models such as peritoneal inflammation (Cash et al. 2008), LPS-induced lung injury (Luangsay et al. 2009), and acute viral pneumonia (Bondue et al. 2011). Additionally, intranasal chemerin treatment (Zhao et al. 2014) or administration of a soluble membrane anchored CMKLR1 agonist (Doyle et al. 2014) both resulted in decreased allergic airway inflammation in animal models. Furthermore, administration of a 15 amino acid peptide derived from the C-terminus of chemerin (Chem-15) has been shown to accelerate wound healing by reducing macrophage accumulation to the immediate wound site, promote inflammation resolution following microbial challenge, and reduce neutrophil adhesion in a myocardial infarction model (Cash et al. 2014; Cash et al. 2013; Cash et al. 2010). Consistent with this, experimental data have shown that under certain experimental conditions, chemerin inhibits the production of pro-inflammatory mediators such as TNFα, IL-1ß, IL-6, IL-12, and CCL5, by classically activated murine macrophages *in vitro* (Cash et al. 2008) and inhibits monocyte adhesion to TNFα-stimulated endothelial cells (Yamawaki et al. 2012). However, an independent group has failed to reproduce these anti-inflammatory effects (Bondue et al. 2012), and the efficacy of Chem-15 administration on known chemerin signalling pathways is unknown, suggesting that other mechanisms might contribute to the anti-inflammatory effects of chemerin. These effects might involve a group of anti-inflammatory mediators termed resolvins, including Resolvin E1, which has been proposed to bind and activate CMKLR1 resulting in anti-

inflammatory function (Arita et al. 2005a). However, this finding has yet to be confirmed by independent groups and it has been shown that Resolvin E1 interacts with other receptors in addition to CMKLR1 (Arita et al. 2007). Thus, independent confirmation and future studies are necessary to elucidate the existence and/or mechanisms of anti-inflammatory chemerin signalling.

Chemerin: pro- or anti-inflammatory?

As current experimental data support both a pro- and anti-inflammatory role for chemerin, it is possible that the primary role of chemerin could to be to indicate local conditions and rapidly establish the appropriate pro-inflammatory or suppressive response. Alternatively, different chemerin isoforms may play contrasting roles in various stages of inflammation, with serine proteases secreted early in the immune response (e.g. by neutrophils (Wittamer et al. 2005)) generating more active chemerin peptides, and later secreted cysteine proteases (e.g. by macrophages (Cash et al. 2008)) generating relatively inactive peptides, thus controlling the severity of inflammatory responses. Moreover, chemerin likely plays different roles depending on which populations of cells are activated in a particular condition. Consequently, while chemerin is known to be involved in immune cell recruitment and pathogenic processes, it remains to be determined if chemerin plays a more important role in inflammation initiation, maintenance, or resolution, particularly with respect to whether increased chemerin activity is playing a protective or pathologic role in these inflammatory disease states.

Role of chemerin in metabolism

In addition to serving as an energy storage depot, WAT is a highly active endocrine organ that secretes a number of bioactive signalling molecules that are collectively termed adipokines. Adipokines comprise a diverse class of highly regulated proteins including leptin, adiponectin, TNFα, and IL-6 (for review, see (Ouchi et al. 2011; Poulos et al. 2010)) and have autocrine/paracrine functions that influence adipose tissue development and function, as well as hormone-like actions on metabolically active tissues such as the brain, liver, and skeletal muscle. Numerous studies have revealed that adipokine secretion is profoundly affected by the degree of adiposity. Given the

regulatory influence of adipokines on numerous biological functions including energy homeostasis, glucose and lipid metabolism, food intake, inflammation, and immunity, it is believed that dys-regulation of adipokine secretion with obesity is a major contributor to the elevated risk for obesity-associated diseases such as type 2 diabetes (T2D) and cardiovascular disease (CVD).

A fundamental shift in our understanding of chemerin biology in human pathology occurred in 2007 when it was first reported that chemerin and CMKLR1 were expressed in WAT (Goralski et al. 2007) and that circulating total chemerin levels were elevated in obese rodents and humans (Bozaoglu et al. 2007; Goralski et al. 2007). Subsequently, *in vitro*, animal, and human studies have firmly established chemerin as an adipokine with significant relevance to obesity and associated metabolic disorders.

Chemerin levels increase with obesity

Fluctuations in circulating chemerin levels are closely related to the degree of overall adiposity. Serum chemerin concentrations are higher in obese animal models including genetic and diet-induced models of obesity (Bozaoglu et al. 2007; Ernst et al. 2012; Ernst et al. 2010; Parlee et al. 2010). In young and adult obese patients, elevated serum or plasma chemerin levels positively correlate with body mass index (BMI) and measures of central adiposity such as waist to hip ratio, waist circumference (Bozaoglu et al. 2007; Chakaroun et al. 2012; Feng et al. 2012; Yoo et al. 2012), and visceral adipose tissue mass (Landgraf et al. 2012; Shin et al. 2012). In obese mice, dys-regulation of chemerin levels is associated with an exaggerated oscillatory pattern with a greater frequency and magnitude of change between minimum and maximum serum chemerin levels (Parlee et al. 2010). Consistent with a positive correlation between chemerin levels and adiposity measures, obese patients who underwent weight loss through either bariatric surgery (Parlee et al. 2015; Ress et al. 2010; Sell et al. 2010; Terra et al. 2013) or exercise-nutrition-based methods (Bluher et al. 2012; Chakaroun et al. 2012; Lloyd et al. 2015; Malin et al. 2014; Saremi et al. 2010; Stefanov et al. 2014), exhibited a significant decline in circulating chemerin levels. Additionally, female patients with restrictive anorexia have decreased systemic chemerin levels (Oswiecimska et al. 2014). Thus, although chemerin is also synthesized and secreted by the liver (Weigert et al.

2010a), as well as some immune and vascular cells, the obesity-associated increase in chemerin levels appears to be primarily adipose tissue derived. This is further supported by reports that adipose tissue explants from obese individuals secrete significantly more chemerin than those isolated from lean individuals, and this secretion correlates with increased body mass index (BMI), waist to hip ratio, and fat cell volume (Sell et al. 2009). Taken together, both experimental and clinical studies indicate that WAT is a dynamic and modifiable source of chemerin. Importantly, adipocytes secrete proteases such as elastase and tryptase, which are able to generate bioactive chemerin isoforms (Parlee et al. 2012). Consistent with this, one study has reported a correlation between the elevations of total and bioactive serum chemerin levels in a murine model of obesity (Ernst et al. 2010). However, while total chemerin levels have been reported in numerous studies, levels of bioactive chemerin in humans, and how these are affected by obesity, remain to be examined.

Chemerin levels influence WAT expansion and inflammation

In obesity, adipose tissue expansion involves a number of remodelling processes that include the enlargement of existing adipocytes (hypertrophy) and an increase in adipocyte number (hyperplasia). One mechanism that contributes to adipocyte hyperplasia is the increased proliferation and differentiation of preadipocytes into adipocytes. Chemerin signalling is essential during the early clonal expansion phase of adipocyte differentiation, where PPARγ, the master regulator of adipogenesis, directly increases chemerin expression (Muruganandan et al. 2011). Reduction of chemerin or CMKLR1 signalling through knock-down or neutralization approaches results in severe impairment of both 3T3-L1 and murine mesenchymal stem cell differentiation into mature adipocytes *in vitro* (Goralski et al. 2007; Muruganandan et al. 2011; Muruganandan et al. 2010). Consistent with this, we have demonstrated that a loss of CMKLR1 *in vivo* is associated with reduced body mass and adiposity, and a resistance to diet-induced obesity (Ernst et al. 2012), suggesting that chemerin signalling promotes adipogenesis *in vivo*. However it is important to note that other groups have demonstrated that CMKLR1 KO mice exhibit increased adiposity with aging or on a high-fat diet (HFD) (Rouger et al. 2013; Wargent et al. 2015) although the reasons for

these discrepancies are unclear. Coincident with hyperplasia and hypertrophy, dilation of existing capillary networks and formation of new blood vessels via angiogenesis is required to increase blood supply to the expanding adipose tissue mass. As chemerin treatment has been shown to activate key angiogenic signalling cascades, to induce proliferation and migration of human endothelial cells, and to promote capillary tube formation (Bozaoglu et al. 2010; Kaur et al. 2010), this adipokine may also support adipose tissue expansion by inducing angiogenesis and promoting vascularization. Moreover, while acute chemerin treatment decreases food intake in mice fed a normal chow diet (Brunetti et al. 2014), constitutive loss of both CMKLR1 and GPR1 results in decreased calorie consumption, suggesting an endocrine role for adipose-derived chemerin to regulate energy intake and adipose tissue expansion (Ernst et al. 2012; Rourke et al. 2014).

Increased adiposity also induces chronic low-grade inflammation in adipose tissue, which is causally linked to obesity itself as well as many obesity-associated comorbidities (for review, see (Lumeng and Saltiel 2011)). Key characteristics of WAT inflammation include the increased secretion of cytokines such as TNFα and IL-6, and the recruitment and infiltration of macrophages, T cells, NK cells and immature DCs to adipose tissue. Several studies have demonstrated that chemerin levels are positively associated with these events (Lehrke et al. 2009; Maghsoudi et al. 2015; Weigert et al. 2010a). As pro-inflammatory cytokines have an established role in up-regulating chemerin expression in adipocytes, chemerin levels may rise as a consequence of increased adipose tissue inflammation (Bauer et al. 2011; Herova et al. 2014; Kralisch et al. 2009; Parlee et al. 2010). Furthermore, consistent with the established role of chemerin as a chemoattractant, adipocyte-derived chemerin acts as a paracrine regulator for the recruitment of CMKLR1-expressing cells to WAT, suggesting that chemerin levels mediate the development of WAT inflammation. For example, studies have shown a lower percentage of CD3+ T cells and macrophages in WAT isolated from CMKLR1 and chemerin KO mice, respectively (Ernst et al. 2012; Takahashi et al. 2011). Additionally, as adipose tissue contains the proteases required for chemerin activation and inactivation (Parlee et al. 2012), context-specific regulation of the ratio of active to total chemerin within adipose tissue likely contributes to the modulation of immune cell

recruitment and consequent inflammation. However, the nature and impact of the relationship between chemerin and adipose tissue inflammation remain to be elucidated as it is unclear which chemerin isoforms are increased in obese adipose tissue and what effect chronically elevated chemerin levels have on adipose tissue and systemic metabolism.

Chemerin levels are associated with obesity comorbidities

The available studies suggest that chemerin expression is dynamic and is substantially elevated in obese individuals. This dys-regulation is closely associated with changes in central adiposity and adipose tissue inflammation, lending support to the potential role of chemerin as a molecular link between obesity, obesity-associated inflammation, and the development of comorbidities. Given the known role of adipokines on both local and systemic processes such as glucose and lipid homeostasis, a number of clinical and experimental studies have investigated the role of chemerin signalling on the pathogenesis of metabolic disorders such as metabolic syndrome, T2D, and CVD.

Metabolic syndrome

Among the most prevalent obesity comorbidities that place individuals at an increased risk for CVD and T2D is metabolic syndrome (MetS), which is characterized by a cluster of metabolic disturbances including impaired glucose homeostasis, high blood pressure, and central adiposity. Consistent with a role for chemerin as a risk factor for MetS, elevated levels of both circulating and adipose-expressed chemerin are significantly elevated in individuals with MetS when compared to healthy controls (Dong et al. 2011; Min et al. 2012; Yan et al. 2012), are predictive for MetS severity (Stejskal et al. 2008), and are often positively correlated with elevations in many individual MetS markers, including circulating triglycerides, low-density lipoprotein (LDL) cholesterol, waist circumference, insulin resistance, fasting insulin/glucose, and systolic as well as diastolic blood pressure (Bozaoglu et al. 2007; Bozaoglu et al. 2009; Chu et al. 2012; Hah et al. 2011; Stejskal et al. 2008; Wang et al. 2013a; Yan et al. 2012; Yang et al. 2010; Yoo et al. 2012). Conversely, with exercise-induced weight loss, decreased serum

chemerin levels correlate with an improvement in MetS markers including visceral fat volume, insulin resistance, fasting glucose, and waist circumference (Saremi et al. 2010). It will be interesting through future studies to determine (i) the regulatory mechanisms supporting the temporal relationship between chemerin and MetS syndrome; (ii) how these changes relate to inflammation and adipose tissue mass in MetS; and (iii) whether chemerin acts as a molecular link between the presence of the metabolic perturbations and increased risk for CVD and T2D.

Glucose homeostasis and T2D

T2D is characterized by deleterious elevations in fasting glucose as well as reduced insulin-stimulated glucose uptake, which derive from sustained hepatic, muscle, and adipose insensitivity to the actions of insulin (insulin resistance). A number of studies have reported that chemerin levels are significantly exacerbated in obese individuals when insulin resistance or T2D is also present (Bozaoglu et al. 2009; Chakaroun et al. 2012; Kloting et al. 2010; Kukla et al. 2010a; Sell et al. 2010; Tonjes et al. 2010; Weigert et al. 2010a; Yamamoto et al. 2010) and that serum chemerin concentrations are strongly associated with insulin sensitivity (Bozaoglu et al. 2009; Ouwens et al. 2012; Tonjes et al. 2010). Consistent with this, decreased chemerin levels subsequent to surgical, exercise-, or diet-induced weight loss in obese patients were significantly correlated with reduced levels of inflammatory markers as well as improved insulin resistance (Chakaroun et al. 2012; Khoo et al. 2015). Importantly, several studies have noted improvements in glycemia and insulin sensitivity, coincident with a decrease in circulating chemerin levels, in T2D patients before any appreciable changes in body weight, indicating that the role of chemerin in T2D may be independent of BMI (Chakaroun et al. 2012; Esteghamati et al. 2014). These observations support a role for chemerin signalling in the regulation of glucose homeostasis and insulin sensitivity.

Consistent with this, animal studies have demonstrated that chemerin signalling influences glucose homeostasis. While some studies have reported no change in glucose tolerance in CMKLR1 KO mice (Gruben et al. 2014; Rouger et al. 2013), others have reported that chemerin, CMKLR1, and GPR1 KO mice all exhibit impaired glucose tolerance with obesity (Ernst et al. 2012; Rourke et al. 2014; Takahashi et al. 2011;

Wargent et al. 2015). Similarly, chronic overexpression of chemerin increased glucose tolerance (Takahashi et al. 2011). The available evidence suggests that decreased levels of chemerin signalling may impair glucose tolerance, at least in part, through impaired glucose-stimulated insulin secretion ((Ernst et al. 2012; Takahashi et al. 2011) and reviewed in (Rourke et al. 2013)). For instance, pancreatic ß-cells isolated from chemerin KO mice have impaired insulin secretion, as does the pancreatic Min6 cell line following chemerin knockdown, suggesting a role for chemerin signalling in the regulation of pancreatic ß-cell function (Takahashi et al. 2011). Thus, an increase in circulating chemerin levels in obese T2D patients might act as a compensatory mechanism to restore glucose handling. Chemerin might also play a direct role in insulin sensitivity and glucose uptake, although investigations to this effect have provided conflicting results. For example, studies have shown both increased (Takahashi et al. 2008) and decreased (Kralisch et al. 2009) insulin-stimulated glucose uptake in 3T3-L1 adipocytes following chemerin treatment. However, experiments with primary human or C2C12 skeletal muscle cells, and chemerin KO mice, are consistent with a role for chemerin signalling in inducing insulin resistance and negatively modulating glucose uptake in skeletal muscle (Ernst et al. 2012; Issa et al. 2012; Sell et al. 2009; Takahashi et al. 2011; Zhang et al. 2014c). Considered altogether, while the precise pathophysiological role of chemerin in T2D is at present unclear, these studies demonstrate that chemerin plays a role in glucose homeostasis, likely as a modulatory factor in insulin secretion and sensitivity.

Chemerin is associated with cardiovascular pathologies

The metabolic perturbations that occur with obesity and MetS contribute to CVD development in approximately one-third of cases (Wilson 2004). Given the alterations in chemerin levels in of these conditions, a limited number of studies have investigated whether chemerin plays a role in cardiovascular pathology. Hyperlipidaemia, generally classified as elevated circulating triglycerides and an increased ratio of LDL/HDL (high-density lipoprotein) cholesterol ratio, occurs in obesity in part as a consequence of altered lipolysis and is associated with an increased risk for the development of CVD. The majority of studies report significant positive correlations with chemerin and circulating

triglycerides, LDL cholesterol, and blood pressure (Bozaoglu et al. 2007; Chakaroun et al. 2012; Chu et al. 2012; Dong et al. 2011; Kunimoto et al. 2015; Ren et al. 2012; Stejskal et al. 2008; Tan et al. 2009; Xiaotao et al. 2012; Yan et al. 2012; Yoo et al. 2012), and negative correlations with HDL cholesterol (Alfadda et al. 2012; Chu et al. 2012; Ren et al. 2012; Sell et al. 2010). However, very few studies have directly examined the effect of chemerin signalling on the regulation of lipolysis. As with glucose uptake, conflicting results have arisen. Some studies with 3T3-L1 and murine primary adipocytes support a role for chemerin in stimulating lipolysis (Goralski et al. 2007; Roh et al. 2007), while another reported decreased basal lipolysis following chemerin treatment (Shimamura et al. 2009). Notably, in the latter study, effects were blunted in CMKLR1 KO mice, indicating that CMKLR1 does affect lipolysis in some manner. To date, only one study has examined the influence of chemerin on lipid homeostasis *in vivo*, with no change in triglyceride and cholesterol levels following chronic overexpression of chemerin in LDL receptor KO mice (Becker et al. 2010). Thus, future studies are necessary to elucidate the involvement of chemerin signalling in lipid homeostasis.

Studies have also shown a role for chemerin signalling in atherosclerosis and cardiovascular disease, with chemerin levels predictive for cardiovascular events (Leiherer et al. 2015). Increased chemerin levels have been associated with atherosclerosis and arterial stiffness (Dessein et al. 2014; Gu et al. 2015; Kostopoulos et al. 2014; Lu et al. 2015), coronary artery disease (Aksan et al. 2014; Hah et al. 2011; Ji et al. 2014; Xiaotao et al. 2012; Yan et al. 2012), dilated cardiomyopathy (Zhang et al. 2015a), acute MI (Kadoglou 2015), and as a risk factor for carotid artery plaque instability and stroke (Zhao et al. 2015). Importantly, chemerin levels generally correlate with the severity of atherosclerotic lesions and overall CVD severity (Gao et al. 2011; Hah et al. 2011; Kostopoulos et al. 2014; Spiroglou et al. 2010; Xiaotao et al. 2012; Yan et al. 2012), lending support to the importance of localized autocrine/paracrine functions of chemerin within the heart. Future studies that investigate the role of chemerin signalling on the regulation of other cardiovascular risk factors and the mechanisms underlying disease pathogenesis will be essential to determine a causal role of both circulating and localized chemerin expression.

Other physiological roles of chemerin signalling

Beyond inflammatory and metabolic disorders, a variety of studies have identified potential roles for chemerin signalling in other physiological processes and diseases. However, it is important to highlight that these roles are not necessarily exclusive from metabolism or inflammation. For example, circulating chemerin levels have been positively associated with other endocrine disorders that are associated with obesity and insulin resistance, such as polycystic ovary syndrome (PCOS) (Ademoglu et al. 2014; Bozaoglu et al. 2009; Guzel et al. 2014; Tan et al. 2009; Yang et al. 2015). In addition to increased serum levels, local ovarian chemerin levels are also increased in rat models of PCOS models (Wang et al. 2012), suggesting an autocrine/paracrine role for chemerin in the regulation of ovarian function. Consistent with this, several studies have demonstrated that both chemerin and 20 aa peptide derived from the C-terminus of chemerin suppress steroidogenesis (Li et al. 2014; Reverchon et al. 2012; Wang et al. 2012), indicating that chemerin signalling might contribute to the pathogenesis of PCOS.

Chemerin levels are increased in patients with osteoporosis (He et al. 2015) and experimental studies have demonstrated that chemerin/CMKLR1 signalling influences bone remodelling by promoting both osteoblastogenesis and osteoclastogenesis (Muruganandan et al. 2013; Muruganandan et al. 2010). Considered together with previous studies on angiogenesis (Kaur 2010), adipogenesis (Goralski et al. 2007; Muruganandan et al. 2011), myogenesis (Issa et al. 2012), and follicular development (Kim et al. 2013), this suggests that chemerin plays a role in the development of numerous tissue types and actively contributes to tissue remodeling during normal physiology and disease pathogenesis. Consistent with this, several studies have implicated a role for chemerin signalling in cancer progression. Notably, increased levels of chemerin in gastric cancer have been reported and shown to correlate with poor survival outcomes (Erdogan et al. 2015; Wang et al. 2014; Zhang et al. 2014a). Mechanistically, chemerin has been proposed to increase the invasiveness of gastric cancer cells (Wang et al. 2014) and increase MSC recruitment to tumors (Kumar et al. 2014), suggesting that inhibition of chemerin signalling might delay tumor progression. In contrast, decreased chemerin levels have been reported in melanoma and intra-tumoral

chemerin injections were shown to inhibit tumor growth (Pachynski et al. 2012), indicating that chemerin might also play a protective role against tumour development.

Consistent with a protective role in host defense, chemerin has been shown to act as an antimicrobial agent. This is not surprising given the similarity in structure with antibacterial cathelicins (Wittamer et al. 2003) and expression in a variety of epithelial cells at barrier sites (reviewed in (Zabel et al. 2014)). Chemerin exhibits direct bacterial lytic activity and inhibits the growth of human pathogens such as *Escherichia coli*, *Candida albicans*, and *Staphylococcus aureus* (Banas et al. 2013; Banas et al. 2015; Kulig et al. 2007). Interestingly, a screen of chemerin-derived peptides revealed that the sequence corresponding to aa 65-85 was responsible for the antimicrobial actions (Banas et al. 2013), suggesting that all other chemerin isoforms identified to date have similar antimicrobial potential. However, the role of chemerin signalling on the regulation of microbial growth beyond host defense against pathogen invasion (ie. impact on the commensal gut microflora) remains to be elucidated.

Contextualizing chemerin function in health and disease

Taken together, persistent elevations in total circulating chemerin levels with obesity and positive correlations with an abundance of metabolic and inflammatory perturbations unify the majority of human studies conducted to date. BMI, insulin sensitivity, and CRP levels are the most predictive of changes in circulating chemerin levels (Chakaroun et al. 2012), suggesting that any disease associated with inflammation, insulin resistance, and/or increased adipose tissue mass as a substantial component of the pathology will also display elevations in circulating or localized chemerin levels. Collectively, human and animal studies suggest dynamic and context-specific regulation of chemerin activity and/or function, dependent on numerous factors, including: location, duration and severity of disease, interactions with other adipokines, genetic and environmental variation, and the signalling events that occur in response to the activation of chemerin receptors on responding cells. Considering the reported pro- and anti-inflammatory functions, as well as enhancement and inhibition of glucose uptake, chemerin may act as both a pathogenic and protective adipokine depending upon the physiological context. Similar to most cytokines, chemerin activity appears highly

regulated and likely also plays essential roles in normal healthy adipose and immune function. Future studies that investigate the regulation of chemerin expression, determine the importance of different chemerin isoforms, characterize chemerin-activated signalling pathways, and elucidate the function of chemerin signalling in health and disease, will help to identify novel therapeutic treatments for the prevention and treatment of inflammatory and metabolic disorders.

Table 1.1. Prochemerin processing

Chemerin is secreted in an inactive precursor form, prochemerin, which is proteolytically processed by a variety of extracellular proteases to generate chemerin isoforms with differing levels of bioactivity. Some proteases are able to cleave chemerin at more than one site and chemerin isoforms may be sequentially processed by different enzymes to modulate activity levels. The coordinated expression and activity of chemerin-modifying enzymes is essential for regulating chemerin bioactivation, inactivation, and consequently, biological function. Activity is in reference to functional assays for chemotaxis or intracellular calcium release. *also generates Chem-125, which has no chemotactic activity but demonstrates antibacterial activity (Kulig et al. 2011)

Protease	Cleaves	Generates	C-terminal sequence	Resulting activity
Prochemerin			…PGQFAFSKALPRS	Inactive
Carboxypeptidase N or B (Du et al. 2009)	Chem-158	Chem-157	…PGQFAFS	Converts high to highest
Cathepsin G (Wittamer et al. 2005)	Chem-163	Chem-156	…PGQFAF	High
Cathepsins K, L* (Kulig et al. 2011)	Chem-163	Chem-157	…PGQFAFS	Highest
Human leukocyte elastase (Wittamer et al. 2005)	Chem-163	Chem-157	…PGQFAFS	Highest
		Chem-155	…PGQFA	Low
		Chem-152	…PG	Inactive
Kallikrein 7 (Schultz et al. 2013)	Chem-163	Chem-156	…PGQFAF	High
Mast cell chymase (Guillabert et al. 2008)	Chem-156	Chem-154	…PGQF	Converts high/highest to inactive
	Chem-157			
Mast cell tryptase (Zabel et al. 2005a)	Chem-163	Chem-158	…PGQFAFSK	Low
		Chem-155	…PGQFA	Low
Plasmin (Zabel et al. 2005a)	Chem-163	Chem-158	…PGQFAFSK	Low
Proteinase 3 (Guillabert et al. 2008)	Chem-163	Chem-155	…PGQFA	Low
Staphopain B (Kulig et al. 2007)	Chem-163	Chem-157	…PGQFAFS	Highest
Factors XIIa, VIIa, plasmin, plasminogen activators (Zabel et al. 2005a)	Described as activators of chemerin, but precise cleavage sites not yet determined			

Table 1.2. Sources of chemerin isoforms

Distinct chemerin isoforms have been identified in several different biological fluids, indicating that chemerin undergoes complex processing *in vivo*. Future studies that investigate the presence of particular isoforms in disease states will contribute to this rapidly growing list.

Biological source	Identified isoforms
Ascites (Wittamer et al. 2005)	Chem-157
Cerebrospinal fluid (Yamaguchi et al. 2011; Zhao et al. 2011)	Chem-158
Hemofiltrate (Meder et al. 2003)	Chem-154
Plasma (Zabel et al. 2005a; Zhao et al. 2011)	Chem-155, -157, -158, -163
Synovial fluid (Zhao et al. 2011)	Chem-158

Thesis objectives

To date, chemerin has primarily been characterized within two different functional contexts: as an adipokine and as a potent chemoattractant for cells that express CMKLR1. The work presented in this thesis addresses the role of chemerin signalling within both of these metabolic and inflammatory contexts. The available evidence suggests that chemerin may act as a protective or pathogenic factor depending on the physiological context. In order to further our understanding of chemerin function, I have examined the role of chemerin signalling in a variety of physiological contexts, including mature adipocytes, where chemerin is highly expressed under healthy conditions, and inflammatory bowel disease (IBD), where chemerin levels are chronically elevated in disease conditions. I hypothesized that chemerin functions to maintain adipose tissue and intestinal homeostasis, and that inhibition of chemerin signalling will influence mature adipocyte function and the development of intestinal inflammation. Furthermore, given the role of chemerin signalling as an antimicrobial agent, and the established role of the commensal gut microflora on health and disease, I hypothesized that chemerin signalling influences metabolism and inflammation through indirect effects on the gut microbiome. Specifically, the objectives of each chapter are as follows:

Chapter 2: Develop novel systems and screen available small molecules that can be used to modulate the expression and/or activity of chemerin signalling, particularly with relevance for use in mature adipocytes

Chapter 3: Identify novel targets of chemerin signalling in mature adipocytes and investigate the role of chemerin signalling in adipose tissue homeostasis

Chapter 4: Examine the role of chemerin signalling in the development of DSS-induced colitis and determine whether a loss of CMKLR1 will protect against development of IBD

Chapter 5: Investigate the impact of a loss of chemerin signalling on the composition of the gut microbiome

CHAPTER 2: DEVELOPMENT AND SCREENING OF TOOLS TO MODULATE CHEMERIN EXPRESSION AND/OR SIGNALLING

Copyright statement

Data presented in Figure 2.11 (hChe9, mChe15, and Dys10 peptide treatments) and methods for the MTT assay have been previously published (Rourke JL, Dranse HJ, Sinal CJ. (2015). CMKLR1 and GPR1 mediate chemerin signalling through the RhoA/ROCK pathway. Molecular and Cellular Endocrinology 417: 36-51). Presentation of the data has been modified for clarity. Re-use is permitted with copyright permission (Appendix A).

Contribution statement

Dr. Shanmugam Muruganandan isolated the bone marrow-derived mesenchymal stem cells (MSCs) used in Figures 2.9 and 2.17. I was responsible for designing and performing all other experiments with guidance from Dr. Christopher Sinal.

Abstract

Chemerin is a potent chemoattractant for cells expressing chemokine-like receptor 1 (CMKLR1) and an adipocyte-secreted signalling molecule that plays important roles in inflammation and metabolism. Mature adipocytes secrete high levels of inactive prochemerin, which undergoes extracellular processing to generate a number of isoforms with differing levels of bioactivity. Activation of CMKLR1 and G protein coupled receptor 1 (GPR1) by bioactive chemerin has been shown to influence a variety of cellular processes including cell migration, proliferation, and differentiation. A number of tools have played essential roles in developing our current understanding of chemerin signalling; however, significant limitations exist regarding their use. In particular, only one chemerin isoform is commercially available and conflicting reports have been presented on the efficacy of small molecule agonists and inhibitors at CMKLR1 and GPR1. In addition, current techniques to modify chemerin levels in mature adipocytes are not robust enough to overcome high levels of basal chemerin expression. The goal of this chapter was to develop novel systems to modulate chemerin expression and signalling, with a focus on the use of these tools in mature adipocytes. We successfully expressed and purified bioactive chemerin using a bacterial expression system. We also generated a lentivirus-mediated chemerin overexpression system that resulted in high levels of chemerin secretion from MSCs and HEK cells, and shifted the distribution of adipocyte-secreted chemerin isoforms. Future modification of these expression systems can be used in order to produce and investigate the biological function of commercially unavailable chemerin isoforms. We also tested the activity of currently available small molecules (hChe9, Dys10, mChe15, humanin, and CCX832) at CMKLR1 and GPR1 using cell-based reporter assays and demonstrated that these molecules function at exponentially higher concentrations than reported but display some receptor specificity. Finally, we generated an inducible knockdown system in order to reduce endogenous levels of chemerin expression. This system was effective in cell types that expressed chemerin at low levels and resulted in a ~40% knockdown in mature adipocytes. The development of these tools was critical for the studies described in Chapter 3. The complementary use of these techniques will also facilitate future studies on the role of specific chemerin isoforms and receptor-specific signalling in physiology and disease.

Introduction

Chemerin is an 18 kDa-secreted protein that has been shown to play important roles in metabolism and immunity as both an adipokine and potent chemoattractant for cells expressing the G protein coupled receptor (GPCR) chemokine-like receptor 1 (CMKLR1). Chemerin is expressed at high levels in the placenta, liver, and white adipose tissue, and white adipocytes are thought to be the primary modifiable source of chemerin levels in circulation (Rourke et al. 2013; Zabel et al. 2014). Chemerin is initially synthesized as a 163 amino acid (aa) protein and the removal of a 20 aa N-terminal signal sequence results in secretion of inactive prochemerin (chemerin-163). The majority of circulating chemerin is believed to exist in this inactive prochemerin form. A number of proteases are responsible for extracellular processing of prochemerin to generate a variety of bioactive chemerin isoforms (for review, see (Rourke et al. 2013)). Characterization of chemerin activity has primarily focused on the removal of amino acids at the C-terminus and a range of isoforms, including chemerin-154, 155, 157, 158, and 163, have been identified in human samples (Meder et al. 2003; Wittamer et al. 2003; Zabel et al. 2005a; Zhao et al. 2011). These isoforms exhibit different levels of activity at CMKLR1 (Du et al. 2009; Guillabert et al. 2008; Kulig et al. 2011; Kulig et al. 2007; Wittamer et al. 2005; Zabel et al. 2005a). More recently, chemerin-157 has also been shown to activate G-protein coupled receptor 1 (GPR1) (Barnea et al. 2008; Rourke et al. 2015). Together, activation of CMKLR1 and GPR1 by chemerin has been shown to play roles in cell migration, proliferation, and differentiation, and influence a range of physiological processes including adipose development and function, energy metabolism, and inflammation.

Several tools have been instrumental in developing our current understanding of chemerin biology. These include the generation of proteins that activate CMKLR1, such as recombinant chemerin-157 and short peptides that are based on the C-terminal sequence of chemerin. Of the developed peptides, hChe9 and a stable analog, Dys10, have been shown to activate CMKLR1, resulting in increased intracellular calcium release (Shimamura et al. 2009; Wittamer et al. 2005). Additionally, mChe15 has been shown to exhibit anti-inflammatory properties (Cash et al. 2014; Cash et al. 2010; Cash et al. 2008). More recently, a patent reported that humanin, a 24 aa peptide with neuro- and

cytoprotective properties (Yen et al. 2013), results in increased recruitment of ß-arrestin to human GPR1 (Leroy 2014).

In contrast to these gain-of-function approaches, the small molecules CCX832 and 2-(α-naphthoyl) ethyltrimethylammonium iodide (α-NETA) have been shown to inhibit CMKLR1 activation and chemotactic activity (Graham et al. 2014; Watts et al. 2013). Similarly, treatment with a neutralizing chemerin antibody has been used to reduce levels of endogenous chemerin signalling (Cash et al. 2008; Muruganandan et al. 2013; Muruganandan et al. 2011). Finally, several genetic methods have been generated to modulate levels of chemerin signalling. These include the generation of chemerin, CMKLR1, and GPR1 knockout mice (Ernst et al. 2012; Rourke et al. 2014; Takahashi et al. 2011), and chemerin and CMKLR1 shRNA expression constructs (Goralski and Sinal 2009; Muruganandan et al. 2010).

While these tools have helped to establish the current understanding of chemerin biology, there are a number of important limitations that exist regarding their use. Firstly, despite the knowledge that chemerin is processed to several bioactive isoforms, the only commericially available isoform is chemerin-157. As a consequence, the role of other bioactive isoforms remains unclear. Additionally, activation of CMKLR1 by chemerin-derived peptides has only been examined in reference to intracellular calcium release and chemotactic activity (Cash et al. 2008; Shimamura et al. 2009; Wittamer et al. 2005). Chemerin is also known to induce ß-arrestin recruitment and activate serum response factor (SRF) signalling through both CMKLR1 and GPR1 (Barnea et al. 2008; Rourke et al. 2015), and the activity of chemerin-derived peptides on these signalling pathways is unknown. Furthermore, the anti-inflammatory action of chemerin-15 has only been reported by one group to date (Cash 2008, 2010, 2014), and there are no peer-reviewed reports on the activity of humanin at GPR1. Finally, the ability of these small molecules to activate CMKLR1 versus GPR1, and mouse versus human receptors, has never been directly compared.

Considered altogether, there is a strong need for the production of other chemerin isoforms, validation of current small molecules that target chemerin receptors, and the generation of reliable systems to genetically manipulate levels of chemerin signalling. For these reasons, the overall goal of this chapter was to develop and screen tools that can

be used to modify chemerin expression and/or signalling. Several approaches were taken as outlined in Figure 2.1. These include the generation of human and mouse chemerin isoforms using both a bacterial expression system and a lentivirus-mediated chemerin overexpression system. Furthermore, the activity of the available small molecules at both mouse and human CMKLR1 and GPR1 were determined using cell-based reporter assays. Finally, an inducible chemerin knockdown system was generated to reduce levels of endogenous chemerin signalling. This work will ultimately have application for a wide range of cell types, but for the purpose of this thesis was focused primarily on modulating chemerin signalling in mature adipocytes. The following chapter discusses and critically evaluates the generation of each of these systems, and concludes with a comparison of the different systems and the implications of their future use.

Methods

Generation of bacterial expression vectors

Recombinant prochemerin and bioactive chemerin expression vectors that contain an N-terminal 6x His tag were generated for both human and mouse chemerin. The N-terminal secretion signal peptide was removed from chemerin, such that human prochemerin (NM_002889) was amplified from Glu21 to Ser163. Human bioactive chemerin was amplified from Glu21 to Ser157 with the addition of a C-terminal stop codon (TAA). Similarly, mouse prochemerin and bioactive chemerin (NM_027852) were amplified from Thr17 to Lys162, and Thr17 to Ser156 with the addition of a C-terminal stop codon (TAA), respectively. Primers (Table 2.1) were designed to incorporate 5'NcoI and 3'HindIII restriction sites to allow incorporation into the pProEx HTb vector (Invitrogen, Burlington, ON) with the incorporation of two additional two bases (CT) to generate an in-frame read. Human chemerin constructs were amplified from a previously generated expression construct and mouse chemerin constructs were amplified from mouse liver cDNA. Liver cDNA was generated with 2 μg of RNA isolated from wildtype C57Bl/6 mice, using Superscript II Reverse Transcriptase (Invitrogen, Burlington, ON), 41.7 μg/mL Oligo (dT) 12-18 primer (Invitrogen, Burlington, ON) in a 12 μL reaction according to manufacturer's recommendations. For all constructs, 10 ng of DNA template was amplified using Pfx polymerase (Invitrogen, Burlington, ON), except for mouse prochemerin, which was amplified using Phusion polymerase (NEB, Whitby, ON), both according to the standard protocol. PCR products were purified using QiaQuick PCR purification kit (Qiagen, Valencia, CA, USA) using the vacuum protocol and verified on a 1% agarose gel. Purified PCR constructs and pProEx vector were digested with NcoI and HindIII, purified, ligated using T4 DNA ligase (NEB, Whitby, ON) overnight at 16ºC, and transformed into DH5α chemically competent cells. Positive transformants were verified using colony PCR performed with Taq polymerase (Invitrogen, Burlington, ON) using standard reaction conditions (10X PCR Buffer (200 mM Tris-HCl pH 8.4, 500 mM KCl), 2.5 mM $MgCl_2$, 0.2 mM dNTPs, 0.1 μM each primer) containing one bacterial colony and cycling conditions of 95ºC for 3 min, and 25 cycles of 95ºC for 30 s, 60ºC for 30 s and 72ºC for 1 min/kb. All constructs were confirmed by restriction digest and sequenced using M13/pUCR Reverse and

PTrcHis Reverse primers through Molecular Cloning Laboratories (MCLab, San Francisco, CA). All sequences used in the expression studies were identical to the published sequences.

In order to transfer the chemerin expression constructs from the pProEx to pET21b vector (Novagen, Madison, WI, USA), a primer (NdeI-pProEX-6HisChemerin) was designed to amplify the 6x His tag and chemerin sequence with a NdeI restriction site incorporated 5' of the His tag (Table 2.1). The pET21b vector carries an N-terminal T7 sequence that was removed by addition of His-Chemerin, and the C-terminal 6x His tag present in pET21b was not utilized. N-terminally His-tagged chemerin was amplified with NdeI-pProEX-6HisChemerin forward primer and the reverse primers used previously for pProEx cloning. This was performed with 10 ng of template (pProEx expression constructs) and Phusion polymerase (NEB, Whitby, ON) using standard conditions as recommended by manufacturer. The cloning protocol was similar to above except using NdeI and HindII restriction sites and colony PCR primers specific for pET21b-HisChemerin to identify positive transformants.

Recombinant protein expression

Expression constructs were transformed into chemically competent BL21(DE3) or Rosetta2(DE3)pLysS cells as indicated for recombinant protein expression. Briefly, starter cultures were generated by spiking 4 mL of LB media with 50 µg/mL ampicillin with 1 colony overnight at 37ºC. Rosetta2(DE3)pLysS cells were also grown in the presence of 34 µg/mL chloramphenicol. Each starter culture was diluted 1:60 in 10 mL of pre-warmed LB media and incubated at 37ºC for approximately 2 h until cells reached mid-log growth (an A_{600} of approximately 0.5-1.0, measured with 100 µL of culture using a PowerwaveX-I plate reader (BioTek, Winooski, VT, USA)). Unless indicated otherwise, isopropyl ß-D-1-thiogalactopyranoside (IPTG) (Invitrogen, Burlington, ON) was added to the culture at a final concentration of 1 mM and incubated at 37ºC until collection at the indicated timepoint(s). Samples were spun for 1 min at 13000 rpm at room temperature (RT), and the pellet frozen at -80ºC until further analysis.

Determination of protein solubility:

Cultures were grown as previously described. Samples were collected 6 h following IPTG induction and spun at 4000 g for 20 minutes at RT. The cell pellet was resupsended in 5 mL of lysis buffer (50 mM NaH_2PO_4, 300 mM NaCl, 10 mM imidazole, pH 8.0) containing 1 mg/mL lysozyme (Sigma, Oakville, ON) and incubated on ice for 30 min. The lysate was sonicated using a microtip probe (Misonix sonicator 3000, Mandel, Guelph, ON) at a power setting of 1.5 for 6 cycles consisting of 10 s sonication: 10 s pause. Following sonication, the lysate was centrifuged at 10000 g for 30 min at 4ºC. The supernatant was decanted and this was considered the soluble crude extract. The pellet was resuspended in 5 mL of lysis buffer (50 mM NaH_2PO_4, 300 mM NaCl, 10 mM imidazole, pH 8.0) and considered the insoluble crude extract.

Purification of recombinant chemerin

For purification of native chemerin, Ni-NTA spin columns (Qiagen, Valencia, CA, USA) were used according to manufacturer's instructions. Briefly, columns were equilibrated with lysis buffer (50 mM NaH_2PO_4, 300 mM NaCl, 10 mM imidazole, pH 8.0) by centrifuging at 700 g for 2 minutes. The lysate (5 mL) was added to the column, spun, washed three times in 600 µL of wash buffer (50 mM NaH_2PO_4, 300 mM NaCl, 20 mM imidazole, pH 8.0), and eluted three times in 200 µL of elution buffer (50 mM NaH_2PO_4, 300 mM NaCl, 250 mM imidazole, pH 8.0). To concentrate eluted chemerin, 300 µL of eluate was added to a 3 kDa Nanosep centrifugal filtration column (Pall, Ville St. Laurent, QC) and spun for 20 min at 13000 rpm. The eluate remaining on top was resuspended in 40 µL of PBS containing 0.1% BSA.

For purification of chemerin under denaturing conditions, cell pellets were resuspended in 2 mL of lysis buffer (100 mM NaH_2PO_4, 10 mM Tris-HCl, 5 M GuHCl, pH 8.0). The lysate was centrifuged at 4000 rpm for 1 min, the supernatant transferred to a new tube, and 500 µL of a 50% slurry of Ni-NTA resin added (Qiagen, Valencia, CA, USA). The lysate/bead mixture was incubated for 30 min with shaking at RT, spun at 5000 g for 10 s, washed twice with 2 mL of wash buffer (100 mM NaH_2PO_4, 10 mM Tris-HCl, 8 M urea, pH 6.3), and eluted three times with 250 µL of elution buffer (100

mM NaH_2PO_4, 10 mM Tris-HCl, 8 M urea, pH 4.5), for 10 min each. For both native and denaturing purification, samples were frozen at -20ºC until further analysis.

SDS-PAGE analysis

To analyse chemerin expression, pellets were thawed at RT for 15 min and lysed. For initial pre-purification experiments (Figure 2.2), pellets were resuspended in 100 µL of 2x SDS-gel-loading buffer (0.09 M Tris-HCl pH 6.8, 20% glycerol, 2% SDS, 0.02% bromophenol blue, 0.1 M DTT). For time course experiments and optimization of incubation temperature, DTT concentration, IPTG concentration, and addition of protease inhibitor (Figure 2.3), pellets were resuspended in lysis buffer (100 mM NaH_2PO_4, 10 mM TrisHCl, 8M urea, pH 8.0) for 1 h at RT with shaking, then spun 10000 g for 30 min and the supernatant transferred to a new tube. For optimization with DTT (Fisher, Toronto, ON) or protease inhibitor cocktail (Sigma, Oakville, ON), reagents were added directly to the lysis buffer. Sample preparation for purification experiments was performed as described above. To estimate protein concentration, protein lysates were diluted 1:40 in distilled water containing a 1:40 dilution of Protein Assay Dye Reagent (BioRad, Mississauga, ON). The mixture was incubated for 5 min at RT and the absorbance read at A_{595} using PowerwaveX-I plate reader (BioTek, Winooski, VT, USA). 0-10 µg dilutions of BSA (stock 1 mg/mL) were used to generate a standard curve to estimate protein concentrations of bacterial samples.

For analysis of chemerin levels by SDS-PAGE, proteins were separated on a 15% gel. Coomassie blue staining was performed by incubating gels with Coomassie blue stain (0.1% w/v Coomassie blue, 40% methanol, 10% acetic acid, 50% distilled water) for 1 h at RT with shaking. Gels were washed with shaking at RT in de-stain solution (40% methanol, 10% acetic acid, 50% distilled water) until bands became clear. Gels were stored in distilled water until drying, which was performed using a Gel-dryer 583 (BioRad, Mississauga, ON) at 80ºC for 2 h, with the vacuum active overnight. Dried gels were scanned using a Perfection 1260 scanner (Epson, Long Beach, CA, USA). For Western blot analysis, proteins were transferred at 100 V for 1 h at 4ºC to nitrocellulose membrane (BioRad laboratories, Missisauga, ON). Blots were blocked with 5% skim milk powder for 1 h at 4ºC and then incubated with primary antibody (1:200 dilution of

human and mouse chemerin antibodies (R&D, Minneapolis, MN, USA) or 1:1000 dilution of His antibody (Novagen, Madison, WI, USA)) overnight at 4ºC. Blots were washed in TBST and incubated with 1:10000 dilution of anti-goat IRDye800-conjugated (chemerin antibodies) or anti-mouse IRDye680-conjugated (His antibody) secondary antibodies (LI-COR, Lincoln, NE, USA) for 1 h at RT. Immunoreactive bands were detected by scanning TBST-washed membranes at 700 or 800 nm using the Odyssey Infrared System (LI-COR Biosciences, Lincoln, NE, USA).

Dectection of chemerin levels and chemerin receptor activation

Chemerin levels were analysed using an ELISA for human chemerin (R&D, Minneapolis, MN, USA) according to manufacturer's recommendations using a 1:100 dilution of eluted chemerin sample resuspended in denatured elution buffer.

The Tango assay measures the recruitment of ß-arrestin to an activated GPCR via the activation of a luciferase reporter gene and was performed as previously described (Barnea et al. 2008; Dranse et al. 2015). Briefly, HTLA cells were transfected with human or mouse CMKLR1 or GPR1. 16-18 h following transfection, the cells were treated with the sample of interest in Optimem (Invitrogen, Burlington, ON). For experiments investigating the activity of CCX832, cells were pre-treated with inhibitor or DMSO control for 1 h at 37ºC before the addition of chemerin. Following 24 h, the cells were lysed and luminescence detected using the luciferase assay system (Promega, Madison, WI, USA) and a Luminoskan Ascent (Thermo Labsystems, Waltham, MA, USA). Luciferase activity was normalized to ß-gal activity as an internal control. Briefly, 30 µL of cell lysate was incubated with an equal volume of ß-gal assay buffer (0.2 M sodium phosphate buffer pH 7.3, 2 mM $MgCl_2$, 0.1 mM 2-mercaptoethanol, and 133 mg/mL ortho-Nitrophenyl-ß-galactoside). When samples turned yellow in colour, 100 µL of 1 M Na_2CO_3 was added to stop the reaction, and absorbance was read at 420 nm. Commerically available human or mouse recombinant chemerin (R&D, Minneapolis, MN, USA) was used as a control for CMKLR1 and/or GPR1 activation.

The SRF signalling luciferase reporter assay was performed as previously described (Rourke et al. 2015). Briefly, HEK cells were transfected with pGL4.34[luc2P/SRF-RE/Hygro), ß-gal control vector, and chemerin receptors. 18 h

following transfection, media was aspirated and replaced with Optimem overnight. 5x concentrated treatments were added to the cells for 4 h, and subsequently lysed in reporter lysis buffer and frozen at -80ºC (Promega, Madison, WI, USA). Luciferase and ß-gal activity was determined as previously described using a FluoStar Omega plate reader (BMG LabTech, Cary, NC, USA).

Generation of pLJM1-Chemerin lentiviral expression constructs

Mouse active chemerin (aa 1-156), prochemerin (aa 1-163), and cherry were directionally cloned into pLJM1 using primers with 5'NheI and 3'XbaI (chemerin) or 3'SalI (cherry) restriction sites (Table 2.1). We included the Kozak consensus sequence (GCCGCC) before the start codon in the mouse chemerin sequence. PCR amplification reactions were performed using 10 ng of liver cDNA generated from mouse liver using Superscript II Reverse Transcriptase (Invitrogen, Burlington, ON) and Phusion polymerase (NEB, Whitby, ON). Positive transformants were sequenced using CMV forward and ChemColPCR reverse primers (Table 2.1, Genewiz, South Plainfield, NJ, USA). The pLJM1 expression vector expresses the gene of interest under control of the CMV promoter. We replaced the CMV promoter with TK, PGK, SV40, and EF1α promoters using directional cloning with primers that included 5' SnaBI and 3' NheI restriction sites (Table 2.1). PCR amplification was performed using Pfx and 10 ng of template (phRL-TK (Promega, Madison, WI, USA), pLJM1, pGL4.34[luc2P/SRF-RE/Hygro (Promega), and genomic DNA amplified from HEK293A cells using DNeasy blood and tissue kit (Qiagen, Valencia, CA, USA), for TK, PGK, SV40, and EF1α promoters, respectively). pLJM1 also incorporates a puromycin resistance marker and this was replaced with GFP (amplified using Pfx (Invitrogen, Burlington, ON)) using 5'BamHI and 3' KpnI cloning primers (Table 2.1). All plasmids were grown using Stbl3 cells (Fisher, Toronto, ON) and positive transformants were confirmed using colony PCR (primers in Table 2.1) and restriction digests.

All plasmids were tested in HEK293A cells before lentivirus generation. Briefly, 17500 HEK cells were plated per well of a 48-well plate. The following day, cells were transfected with 0.25 µg of plasmid using PEI (Sigma, Oakville, ON). After 24 h, fresh media was replaced and cells were allowed to growth for 48 h. GFP expression was then

imaged and chemerin levels in conditioned media were examined using both western blot analysis (2 μL) and the Tango assay (1:2 dilution).

To generate bone marrow-derived mesenchymal stem cells (MSCs) with stable integration of pLJM1-chemerin-puro constructs, MSCs were transfected with lipofectamine 2000 (Invitrogen, Burlington, ON). MSCs were isolated and cultured as previously described (Muruganandan et al. 2010). The day before transfection, 15000 MSCs per well of a 24-well plate were plated. Cells were then transfected with 1 μg of DNA and fresh media was replaced after 24 h. When cells were ~50% confluent, 5 μg/mL of puromycin was added to select for cells with stable integration. ~10 independent colonies for each of pLJM1-GFP-puro, pLJM1-mChem(active)-puro, and pLJM1-mChem(pro)-puro were isolated, expanded, and tested for GFP or chemerin expression levels through imaging, qPCR and/or western blot analysis. Approximately 15000 MSCs were plated per well of a 48-well plate and lysed the following day for analysis of undifferentiated MSCs, or differentiated into adipocytes as previously described (Muruganandan et al. 2010). Experiments were performed with three independent colonies for each overexpression construct.

Lentivirus production and transduction

Approximately $1.06x10^7$ human embryonic kidney (HEK) 293T/17 cells (ATCC, Manassa, VA, USA) were plated in a 15 cm dish (Corning, NY, USA). The following day, cells were washed twice with serum-free media, and transfected with 9.9 μg pLJM1 vector, 3 μg MDG, and 6 μg pSPAX2 using PEI (Sigma, Oakville, ON) in antibiotic and serum-free media. After 24h, fresh serum-containing media was replaced and incubated on the cells for 48 h. Supernatant was collected, filtered through a 0.45 μm filter (BD Biosciences, San Jose, CA, USA), and virus concentrated by spinning at 28000 rpm for 2 h at 4ºC using a SW32 rotor and Optima L-90K ultracentrifuge (Beckman, Mississauga, ON). The pellet was resuspended in filtered PBS containing 1% BSA (Invitrogen, Burlington, ON) on ice and stored in aliquots at -80ºC until use.

The day before transduction, approximately 40000 HEK cells or 15000 MSCs were plated per well of a 12-well plate. 10 μL of concentrated virus was added to each well in media containing serum and 4 μg/mL polybrene (Sigma, Oakville, ON). After 72

h, fresh serum-free media (1 mL) was replaced. Following 24 h, cells were lysed for RNA/protein isolation and conditioned media collected. MSCs were differentiated into adipocytes as previously described (Muruganandan et al. 2010). MSC-derived adipocytes were transduced on day 4 following induction of differentiation. 10 µL of virus was added directly to each well in adipocyte maintenance media containing serum, insulin, and 4 µg/mL polybrene. After 72 h, fresh maintenance media was replaced and replenished every 48 h until cells were fully differentiated. Mature MSC-derived adipocytes (~day 10) were then incubated in serum-free media (200 µL) for 24 h, lysed, and media collected for further analysis. Samples stored at -80ºC until further analysis (western blot, 10-20 µL; Tango assay, 1:5 dilution).

Protein lysis

Cells were washed twice with ice-cold PBS before the addition of RIPA lysis buffer (1% NP-40, 0.5% sodium deoxycholate, 0.5% SDS, 150 mM NaCl, 50 mM Tris, 1mM EDTA, pH 8.0) containing phosphatase and proteinase inhibitors (Fisher 78443, Toronto, ON). Cells were scraped into a pre-chilled tube, thoroughly mixed, and incubated on ice for 20 min. Samples were then centrifuged for 10 min at 14000 g at 4ºC. Cleared supernatant was transferred to a new tube and stored at -20ºC until further analysis.

RNA isolation and qPCR

RNA was isolated using the RNeasy Plus kit (Qiagen, Valencia, CA, USA) according to manufacturer's recommendations and eluted in 40 µL of RNase-free water. RNA was quantified using a FLUOstar Omega (BMG LabTech, Cary, NC, USA) and cDNA was generated using EcoDry Premix Double-primer (Clontech, MountainView, CA, USA). cDNA was diluted to 5 ng/µl (overexpression studies) or 6 ng/µL (PiggyBac experiments) and qPCR performed using 1 µL of cDNA per reaction, with 0.5 µM primers, and FastStart SYBR green master mix (Roche, Laval, QC). qPCR was performed using a LightCycler96 according to manufacturer's recommendations and analysed using LightCycler96 software (Roche, Laval, QC). Relative gene expression was calculated using ΔΔCt method (Livak and Schmittgen 2001) where each sample was

normalized to cyclophilin A as a reference gene. Primer sequences are listed in Table 2.2 for mouse chemerin (NM_027851) and cyclophilin A (NM_008907).

Modulation of CMKLR1 and GPR1 activity with small molecules

hChe9, mChe15, mChe15MUT, Dys10, and Humanin were obtained from GenScript (Piscataway, NJ, USA) and stored in aliquots at -20ºC. hChe9, mChe15, and mChe15MUT were resuspended in PBS at a stock concentration of 1 mM while Dys10 was resuspended in PBS at a stock concentration of 1 mg/mL. Humanin was resuspended in water at a stock concentration of 1 mM. CCX832 and CCX826 were donated from ChemoCentryx (Mountain View, CA, USA) at a stock concentration of 1 mM in DMSO and stored in aliquots at RT.

L1.2 migration assay

The ability of human CMKLR1-expressing murine pre-B lymphoma L1.2 cells to migrate towards chemerin was assessed as previously described (Rourke et al. 2015). Briefly, L1.2 cells ($1x10^6$ cells/mL) were treated with 5 µM butyric acid overnight. The next day, cells ($5x10^6$ cells/mL) were pre-labelled with 2.5 µM calcein AM (Invitrogen, Burlington, ON) for 90 min at 37ºC in complete growth media (RPMI 1640 with 10% FBS, 10 mM HEPES, 1 mM sodium pyruvate, and 10 mM non-essential amino acids). Cells were then resuspended in chemotaxis medium (RPMI 1640 with 1% FBS) at a concentration of $2.5x10^6$ cells/mL and pre-treated with DMSO, CCX832 (inhibitor), or CCX826 (control) for 1 h at 37ºC. 100 µL of cells were placed in the upper chamber of a 5 µm pore transwell insert (Corning, Corning, NY, USA) and 600 µL of treatment (vehicle or 3 nM human chemerin (aa 21-157, R&D, Minneapolis, MN, USA) placed in the lower chamber. Cells were allowed to migrate for 4 h and then the cells present in the lower chamber were collected, centrifuged for 5 min at 10000 rpm and resuspended in PBS. Fluorescence was determined using a FluoStar Omega plate reader (BMG LabTech, Cary, NC, USA) using 485 nm excitation and 520 nm emission. Fold change migration was calculated relative to control (DMSO pre-treatment with no chemerin).

Generation of inducible Piggybac (PB) transposase shRNA constructs

The PiggyBac transposon PB-CuO-shMCS-IRES-GFP-EF1-CymR-Puro expression vector (SBI, Mountain View, CA, USA) was used to generate an inducible knockdown system. The PiggyBac expression vector was transformed into TOP10 cells and grown in LB with 50 µg/mL ampicillin at 30ºC overnight. shRNA sequences were designed using RNAi oligo designer (Paddison et al. 2004) and are indicated in Table 2.2. Primers universal for all shRNA sequences were designed to incorporate 5'-BstBI and 3'-SwaI restriction sites. Ultramer oligonucleotides were designed that consisted of: miR30 sequence (TGCTGTTGACAG), Drosha recognition site (TGAGCG), sense shRNA sequence, loop sequence (TAGTGAAGCCACAGATGTA), antisense shRNA sequence, Drosha recognition site (TGCCTA), and miR30 sequence (CTGCCTCGGA) based on a previously published protocol (Paddison et al. 2004). Ultramers were resuspended at a concentration of 3 µg/uL in water (IdtDNA, Coralville, Iowa, USA). When the first base in the shRNA sequence was a pyrimidine, it was replaced with adenine on the sense sequence. shRNA sequences were amplified using Phusion polymerase (NEB, Whitby, ON) with 10x GC buffer, 10 mM dNTPs, 0.5 µM each primer, 1 µL of a 1:30 dilution of each ultramer, 3% DMSO, and 1 µL Phusion in a 100 µL reaction and the following cycling conditions: 98ºC for 30 s, 25 cycles of 98ºC for 10 s, 60ºC for 30 s, 72ºC for 30 s/kb, and 72ºC for 5 min. PCR products were analysed on a 2.5% agarose gel and purified using a PCR purification kit (Qiagen, Valencia, CA, USA). Purified DNA and Piggybac expression vector were digested with BstBI and SwaI, ligated overnight at 16ºC with T4 ligase (NEB, Whitby, ON), and transformed into TOP10 cells. Colonies were grown overnight in 4 mL LB with 50 µg/mL ampicillin and positive transformants were identified using colony PCR with 1 µL of culture with the primers indicated in Table 2.2. Colony PCR primers were based on the vector sequence that flank the insertion sites and generate a product 45 bp longer if the shRNA insert is present. Positive transformants were confirmed with restriction digests and all expression constructs were sequenced using the Colony PCR Reverse primer (Genewiz, South Plainfield, NJ, USA).

Expression of PB transposase shRNA constructs

To test whether the PB transposon vectors were inducible following cumate addition, empty PB vector was transfected into HEK cells. Briefly, 17500 HEK cells per well were plated in a 48-well plate and transfected the following day with 100 ng of PB expression vector using polyethylenimine (PEI) (Sigma, Oakville, ON). Fresh media was replaced every 24 h with 0, 1, 5, or 10x cumate solution. The 10000x stock solution of cumate (300 mg/mL cumic acid suspended in 95% EtOH, SBI, Mountain View, CA, USA) was warmed at 37ºC to re-dissolve precipitate before each use. After 48 h, GFP expression was visualized.

To test the efficiency of PB-LacZ-KD or PB-Chem-KD expression vectors, HEK cells were co-transfected with 200 ng of LacZ or Chem KD PiggyBac expression vectors and 25 ng of ß-gal or chimeric chemerin-luciferase expression constructs, respectively, in the presence or absence of 1x cumate (SBI, Mountain View, CA, USA). The next day, fresh media (± cumate) was replaced. After 48-72 h, GFP expression was evaluated, the cells were lysed in 100 µL RLB (Promega, Madison, WI, USA), and lysates frozen at -80ºC. ß-gal or luciferase assays were performed as previously described.

Generation of stable PB-expressing MSCs

Mouse bone-marrow derived MSCs (15000 cells per well in 12-well plate) were transfected with 700 ng of empty, LacZ KD, or mouse chemerin KD PB expression vector and 300 ng of Super PiggyBac transposase expression vector (SBI, Mountain View, CA, USA) using Lipofectamine 2000 (Invitrogen, Burlington, ON). Transfection conditions were optimized for transfection of MSCs as follows: 100 µL of Optimem (Invitrogen, Burlington, ON) and 3.5 µL of lipofectamine, and 100 µL of Optimem and DNA, were incubated separately at RT for 5 min, and then combined, vortexed, and incubated at RT for 20 min. 200 µL of transfection mixture was added to each well with 800 µL of fresh media (MEMα containing 2 mM L-glutamine, 10% FBS, 100 U/mL penicillin, and 100 µg/mL streptomycin) and incubated on cells overnight. The following day, cells were given fresh media and 24-48 h later 5 µg/mL of puromycin dihydrochloride (Santa Cruz, Dallas, TX, USA) was added to select for PB-expressing cells. Cells were passaged until growing in a T75 flask and either assayed as a crude

population, or colonies isolated and tested independently for high-expressing clones and robust adipogenic differentiation. Stable PB-expressing MSCs were maintained in 5 µg/mL of puromycin.

To test the efficiency of LacZ or chemerin KD in MSCs, cells (15000 per well of a 48-well plate) were transfected with 150 ng of ß-gal or a chemerin-luciferase construct using Lipofectamine (50 µL of transfection mixture in 200 µL of media). The following day, fresh media with or without cumate was added to the cells. After 48-72 h, GFP expression was evaluated, cells were lysed in 100 µL of RLB (Promega, Madison, WI, USA), and stored at -80ºC until further analysis.

To examine the effect of LacZ or chemerin KD in mature adipocytes, MSCs were differentiated into adipocytes as previously described (Muruganandan et al. 2010). On day 8 following the induction of differentiation, adipocytes were treated with 0, 1, 5, or 10x cumate in adipocyte maintenance media (basal growth media plus 5 µg/mL insulin). Cumate-containing media was replaced every 48 hours. Cells were lysed on day 12 in 350 µL of RLT+ buffer containing 143 mM 2-mercaptoethanol (Qiagen, Valencia, CA, USA) and the lysate stored at -80ºC until qPCR analysis.

MTT assay

Cells were grown as described previously. To assess viability, cells were incubated with 100 µL of 0.5 mg/mL thiazolyl blue tetrazolium bromide (MTT) (Sigma, Oakville, ON) diluted in fresh serum-free culture medium at 37ºC. After 4 h, the MTT reagent was aspirated from each well and the formazan product was solubilized in 200 µL of DMSO. The absorbance of each sample was measured at 540 and 690 nm using a FLUOStar Omega plate reader (BMG LabTech, Cary, NC, USA). To calculate fold change, the absorbance at (540-690 nm) was expressed relative to vehicle-treated cells (considered as 100% cell viability).

Oil Red O staining

Oil Red O staining was performed to assess the extent of adipogenic differentiation. Cells were washed with PBS and fixed in 4% PFA at 4ºC overnight. The next day, cells were washed in PBS and incubated with Oil Red O (0.3% Oil red O in

60% isopropanol) for 15 min at RT with shaking. Cells were rinsed in PBS, imaged, and stain eluted from cells by the addition of isopropanol, and the absorbance at 520 nm measured using a FLUOStar Omega plate reader (BMG LabTech, Cary, NC, USA).

Imaging

Cells were imaged at ex 546/12; em 575-640 nm (GFP) or ex 480/20; em 510/20 nm (cherry) using an Axiovert 200M fluorescent microscope (Zeiss, Toronto, ON), Orca R2 C10600 camera (Hamamatsu, Boston, MA, USA), and AxioVision 4.8 software (Zeiss). Oil Red O stained-cells were imaged using an Eclipse TS100 microscope (Nikon, Melville, NY, USA), a Go-3 colour camera (Qimaging, Surrey, BC), and QCapture Pro6 software (Qimaging).

Molecular biology and statistics software

Sequence analysis, primer design, vector map assembly, and database searching was performed using MacVector (Version 12.7, Cary, NC, USA). All statistical analysis was performed using GraphPad Prism (version 5.0b, La Jolla, CA, USA). Data is represented as mean ± SEM. For parametric data, statistical significance was determined using a two-way unpaired Student's t-test (two groups), one-way ANOVA with Tukey post-test (three+ groups), or a two-way ANOVA with Bonferonni post-test (two factors).

Results

Generation of recombinant chemerin using a bacterial expression system

In order to produce recombinant chemerin isoforms that are not commercially available, we used a bacterial expression system because it offers the advantage of the relative ease of working with bacteria and recombinant protein expression at a reasonably low cost. The ultimate goal was to establish a robust and reliable system capable of producing any particular chemerin isoform. However, in this project, we focused on the expression and purification of both human and mouse prochemerin and active chemerin-157.

Generation of pProEx-chemerin expression constructs

The pProEx HT prokaryotic expression vector incorporates a polyhistidine (6x His) sequence at the amino terminus of the expressed protein of interest, which is under control of the Trc promoter. This allows for induction of protein expression following the addition of IPTG to bacterial cultures. Using pProEx HTb, the expression constructs outlined in Figure 2.2A,B (His-tagged human prochemerin (aa 21-163), human active chemerin (aa 21-157), mouse prochemerin (aa 17-162), and mouse active chemerin (aa 17-156)) were generated successfully. All sequences used were identical to those published (human: NM_002889; mouse: NM_027852). We first examined expression of pProEx-hChem(active) and pProEx-hChem(pro) in BL21(DE3) cells. BL21(DE3) cells grow in minimal media and are deficient in key proteases such as *lon* and *omp*T, which degrade intracellular and extracellular proteins, respectively. Using standard growth conditions (37ºC, 4 h collection, 1 mM IPTG induction) the presence of bands that match the predicted sizes (Figure 2.2C) of His-tagged human pro- (19.6 kDa) and active (19.2 kDa) chemerin were observed from cell lysates expressing pProEx-hChem compared to untagged human chemerin control (15.8 kDa) (Figure 2.2D). However, analysis of the cell lysate also revealed the presence of additional lower and high bands. Similarly, expression of pProEx-mChem(active) and pProEx-mChem(pro) resulted in the expression of bands that match to the predicted sizes (20.0 kDa and 19.2 kDa, respectively, Figure 2.2C) compared to untagged mouse chemerin control (15.9 kDa) (Figure 2.2E). While there was a modest band underneath mouse chemerin, there were

fewer bands present in the immunoblot of mouse chemerin compared to human. As expected, expression of pProEx-empty vector did not result in the presence of any immunodetectable bands (Figure 2.2D,E).

Optimization of pProEx-chemerin expression

We next investigated the conditions required for optimal expression of chemerin from pProEx constructs, including collection time, lysis conditions, concentration of IPTG for induction of expression, incubation temperature, and host cell strain. First, we examined the expression of chemerin in BL21 cells at 6, 12, 18, and 24 h following induction with 1 mM IPTG at 30ºC. There was no significant difference between chemerin expression at the different time points for human active or prochemerin (Figure 2.3A) or for mouse active or prochemerin (Figure 2.3B). Future optimization experiments in BL21 cells were continued using a 6 h collection period. For simplicity, although further experiments were performed for all four isoforms (human/mouse and pro/active chemerin), only mouse active chemerin expression is shown.

The presence of an extra band (~15 kDa) below chemerin led us to believe that bacterially-expressed chemerin was being cleaved, degraded, and/or undergoing misfolding. We tested the impact of adding DTT or protease inhibitors to the lysis buffer in an attempt to improve the stability of expressed chemerin (Figure 2.3C). We also examined the effect of lowering the concentration of IPTG used to induce chemerin expression (Figure 2.3D). There was no influence on chemerin expression following any of these modifications. We then investigated potential differences in chemerin expression following growth of BL21 cells at various temperatures. We noticed a dramatic increase in chemerin expression following incubation at 16ºC compared to 23ºC and 30ºC (Figure 2.3E). Interestingly, presence of the lower band observed in earlier experiments was reduced in these cultures.

Finally, codon analysis of human and mouse chemerin sequences revealed the presence of codons (~16% and ~13% of total sequence, respectively) that are rarely used in *E. coli* (Table 2.3). Rosetta2(DE3)pLysS cells are BL21 derivatives that are designed to enhance the expression of eukaryotic proteins by expressing tRNAs for 7 rare codons including AUA, AGG, AGA, CUA, CCC, and GGA. We compared whether there was a

difference in the expression of recombinant chemerin from BL21(DE3) or Rosetta2(DE3)pLysS cells and observed a dramatic increase in chemerin expression in Rosetta2 cells compared to BL21 cells at 3 different temperatures (Figure 2.3F). We repeated the time course experiments to optimize chemerin expression in Rosetta2 cells and determined that 6 h is the optimal collection time for cells grown at 16ºC following 1 mM IPTG induction (Figure 2.3G).

Generation and optimization of pET21b-chemerin expression constructs

We next examined whether expression of chemerin under control of the T7 promoter, which is generally regarded as "stronger" compared to the Trc promoter, would increase levels of recombinant chemerin expression. To do this, we transferred the His-tagged chemerin sequence from the pProEx vector to the pET21b vector. We then grew cultures in parallel conditions (based on the optimization experiments with the pProEx constructs) and compared chemerin expression levels. Interestingly, we were able to observe recombinant chemerin expression from cells expressing the pET21b-chemerin vectors but not from empty pET21b or pProEx vectors (Figure 2.4A). The observed band sizes were consistent with the expected sizes of His-tagged pro- and active chemerin. As we were previously unable to detect chemerin expression on Coomassie-stained gels with pProEx vectors (data not shown), this confirmed that pET21b was a better expression vector for production of recombinant chemerin.

We then optimized the conditions for expression of chemerin from pET21b. Ultimately, expression of pET21b-chemerin was highest following 6 h incubation at 23ºC after induction with 1 mM IPTG (Figure 2.4B). This was confirmed by Coomassie blue staining, which demonstrated high levels of chemerin expression under these conditions (Figure 2.4C).

Purification of recombinant chemerin

Having established the optimal growth conditions for chemerin expression, we next investigated the conditions necessary for purification of recombinant chemerin. This was performed for both human and mouse chemerin and similar results were achieved for both species. However, only human data is presented for simplicity.

In order to determine the appropriate lysis and purification procedures, we first examined whether *E. coli*-expressed chemerin was present in a soluble or insoluble form. We observed that chemerin was present in both the soluble and insoluble fractions, and in approximately equal amounts (Figure 2.5A). As a result, we first attempted to purify chemerin under native conditions. 6x His has a high affinity for Ni-NTA (Ni^{2+}-nitrilo-triacetic acid) resin and we performed purification with native buffers using both Ni-NTA spin columns and a 50% Ni-NTA resin slurry. We had the most success with Ni-NTA spin columns (Figure 2.5B). However, the yield of chemerin in eluted fractions was extremely low compared to the amount of chemerin present in the lysate. Analysis of the flow-through (unbound chemerin) revealed that a significant proportion of chemerin was not binding to the column. Furthermore, a significant amount of chemerin was eluted from the column in the wash buffer. We attempted to decrease the amount of chemerin eluted in earlier steps by decreasing the imidazole concentration in both the lysis and wash buffers (from 20 mM to 1 mM) but this did not affect the amount of purified chemerin (data not shown).

Due to the low yield of recombinant chemerin following native purification, we investigated whether chemerin could be purified in larger amounts under denaturing conditions. In contrast to the native purification procedure, we had more success with purification with beads compared to spin columns (Figure 2.5C). Importantly, significantly higher levels of chemerin were present in the eluted fractions following purification under denaturing conditions as compared to native conditions. However, a significant proportion of chemerin did not bind to the beads, was eluted in the washes, or was found remaining to the beads after elution. Despite this, analysis of chemerin levels using an ELISA indicated that at least 200 ng/mL of denatured chemerin was purified from a 10 mL bacterial culture.

Bacterially-expressed recombinant chemerin is bioactive at CMKLR1

To investigate whether chemerin purified under native conditions was bioactive, we performed the Tango assay, which is a HEK cell-based assay that measures ß-arrestin recruitment as an indicator of GPCR activation (Barnea et al. 2008). Initial experiments suggested that there was no activity of mouse or human chemerin at CMKLR1 (data not

shown). To rule out that the elution buffer was not toxic to the cells, we concentrated and resuspended purified chemerin in PBS with 0.1% BSA using a 3 kDa centrifugal filter column. Notably, application of a 1:5 (10 μL) or 1:10 (5 μL) dilution of purified human chemerin (of total 40 μL obtained) exhibited activity at human CMKLR1, whereas buffer alone or a 1:50 dilution of purified chemerin did not (Figure 2.6). Comparison with commercially available chemerin indicates that the total eluted volume was between 3 and 10 nM, which is equivalent to ~8 ng of purified chemerin per 10 mL of bacterial culture.

Overexpression of chemerin using a lentiviral approach

In addition to the bacterial expression system, we decided to explore an alternative approach to producing commercially unavailable chemerin isoforms. We sought to overexpress chemerin in mammalian cells and were particularly interested in developing this system for use in mature adipocytes, which are traditionally very difficult to manipulate genetically. For this reason we chose to use a lentiviral-mediated delivery system that would allow for efficient stable integration of chemerin expression constructs into non-dividing cells. It is important to note that while we chose to focus on mature adipocytes, this overexpression system is also applicable to numerous other cell types.

Overexpression of chemerin in HEK cells results in increased chemerin secretion and bioactivity

In order to overexpress chemerin in mammalian cells, we cloned mouse active chemerin (aa 1-156), mouse prochemerin (aa 1-163), or cherry (control) into the pLJM1 lentiviral expression vector under control of the CMV promoter. We also incorporated a GFP marker under control of the hPGK promoter in order to visualize integration and expression levels in transduced cells (Figure 2.7A). Transduction of HEK293A cells with pLJM1-empty-GFP, pLJM1-cherry-GFP, pLJM1-mChem(active)-GFP, and pLJM1-mChem(pro)-GFP resulted in GFP expression as early as one day post-transduction and reached maximal expression approximately 4 days following transduction (Figure 2.7B). This indicated that the virus successfully integrated into cells. As expected, chemerin was expressed and secreted at high levels from cells expressing mChem(active) and

mChem(pro) but not from cells expressing empty vector or cherry control (Figure 2.7C). Conditioned media from cells expressing mChem(active) or mChem(pro) resulted in significant activation of CMKLR1 in the Tango assay (Figure 2.7D). However, conditioned media from cells expressing mChem(active) exhibited ~16-fold more bioactivity than cells expressing mChem(pro), suggesting that while HEK cells appear to process inactive prochemerin to bioactive isoforms, overexpression of the active isoform is more efficacious in terms of inducing ß-arrestin recruitment to CMKLR1.

Previous studies have demonstrated that the strength of constitutive promoters and their ability to drive ectopic gene expression, including CMV, can vary considerably between different cell types and species (Qin et al. 2010b). In order to generate a chemerin overexpression system that will function in multiple cell types, we replaced the CMV promoter in pLJM1-CMV-mChem(active)-PGK-GFP with TK, PGK, SV40, and EF1α promoters. Transduction of HEK cells with lentivirus encoding mChem(active) under control of these promoters resulted in changes in GFP expression from the PGK promoter in the same construct (Figure 2.7E). In particular, GFP expression was relatively modest, but detectable, following transduction of PGK-mChem(active) and EF1α-mChem(active), confirming that the lentiviral constructs are expressed following transduction. Chemerin was detected in conditioned media isolated from HEK cells expressing mChem(active) under control of the TK, SV40, EF1α, and CMV promoters (Figure 2.7F). This was highest for the CMV and SV40 promoters. As expected, expression of the empty vector (CMV promoter) did not result in chemerin expression. Interestingly, chemerin expression did not correlate with GFP expression, suggesting that GFP expression is more useful as an indicator of whether the virus has entered the cells versus a quantitative measure for determining the amount of integration into cells.

Overexpression of chemerin in MSC-derived adipocytes modifies chemerin bioactivity but not chemerin mRNA or protein levels

We next transduced mature MSC-derived adipocytes with pLJM1-mChem(active)-GFP lentivirus, where chemerin expression is under control of the various constitutive promoters tested in Figure 2.7. We observed high GFP expression in lentivirus-transduced cells but not in the polybrene control, suggesting efficient

integration of lentivirus into mature adipocytes (Figure 2.8A). Analysis of chemerin mRNA (Figure 2.8B), intracellular chemerin (Figure 2.8C), and secreted chemerin levels (Figure 2.8D), suggested that there was no change in chemerin expression or secretion over basal levels following chemerin overexpression with the various promoters. However, conditioned media from mature adipocytes expressing mChem(active) under control of CMV, TK, SV40, and EF1α promoters resulted in increased levels of mouse CMKLR1 activation in the Tango assay compared to media from adipocytes transduced with polybrene control or empty lentivirus (Figure 2.8E). This suggests that despite no observable change in chemerin levels, the ratio of bioactive chemerin in adipocyte-conditioned media is increased following mChem(active) overexpression. We observed similar results following transduction of SVF-derived adipocytes with pLJM1-mChem(active)-GFP (data not shown).

Generation of MSCs with stable integration of mChem(active) and mChem(pro)

As transduction of mature adipocytes with chemerin overexpression lentivirus resulted in a relatively modest influence on chemerin expression and bioactivity, we pursued an alternative approach in which we generated undifferentiated MSCs and subsequently MSC-derived adipocytes, with stable overexpression of chemerin. We first tested which promoter had the highest activity in MSCs using the expression constructs outlined in Figure 2.8. We observed chemerin expression from TK, PGK, SV40, EF1α, and CMV promoters, compared to empty vector control; however chemerin expression was highest under control of the EF1α promoter (Figure 2.9A). We then generated pLJM1-EF1α-GFP, mChem(active), or mChem(pro) expression constructs with a puromycin selection marker under control of the PGK promoter (Figure 2.9B). Undifferentiated MSCs were transfected with pLM1-EF1α-GFP, mChem(active), or mChem(pro), and stable cell lines were generated by puromycin selection. qPCR analysis of puromycin-resistant cells revealed significantly higher levels of chemerin mRNA in mChem(active) or mChem(pro)-expressing cells compared to GFP-expressing cells (Figure 2.9C). Consistent with this, analysis of MSC-conditioned media revealed the presence of bands that corresponded in size to active chemerin and prochemerin (Figure 2.9D) and exhibited bioactivity at mouse CMKLR1 (Figure 2.9E). Importantly,

the appearance of an extra band and bioactivity at CMKLR1 in samples isolated from mChem(pro)-expressing MSCs suggests the occurrence of prochemerin processing to bioactive chemerin isoforms.

MSCs with stable expression of GFP, mChem(active), or mChem(pro) were then differentiated into adipocytes. There was no obvious difference in adipocyte morphology between the various overexpression lines (data not shown). qPCR analysis revealed significantly higher levels of mChem(active) but not mChem(pro) compared to GFP-expressing adipocytes (Figure 2.9F). However, western blot analysis revealed modestly higher levels of both mChem(active) and mChem(pro) (Figure 2.9G). Application of media isolated from adipocytes overexpressing mChem(active) had ~8-fold higher activity at mouse CMKLR1 compared to media isolated from GFP-expressing adipocytes (Figure 2.9H). Additionally, there was a moderate increase in bioactivity at CMKLR1 with media isolated from mChem(pro)-expressing adipocytes (Figure 2.9H). Altogether, this data suggests that stable overexpression of chemerin in undifferentiated MSCs is a viable strategy to increase endogenous chemerin levels in mature MSC-derived adipocytes.

Identification of an alternative splice variant in mouse chemerin

During the cloning process for mouse chemerin expression in both *E. coli* and lentivirus-mediated overexpression studies, sequencing of positive transformants revealed the presence of three extra nucleotides (CAG) compared to the published sequence. This occurred despite using liver RNA that was isolated from two different animals 4 years apart as the starting template for cDNA synthesis. In total, the extra nucleotides appeared in 14 of 24 clones suggesting that this sequence is relatively abundant. Mouse chemerin is composed of 6 different exons, and further analysis of the mouse chemerin sequence revealed that these three nucleotides occur on the boundary between exons 4 and 5. In addition, these nucleotides are present on the 3' terminus of the intron sequence immediately before exon 5, suggesting that this is a result of alternative splicing (Figure 2.10A).

The identified splice variant would result in the addition of an extra glutamine compared to the published sequence. Glutamine is a polar amino acid that is frequently

involved in protein binding sites and insertion of a glutamine has been linked to both disease (Terrinoni et al. 2000) and decreased ligand binding (Zapf et al. 1993). In order to determine whether the alternative splice variant influences chemerin secretion or activity, we overexpressed the two prochemerin variants in HEK cells. Western blot analysis of 24 h conditioned media revealed no obvious difference in chemerin secretion between the two constructs (Figure 2.10B). The presence of two bands indicates that both forms of prochemerin are actively processed to smaller isoforms that are similar in size to recombinant and overexpressed bioactive chemerin. In addition, both prochemerin forms have similar levels of activity at mouse CMKLR1 (Figure 2.10C), suggesting that the presence of the three extra nucleotides does not alter chemerin secretion or activity in HEK cells.

Screening small molecules for activity at CMKLR1 and GPR1

A number of publications have identified small molecule agonists and antagonists with reported activity at CMKLR1 (Cash et al. 2008; Graham et al. 2014; Leroy 2014; Shimamura et al. 2009; Watts et al. 2013; Wittamer et al. 2003). In order to confirm the influence of these peptides on CMKLR1 activation and investigate potential activity at GPR1, we performed cell-based activity assays using both human and mouse chemerin receptors.

First, we determined the activity of small peptides derived from the C-terminal sequence of chemerin at CMKLR1 and GPR1. This was assessed using the serum response factor (SRF)-based signalling assay, for which chemerin-157 has previously been shown to activate signalling through both CMKLR1 and GPR1 (Rourke et al. 2015). Application of high doses (100-1000 nM) of both hChe9 and Dys10 on cells expressing human or mouse CMKLR1, and mouse GPR1, resulted in a significant induction of SRF signalling (Figure 2.11A,B). This was highest (~30-fold) for mouse CMKLR1 compared to mGPR1 (~10-fold). There was also a modest (~4-fold) increase in human GPR1 activation following treatment with hChe9AP and Dys10. In contrast, treatment of CMKLR1 or GPR1-expressing cells with mChe15 (Figure 2.11C) or the control peptide mChe15MUT (data not shown) did not result in SRF activation. Similar results were

obtained using the Tango assay for ß-arrestin recruitment to CMKLR1 and GPR1 (data not shown).

We next assessed the activity of humanin at human and mouse chemerin receptors (Leroy 2014). Using the Tango assay, we observed ~20-fold induction of human, but not mouse, GPR1 in response to 10 μM humanin treatment, but not at lower doses (Figure 2.12A). Additionally, there was no activation of either human or mouse CMKLR1 in response to humanin treatment (Figure 2.12B). In order to further investigate human GPR1 activation by humanin, we treated human GPR1-expressing cells with a higher range of humanin concentrations and observed a dose-dependent increase in ß-arrestin recruitment corresponding to an EC_{50} of 18.7 μM (Figure 2.12C). We also examined the effect of co-treating human GPR1-expressing cells with both human recombinant chemerin and humanin and observed an additive effect (Figure 2.12D).

Finally, we assessed the ability of the recently characterized human CMKLR1 inhibitor, CCX832, to inhibit CMKLR1 and GPR1 activation using the Tango assay. Treatment of human CMKLR1-expressing cells with increasing doses of chemerin resulted an increase in ß-arrestin recruitment, indicative of receptor activation (Figure 2.13A). Notably, treatment with 300 nM or 1 μM CCX832 decreased basal levels of CMKLR1 activation, and reduced chemerin activation of CMKLR1 by ~10-fold at all chemerin concentrations tested. Lower concentrations of CCX832 (3-100 nM) also decreased human CMKLR1 activation by high doses of chemerin (30 nM); however, this reduction was relatively modest (~2-fold). Consistent with this, 1 μM CCX832 decreased the basal activation of mouse CMKLR1, with lower doses (100 and 300 nM) inhibiting mouse CMKLR1 activation by higher doses of chemerin (Figure 2.13B). Treatment with the negative control compound CCX826, a close analog to CCX832 that has low binding affinity for CMKLR1, decreased receptor activation by 30 nM chemerin at a concentration of 1 μM, suggesting the presence of potential toxic effects (Figure 2.13A,B). Higher doses of both CCX832 and CCX826 resulted in significant toxic effects (data not shown).

In order to further examine the potential inhibitory effects of CCX832, we tested the ability of human CMKLR1-expressing L1.2 pre B lymphocytes to migrate towards chemerin. Cells pre-incubated with DMSO or control compound (CCX826) exhibited a

3.5-fold increase in migration towards the lower chamber of a cell culture insert containing 1 nM human chemerin compared to vehicle (Figure 2.13C). Pre-treatment with CCX832 resulted in a 20% reduction in the migration of CMKLR1-expressing L1.2 cells towards chemerin. Considered altogether, this indicates that CCX832 treatment is capable of inhibiting CMKLR1 function, although the effects are relatively modest. We also tested the effect of CCX832 to inhibit human or mouse GPR1 activation. In contrast to CMKLR1, the control compound CCX826 had a significant effect on GPR1 activation (Figure 2.14A,B). As a result we are unable to determine whether any decrease in chemerin activation of GPR1 following CCX832 treatment is the result of GPR1 inhibition or non-specific and/or toxic effects.

Generation of an inducible chemerin knockdown system

As a final approach to modulate levels of chemerin signalling, we generated a knockdown system to examine the effect of reduced levels of endogenous chemerin signalling. The primary goal of this project was to decrease chemerin expression in mature adipocytes. Previous attempts using adenovirus and lentivirus-mediated shRNA delivery in adipocytes achieved minimal knockdown (data not shown), suggesting that virus-mediated shRNA delivery is not a viable approach. As adipocytes have significantly low transfection efficiency, we opted for a system in which we could manipulate preadipocytes, which are relatively easier to transfect. However, knockdown of chemerin signalling in preadipocytes inhibits adipogenic differentiation (Goralski et al. 2007). Thus we opted for an inducible knockdown system in which we could transfect undifferentiated MSCs and then later activate shRNA expression in mature adipocytes.

To do this, we used the cumate-inducible Piggybac (PB) knockdown system outlined in Figure 2.15. This is a miRNA-based expression system that operates on the cumate switch where the repressor, cymR, is expressed robustly and functions to prevent background leakiness (Mullick et al. 2006). In addition, the transposon-based system facilitates shRNA integration into the host genome, which will accelerate the generation of stable shRNA expression in cells with low transfection efficiency, such as MSCs.

Cumate induces the expression of PB in HEK cells, MSCs, and adipocytes, but has effects on cell viability

We first determined the optimal concentration of cumate for shRNA expression. As the cumate-inducible switch regulates both shRNA and GFP expression (Figure 2.15), we assessed levels of GFP expression in cells expressing the empty PB vector to estimate levels of shRNA induction. Treatment of empty PB-expressing HEK cells, MSCs, and mature adipocytes with increasing doses of cumate resulted in GFP expression (Figure 2.16A). Importantly, there was no background GFP expression in the absence of cumate indicating that there is no background leakiness of the PB system. GFP expression was highest in HEK cells compared to MSCs and adipocytes. Notably, while both HEK cells and MSCs expressed similar levels of GFP following 1, 5, and 10x cumate addition, GFP expression in mature adipocytes was dose-dependent, with the highest level of GFP expression occurring in response to 10x cumate treatment (Figure 2.16A).

We also assessed the effect of cumate treatment on cell viability and observed a significant decrease in cell viability following 5 or 10x treatment in both HEK cells and MSCs (Figure 2.16B). The viability of mature adipocytes was not affected by cumate treatment.

Expression of PB-LacZ-KD and PB-Chem-KD constructs in HEK cells and MSCs results in ~50% decrease in levels of ß-gal activity and chemerin-luciferase, respectively

We then generated inducible PB vectors that expressed 3 different LacZ (PB-LacZ-KD 348, 632, and 1190) or 5 different chemerin (PB-Chem-KD 95, 297, 362, 490, 537) shRNA sequences, where the numbers indicate the region of the LacZ or chemerin mRNA sequence targeted. These constructs were designed to include a Drosha recognition site and miR30 sequences that flank the shRNA (based on (Paddison et al. 2004)), as preliminary experiments using the PB vector as provided from the manufacturer did not result in shRNA activity (data not shown). We tested the efficiency of PB-LacZ-KD constructs in ß-gal-expressing HEK cells and observed ~50% decrease in ß-gal activity with all three sequences (Figure 2.17A). Unexpectedly, treatment of empty PB-expressing cells with 1x cumate resulted in a modest decrease in ß-gal activity. This suggests the presence of effects on cell viability that were not evident in Figure

2.16B. To test the efficiency of PB-Chem-KD vectors, we examined the ability of each sequence to reduce levels of a chimeric chemerin-luciferase fusion construct expressed in HEK cells. We observed a significant decrease in chemerin-luciferase levels following induction of 3 chemerin shRNA sequences (PB-Chem-KD 95, 362, and 490), where PB-Chem-KD-95 had the greatest effect with a 60% knockdown. There was no effect of the other two chemerin shRNA sequences on chemerin-luciferase levels (Figure 2.17B).

In order to generate an inducible knockdown in mature adipocytes, the PB expression constructs were transfected into undifferentiated MSCs and PB-expressing stable MSC lines generated. Similar to the results with HEK cells, MSCs expressing each of the 3 LacZ shRNA sequences reduced the level of ß-gal activity in ß-gal-expressing MSCs (Figure 2.17C). The knockdown was similar (~50% reduction) following treatment with 1-10x cumate treatment. In contrast to Figure 2.16B, only 10x cumate addition appeared to have a toxic effect on MSCs expressing the empty PB vector (Figure 2.17C). MSC lines stably expressing PB-ChemKD 95, 362, or 490 were also generated. Interestingly, when transfected with a chemerin-luciferase fusion protein, only PB-Chem-KD-95 was able to reduce chemerin-luciferase levels following treatment with 1x cumate (~50% reduction). However, all three sequences reduced chemerin-luciferase expression levels at higher concentrations of cumate treatment (Figure 2.17D). Considered altogether, this indicates that stable PB-LacZ-KD and PB-Chem-KD MSC lines function as expected. In further studies, only PB-LacZ-KD-348 was used as a control vector.

Inducible PB-Chem-KD-95 has a modest effect on chemerin levels in mature adipocytes

We next differentiated the stable PB-expressing MSCs into mature adipocytes in the absence of cumate. We performed Oil Red O staining to confirm that expression of PB vectors did not affect adipocyte differentiation. There was no difference in the morphology or accumulation of lipid droplets between MSCs expressing PB-LacZ-KD-348 (control) and PB-Chem-KD-95, 362, or 490 (Figure 2.18A). We then treated mature adipocytes with 10x cumate to induce shRNA expression. GFP expression was visible 24 h following the addition of cumate (data not shown) and reached maximum expression after 4 d of cumate treatment (Figure 2.18B). As expected, treatment of PB-LacZ-KD-

348-expressing adipocytes did not have an effect on chemerin expression (Figure 2.18C). We observed a significant decrease in chemerin levels following cumate treatment in cells expressing PB-Chem-KD-95 (Figure 2.18C). However, this decrease was relatively modest (~20%). Expression of both PB-Chem-KD-362 and 490 did not have any effect on chemerin mRNA levels. We then treated PB-expressing adipocytes with higher doses of cumate in order to achieve a greater knockdown, but this resulted in toxicity (data not shown). Altogether, this data suggests that while it is possible to reduce endogenous chemerin levels in mature adipocytes, the efficiency of the knockdown is relatively modest.

Discussion

In this chapter, I have described the generation and testing of several methods to modify chemerin expression and signalling with a focus on the use of these systems primarily in mature adipocytes. Herein, I critically evaluate the use of the systems and discuss the potential implications of their future use.

Production of chemerin isoforms

We successfully generated bioactive chemerin isoforms using two different methods. First, we expressed high levels of recombinant chemerin in *E. coli* using two different expression vectors, pProEx HTb and pET21b. We optimized the bacterial growth conditions for maximal chemerin expression, including temperature, collection time, IPTG concentration, and host cell strain. Using the established expression conditions we were able to successfully purify chemerin using both native and denaturing conditions. Importantly, chemerin purified under native conditions retained bioactivity at CMKLR1. This is ideal because previous recombinant chemerin expression systems required extensive re-folding protocols (Xiang et al. 2010). The successful expression and purification of bioactive chemerin provides a basis for future studies to scale up production in order to generate larger quantities of recombinant chemerin.

There are several areas for improvement in the future use of this recombinant chemerin expression system. Firstly, while we were interested in expressing chemerin that was as similar to the published sequence as possible, the improved levels of chemerin expression in the presence of rare tRNAs using Rosetta cells suggests that codon-optimizing the sequence may further improve expression levels. Furthermore, while expression of chemerin resulted in the presence of immunodetectable chemerin that was similar in size to the expected protein, we also observed the presence of additional smaller bands throughout the project. It is possible that this is a result of degradation by bacterial proteases; however, the addition of protease inhibitor cocktail to the lysis buffer did not affect the intensity of these bands. Another possibility is that intra- or extracellular proteases are cleaving chemerin before lysis, and studies involving the addition of protease inhibitors to the bacterial culture may improve the expression of chemerin. Future studies to improve purification conditions are also warranted, as the

yield of chemerin was relatively low under both native and denaturing purification protocols. Both time and temperature, in addition to host cell strain, influence the distribution between soluble and insoluble chemerin, and therefore the growth and lysis conditions for optimal purification conditions should be further investigated. Finally, the level of bioactivity was modest compared to commercially available recombinant chemerin. It is possible that the N-terminal His tag interferes with chemerin binding at CMKLR1 and experiments that examine the effect of removing the His tag might improve chemerin bioactivity. Further optimization studies such as these will likely improve the success of recombinant chemerin production in *E. coli*.

We also successfully generated chemerin isoforms using a lentivirus-mediated overexpression system. In contrast to recombinant chemerin, this system results in the generation of chemerin similar to endogenously produced chemerin, including translation of the 17 aa signal peptide that is removed in commercially produced chemerin. Use of a lentiviral approach allows for stable integration and expression of chemerin in cells that are difficult to modify genetically; for example, non-dividing cells such as adipocytes. Inclusion of a GFP marker allowed visualization of lentivirus integration into cells, and we observed robust GFP expression in all cell types investigated. This suggests that this chemerin overexpression system is applicable to a wide range of cell types and species. Importantly, generation of constructs with a variety of promoters will enable optimization for numerous cell types, and different promoters could potentially be used within a particular cell type to achieve low or high levels of chemerin expression depending on the desired effect. Additionally, inclusion of a puromycin resistance marker allows for the rapid selection of cells with high levels of chemerin overexpression in cases where robust lentivirus integration is not achieved.

Lentiviral-mediated overexpression of chemerin resulted in high levels of chemerin secretion and activity from both HEK cells and MSCs. However, it was difficult to achieve high levels of chemerin expression in mature adipocytes, either directly through lentiviral infection or via the differentiation of MSCs with stable chemerin overexpression. This is likely because mature adipocytes naturally secrete high levels of chemerin. Alternatively, techniques to measure chemerin levels might not be sensitive enough to measure changes in chemerin secretion and/or activity. Importantly,

despite no detectable change in chemerin expression or secretion in mature adipocytes, there was an observed shift in chemerin bioactivity following expression of mChem(active) using both stable MSC-expressing cells and lentiviral transduction of mature adipocytes. This suggests that despite no difference at the mRNA level, there was a shift towards the production of the overexpressed active chemerin isoform. Considered altogether, the lentiviral-mediated overexpression system was robust, efficient, and appears promising for the expression of chemerin isoforms in low-chemerin expressing cells types, and for influencing the balance of chemerin isoform production in naturally high-expressing chemerin cell types.

The development of recombinant and endogenous chemerin expression systems will allow for investigations into the biological function of chemerin isoforms that are not commercially available. Modifications can also be introduced in order to study the resulting effect on chemerin activity. For example, we identified a novel splice variant of chemerin and used the lentivirus-mediated overexpression system to examine whether this variant had any effect on chemerin secretion or activity at CMKLR1. Each of the two expression systems offer distinct advantages and the use of both will aid in future studies. Production of chemerin isoforms using an *E. coli* expression system offers the benefit of producing large amounts of chemerin that can easily be applied to any cell type at little cost. In contrast, the lentiviral-mediated overexpression system is more tedious to use, but has the advantage that chemerin will be secreted and processed in an endogenous form. As we know very little about chemerin processing, the presence of post-translational modifications, protein folding, and whether chemerin exerts any intracellular functions, this is essential to furthering our understanding of chemerin signalling. These systems are promising and useful tools to enable the characterization of unavailable or modified chemerin isoforms.

The use of small molecules to activate chemerin receptors

As a complementary approach to the expression of full-length chemerin isoforms, the use of small molecules that activate CMKLR1 and GPR1 provide additional insights into chemerin signalling. In this chapter, we tested several small molecules that have been shown to activate chemerin receptors and interestingly, none of the tested peptides

activated SRF signalling or induced ß-arrestin recruitment at the previously reported concentrations. hChe9 and Dys10 have been reported to activate CMKLR1 with an EC_{50} of 7 nM and 26.4 nM, respectively (Shimamura et al. 2009; Wittamer et al. 2003), whereas our studies confirmed that these peptides activate CMKLR1, but at much higher concentrations (0.1- 1 μM). This is consistent with a recent commentary that hChe9 is 100-fold less potent than originally reported (Zabel et al. 2014). We also confirmed that humanin activates human GPR1, but at much higher concentrations than previously reported with an EC_{50} of 18.7 μM compared to 60.9 nM (Leroy 2014). Finally, we did not observe activation of CMKLR1 or GPR1 by mChe15. This is similar to a previous report that mChe15 does not induce intracellular calcium release (Luangsay et al. 2009). It is entirely possible that the peptides do not work as originally reported. Alternatively, the discrepancies in peptide potency might be explained by the presence of multiple intracellular signalling pathways downstream of CMKLR1 or GPR1 activation. Initial reports characterizing hChe9AP and Dys10 assayed intracellular calcium release and chemotactic activity, whereas we measured SRF signalling and ß-arrestin recruitment (Shimamura et al. 2009; Wittamer et al. 2003). Thus it is possible that specific peptides preferentially activate different signalling pathways and future studies that are specifically designed to examine this concept will provide further insight into the mechanisms of chemerin signalling.

Our results also indicate that different peptides exhibit receptor selectivity. We demonstrated that while both hChe9 and Dys10 activated GPR1 in addition to CMKLR1, these peptides had higher activity at CMKLR1. Additionally, humanin activated human GPR1 but not CMKLR1. This is the first evidence of a chemerin receptor agonist that displays specificity for one chemerin receptor, although humanin has been shown to activate other GPCRs (Yen et al. 2013). Future studies that exploit the specificity of peptides for receptors and signalling pathway activation will help to fully elucidate the role of chemerin signalling.

Methods to decrease endogenous chemerin signalling

Similar to the results obtained with the peptide agonists, we observed that the CMKLR1 inhibitor CCX832 did not work at concentrations previously reported (IC_{50} of

5 nM) (Watts et al. 2013). Our results indicated that 300 nM or 1 μM caused a modest reduction in ß-arrestin recruitment in the presence of chemerin-157 and on the recruitment of CMKLR1-expressing cells. This suggests that while CCX832 does inhibit CMKLR1 activation, the effect is relatively modest. CCX832 was originally shown to inhibit CMKLR1 activation by hChe9 (Watts et al. 2013) and it is possible that activity in combination with full-length chemerin-157, versus the short peptide, is different. In addition, both CCX832 and the control compound had some effects on GPR1 activity. It is unclear whether the control compound has affinity for GPR1 or if these are toxic effects. Regardless, our results suggest that use of CCX832 should be restricted to cells with low levels of endogenous chemerin secretion in order to maximize the inhibition of CMKLR1.

The inducible PB system offers a unique method to reduce levels of endogenous chemerin signalling in mature adipocytes as well as numerous other cell types. Importantly, there was essentially zero background shRNA activity in the absence of cumate. This is crucial to prevent shRNA expression in un-induced cells that might affect cell function; for example, decreased adipogenic differentiation with chemerin knockdown in MSCs. However, the tight regulation of the cumate operon also raised several problems. Firstly, we observed low GFP expression in PB-expressing cells, suggesting relatively low induction of the CMV promoter that controls both shRNA and GFP expression. Importantly, the maximum knockdown achieved was 50%. As a result, higher concentrations of cumate were necessary in order to displace the CymR repressor from the cumate switch operon. However, cumate treatment had a negative effect on cell viability. This was greatest in proliferating cells (HEK cells, MSCs) versus differentiated cells (adipocytes). Additionally, only 1 chemerin shRNA sequence (of 3 verified to work in HEK cells) was functional in differentiated adipocytes. It is likely that the relatively low induction of shRNA expression was not sufficient to overcome high basal levels of chemerin expression in adipocytes. Further optimization of the inducible PB system, including the selection of colonies with a high copy number of PB transposon integration, and determining the optimal balance between cumate concentration and shRNA expression, will help to improve the efficacy of this system. Considered altogether, while this system was functional in adipocytes, it is likely to be more successful in low-

proliferative or differentiated cell types with relatively low levels of basal chemerin expression.

This work highlights the need for novel small molecules to manipulate chemerin signalling. The generation of specific receptor inhibitors, or knockdown systems for chemerin receptors, will also prove useful in delineating the role of chemerin signalling. This is particularly relevant for studying the role of chemerin signalling in adipocytes, where high basal levels of chemerin expression reduce the sensitivity of inhibitors and knockdown techniques.

Perspective on the complementary use of these tools

There are several benefits and limitations to the use of each of these systems, which are described in Table 2.4. Ultimately, the complementary use of these systems will help to further elucidate the biological role of chemerin signalling. For example, previous studies have shown that full-length chemerin isoforms are significantly more active than chemerin-derived peptides, indicating that the N-terminus plays a role in engaging the receptor (Yamaguchi et al. 2011). Our results are consistent with these findings and suggest that performing studies with both full-length chemerin isoforms and peptides will provide the most insight into chemerin signalling, particularly with relevance to differences in intracellular signalling pathways and receptor selectivity. Furthermore, the systems described in this chapter (ie lentivirus-mediated overexpression or inducible PB knockdown) can be modified to overexpress or knockdown specific chemerin receptors, which will complement the current studies with chemerin receptor inhibitors and confirm the specificity of peptides. Furthermore, although this chapter was primarily focused on modulating chemerin levels in mature adipocytes, and highlighted the difficulty of manipulating levels of chemerin signalling in these cells, these tools are applicable to a broad range of cell types. Ultimately, the complementary use of systems such as these will facilitate studies that improve our understanding of the role and function of chemerin and signalling in numerous physiological systems.

Tables and figures

Figure 2.1. Different approaches used to modulate chemerin expression and/or activity of chemerin receptors in mature adipocytes

Several different approaches were used to manipulate levels of chemerin signalling in MSC-derived adipocytes. Recombinant prochemerin and bioactive chemerin were produced using a bacterial expression system (1) and chemerin was overexpressed in adipocytes using a lentiviral-mediated approach (2). Additionally, several small molecules, including agonists (3A) and an antagonist (3B), were screened for activity at CMKLR1 and GPR1. Finally, a cumate-inducible chemerin shRNA expression system was established in MSCs to enable chemerin knockdown in mature adipocytes (4).

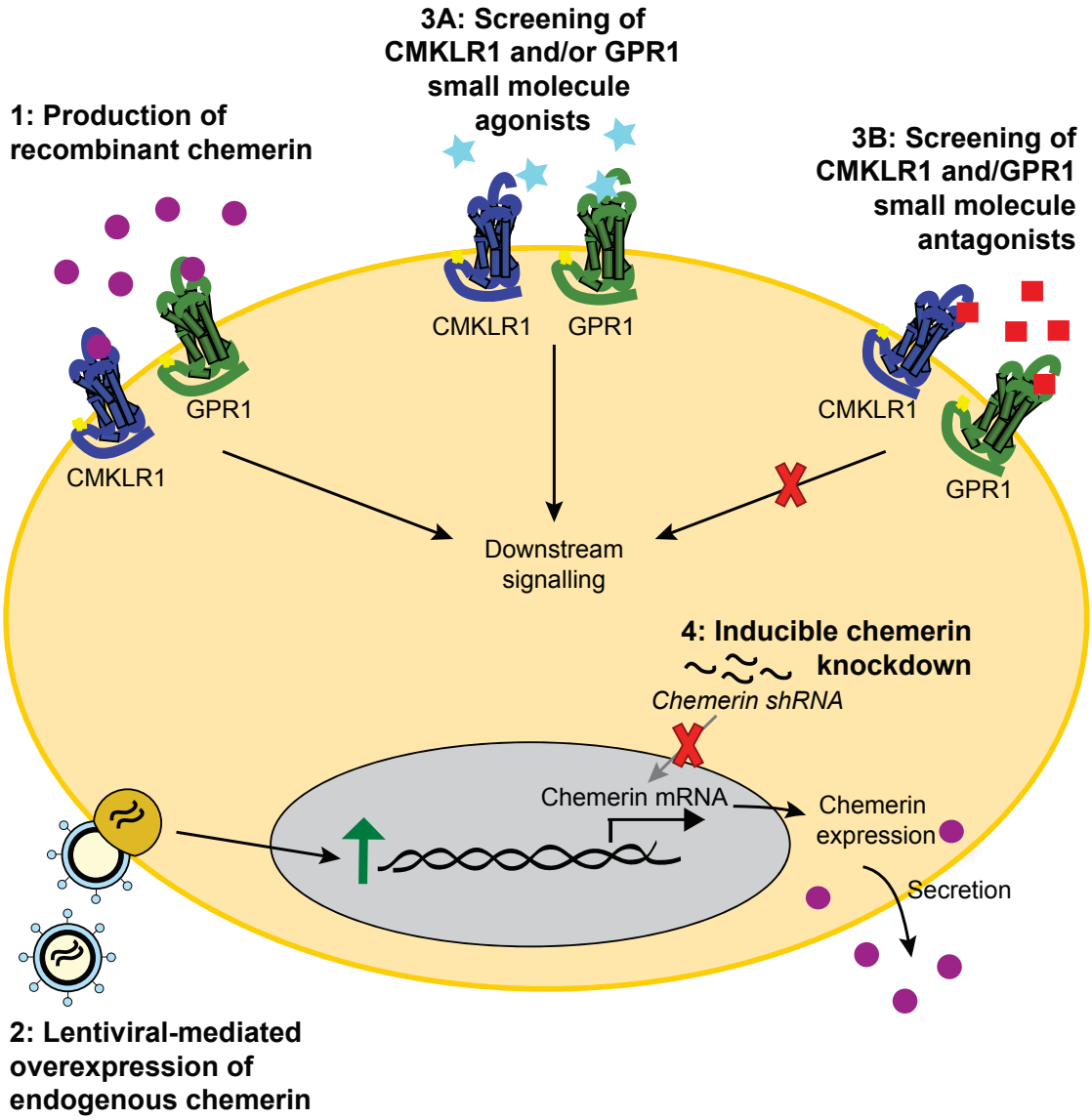
3A: Screening of CMKLR1 and/or GPR1 small molecule agonists
1: Production of recombinant chemerin
3B: Screening of CMKLR1 and/GPR1 small molecule antagonists
CMKLR1
GPR1
GPR1
CMKLR1
CMKLR1
GPR1
Downstream signalling
4: Inducible chemerin knockdown
Chemerin shRNA
Chemerin mRNA
Chemerin expression
Secretion
2: Lentiviral-mediated overexpression of endogenous chemerin

Table 2.1. Primer sequences used for cloning chemerin expression constructs

Primer	Sequence (5'-3')
Bacterial expression constructs:	
NcoI-mChemThr17 Forward	AAAACCATGGCTACACGTGGGACAGAGCCCGAACT
HindIII-mChemSer156 Reverse	AAAAAAGCTTTTAGGAGAAGGCAAACTGTCCAGGTAG
HindIII-mChemLys162 Reverse	AAAAAAGCTTTTATTTGGTTCTCAGGGCCCTGGA
NcoI-hChemGlu21 Forward	AAAACCATGGCTGAGCTCACGGAAGCCCAGCGC
HindIII-hChemSer157 Reverse	AAAAAAGCTTTTAGGAGAAGGCGAACTGTCCAGGGAA
HindIII-hChemSer163 Reverse	AAAAAAGCTTTTAGCTGCGGGGCAGGGCCTT
M13/pUCR Reverse	CAGGAAACAGCTATGAC
pTrcHis Reverse	GATTTAATCTGTATCAGG
NdeI-pProEx-6HisChemerin	AAAACATATGTCGTACTACCATCACCATCAC
Lentiviral expression constructs:	
NheI-mChem Forward	AAAAGCTAGCGCCGCCATGAAGTGCTTGCTGATCT
XbaI-mChem(active) Reverse	AAAATCTAGATTAGGAGAAGGCAAACTGTCCAGG
XbaI-mChem(pro) Reverse	AAAATCTAGATTATTTGGTTCTCAGGGCCCTGGA
NheI-cherry Forward	AAAAGCTAGCATGGTGAGCAAGGGCGAGGAGGATAAC
SalI-cherry Reverse	AAAAGTCGACCTTGTACAGCTCGTCCATGCCG
SnaBI-TK Forward	AAAATACGTAAAATGAGTCTTCGGACCTCGCGG
NheI-TK Reverse	AAAAGCTAGCTTAAGCGGGTCGCTGCAGGGTC
SnaBI-PGK Forward	AAAATACGTAGGGGTTGGGGTTGCGCCTTTTC
NheI-PGK Reverse	AAAAGCTAGCCTGGGGAGAGAGGTCGGTGATT
SnaBI-SV40 Forward	AAAATACGTAGCGCAGCACCATGGCCTGAAATAAC
NheI-SV40 Reverse	AAAAGCTAGCGAGCTTTTTGCAAAAGCCTAGGCCTC
SnaBI-EF1α Forward	AAAATACGTAGGCTCCGGTGCCCGTCAGTG
NheI-EF1α Reverse	AAAAGCTAGCTCACGACACCTGAAATGGAAGAAAAA
BamHI-GFP Forward	AAAAGGATCCGCCACCATGGTGAGCAAGGGCGA
KpnI-GFP Reverse	AAAAGGTACCTTACTTGTACAGCTCGTCCATGCC
Chem ColPCR Forward	GGAGGAGTTCCACAAACAC
Chem ColPCR Reverse	CTGTCCCTGTAATAAACCCG
Cherry ColPCR Forward	TCCCACAACGAGGACTACAC
Cherry ColPCR Reverse	ATGTCTGCCCGTATTTCGC
Promoter ColPCR Forward	GACCTTATGGGACTTTCCTAC
TK ColPCR Reverse	GAGAGTGTTTCGTTCCTTCC
PGK ColPCR Reverse	GTGAAGAATGTGCGAGACC
SV40 ColPCR Reverse	TGACACACATTCCACAGC
EF1α ColPCR Reverse	TTACCTGTGTTCTGGCGGCAAACC
GFP Forward	CAAAGACCCCAACGAGAAG
GFP Reverse	AGAGTCACACAACAGACGG
CMV Forward (sequencing)	CGCAAATGGGCGGTAGGCGTG

Table 2.2. Primer sequences used for cloning and testing Piggybac knockdown constructs

Primer	Sequence (5'-3')
BstBI-miR30 Forward	AAAATTCGAAAAGGTATATTGCTGTTGACAGTGAGCG
SwaI-miR30 Reverse	AAAAATTTAAATTCCGAGGCAGTAGGCA
miRNA30-LacZ KD 348 (sense:CTCACATTTAATGTTGATGAAA)	TGCTGTTGACAGTGAGCGATCACATTTAATGTTGATGAAATAGTGAAGCCACAGATGTATTTCATCAACATTAAATGTGAGTGCCTACTGCCTCGGA
miRNA30-LacZ KD 632 (sense:CTACACAAATCAGCGATTT)	TGCTGTTGACAGTGAGCGATACACAAATCAGCGATTTTAGTGAAGCCACAGATGTAAAATCGCTGATTTGTGTAGTGCCTACTGCCTCGGA
miRNA30- LacZ KD 1190 (sense:CGGCCTGTATGTGGTGGATGAA)	TGCTGTTGACAGTGAGCGAGGCCTGTATGTGGTGGATGAATAGTGAAGCCACAGATGTATTCATCCACCACATACAGGCCGTGCCTACTGCCTCGGA
miRNA30-mChem KD 95 (sense:AAGCCATGAAGTGCTTGCTGAT)	TGCTGTTGACAGTGAGCGCAGCCATGAAGTGCTTGCTGATTAGTGAAGCCACAGATGTAATCAGCAAGCACTTCATGGCTTTGCCTACTGCCTCGGA
miRNA30-mChem KD 297 (sense:CTTTGTGAGGTTGGAATTTAAG)	TGCTGTTGACAGTGAGCGATTTGTGAGGTTGGAATTTAAGTAGTGAAGCCACAGATGTACTTAAATTCCAACCTCACAAAGTGCCTACTGCCTCGGA
miRNA30-mChem KD 362 (sense:GAGTGCACAATCAAACCAAAC)	TGCTGTTGACAGTGAGCGAAGTGCACAATCAAACCAAACTAGTGAAGCCACAGATGTAGTTTGGTTTGATTGTGCACTCTGCCTACTGCCTCGGA
miRNA30-mChem KD 490 (sense:GGAGTTGCAATGCATTAAGAT)	TGCTGTTGACAGTGAGCGAGAGTTGCAATGCATTAAGATTAGTGAAGCCACAGATGTAATCTTAATGCATTGCAACTCCTGCCTACTGCCTCGGA
miRNA30-mChem KD 537 (sense:GCTACTTCCTACCTGGACAGT)	TGCTGTTGACAGTGAGCGACTACTTCCTACCTGGACAGTTAGTGAAGCCACAGATGTAACTGTCCAGGTAGGAAGTAGCTGCCTACTGCCTCGGA
Piggybac colony PCR Forward	TCTCTCCACAGGTGTCCACT
Piggybac colony PCR Reverse	AGACCCCTAGGAATGCTCGT
Cyclophilin A qPCR Forward	GAGCTGTTTGCAGACAAAGTTC
Cyclophilin A qPCR Reverse	CCCTGGCACATGAATCCTGG
mChemerin qPCR Forward	TACAGGTGGCTCTGGAGGAGTTC
mChemerin qPCR Reverse	CTTCTCCCGTTTGGTTTGATTG

Figure 2.2. Chemerin is expressed from pProEx-hChemerin and pProEx-mChemerin expression constructs in BL21 cells

His-tagged chemerin expression constructs were generated using the pProEx expression system. The amino acid sequence for the general expression construct, including His-tag, spacer region and rTEV protease cleavage site, is outlined (A). Human chemerin was amplified from Glu21 to Ser163 (prochemerin) or Ser157 (bioactive chemerin). Mouse chemerin was amplified from Thr17 to Lys162 (prochemerin) or Ser156 (bioactive chemerin). Bold sequence indicates the difference between pro- and active chemerin isoforms (B). The predicted molecular weight of each expressed protein is shown (C). pProEx vectors were transformed into BL21 cells, cultured at 37ºC, and samples collected 4 h following 1 mM IPTG induction. 10 µg of each cell lysate was loaded for Western blot analysis with human (D) or mouse (E) antibodies. 100 ng of commerically available human (aa 21-157, D) or mouse (aa 17-156, E) recombinant chemerin was loaded as a positive control. The molecular weight of the marker is indicated in (D) and is similar for (E).

A

MSYYHHHHHHDYDIPTTENLYFQGAMA-Chemerin

6x His Tag — spacer region — rTEV protease cleavage site

B

Human: 21 ELTEA... 141 AGEDPHSFYFPGQFAFS 157 **KALPRS** 163

Mouse: 17 TRGTE... 140 AGEDPHGYFLPGQFAFS 156 **RALRTK** 162

C

	Sequence	**Weight (kDa)**	**+ His-tag (kDa)**
Human prochemerin	Glu21-Ser163	16.53	19.85
Human active chemerin	Glu21-Ser157	15.88	19.20
Mouse prochemerin	Thr17-Lys162	16.65	19.97
Mouse active chemerin	Thr17-Ser156	15.92	19.24

D

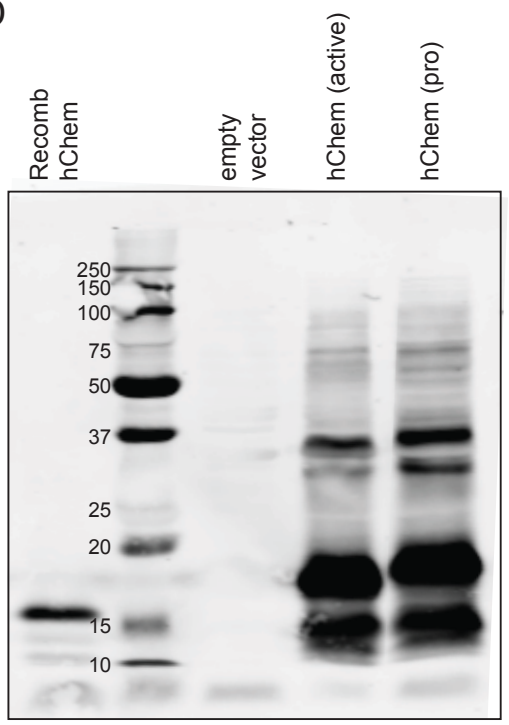

E

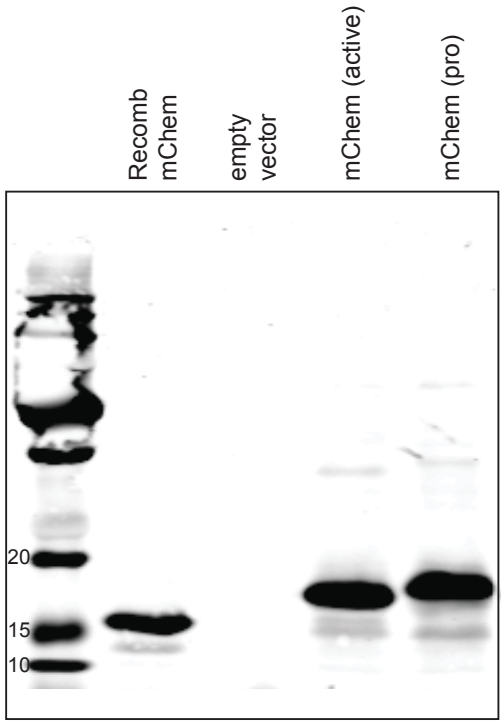

Figure 2.3. Optimization of pProEx-chemerin expression

The effect of collection time (A, B), DTT and protease inhibitor cocktail addition to lysis buffer (C), IPTG concentration (D), temperature (E), and host cell strain type (F) was evaluated in *E. coli* expressing pProEx-chemerin constructs. BL21 cells expressing human (A) or mouse (B) chemerin isoforms were induced with 1mM IPTG and samples collected 6, 12, 18, or 24 h following induction at 30ºC (A, B). Increasing amounts of DTT or protease inhibitor cocktail were added to the lysis buffer following 6 h incubation at 37ºC (C). Increasing concentrations of IPTG were used to induce chemerin expression and samples collected 6 h after induction at 37ºC (D). Cells were grown at 16, 23, or 30ºC and collected 6 h following the induction of chemerin expression (E). To compare levels of chemerin expression in BL21 cells versus Rosetta cells, cells were grown for 6 h at 16, 23, or 30ºC (F). Expression of chemerin following 4, 6, 10, 18 and 24 h after induction at 23ºC was then assessed in Rosetta cells (G). Expression studies were performed for all four isoforms (human/mouse and pro/active chemerin) but mouse active chemerin is represented in C-G. 10 µg of protein were loaded in A and B, and 5 µg in C-G. All blots were incubated with anti-His antibody. In A, the empty vector is representative of the 12 h timepoint; in E-F the empty vector is representative of 30ºC. The molecular weight marker is shown in A and is similar for all panels.

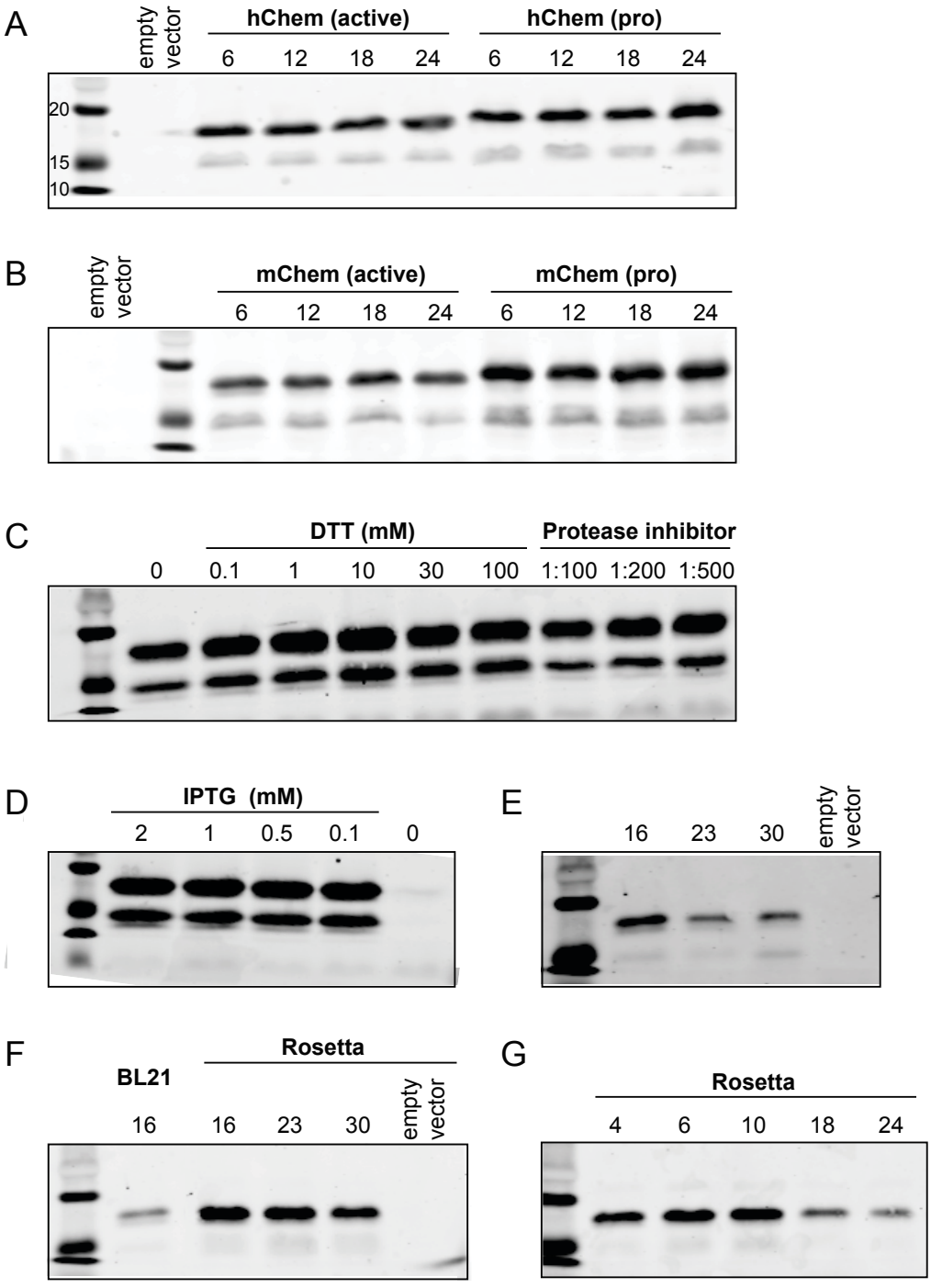
A
empty vector
hChem (active)
hChem (pro)
6 12 18 24 6 12 18 24
20
15
10
B
empty vector
mChem (active)
mChem (pro)
6 12 18 24 6 12 18 24
C
DTT (mM)
Protease inhibitor
0 0.1 1 10 30 100 1:100 1:200 1:500
D
IPTG (mM)
2 1 0.5 0.1 0
E
16 23 30 empty vector
F
BL21
Rosetta
16 16 23 30 empty vector
G
Rosetta
4 6 10 18 24

Table 2.3. Rare codon usage in chemerin sequences

Codon	# times used			
	Human prochemerin (aa21-163)	Human active chemerin (aa21-157)	Mouse prochemerin (aa17-162)	Mouse active chemerin (aa17-156)
AGA	0	0	3	2
AGG	5	5	4	3
AUA	2	2	2	2
CUA	0	0	3	3
GGA	2	2	1	1
CCC	7	6	4	4
CGG	6	6	2	2
Total	**22**	**21**	**19**	**17**

Figure 2.4. Expression and optimization of pET21b-Chemerin expression

His-chemerin was amplified from pProEx constructs and inserted into the pET21b expression vector. Expression of chemerin (6 h following induction at 37ºC in Rosetta cells) from pProEx versus pET21b constructs was compared by running 10 µg on a SDS-PAGE gel and staining with Coomassie blue (A). The white box indicates the expected area for chemerin expression. 1 µg of commercially-available recombinant human chemerin (aa 21-157) was loaded as a control. The incubation time and temperature for optimal chemerin expression from pET21b in Rosetta cells was evaluated (B). 2 µg of lysate from cells expressing pET21b-hChem(active) was loaded for Western blot analysis with anti-His antibody. The blots are cropped for presentation but were run concurrently under identical processing conditions and are directly comparable. 10 µg of lysate from Rosetta cells expressing pET21b-hChem(active) for 6 h at 16ºC or 23ºC was run on a SDS-PAGE gel and stained with Coomassie blue. Molecular weight markers are indicated for each blot.

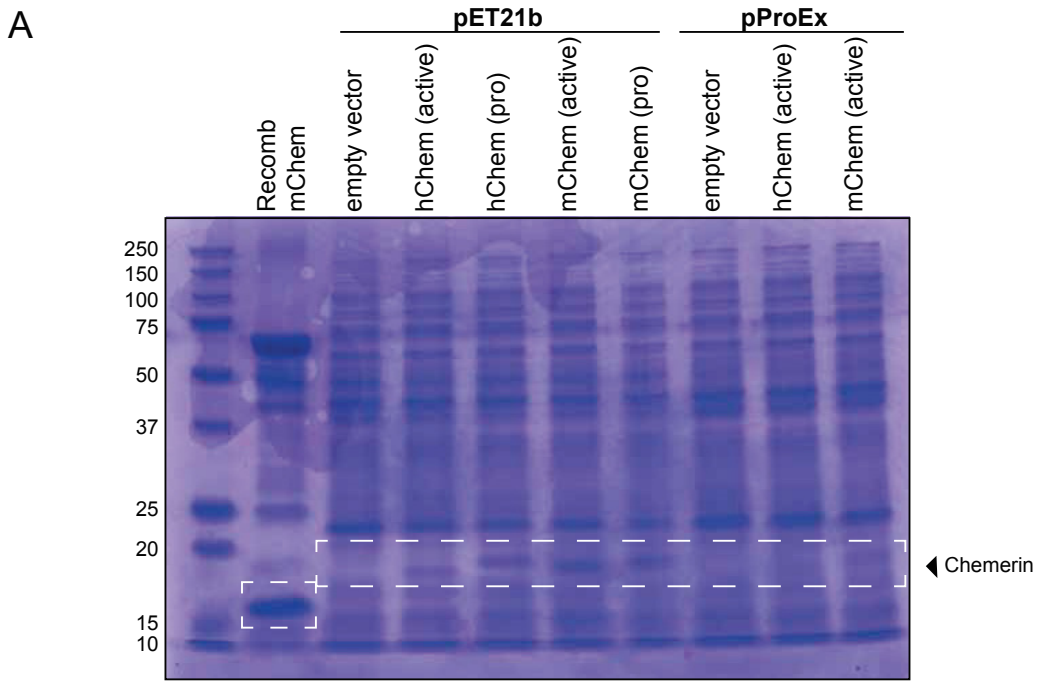
A
pET21b
pProEx
Recomb mChem
empty vector
hChem (active)
hChem (pro)
mChem (active)
mChem (pro)
empty vector
hChem (active)
mChem (active)
250
150
100
75
50
37
25
20
15
10
Chemerin
B
empty vector
16C
23C
30C
6
12
18
24
6
12
18
24
6
12
18
24
20
15
10
C
Recomb mChem
empty vector
16
23
250
150
100
75
50
37
25
20
15
10
Chemerin

Figure 2.5. Purification of recombinant chemerin using both native and denaturing conditions generates a low yield of chemerin

Rosetta cells expressing pET21b-hChem(active) were grown at 6 h for 37ºC following IPTG induction, a solubility test performed, and chemerin levels analysed using Western blot analysis with an anti-His antibody (A). The induction control (no IPTG addition), lysate, and crude extracts represent 0.8%, 0.4% and 0.1% of total lysate, respectively. Purification of human active chemerin under native conditions was performed using Ni-NTA spin columns (B) and under denaturing conditions using a 50% Ni-NTA resin slurry (C). In both (B) and (C), 20 μL of each sample was loaded and chemerin was detected using an anti-human chemerin antibody. Molecular weight markers are indicated in panel A and are similar for B-C.

A

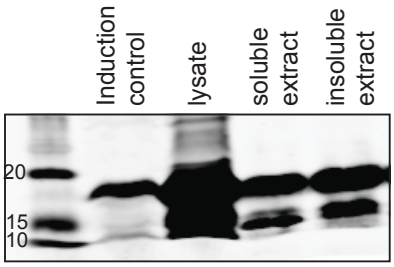

B **Native purification**

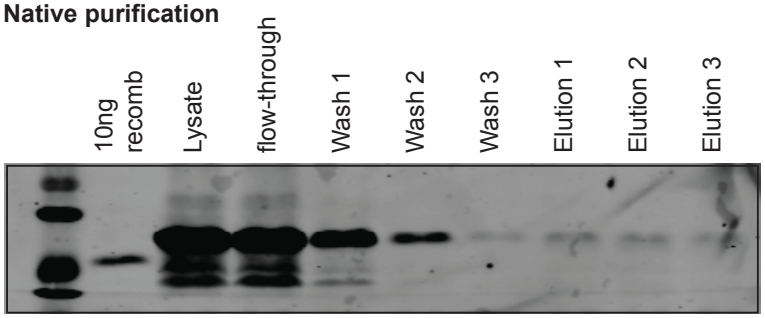

C **Denatured purification**

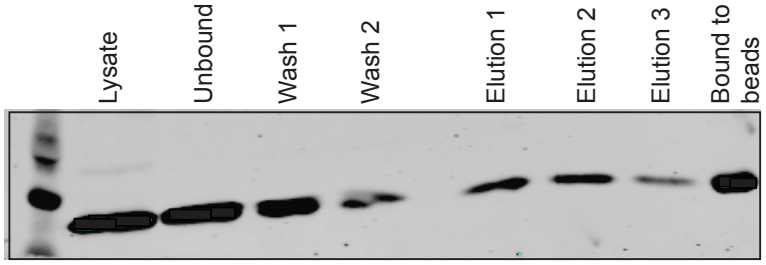

Figure 2.6. Recombinant human active chemerin purified under native conditions has activity at hCMKLR1

Rosetta cells expressing pET21b-hChem(active) were grown for 6 h at 23ºC following induction with 1 mM IPTG. Recombinant chemerin was purified under native conditions, concentrated, and resuspended in PBS with 0.1% BSA. Bioactivity at human CMKLR1 was performed using the Tango assay following treatment of cells with 1:50, 1:10, or 1:5 dilutions of concentrated eluate. 0.3 or 1 nM of commercially available recombinant human chemerin (aa 21-157) was used as a positive control. Values are normalized to the media control where * represents $p<0.05$ compared to the media control.

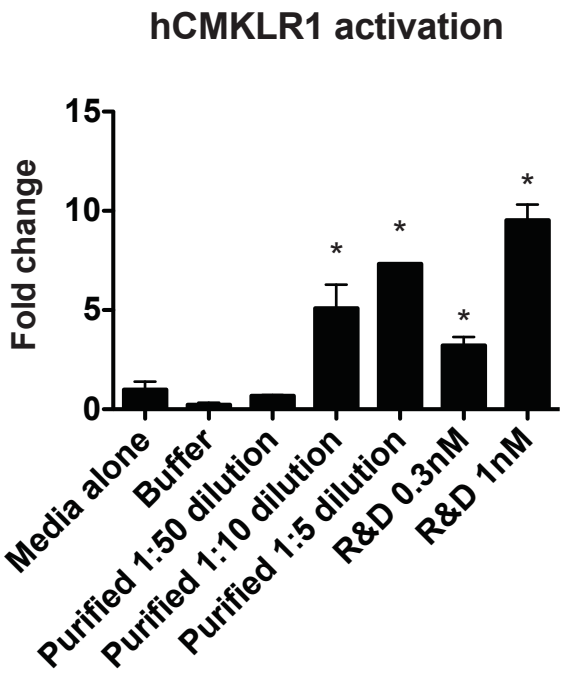
hCMKLR1 activation
Fold change
15
10
5
0
*
*
*
*
Media alone
Buffer
Purified 1:50 dilution
Purified 1:10 dilution
Purified 1:5 dilution
R&D 0.3nM
R&D 1nM

Figure 2.7. Lentivirus-mediated chemerin overexpression in HEK cells results in high levels of secreted bioactive chemerin

Mouse active chemerin (aa 1-156), mouse prochemerin (aa 1-163), or cherry was directionally cloned into the pLJM1 expression vector under the control of the CMV, TK, PGK, SV40, or EF1α promoters. The vector also expresses GFP under control under the hPGK promoter (A). pLJM1-CMV-mChem(active), mChem(pro), or cherry virus was generated and tested in HEK293A cells. GFP expression was imaged 4 d following transduction (B, 10x magnification). Cell lysate and 24 h-conditioned media were collected and chemerin expression and secretion was examined using western blot analysis (C). Bioactivity of conditioned media at mouse CMKLR1 was investigated using the Tango assay for ß-arrestin recruitment (D). pLJM1-mChem(active) virus under the control of TK, PGK, SV40, EF1α, and CMV promoters was generated and tested in HEK293A cells. GFP expression was imaged 4 d following transduction (E, 10x magnification) and levels of secreted chemerin were examined using western blot analysis of 24 h-conditioned media (F). Representative GFP images (n=6) and western blots (n=4) are shown. Blots were cropped for simplicity and molecular weight markers are indicated. Values are expressed relative to empty vector control where * represents $p<0.05$ compared to empty vector control (D, n=4).

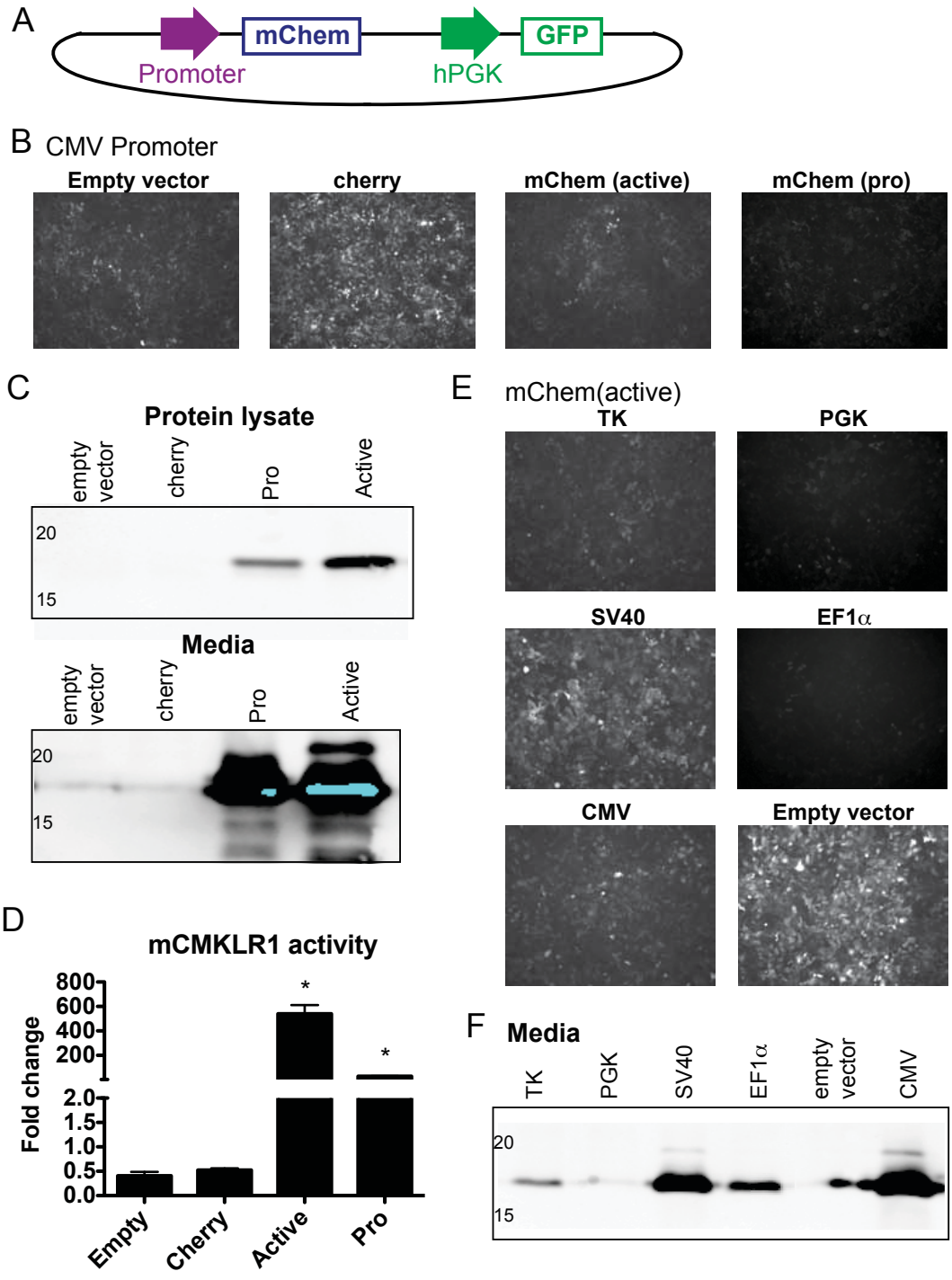
A
mChem
GFP
Promoter
hPGK
B CMV Promoter
Empty vector
cherry
mChem (active)
mChem (pro)
C
Protein lysate
empty vector
cherry
Pro
Active
20
15
Media
empty vector
cherry
Pro
Active
20
15
D
mCMKLR1 activity
Fold change
800
600
400
200
2.0
1.5
1.0
0.5
0.0
*
*
Empty
Cherry
Active
Pro
E
mChem(active)
TK
PGK
SV40
EF1α
CMV
Empty vector
F
Media
TK
PGK
SV40
EF1α
empty vector
CMV
20
15

Figure 2.8. Lentivirus-mediated chemerin overexpression in MSC-derived adipocytes does not result in a detectable change in chemerin RNA or protein levels but results in modified bioactivity at mCMKLR1 in adipocyte-conditioned media

Mature MSC-derived adipocytes were transduced with pLJM1-mChem(active), where mouse chemerin is under control of the CMV, TK, PGK, SV40, or EF1α promoter. GFP expression in non-transduced cells (polybrene control), empty vector control, or chemerin-transduced cells was evaluated 7 d following transduction (A, 10x magnification). Chemerin mRNA levels (B, n=2) and protein levels in cell lysate (C, n=4) or 24 h-conditioned media (D, n=10) were evaluated using qPCR or western blot analysis, respectively. Bioactivity of conditioned media at mouse CMKLR1 was tested using the Tango assay (E, n=2). Representative GFP images (n=10) and western blots are shown. Molecular weight markers are indicated. All values are expressed relative to polybrene control where * represents $p<0.05$ compared to polybrene control.

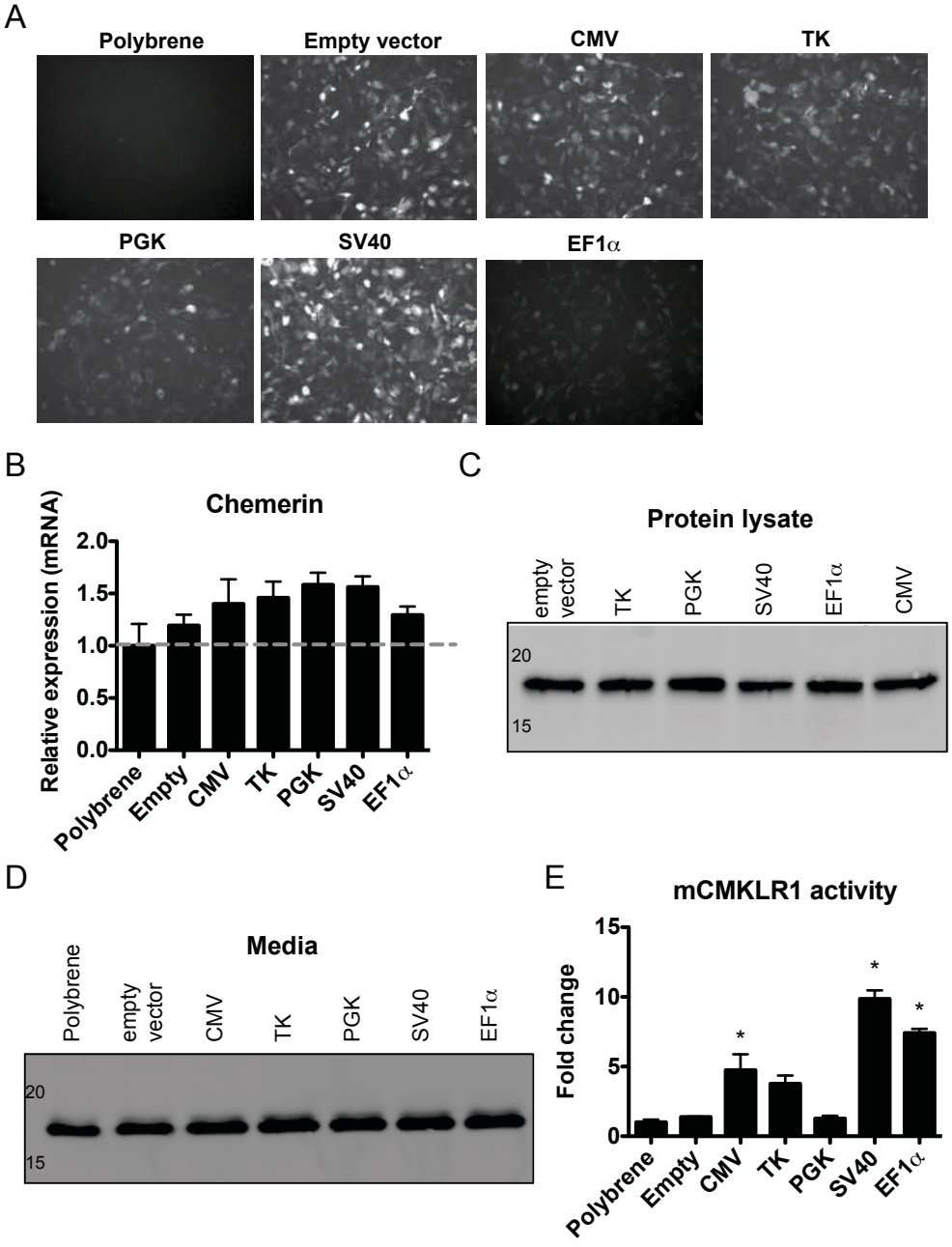
A
Polybrene
Empty vector
CMV
TK
PGK
SV40
EF1α
B
Chemerin
Relative expression (mRNA)
2.0
1.5
1.0
0.5
0.0
Polybrene
Empty
CMV
TK
PGK
SV40
EF1α
C
Protein lysate
empty vector
TK
PGK
SV40
EF1α
CMV
20
15
D
Media
Polybrene
empty vector
CMV
TK
PGK
SV40
EF1α
20
15
E
mCMKLR1 activity
Fold change
15
10
5
0
*
*
*
Polybrene
Empty
CMV
TK
PGK
SV40
EF1α

Figure 2.9. Differentiation of MSCs with stable integration of chemerin overexpression constructs results in increased endogenous chemerin levels in mature MSC-derived adipocytes

Undifferentiated MSCs were transduced with empty pLJM1 vector (control) or pLJM1-mChem(active) lentivirus in which chemerin is under the control of the TK, PGK, SV40, EF1α, or CMV promoters. Chemerin levels were assessed in 24 h-conditioned media using western blot analysis (A, n=3). A lentivirus construct encoding GFP, mChem(active), or mChem(pro) under control of the EF1α promoter, as well as a puromycin resistance marker under control of the PGK promoter, was generated (B). Undifferentiated MSCs were transfected with GFP, mChem(active), or mChem(pro) overexpression constructs and chemerin mRNA levels assessed using qPCR (C, n=7). Chemerin levels and bioactivity at mouse CMKLR1 were investigated using western blot analysis (D, n=7) and the Tango assay (E, n=3) in 24 h-conditioned media. Stable GFP-, mChem(active)-, or mChem(pro)-expressing MSC lines were differentiated into adipocytes. On day 8 following induction of differentiation, mRNA levels (F, n=3) were assessed using qPCR. Secreted chemerin levels (G, n=3) and bioactivity at mouse CMKLR1 (H, n=3) in 24 h-conditioned media were assessed using western blot analysis and the Tango assay, respectively. Molecular weight markers are indicated. Recombinant chemerin (aa 17-156) was loaded as a positive control in western blot analysis. All values are expressed relative to GFP control where * represents $p<0.05$ compared to GFP control.

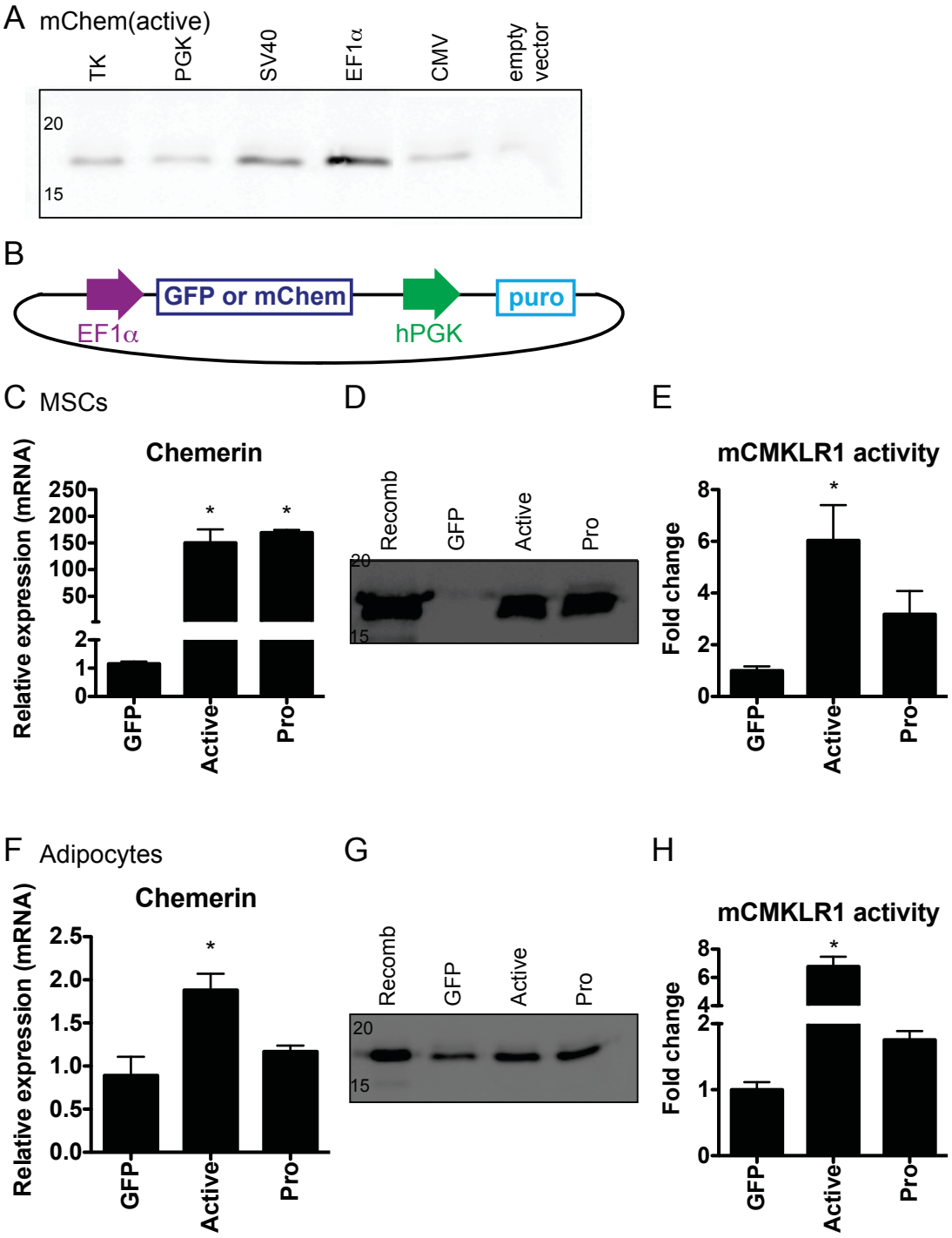
A mChem(active)
TK
PGK
SV40
EF1α
CMV
empty vector
20
15
B
GFP or mChem
puro
EF1α
hPGK
C MSCs
Chemerin
Relative expression (mRNA)
250
200
150
100
50
2
1
0
GFP
Active
Pro
D
Recomb
GFP
Active
Pro
20
15
E
mCMKLR1 activity
Fold change
8
6
4
2
0
GFP
Active
Pro
F Adipocytes
Chemerin
Relative expression (mRNA)
2.5
2.0
1.5
1.0
0.5
0.0
GFP
Active
Pro
G
Recomb
GFP
Active
Pro
20
15
H
mCMKLR1 activity
Fold change
8
6
4
2
1
0
GFP
Active
Pro

Figure 2.10. Identification of an extra amino acid on the boundary of exons 4 and 5 in mouse chemerin

Mouse chemerin (located on the reverse strand of chromosome 6) is comprised of 6 exons, 2 of which code for untranslated regions (shown in grey). Sequencing analysis of chemerin that was originally cloned from mouse liver mRNA revealed the presence of an extra amino acid (CAG) on the boundary between exons 4 (pink) and 5 (green). Analysis of the intron sequence between exons 4 and 5 revealed the presence of 3' CAG. Numbering is relative to the published sequence (A). Empty pLJM1 vector, or pLJM1-mouse chemerin constructs expressing either active chemerin (aa 17-156), prochemerin (aa 17-162), or prochemerin with the extra amino acid, were transfected into HEK cells. Chemerin levels in 24 h conditioned media were analysed by Western blot analysis (B) or using the Tango assay for mouse CMKLR1 activity (C). Recombinant mouse chemerin (aa 17-156) was loaded as a positive control. Values are expressed relative to control (media alone) where * represents $p<0.05$ compared to control. n=2.

A

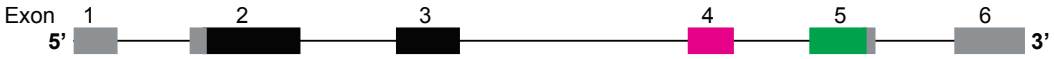

Exon 4 (386-481): Exon 5 (482-600):

460 481 482 510

Published: ...AATTCTGAAGCAAGGGCCTCAG---GATCCTCAGGAGTTGCAATGCATTAAGA...

Sequenced: ...AATTCTGAAGCAAGGGCCTCAG**CAG**GATCCTCAGGAGTTGCAATGCATTAAGA...

Intron 4-5: ...ctgcagcaaacactggttctagcag

B

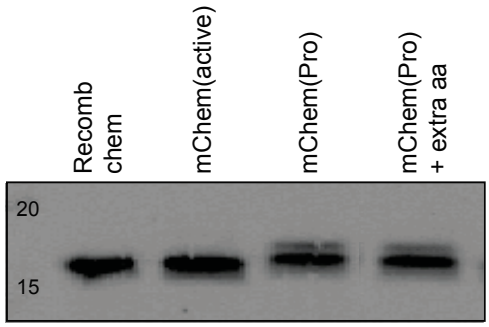

C

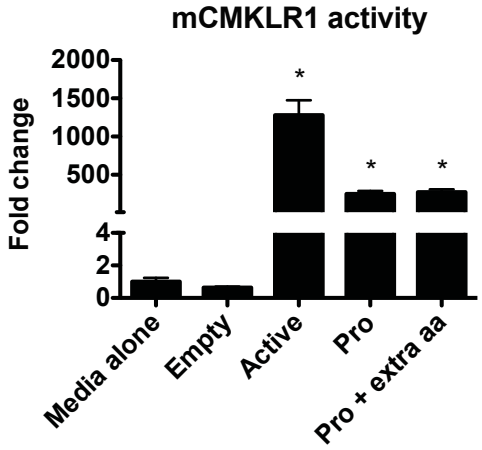

Figure 2.11. hChe9 and Dys10, but not mChe15, activate SRF signalling through chemerin receptors

HEK cells were transfected with SRF-RE luciferase reporter and human or mouse CMKLR1 and GPR1. Cells were treated for 4 h with the indicated concentrations of hChe9 (A, n=4), Dys10 (B, n=3), or mChe15 (C, n=4). Luminescence (relative light units, RLU) was measured as a read-out of chemerin receptor activation and is normalized to ß-gal activity. Data is represented relative to vehicle control. Statistical significance was determined where * represents $p<0.05$ compared to vehicle (0 nM peptide) treatment. n=3-4.

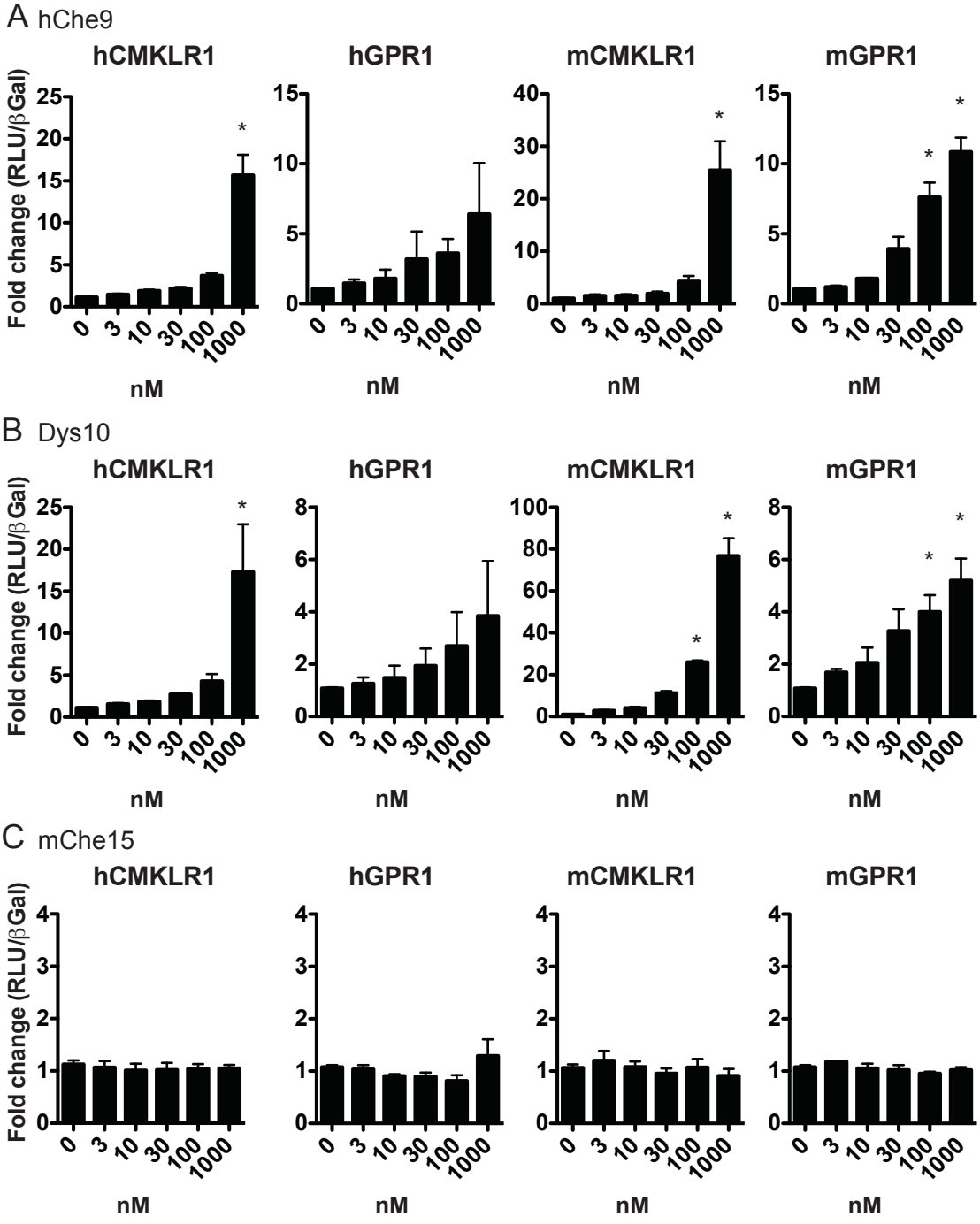
A hChe9
hCMKLR1
hGPR1
mCMKLR1
mGPR1
Fold change (RLU/βGal)
nM
B Dys10
hCMKLR1
hGPR1
mCMKLR1
mGPR1
Fold change (RLU/βGal)
nM
C mChe15
hCMKLR1
hGPR1
mCMKLR1
mGPR1
Fold change (RLU/βGal)
nM

Figure 2.12. Humanin induces beta-arrestin recruitment to human GPR1 but not mouse GPR1 and human/mouse CMKLR1

The bioactivity of humanin at CMKLR1 and GPR1 was investigated using the Tango assay. Increasing doses of humanin were applied for 24 h to cells expressing human or mouse receptors as indicated (A, n=2). 30 nM of recombinant human chemerin was used as a positive control. Using a wider dose-range, the EC_{50} of humanin at hGPR1 was determined using the Tango assay (B, n=3). Cells expressing hGPR1 were co-treated with 1 μM of humanin and increasing doses of human chemerin (C, n=2). Values are expressed relative to vehicle control where * represents $p<0.05$ compared to vehicle control (A, B) or vehicle (no humanin) within each chemerin dose (C).

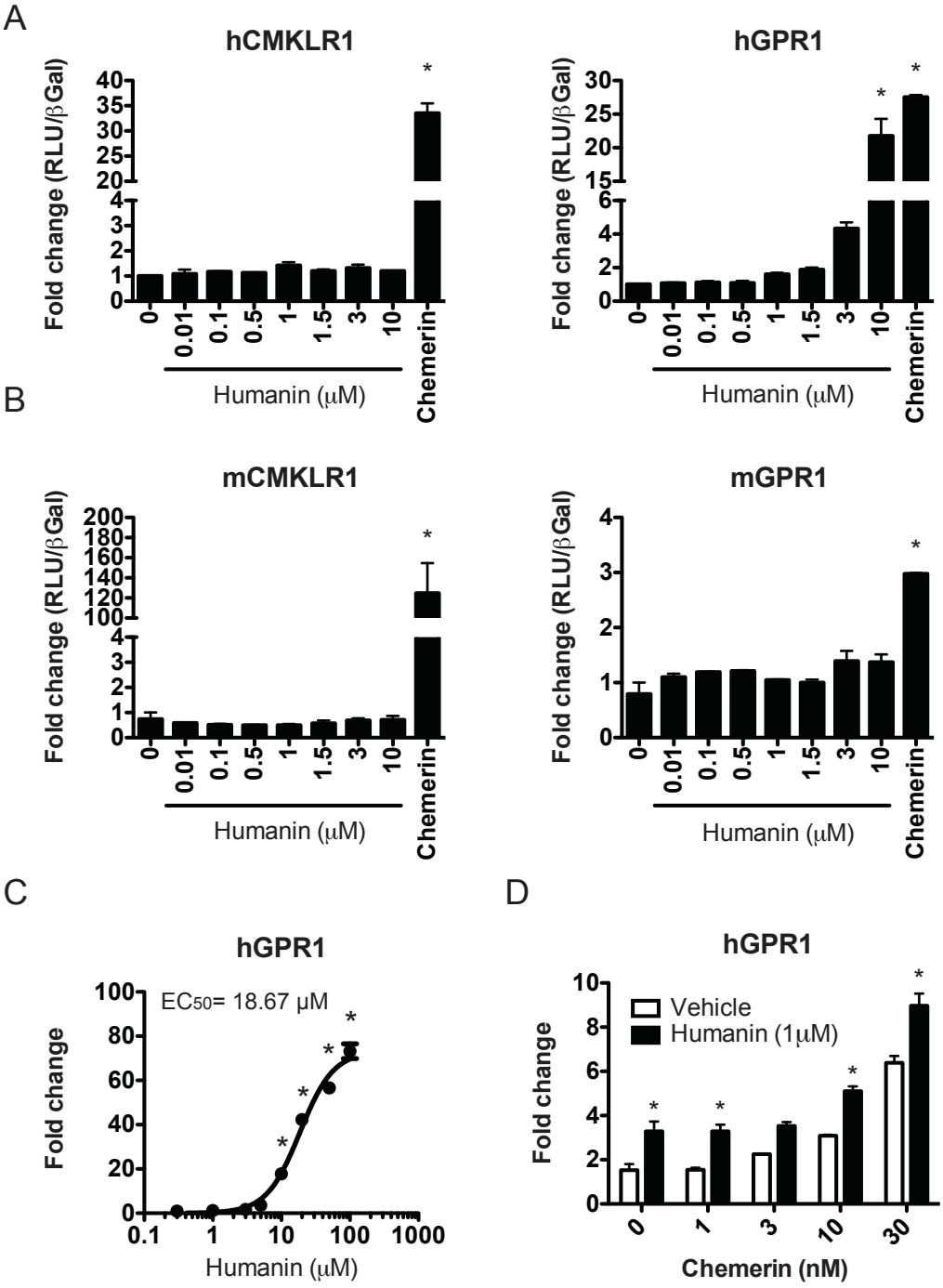
A
hCMKLR1
hGPR1
Fold change (RLU/βGal)
Humanin (μM)
Chemerin
B
mCMKLR1
mGPR1
C
hGPR1
EC50= 18.67 μM
Fold change
Humanin (μM)
D
hGPR1
Vehicle
Humanin (1μM)
Chemerin (nM)

Figure 2.13. CCX832 inhibits the activation of human and mouse CMKLR1 by chemerin at high doses and modestly inhibits CMKLR1-mediated chemotaxis

The activity of the CMKLR1 inhibitor CCX832, and control CCX826, at human and mouse CMKLR1 was investigated using the Tango assay. Increasing concentrations of recombinant chemerin (3-30 nM) and CCX832 or CCX826 (1-1000 nM) were incubated on cells expressing human (A, n=3) or mouse (B, n=3) CMKLR1. The next day, cells were lysed and luminescence detected as a measure of receptor activation. The effect of 300 nM CCX832 or CCX826 on the ability of CMKLR1-expressing L1.2 cells to migrate towards 1 nM human recombinant chemerin was investigated (C, n=4). In (A), values are expressed relative to vehicle control (no chemerin, no inhibitor) where * represents $p<0.05$ compared to vehicle control within each chemerin dose. In (C), values are expressed relative to vehicle/vehicle (top/bottom) where * represents $p<0.05$ compared to vehicle/vehicle and # represents $p<0.05$ compared to vehicle/chemerin.

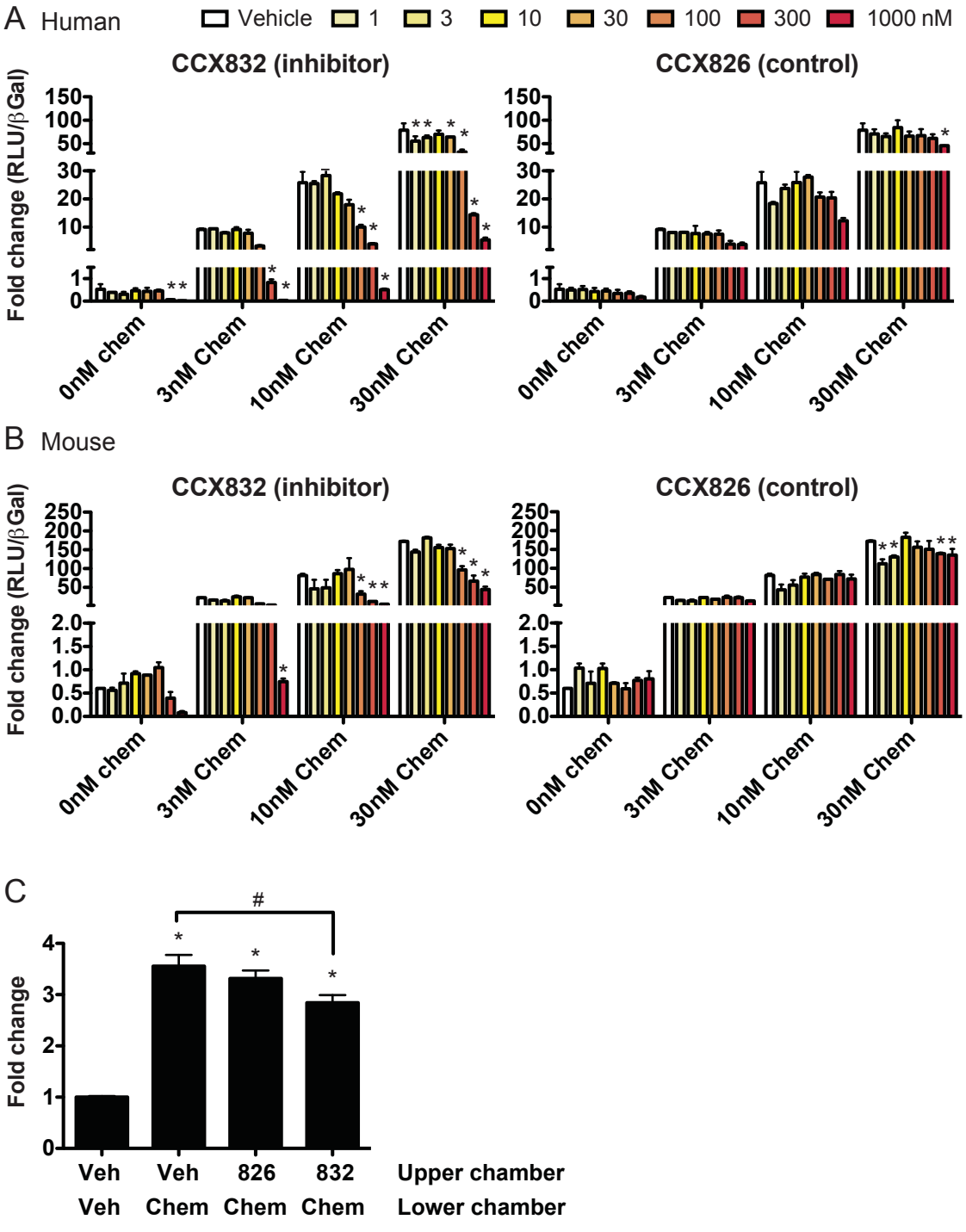
A Human
Vehicle
1
3
10
30
100
300
1000 nM
CCX832 (inhibitor)
CCX826 (control)
Fold change (RLU/βGal)
0nM chem
3nM Chem
10nM Chem
30nM Chem
B Mouse
C
Fold change
Veh
Veh
Veh
Chem
826
Chem
832
Chem
Upper chamber
Lower chamber

Figure 2.14. CCX832 inhibits the activation of human and mouse GPR1 by chemerin at high doses

The activity of the CMKLR1 inhibitor CCX832 and control CCX826 at human and mouse GPR1 was investigated using the Tango assay. Increasing concentrations of recombinant chemerin (3-30 nM) and CCX832 or CCX826 (10-1000 nM) were incubated on cells expressing human (A, n=2) or mouse (B, n=2) GPR1. The next day, cells were lysed and luminescence detected as a measure of receptor activation. Values are expressed relative to vehicle control (no chemerin, no inhibitor) where * represents $p<0.05$ compared to vehicle control within each chemerin dose.

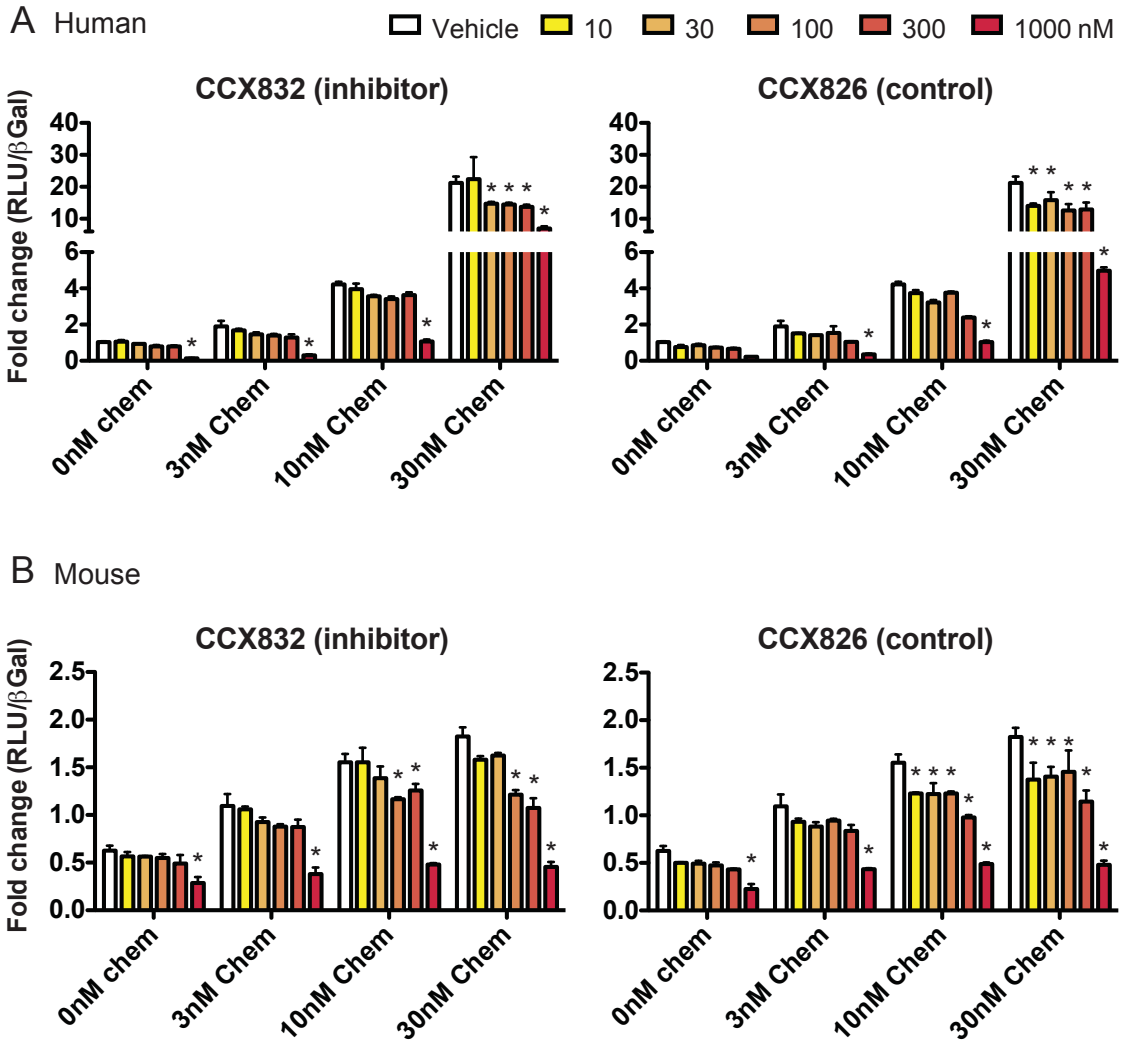
A Human
Vehicle
10
30
100
300
1000 nM
CCX832 (inhibitor)
CCX826 (control)
Fold change (RLU/βGal)
0nM chem
3nM Chem
10nM Chem
30nM Chem
B Mouse
CCX832 (inhibitor)
CCX826 (control)
Fold change (RLU/βGal)
0nM chem
3nM Chem
10nM Chem
30nM Chem

Figure 2.15. The Piggybac transposon system is easily mobilized into target genomes and is cumate-inducible

Diagram of the Piggybac expression system, modified from the PiggyBac transposon website (https://www.systembio.com/piggybac). The shRNA of interest is flanked by a miR-30 precursor sequence at the 5' and 3' ends, which is controlled by the CMV5 promoter upstream of the inducible cumate switch element. Expression of GFP is regulated by the cumate switch; however, translation is directed by the IRES element upstream of the GFP. Thus, the vector has to be turned on to show GFP expression. The PiggyBac expression vector also contains a puromycin cassette (to establish stable cell lines) and the CymR repressor element (regulates the cumate switch), which are both driven by the constitutive EF1α promoter. The super PiggyBac transposase recognizes transposon-specific inverted terminal repeat sequences (ITRs) located on both ends of the transposon vector. The transposase catalyzes the efficient integration of ITRs into TTAA chromosomal sites and allows the gene of interest between the two ITRs to be easily mobilized in target genomes (A). In the absence of cumate, the CymR repressor binds the cumate operator sequence with high affinity. The addition of cumate alleviates the repression and allows transcription to occur (B).

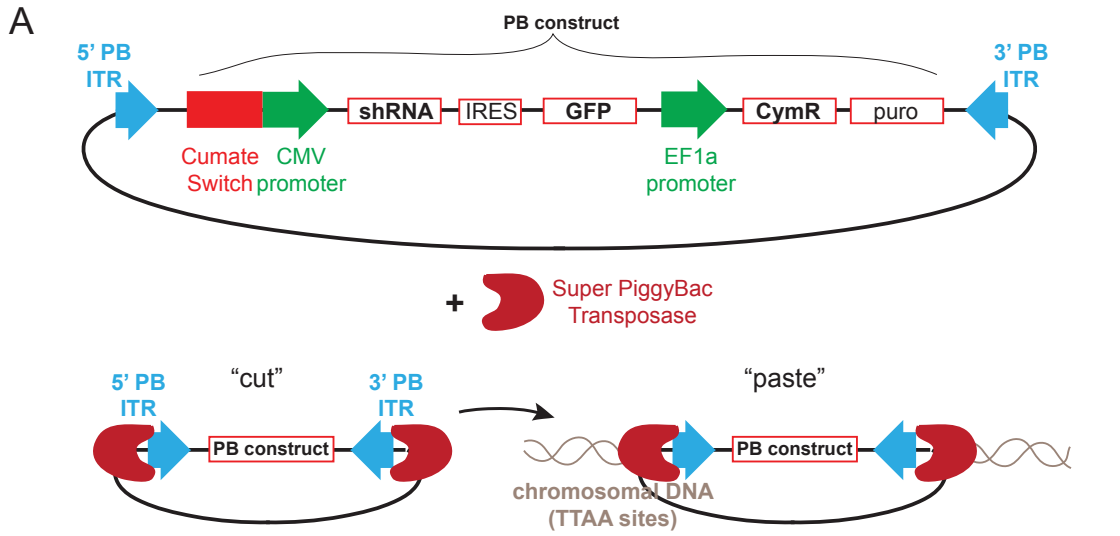
A
PB construct
5' PB ITR
3' PB ITR
shRNA
IRES
GFP
CymR
puro
Cumate Switch
CMV promoter
EF1a promoter
+
Super PiggyBac Transposase
"cut"
"paste"
PB construct
chromosomal DNA (TTAA sites)

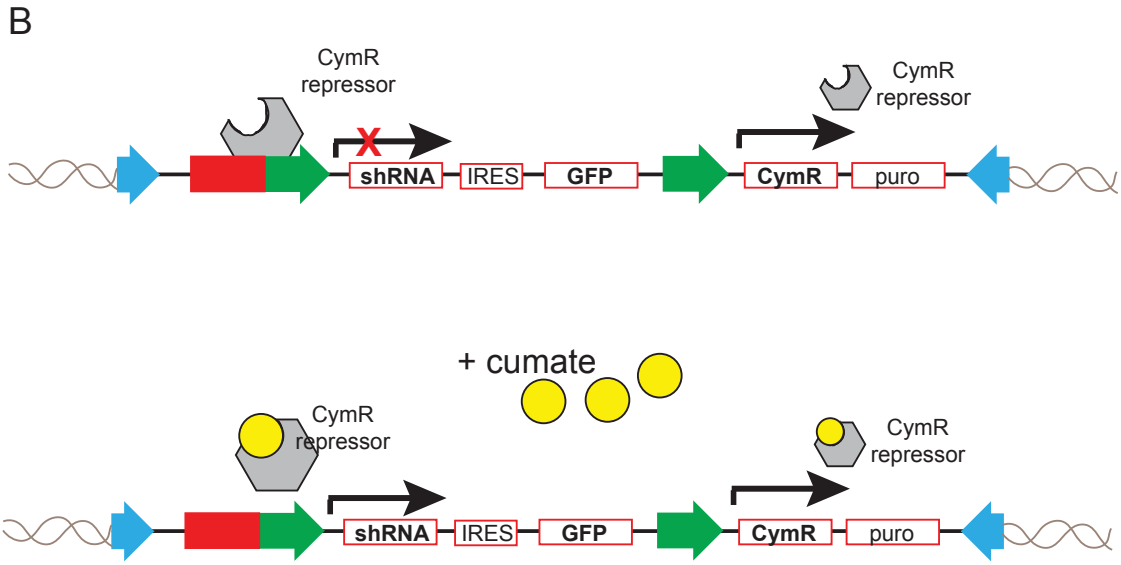
B
CymR repressor
shRNA
IRES
GFP
CymR
puro
+ cumate

Figure 2.16. The Piggybac knockdown has no toxic effects on HEK cells, MSCs, or mature adipocytes following 1x cumate addition

HEK cells and MSCs were transfected with empty PiggyBac expression vector and treated with 0-10x cumate for 48 or 72 h, respectively. MSCs with stable expression of empty PiggyBac vector were differentiated into adipocytes and treated with cumate from days 8-12 following induction of differentiation. GFP expression was visualized using different exposure times for each cell type (A, 10x magnification). Cell viability was assessed in cells treated with cumate (B, n=2). Cell viability is expressed relative to the no cumate control within each cell type. Statistical significance was determined for each cell type independently where * represents $p<0.05$ compared to control (no cumate).

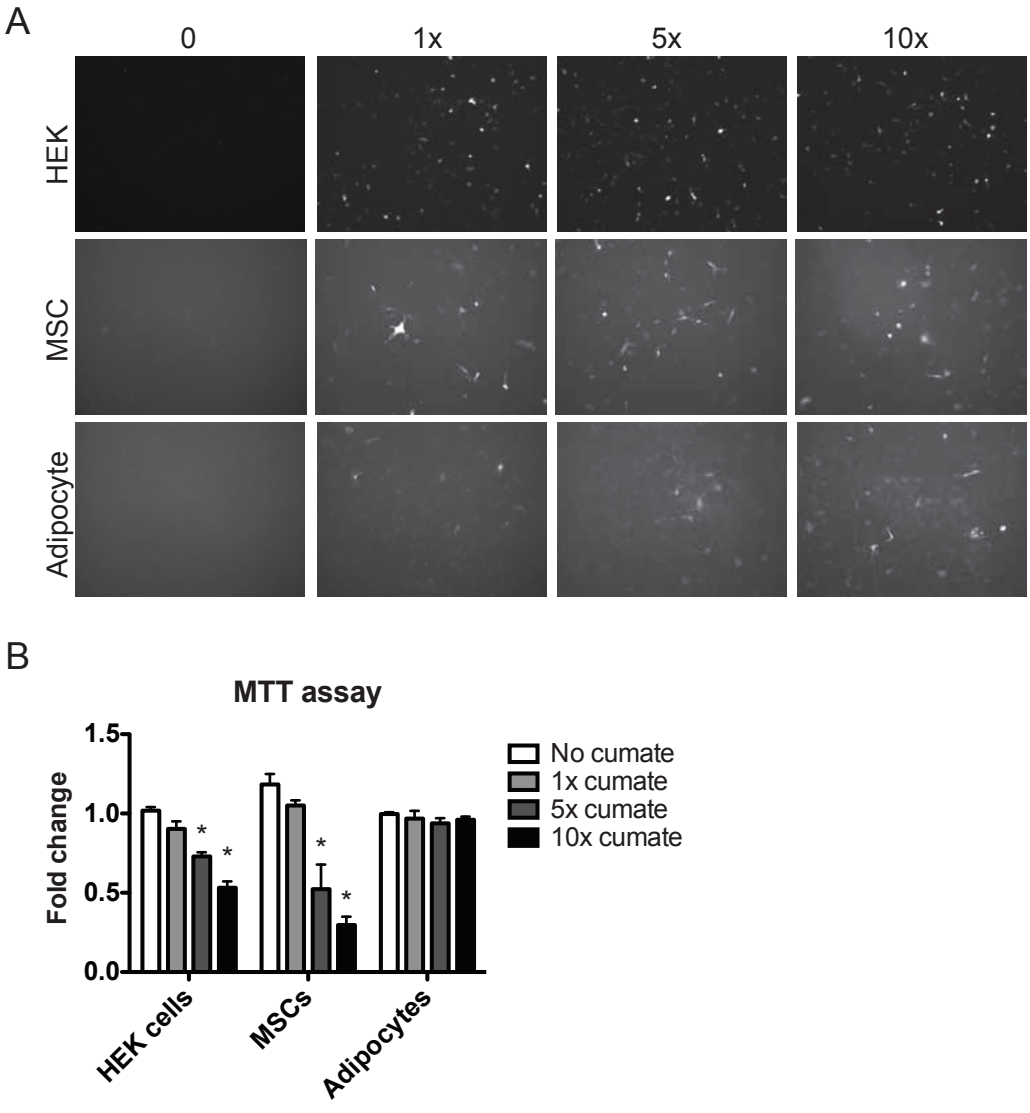
A
0
1x
5x
10x
HEK
MSC
Adipocyte
B
MTT assay
Fold change
1.5
1.0
0.5
0.0
No cumate
1x cumate
5x cumate
10x cumate
HEK cells
MSCs
Adipocytes

Figure 2.17. Expression of PB-LacZKD and PB-ChemKD leads to a reduction in ß-gal activity and chemerin-luciferase levels in HEK cells and undifferentiated MSCs

HEK cells were co-transfected with a ß-gal expression construct and empty PiggyBac vector, PB-LacZKD 348, 632, or 1190. 72 h following cumate addition, bGal activity was determined as a measure of shRNA efficacy (A, n=4). HEK cells were co-transfected with a chemerin-luciferase fusion construct and PB-ChemKD expression vectors. 48 h following cumate addition, luciferase activity was determined as a measure of shRNA efficacy (B, n=4). MSCs were transfected with the indicated PiggyBac vector and PiggyBac transposase. Cells positive for PiggyBac integration were selected with puromycin treatment to generate stable PiggyBac-expressing MSC lines. Undifferentiated MSCs were transfected with ß-gal (C, n=3) or chemerin-luciferase (D, n=3) to determine shRNA efficacy. In (A-B), values are normalized to empty vector control (no cumate addition) where * represents $p<0.05$ compared to the no cumate control for each construct. In (C-D), values are normalized to the control (no cumate addition) within each sequence/cell line where * represents $p<0.05$ compared to the no cumate control.

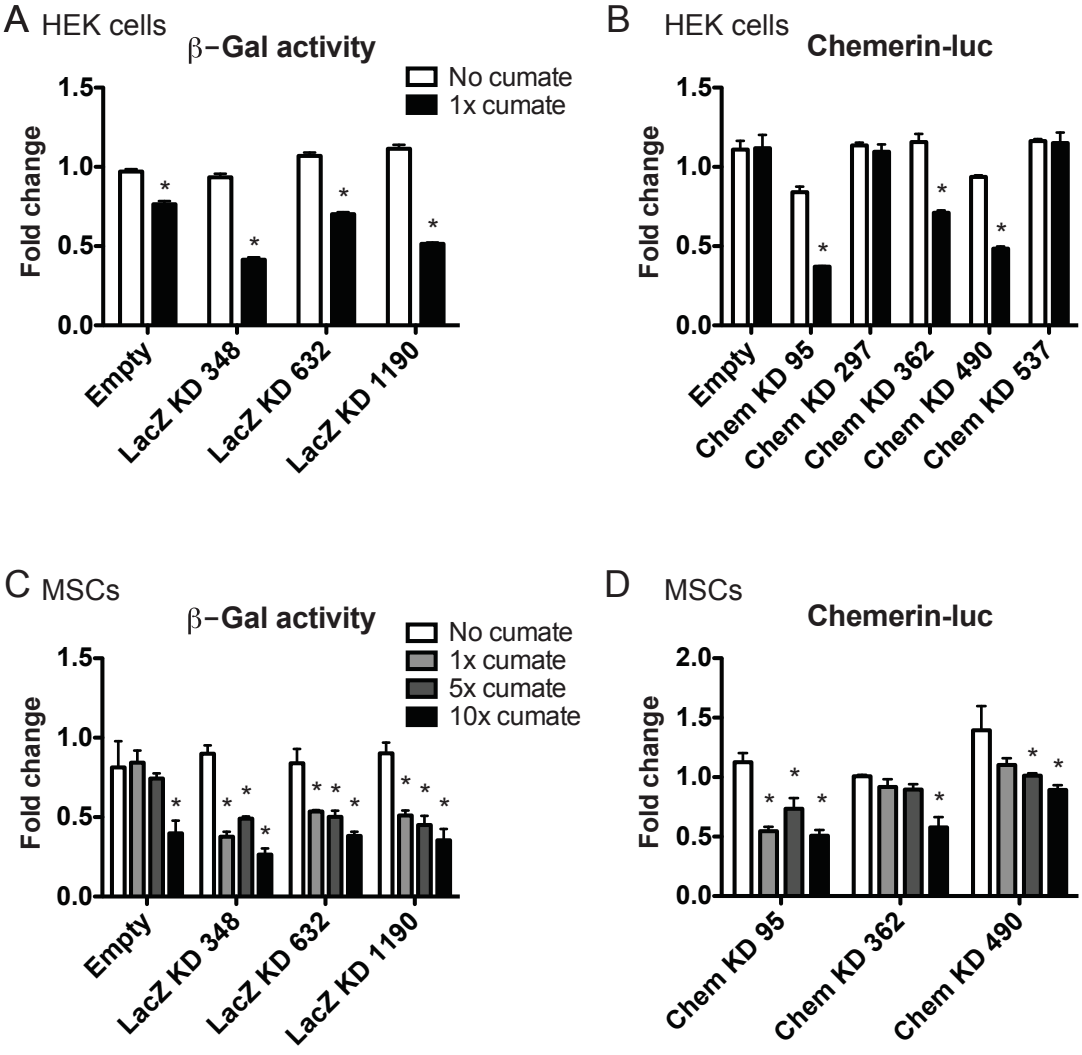
A HEK cells
β−Gal activity
No cumate
1x cumate
Fold change
1.5
1.0
0.5
0.0
Empty
LacZ KD 348
LacZ KD 632
LacZ KD 1190
B HEK cells
Chemerin-luc
Fold change
1.5
1.0
0.5
0.0
Empty
Chem KD 95
Chem KD 297
Chem KD 362
Chem KD 490
Chem KD 537
C MSCs
β−Gal activity
No cumate
1x cumate
5x cumate
10x cumate
Fold change
1.5
1.0
0.5
0.0
Empty
LacZ KD 348
LacZ KD 632
LacZ KD 1190
D MSCs
Chemerin-luc
Fold change
2.0
1.5
1.0
0.5
0.0
Chem KD 95
Chem KD 362
Chem KD 490

Figure 2.18. Expression of PB-ChemKD in mature adipocytes results in a modest decrease in chemerin mRNA levels

MSCs with stable expression of PiggyBac LacZ or Chem shRNA vectors were differentiated into mature adipocytes. Adipogenenic differentiation was evaluated using Oil Red O staining and compared to LacZ control (A, n=2). Adipocytes were treated with 10x cumate starting on day 8 following the induction of differentiation. Following 4 d of cumate treatment, GFP expression was evaluated (B, 10x magnification). The LacZKD and ChemKD photos were taken on different exposures. Chemerin expression was evaluated in adipocytes using qPCR analysis (C, n=3). Values are expressed relative to LacZKD control (no cumate) where * represents $p<0.05$ compared to the no cumate control within each sequence.

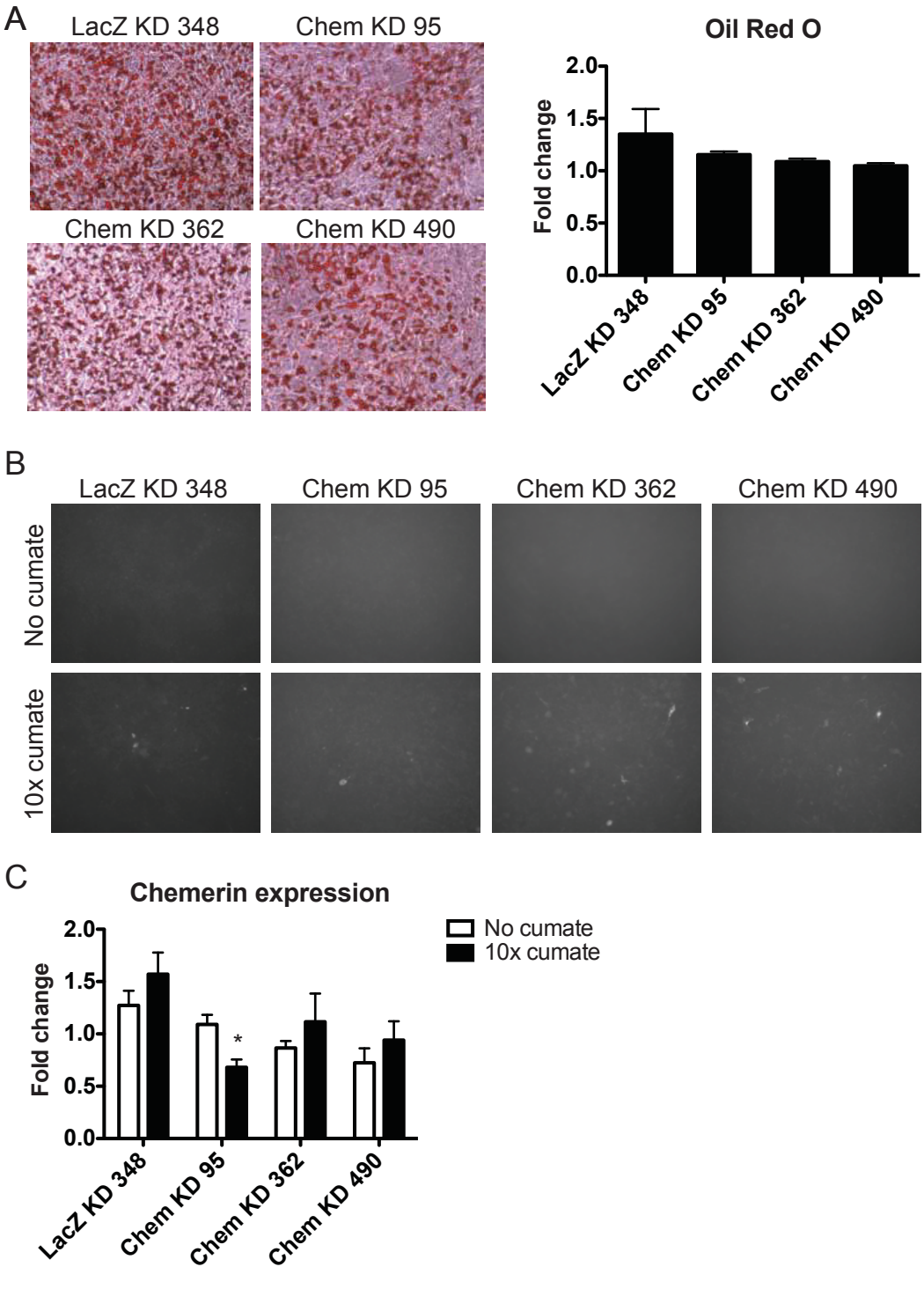
A
LacZ KD 348
Chem KD 95
Chem KD 362
Chem KD 490
Oil Red O
Fold change
2.0
1.5
1.0
0.5
0.0
LacZ KD 348
Chem KD 95
Chem KD 362
Chem KD 490
B
LacZ KD 348
Chem KD 95
Chem KD 362
Chem KD 490
No cumate
10x cumate
C
Chemerin expression
No cumate
10x cumate
Fold change
2.0
1.5
1.0
0.5
0.0
*
LacZ KD 348
Chem KD 95
Chem KD 362
Chem KD 490

Table 2.4. Comparison of the different strategies used to modulate chemerin expression and/or signalling

Technique	Advantages	Disadvantages
Recombinant protein expression	• Generate any isoform (including those not commercially available) • Generate modified forms with mutation of interest • High yield • Ease of working with bacteria	• Missing mammalian PTMs • Purification protocol requires optimization
Lentivirus-mediated overexpression	• Generate any isoform (including those not commercially available) • Potential to overexpress modified forms of chemerin or chemerin receptors • Endogenously expressed (contains PTMs, properly folded, etc) • Stable integration into cells of interest	• Variability in expression • Difficult to overcome high basal levels • Some cell types difficult to transduce
Small molecule treatment	• Acute treatment • Inexpensive • Specificity (species and receptor)	• Does not study role of full molecule (may have other functions)
Inducible knockdown system	• Inducible • Temporal regulation with cumate addition/removal • Foot-print free transposon excision • Potential to knockdown chemerin receptors if necessary	• Requires some time to “turn on” • Difficult to overcome high basal levels • Needs high cumate concentration to displace CymR; cumate negatively influences cell viability

CHAPTER 3: ADIPOCYTE-SECRETED CHEMERIN IS PROCESSED TO A VARIETY OF ISOFORMS AND INFLUENCES MMP3 AND CHEMOKINE SECRETION THROUGH AN NFKB-DEPENDENT MECHANISM

Copyright statement

Data presented in Figure 3.11A,B was previously published (Ernst, MC, Haidl, ID, Zuniga, LA, Dranse, HJ, Rourke, JL, Zabel, BA, Butcher, EC, and Sinal, CJ. 2012. Disruption of the chemokine-like receptor-1 (CMKLR1) gene is associated with reduced adiposity and glucose intolerance. Endocrinology 153: 672-82). Presentation of the data has been modified for clarity. Re-use is permitted with copyright permission (Appendix A).

Contribution statement

Dr. Shanmugam Muruganandan isolated MSCs and generated SVF-derived adipocytes. Dr. Matthew Ernst monitored the weight of wildtype and CMKLR1 knockout mice over a 24-week period and generated Figure 3.11A,B. He also isolated the RNA used for qPCR analysis in Figure 3.11B,C. Dr. Alejandro Cohen (Proteomics and Mass Spectrometry Core Facility) assisted with the design and analysis of mass spectrometry experiments. I was responsible for designing and performing all other experiments with guidance from Dr. Christopher Sinal.

Abstract

Obesity is associated with accelerated white adipose tissue (WAT) remodelling that is characterized by changes in cellular composition, size, and dysregulation of adipokine secretion. Pathological WAT remodelling is believed to contribute to the development of a chronic state of low-grade inflammation, insulin resistance, and obesity-associated diseases. Clinical and experimental studies have demonstrated that levels of the adipokine chemerin are positively associated with adiposity and the development of obesity-associated diseases. However, the mechanisms and biological function of chemerin signalling in WAT, and specifically mature adipocytes, are poorly understood. In this study, we demonstrated that mesenchymal stem cell (MSC) and stromal vascular fraction (SVF)-derived adipocytes secrete high levels of bioactive chemerin isoforms and abundantly express the chemerin receptor chemokine-like receptor 1 (CMKLR1), suggesting that mature adipocytes act as both a source and target of chemerin signalling. Using a neutralizing antibody to reduce levels of endogenous chemerin signalling, we identified factors involved in adipose tissue remodelling, including matrix metalloproteinase (Mmp)3 and numerous chemokines (Ccl2, 3, 5, 7), as novel targets of chemerin signalling in mature adipocytes. Inhibition of chemerin signalling increased expression of Mmp3 and chemokine expression with resultant increases in MMP activity and on the recruitment of macrophages towards adipocyte-conditioned media. We demonstrated that these effects are mediated through an increase in NFkB signalling, suggesting that chemerin signalling exerts an anti-inflammatory influence in mature adipocytes. We also showed for the first time that multiple chemerin isoforms are present in adipocyte-conditioned media, and that concentration of conditioned adipocyte media or overexpression of adipocyte-secreted chemerin, but not treatment with recombinant chemerin or synthetic peptides, recapitulate the activities of endogenous adipocyte-secreted chemerin. Considered altogether, this suggests that a uniquely processed chemerin isoform plays an autocrine and paracrine role in WAT remodelling and identifies chemerin as a novel therapeutic target to modulate adipose tissue remodelling during obesity.

Introduction

White adipose tissue (WAT) plays a central role in lipid and glucose metabolism by acting as both an energy storage depot and an endocrine organ that secretes a number of biologically active molecules termed adipokines. WAT exhibits continuous and dynamic changes in structure and function in response to nutrient availability (Sun et al. 2011). Obesity, characterized as the accumulation of abnormal or excessive amounts of WAT, generally results from situations in which energy intake exceeds energy expenditure. Recent reports published by the World Health Organization demonstrate that the worldwide prevalence of obesity has doubled since 1980 and that currently more than 1.9 billion adults are overweight or obese (WHO 2015). This is an alarming health concern because obesity is a risk factor for a number of diseases including chronic low-grade inflammation, hypertension, cardiovascular disease, diabetes, musculoskeletal disorders, and some cancers (Haslam and James 2005).

Pathological changes in WAT structure and function with obesity are thought to contribute to the increased risk for obesity-associated disorders. WAT is comprised primarily of lipid-filled adipocytes, but also contains a number of other cell types including preadipocytes, macrophages, endothelial cells, fibroblasts, and leukocytes. These cells are supported by a rich extracellular matrix (ECM), which consists of a variety of ECM proteins including collagen, laminin, fibronectin, and proteoglycans (Mariman and Wang 2010; Divoux and Clement 2011; Martinez-Santibanez and Lumeng 2014). In obesity, adipose tissue remodelling is pathologically accelerated and is characterized by adipocyte hypertrophy and hyperplasia, which occur due to excessive lipid storage and preadipocyte differentiation into mature cells. Adipose tissue expansion is also associated with increased angiogenesis, macrophage infiltration, endothelial cell activation, and changes in ECM composition and structure that occur in order to accommodate tissue growth (Sun et al. 2011; Martinez-Santibanez and Lumeng 2014). These changes are associated with altered production of inflammatory mediators and signalling molecules from both infiltrating immune cells and adipocytes. In particular, obesity is associated with dysregulated adipokine secretion from adipocytes resulting in the increased secretion of pro-inflammatory adipokines and decreased secretion of anti-inflammatory adipokines. Altered adipokine secretion has effects on local processes such

as adiposity, adipocyte metabolism and adipose tissue inflammation, as well as systemic processes including energy metabolism, neuroendocrine functions, and inflammation (Ouchi et al. 2011; Poulos et al. 2010). Considered altogether, changes in WAT cellular composition, size, and the production of adipokines are believed to promote a state of chronic-low grade inflammation, insulin resistance, and contribute to the development of obesity-associated disorders (Sun et al. 2011; Suganami et al. 2012). Therefore, a primary interest in the prevention and treatment of obesity and obesity-associated disorders is to understand the mechanisms that underlie adipose tissue remodelling and changes in WAT function with obesity.

Clinical and experimental studies have demonstrated that circulating levels of the adipokine chemerin, originally identified as a potent chemoattractant for cells expressing chemokine-like receptor 1 (CMKLR1)(Wittamer et al. 2003), are positively correlated with adiposity and the development of metabolic disorders including metabolic syndrome, type 2 diabetes, and cardiovascular disease (for review, see (Rourke et al. 2013)). Chemerin is expressed at high levels in mature adipocytes and WAT is considered a primary modifiable source of both local and systemic chemerin. Chemerin is secreted from adipocytes as inactive prochemerin, which undergoes extracellular processing to a variety of bioactive isoforms through the removal of a number of amino acids from the C-terminus (Rourke et al. 2013; Zabel et al. 2014). Adipocytes express several proteases, including the serine proteases elastase and tryptase, which are capable of bioactivating chemerin (Parlee et al. 2012). However, to date, the distribution of adipocyte-derived chemerin isoforms remains unclear and the majority of studies focus on the role of the chemerin-157 isoform. Bioactive chemerin binds and activates two receptors – CMKLR1 and G protein coupled receptor 1 (GPR1) – as well as the non-signalling receptor C-C chemokine receptor-like 2 (CCRL2) (Barnea et al. 2008; Meder et al. 2003; Wittamer et al. 2003; Zabel et al. 2008). Both CMKLR1 and GPR1 are highly expressed in WAT, with CMKLR1 expressed in adipocytes and the stromal vascular fraction (SVF), while GPR1 is enriched in the SVF (Goralski et al. 2007; Rourke et al. 2014). Previous studies have demonstrated that chemerin expression is induced by adipocyte hypertrophy (Bauer et al. 2011) and plays a role in adipogenic processes including adipocyte differentiation (Goralski et al. 2007; Muruganandan et al. 2011;

Muruganandan et al. 2010), glucose uptake (Kralisch et al. 2009; Takahashi et al. 2008), and lipolysis (Goralski et al. 2007; Roh et al. 2007; Shimamura et al. 2009). However, the mechanisms of chemerin signalling in adipocytes, including chemerin isoform distribution and the activation of intracellular signalling pathways, remain unclear.

As chemerin levels are altered with obesity and are associated with the development of obesity-associated disorders, we hypothesized that chemerin signalling plays a fundamental role in processes associated with adipose tissue remodelling. The goals of this study were to identify novel molecular targets of chemerin signalling in mature adipocytes and elucidate the signal transduction pathways downstream of CMKLR1 and/or GPR1 activation. We report that neutralization of endogenous chemerin signalling using an antibody-mediated approach alters the expression and activity of factors involved in adipose tissue remodelling through an NFkB-dependent pathway. Furthermore, we provide evidence that these effects are mediated through a uniquely modified adipocyte-derived chemerin isoform.

Methods

Reagents

Neutralizing mouse chemerin antibody and IgG control (R&D, Minneapolis, MN, USA) were reconstituted in sterile filtered PBS at a concentration of 1 mg/mL. Recombinant mouse tumor necrosis factor (TNF)α, mouse chemerin (aa 17-156), and human chemerin (aa 21-157) were purchased from R&D (Minneapolis, MN, USA). Lipopolysaccharide (LPS) and Bay11-7082 were obtained from Sigma Aldrich (Oakville, ON). CCX832/CCX826 was kindly gifted from Chemocentryx (Mountain View, CA, USA). Dys10 and hChe9AP were purchased from Genscript (Piscataway, NJ, USA).

Animals

C57Bl/6 mice were obtained from the Jackson Laboratory (Bar Harbor, ME). CMKLR1 knockout mice were fully backcrossed onto the C57Bl/6 background and have been previously described (Dranse et al. 2015; Ernst et al. 2012). Bone marrow-derived mesenchymal stem cells (MSCs) were isolated from 8-10 week old male mice and stromal vascular fraction cells were isolated from the subcutaneous white adipose depots of 10-14 week old female mice. There was no reason for the difference in age or sex between isolated cell types other than the availability of animals. Male wildtype or CMKLR1 KO mice were fed a low-fat diet and monitored for 6 or 24 weeks beginning at week 6 of age as previously described (Ernst et al. 2012). Mice were maintained under specific pathogen free conditions, at 21°C in a 12 h light:dark cycle with free access to food and water. Animals were sacrificed using an overdose (90 mg/kg) of pentobarbital sodium injected intraperitoneally followed by exsanguination via cardiac puncture. All experimental protocols were approved by the Dalhousie University Committee on Laboratory Animals and in accordance with the Canadian Council on Animal Care guidelines.

Primary cell isolation, culture, and treatment

MSCs were isolated from the bone marrow of wildtype mice as previously described (Muruganandan et al. 2010). Briefly, the hindlimbs were removed from each mouse, and the fat and tissue was removed from both the femur and tibia. Each bone was

rinsed with warm MSC media (MEMα containing 2 mM L-glutamine, 10% FBS, 100 U/mL penicillin, and 100 µg/mL streptomycin) and then the ends of each bone were cut off and the marrow flushed out by inserting a 22-gauge needle and passing warm media through the bone. Cells in the crude bone marrow were separated by passing through a 22-gauge needle several times and then filtered through a 70 µm cell strainer (BD, Mississauga, ON). The cells were washed three times in fresh media by spinning at 2500 rpm and then plated in a T25 flask (Corning, Corning, NY, USA). Fresh media was replaced the following day to remove non-adherent hematopoietic cells and then subsequently every 48 h until cells were approximately 80% confluent and passaged into a T75 flask (Corning). Single colonies were isolated from this crude population of MSCs and tested for their ability to differentiate into adipocytes. Briefly, MSCs (~15000 cells/48 well-plate, or 50000 MSCs/24-well plate for microarray analysis) were plated and grown to confluence. To induce adipocyte differentiation, cells were grown in adipocyte induction media containing 50 µM ascorbic acid (Sigma, Oakville, ON), 5 µg/mL insulin (Roche, Missisauga, ON), 50 µM indomethacin (Sigma, Oakville, ON), and 0.1 µM dexamethasone (Sigma, Oakville, ON). This was considered day 0 of adipocyte differentiation. After 48 h, fresh maintenance media (250 µL) containing 5 µg/mL insulin was replaced and refreshed every 48 h thereafter. MSCs with high adipogenic potential were expanded and stored in liquid nitrogen. For experiments, MSCs were used until approximately passage 20.

The stromal vascular fraction (SVF) was isolated from subcutaneous adipose tissue depots from mice as previously described (Muruganandan et al. 2011). Briefly, fat pads were minced in HEPES buffer using scissors and incubated with 2500 U of collagenase I (Sigma, Oakville, ON) for 60 min at 37ºC with 5% CO_2 with occasional mixing. The suspension was then diluted in DMEM/F-12 and undigested tissue was removed by filtering through a 100 µm mesh filter (BD Biosciences, San Jose, CA, USA). The filtrate was centrifuged at 50 g for 5 min, the supernatant underneath the adipocyte layer transferred to a new tube, and centrifuged at 200 g for 10 min. The pellet was then resuspended in DMEM/F-12, red blood cells lysed, and filtered through a 20 µm filter. The filtrate was spun at 200 g for 10 min, resuspended at a concentration of 50000 cells/mL and 500 µL plated per well of a 48-well plate (Costar, Corning, NY,

USA). Cells were grown for 24-48 h in complete growth media (MEMα, 10% FBS, 100 U/mL penicillin, and 100 µg/mL streptomycin) with fresh media replaced every day. On day 3 following isolation, media was replaced with adipocyte differentiation cocktail containing 50 µM ascorbic acid, 10 µg/mL insulin, 50 µM indomethacin, and 0.1 µM dexamethasone. Adipocyte differentiation cocktail was replaced every 48 h until cells were fully differentiated and then maintained in adipocyte maintenance media (250 µL) containing 5 µg/mL insulin. All experiments were performed on freshly isolated cells.

Experiments were performed on days 8-10 (MSC-derived adipocytes) or days 10-17 (SVF-derived adipocytes) following induction of differentiation and all treatments were performed in 100 µL of serum-free media (MEMα with 100 U/mL penicillin and 100 µg/mL streptomycin). Lysate and media samples were stored at -80ºC until further analysis.

Oil Red O staining

Cells were washed in PBS and fixed in 4% PFA at 4ºC overnight. The following day, cells were washed three times and stored in PBS at 4ºC. When all time-points had been collected, cells were stained in freshly diluted Oil Red O stain (0.3% Oil red O in 60% isopropanol) for 15 min with gentle shaking. Cells were then rinsed in PBS and imaged using an Eclipse TS100 microscope (Nikon, Melville, NY, USA), a Go-3 colour camera (Qimaging, Surrey, BC), and QCapture Pro6 software (Qimaging). All images were taken at the same exposure and adjustments made equally using Photoshop (Adobe, San Jose, CA, USA). Following imaging, PBS was removed from each well and 100 µL of isopropanol added to each well. The absorbance of eluted stain was measured at 520 nm using a FLUOStar Omega plate reader (BMG LabTech, Cary, NC, USA).

RNA isolation

Cells were lysed for RNA isolation in 350 µL of buffer RLT+ with 143 mM 2-mercaptoethanol with scraping and gentle mixing by pipette. RNA for downstream microarray experiments was isolated using the RNeasy RNA isolation kit with on-column DNAse digestion (Qiagen, Valencia, CA, USA). RNA from white adipose tissue was isolated using Trizol as previously described (Ernst et al. 2012). For all other

experiments, RNA was isolated using the RNeasy Plus RNA isolation kit with genomic DNA eliminase columns (Qiagen, Valencia, CA, USA) according to manufacturer's recommendations. RNA was eluted in 40 µL of RNase-free water and quantified by measuring the absorbance at 260 and 280 nm using a FLUOStar Omega plate reader (BMG LabTech, Cary, NC, USA).

Microarray analysis

Samples for microarray analysis were generated in triplicate and isolated independently. RNA was concentrated to a final volume of ~10 µL using a Speed Vac Plus SC100A with a universal vacuum system UVS400 (Savant, Fisher, Toronto, ON) for approximately 20 min with no heating. RNA integrity was examined by running an RNA gel. Briefly, 10 µg of RNA was denatured in MOPS electrophoresis buffer containing 7.4% formaldehyde, 50% formamide, and 2 µg/mL ethidium bromide by incubation at 55ºC for 60 min. After cooling at 4ºC for 10 min, 10x RNA gel loading buffer (50% glycerol, 10 mM EDTA (pH 8.0), 0.25% bromophenol blue, 0.25% xylene cyanol) was added to each sample. 28S and 18S rRNA bands were visualized by running samples on a 1.5% agarose gel containing 2.2 M formaldehyde. Samples for each treatment were pooled together in equal concentrations and shipped overnight on dry ice to The Centre for Applied Genomics at the Hospital for Sick Children (Toronto, ON). RNA BioAnalyzer analysis (Agilent, Santa Clara, CA, USA) was performed to verify quantity and quality of RNA samples, and microarray analysis was performed using a Mouse Gene 1.0 ST chip (Affymetrix, Santa Clara, CA, USA). The publicly available DNA-Chip Analyzer (dChip) software was used to analyze changes in gene expression between samples (Li and Wong 2001).

qPCR analysis

cDNA was generated using Affinity Script RT (Agilent, Santa Clara, CA, USA) with 0.5 µg of total RNA in a volume of 25 µL. 1 µL of cDNA was used as a template for qPCR using Brilliant II Fast SYBR Green master mix (Agilent) as per manufacturer's instructions. qPCR was performed using an MX3000p thermocycler (Stratagene) and analysed using MxPro qPCR software (Stratagene). Alternatively, 2 µg of total RNA

was transcribed to cDNA using EcoDry Premix Double-primed (Clontech, MountainView, CA, USA). cDNA was diluted to 10 ng/µl and qPCR performed using 1 µL of cDNA per reaction, with 0.5 µM primers, and FastStart SYBR green master mix (Roche, Laval, QC). qPCR was performed on a LightCycler96 according to manufacturer's recommendations and analysed using LightCycler96 software (Roche, Laval, QC).

Exon-spanning primers (Table 3.1) were designed using Primer-BLAST (http://www.ncbi.nlm.nih.gov/tools/primer-blast). For all primer sets, a melt curve analysis, confirmed by agarose gel electrophoresis, was performed to verify that a single gene-specific product was produced. In addition, amplification efficiency was tested through the generation of a calibration curve and using a cut-off efficiency of 90-105%. Relative gene expression was determined using the ΔΔCt method (Livak and Schmittgen 2001) where each sample was normalized to cyclophilin A as the reference gene.

Western blotting

To investigate the abundance of proteins in adipocyte-conditioned media, SDS-PAGE analysis was performed. 6X SDS-PAGE sample buffer was added to 30-40 µl of conditioned adipocyte media, boiled for 5 min, and proteins separated on a 10% (MMP3) or 15% polyacrylamide gel (chemerin, CCL2). For analysis of non-denatured chemerin, 6X SDS-PAGE sample buffer without 2-mercaptoethanol was added to adipocyte media and samples were not boiled. Proteins were transferred at 100 V for 1 h at 4ºC to nitrocellulose membrane (BioRad laboratories, Mississauga, ON), blocked for 1 h in Odyssey blocking buffer (LI-COR, Lincoln, NE, USA) or 5% skim milk powder (MMP3), and incubated with primary antibody (goat anti-mouse chemerin, CCL2, and MMP3; R&D, Minneapolis, MN, USA) overnight at 4ºC in blocking buffer with shaking. The next day, blots were washed with TBST and incubated with 1:10000 dilution of anti-goat IRDye800-conjugated secondary antibody (LI-COR) for 1 h at RT without exposure to light. Blots were imaged in TBST by scanning at 800 nm using an Odyssey Infrared System (LI-COR Biosciences, Lincoln, NE, USA).

Tango assay

The cell-based Tango assay was used to evaluate levels of bioactive chemerin in adipocyte-conditioned media as previously described (Barnea et al. 2008; Ernst et al. 2010; Parlee et al. 2010). Briefly, HTLA cells were transfected with mouse CMKLR1 or GPR1. After 24 h, the cells were treated with 50 µL of the sample of interest. For treatment with adipocyte-conditioned media, 50 µL was applied to HTLA cells (no dilution). The next day, cells were lysed and luminsence detected as a read-out of beta-arrestin recruitment/GPCR activation. Luciferase activity was normalized to ß-gal activity as an internal control and the bioactivity of each sample normalized to vehicle control.

MTT assay

To assess cell viability, adipocytes (day 8 of differentiation in a 48-well plate) were treated as indicated for 24 h in serum-free media. Cells were then incubated with 100 µL of 0.5 mg/mL thiazolyl blue tetrazolium bromide (MTT) (Sigma Aldrich, Oakville, ON) diluted in fresh serum-free media at 37ºC. After 3 h, the MTT reagent was aspirated from each well and the formazan product was solubilized in 100 µL of DMSO at 37ºC for 10 min. The absorbance of each sample was measured at 540 and 690 nm using a FLUOStar Omega plate reader (BMG LabTech, Cary, NC, USA). To calculate fold change, the absorbance at (540-690) nm was expressed relative to vehicle control (considered as 100% cell viability).

MMP assay

The fluorometric SensoLyte 520 MMP-3 assay kit or general MMP assay kit (Anaspec, Fremont, CA, USA) were used to determine levels of MMP3/12 or general MMP activity, respectively, in conditioned adipocyte media according to manufacturer's recommendations. Assay conditions were optimized to include a 1:100 dilution of MMP3/12 substrate in assay buffer and 10 µL of conditioned adipocyte media (or substrate/media control) in a total volume of 100 µL. Fluorescence (excitation 485 nm and emission 520 nm) was monitored via a kinetic reading at 37ºC with 25 cycles of 20 flashes/well with a cycle time of 150 s. Orbital shaking (10 s at 200 rpm) was included

before each cycle. Data was recorded as relative fluorescence units (RFU)/min and is presented as the endpoint reading (RFU).

RAW 264.7 cell migration assays

RAW264.7 cells were obtained from ATCC (Manassas, VA, USA) and maintained in growth media (DMEM, 10% FBS, 100 U/mL penicillin, and 100 µg/mL streptomycin) and passaged as recommended by distributor. For experiments involving the addition of the Ccl2 neutralizing antibody (Figure 3.6C, R&D, Minneapolis, MN, USA), migration assays were performed using clear 8 µm pore ThinCert tissue culture inserts (Greiner, Monroe, NC, USA). 300 µL of cells ($2x10^6$ cells/mL) were placed in the upper chamber of the insert and 500 µL of serum-free media and 100 µl of conditioned adipocyte media (or serum-free media control) was placed in the lower chamber. Adipocyte-conditioned media was incubated with anti-Ccl2 antibody (20 µg/mL) for 2 h with gentle shaking prior to initiation of the migration assay. Cells were allowed to migrate for 4 h and then the inserts were washed in PBS and cells present in the upper chamber removed by scraping with a Q-tip. Cells were fixed in ice-cold methanol for 10 min at -20ºC and then stained with 1 mg/mL Hoescht 33258 (Biotium, Hayward, CA, USA) for 30 min in the dark. Membranes were mounted onto glass slides using Fluoromount aqueous mounting medium (Sigma, Oakville, ON, USA) and imaged using an Axiovert 200M fluorescent microscope (Zeiss, Toronto, ON), Orca R2 C10600 camera (Hamamatsu, Boston, MA, USA), and AxioVision 4.8 software (Zeiss). Approximately 10 random images were taken per slide. All images were taken at the same exposure and cells on the lower side of the membrane were counted manually.

For experiments involving the addition of Bay-7082 (Figure 3.8E), migration assays were performed using FluoroBlok 8um cell culture inserts (Corning, Corning, NY, USA). 300uL of cells ($2x10^6$ cells/mL) were placed in the upper chamber of the insert and 700 µL of serum-free media and 100 µL of conditioned adipocyte media or control (serum-free media) was placed in the lower chamber. Cells were allowed to migrate for 8 h. Membranes were washed with PBS and stained with 2.5 µM Calcein AM (Invitrogen, Burlington, ON) in PBS for 1 h at 37ºC. Inserts were then placed in fresh PBS and imaged using a FLUOStar Omega plate reader (BMG LabTech, Cary, NC, USA). The

fluorescence (excitation 485 nm, emission 520 nm) of each insert was read using a 30x30 scan matrix and 10 flashes per scan point. The average RFU of each well was normalized to vehicle control to determine the relative number of migrated cells.

Analysis of NFkB activity

In order to monitor NFkB signalling pathway activity in mature MSC-derived adipocytes, a stable NFkB-luciferase reporter MSC line was generated. MSCs (30000 cells per well, 12-well plate) were transduced with 30 µL of Cignal Lenti NFkB Reporter (SA Bioscience, Toronto, ON) in growth media containing 6 µg/mL hexadimethrine bromide (Sigma Aldrich, Oakville, ON). 48 h following transduction, fresh media containing 5 µg/mL puromycin dihydrochloride (Santa Cruz, Dallas, TX, USA) was replaced to select for positive transformants. After 72 h in selection media, cells were plated at a low density to isolate single NFkB-luciferase colonies. Clones were tested for NFkB reporter activity using LPS stimulation as well as the ability to differentiate into adipocytes, and an optimal NFkB-luciferase MSC cell line was used for all further experiments.

To monitor NFkB activity in SVF-derived adipocytes, mature adipocytes were transduced with 5 µL of Cignal Lenti NFkB Reporter lentivirus (SA Bioscience, Toronto, ON) per well of a 48-well plate in adipocyte differentiation cocktail containing 6 µg/mL hexadimethrine bromide. 72 h following transduction, fresh media/treatment was replaced as indicated and NFkB activity assessed.

For both MSC and SVF-derived adipocytes, cells were lysed in 100 µL of Reporter Lysis Buffer (Promega, Madison, WI, USA) with shaking for 5 min and then frozen at -80ºC. Thawed lysate was transferred to a 0.5 mL tube and spun for 5 min at 13000 rpm. To estimate protein concentration, cleared lysate (diluted 1:10 in distilled water) or dilutions of bovine serum albumin (assay standard) was mixed with a 1:40 dilution of Protein Assay Dye Reagent (BioRad, Mississauga, ON). The sample was incubated for 5 min at RT and then the absorbance read at A_{595} using a FLUOStar Omega plate reader (BMG LabTech, Cary, NC, USA). To determine levels of NFkB activity, 80 µL of luciferase reagent (Promega) was added to 10 µL of cleared supernatant in a white 96-well plate and luminescence measured using a FLUOStar Omega plate reader (BMG

LabTech, Cary, NC, USA). Relative light units (RLU) were normalized to total protein concentration and fold change calculated relative to vehicle control.

Ccl2-luciferase reporter constructs

DNA sequences containing the proximal -5800/+10 region of the mouse Ccl2 promoter were amplified from genomic DNA isolated from C57/Bl6 ear clips using the DNeasy tissue/blood kit (Qiagen, Valencia, CA, USA). Primer sequences (Table 3.1) included 5' MluI and 3' NheI restriction sites. Putative NFkB response elements (consensus sequence GGGRNNYYCC) were identified in this region. PCR was performed using Takara ExTaq DNA Polymerase (Clontech, Mountain View, CA, USA) according to manufacturer's recommendations (optimized to include 0.3 μM primers, 500ng template, and cycling conditions of 98ºC for 30 sec, and cycles of 98ºC for 10 s, 55ºC for 30 s and 72ºC for 5.5 min). Amplified products were directionally cloned into pGL3-basic (Promega, Madison, WI, USA) using MluI and NheI restriction sites.

For functional testing, NFkB-luciferase plasmid or Ccl2-luciferase plasmid were transfected into Cos7 cells using PEI (Sigma, Oakville, ON). Briefly, 20000 cells/well were plated in a 48-well plate and transfected with 100 ng mCMKLR1 or pBSK, 100 ng of luciferase construct, and 50 ng of ß-gal. The following day, cells were treated with 50 ng/mL of mouse TNFα and/or 30 nM recombinant mouse chemerin (aa 17-156) in Optimem. After 24 h, cells were lysed and luminescence detected as described above. RLU were normalized to ß-gal activity and fold change calculated relative to pBSK vehicle control.

Inducible chemerin knockdown

Inducible Piggybac transposase shRNA constructs and stable Piggybac-chemerin shRNA expressing MSCs were generated as previously described (Chapter 2). Mature adipocytes were treated for 4 d with 10x cumate solution before cell lysis and RNA isolation.

L1.2 migration assay

The L1.2 migration assay was performed as previously described (Goralski et al. 2007; Rourke et al. 2015). Murine pre-B lymphoma CMKLR1-expressing L1.2 cells were maintained in growth media (RPMI 1640 with 10% FBS, 10 mM HEPES, 1mM sodium pyruvate, and 10 mM non-essential amino acids). Cells ($1x10^6$ cells/mL) were treated overnight with 1 mM butyric acid. The next day, $5x10^6$ cells/mL were pre-labelled with 2.5 µM Calcein AM (Invitrogen, Burlington, ON) for 1 h at 37ºC. Cells were then resuspended at a concentration of $2.5x10^6$ cells/mL in chemotaxis media (RPMI 1640 with 1% FBS). 100 µL of cells were added to the upper chamber of a 5 µm pore transwell insert (Corning, Corning, NY, USA). 600 µL of the indicated treatment was added to the lower chamber and cells were allowed to migrate for 4 h at 37ºC. Cells present in the lower chamber were centrifuged at 13000 rpm, resuspended in 100 µl of PBS, and the fluorescence measured at 485 nm excitation/520 nm emission using a FLUOStar Omega plate reader (BMG LabTech, Cary, NC, USA).

Concentration of chemerin using spin columns

Mature MSC-derived adipocytes were washed in warm serum-free media and incubated in fresh serum-free media for 24 h. The next day, conditioned media was collected and filtered through a 10 kDa or 100 kDa centrifugal filter column (EMD Millipore Microcon, Pittsburgh, PA, USA). 1500 µL of adipocyte-conditioned media was filtered through each column by spinning at 10000 rpm for 10 min (100 kDa filter) or 30 min (10 kDa filter) in 500 µL increments. Following centrifugation, ~150 µL of media remained on the top portion of the 10 kDa filter. The concentrated proteins on top of the 100 kDa filter were resuspended in 150 µL of serum-free media. 10x concentrated samples were immediately transferred to cells for further analysis or frozen at -20ºC until Western blot analysis.

Chemerin immunoprecipitation

Mature adipocytes were washed two times in warm serum-free media and then incubated for 24 h with fresh serum-free media. Conditioned adipocyte media was stored in aliquots at -80ºC until immunoprecipitation. Briefly, 1 mL of conditioned adipocyte

media was incubated with 100 µl of RIPA buffer (1% NP-40, 0.5% sodium deoxycholate, 0.5% SDS, 150 mM NaCl, 50 mM Tris, 1 mM EDTA, pH 8.0) and 0.5 µg of anti-mouse chemerin antibody or IgG control (R&D, Minneapolis, MN, USA) at RT with shaking for 1 h. 100 µL of protein G agarose slurry (reconstituted at 10% w/v in distilled water) was added to each tube and incubated overnight with shaking at 4ºC. The next day, media was spun at 13000 rpm for 1 min, and the supernatant transferred to a fresh tube. The pellet was washed three times with PBS and then resuspended in 40 µL of 6x SDS-PAGE buffer. Supernatant and pellets were stored at -20ºC until further analysis.

Silver staining

Silver staining was performed in order to isolate chemerin for mass spectrometry sequencing analysis. Recombinant mouse chemerin (aa 17-156, R&D, Minneapolis, MN, USA) or immunprecipitated chemerin from conditioned adipocyte media was separated using SDS-PAGE on a Novex 14% Tris-glycine gel (Invitrogen, Burlington, ON). The gel was washed in distilled water for 30 min, and then washed in a 45% methanol/ 5% acetic acid solution for 20 min. The gel was then sensitized with 0.02% sodium thiosulphate for 2 min, rinsed in water twice, and incubated in chilled 0.1% silver nitrate for 20 min. After rinsing, the gel was developed in 2% sodium carbonate/0.04% formaldehyde solution. Images of the gel were captured with a Powershot SD700IS (Canon, Melville, NY, USA) and silver-stained gels were stored in 1% acetic acid at 4ºC until further analysis.

Mass spectrometry

Recombinant mouse chemerin (aa 17-156) or chemerin immunoprecipatated from adipocyte-conditioned media was subjected to SDS-PAGE analysis under denaturing conditions. Bands (~1 mm by 4 mm) were excised from silver-stained gels using gel cutting pipette tips, transferred to a clean microcentrifuge tube, and stored at -80ºC until mass spectrometry analysis. Gel bands were prepared as described previously (Shevchenko et al. 2006). Briefly, gel bands were reduced with 10 mM dithiothreitol for 30 min at 56ºC, alkylated with 55 mM iodoacetamide for 30 min at RT, and digested with trypsin (Promega, Madison, WI, USA) or Lys-C (Pierce, ThermoFisher Scientific,

Burlington, ON) for 12 h at 37ºC. Peptides were then extracted in 100 µL of a 50% acetonitrile: 5% formic acid solution, extracts dried using vacuum centrifugation (SPD SpeedVac Thermo Electron Corp., Waltham, MA), and resuspended in 20 µL of a 3% acetonitrile: 0.5% formic acid solution. Liquid chromatography-tandem mass spectrometry (LC-MS/MS) was performed using a nano flow liquid chromatography system (Ultimate3000, ThermoScientific, Burlington, ON) interfaced to a VelosPro hybrid ion trap-orbitrap high resolution tandem mass spectrometer (ThermoScientific) operated in data dependent acquisition mode. 1 µL of each sample was injected onto a C18 Onyx Monolithic capillary column (0.1 x 150 mm, Phenomenex, Torrance, CA, USA) with a flow rate of 300 nL/min. Samples were electro-sprayed at 1.2 kV using a dynamic nanospray probe with fused silica non-coated emitters. Chromatographic separation was performed using 90 min linear gradients (mobile phase A: 0.1% formic acid in water; mobile phase B: 0.1% formic acid in acetonitrile) from 3% B to 35% B over 60 min, and then increasing to 95% B over 5 min. MS/MS spectra were acquired using both collision-induced dissociation (CID) and higher-energy collisional dissociation (HCD) for the top 15 peaks in the survey 30000-resolution MS scan. Files were acquired using Xcalibur software (ThermoScientific) and exported to Proteome Discoverer 2.0 software (ThermoScientific). Peptide and protein identification was performed using SequestHT search algorithm (semi- tryptic or LysC digests with 2 maximum missed cleavages, 20 ppm precursor mass tolerance, and 0.8 Da fragment mass tolerance). The resulting MS/MS spectra were searched using the UniProt full mouse and the common repository of adventitious proteins (cRAP) databases. After further analysis, peptides corresponding to mammalian keratin, trypsin, or LysC were removed. The threshold for protein identification was the detection of at least 3 unique peptides.

For multiple reaction monitoring (MRM) of chemerin peptides in adipocyte-conditioned media, proteins were precipitated from adipocyte-conditioned media (no IP) using acetone precipitation. Briefly, 4x the sample volume of cold acetone was added to conditioned adipocyte media (400 µL). Samples were mixed and incubated for 60 min at -20ºC. Samples were then centrifuged at 13000 rpm for 10 min, the supernatant discarded, and the pellet dried using vacuum centrifugation (SPD SpeedVac Thermo Electron Corp., Waltham, MA) and stored at -20ºC until mass spectrometry analysis.

Protein concentration was estimated prior to acetone precipitation using Protein Assay Dye Reagent (BioRad, Mississauga, ON). To prepare samples for MRM analysis, each sample was resuspended in 200 µL of denaturing buffer (8 M urea, 0.4 M ammonium bicarbonate), sonicated for 15 min, reduced with 25 mM dithiothreitol for 30 min at 60ºC, alkylated with 70 mM iodoacetamide for 30 min at RT, and digested with LysC (Pierce, ThermoFisher Scientific, Burlington, ON) for 12 h at 37ºC. The pH was adjusted to 3 using trifluoroacetic acid (TFA) and solid phase extraction performed using Oasis HLB 3 cc vacuum cartridges (30 µm particle size, Waters Corporation, Milford, MA, USA) with 0.1% TFA column washes and elution in 50 and 80% acetonitrile-0.1% TFA. Extracts were dried using vacuum centrifugation (SPD SpeedVac Thermo Electron Corp., Waltham, MA), and resuspended in 25 µL of resuspension buffer (3% acetonitrile with 0.1% formic acid).

A MRM method was developed using Skyline (MacLean et al. 2010). Table 3.2 contains details of the acquisition method. 1 µL of each sample was subjected to electrospray LC-MS/MS using a nano flow liquid chromatography system (Ultimate3000, ThermoScientific, Burlington, ON) equipped with a C18 Synergi 4 µm Fusion RP80A column (0.3 x 150 mm) (Phenomenex, Torrance, CA, USA). The separation was carried out over the gradients indicated in Table 3.3. The HPLC was interfaced to an AB/SCIEX QTrap 5500 mass spectrometer via a Turbo ionspray source. A potential of 5500 V was applied and the ionization parameters were set to: declustering potential: 30 V; interface heater temperature: 55ºC; curtain gas: 20 psi; collision gas pressure: 12 psi; gas1: 13 psi; gas2: 0 psi. Data were acquired using the MRM method with Analyst 1.6.2 software and analysed using Skyline-daily software.

Generation of adipocytes with stable overexpression of chemerin

MSCs with stable integration of pLJM1-GFP, mouse chemerin (active) or pLJM1-mouse chemerin (pro) were generated as described in chapter 2. Single colonies were isolated and expanded, and all experiments were performed with three independent colonies for each overexpression line. GFP or chemerin overexpression was confirmed by imaging cells and/or western blot analysis of conditioned media, respectively. Stable MSCs were differentiated into adipocytes and treated on day 8 following differentiation

in serum-free media. After 24 h, media was collected and cells were lysed in 350 µL of buffer RLT+ (Qiagen, Valencia, CA, USA) for RNA isolation.

Statistical analysis

All statistical analysis was performed using GraphPad Prism (version 5.0b, La Jolla, CA, USA). Data is represented as mean ± SEM. For parametric data, statistical significance was determined using a two-way unpaired Student's t-test (two groups), one-way ANOVA with Tukey post-test (three+ groups), or a two-way ANOVA with Bonferonni post-test (two factors). Non-parametric data (migration assay counts, Figure 3.6C) were evaluated using a Kruskal-Wallis test with Dunn's multiple comparison post-test.

Results

Characterization of MSC-derived adipocytes

In order to identify novel targets of chemerin signalling in mature adipocytes, a microarray-based discovery approach was used (Figure 3.1). We first isolated and cultured mesenchymal stem cells from the bone marrow of wildtype mice. Colonies derived from single cells were established and differentiated into adipocytes using previously defined adipogenic conditions (Muruganandan et al. 2010). Oil Red O staining of cells throughout the course of differentiation revealed that lipid droplets formed as early as day 2 of differentiation (Figure 3.2A) and were present in the majority of cells. Maximum lipid accumulation was achieved by day 8 of differentiation (Figure 3.2B). qPCR analysis of the MSC cell surface marker CD44 revealed a dramatic decrease in expression as early as day 2, suggesting that very few MSCs or undifferentiated cells remained (Figure 3.2C). The expression of the early adipogenic differentiation markers adipocyte protein (AP2, or fatty acid binding protein 4, FABP4) and adipose differentiation related protein (ADRP, or perilipin 2, Plin2) increased dramatically on day 2 of differentiation and remained ~10-fold higher than undifferentiated cells throughout differentiation (Figure 3.2D). Additionally, expression of the adipocyte markers PPARγ and adiponectin increased throughout differentiation (Figure 3.2D). Considered altogether, this data demonstrates that adipogenic differentiation occurs in a robust and reliable manner using the established MSC lines.

MSC-derived adipocytes express CMKLR1 and secrete high levels of bioactive chemerin

We next investigated the expression of chemerin and chemerin receptors in MSC-derived adipocytes throughout differentiation. qPCR analysis revealed that chemerin mRNA levels increased approximately 50-fold as early as day 2 of differentiation and continued to increase throughout differentiation, reaching peak expression on day 8 (Figure 3.3A). Consistent with this, the expression of CMKLR1 also increased throughout differentiation (Figure 3.3A). There were no changes in the expression of GPR1 or CCRL2 throughout adipogenic differentiation of MSCs (Figure 3.3A).

To further examine the increase in chemerin levels throughout differentiation, western blot analysis of adipocyte-conditioned media was performed. Analysis of

denatured media collected throughout the course of adipocyte differentiation revealed a dramatic increase in the secretion of chemerin from maturing adipocytes (Figure 3.3B). Interestingly, two bands that were very similar in size were observed with the lower, stronger band corresponding in size to recombinant mouse chemerin (aa 17-156). These two bands were also apparent when conditioned adipocyte media was subjected to SDS-PAGE under non-denaturing conditions (Figure 3.3B), suggesting that one or more chemerin isoforms, or potentially modified forms of chemerin, are present in adipocyte-conditioned media.

To determine whether adipocyte-secreted chemerin was bioactive, we applied adipocyte-conditioned medium to the cell-based Tango assay. The Tango assay assesses levels of GPCR activation by measuring ß-arrestin recruitment via the expression of a luciferase reporter gene (Barnea et al. 2008). Treatment of cells expressing both mouse CMKLR1 and GPR1 with adipocyte-conditioned media resulted in reporter activity indicating that adipocyte-secreted chemerin is bioactive. The activation of both CMKLR1 and GPR1 increased significantly when treated with media collected from differentiated adipocytes compared to undifferentiated MSCs (Figure 3.3C). Notably, activation of CMKLR1 (~50-fold) was significantly higher than GPR1 (~2-fold). Considered together, the high level of bioactive chemerin secretion and CMKLR1 expression, suggest that MSC-derived adipocytes are both a source and target of chemerin signalling.

Treatment with mouse chemerin antibody neutralizes adipocyte-secreted chemerin and dramatically alters the expression of numerous genes

To reduce levels of endogenous chemerin signalling, mature MSC-derived adipocytes were treated with a neutralizing chemerin antibody or IgG control (Figure 3.1). To confirm that antibody treatment neutralized chemerin signalling, we transferred 24- or 48 h-conditioned media from adipocytes treated with the chemerin antibody to CMKLR1- or GPR1-expressing cells in the Tango assay (Figure 3.4A,B). As expected, treatment with vehicle or IgG control did not have any effect on chemerin bioactivity but increasing concentrations of chemerin antibody decreased the activation of both CMKLR1 and GPR1. Notably, 48 h conditioned media had approximately 8- and 2-fold

higher activity at CMKLR1 and GPR1 compared to vehicle-treated 24 h conditioned media, respectively, and higher concentrations of chemerin antibody were required to inhibit CMKLR1 activation. Treatment of mature adipocytes with the neutralizing chemerin antibody for 24 or 48 h did not have any effect on cell viability (Figure 3.4C).

In order to identify genes that were differentially regulated in MSC-derived adipocytes following neutralization of endogenous chemerin signalling, Affymetrix microarray analysis was performed. Over 3000 genes were up- or down-regulated following antibody treatment. The expression of genes that were more than 2.5-fold higher or lower compared to IgG control are highlighted in Tables 3.4 and 3.5, respectively.

Mmp3 expression and activity increase following neutralization of chemerin signalling

Matrix metalloproteinase (MMP) 3 was the third most differentially regulated gene identified in the microarray analysis (Table 3.4). Mmp3, or stromelysin-1, is a soluble enzyme that degrades many ECM proteins such as proteoglycans, gelatin, and fibronectin, and contributes to the activation of other MMPs including gelatinases, MMP1, and MMP13 (Fanjul-Fernandez et al. 2010; Klein and Bischoff 2011b; Visse and Nagase 2003). We confirmed the microarray findings using an independent set of primers and observed that 24 h treatment of MSC-derived adipocytes with increasing doses of chemerin antibody resulted in a dramatic dose-dependent increase in Mmp3 expression (Figure 3.5A). This was highest (~100-fold induction) with 100 µg/mL chemerin antibody treatment. Notably, the up-regulation of Mmp3 expression was similar following a 48 h antibody treatment (Figure 3.5B) indicating that Mmp3 up-regulation is maintained over days. Analysis of secreted MMP3 protein levels from 24 h adipocyte-conditioned media revealed the presence of MMP3 following 30 and 100 µg/mL antibody treatment, but not with lower antibody doses (0-10 µg/mL), vehicle (PBS), or IgG control treatments (Figure 3.5C).

We also investigated the expression of other MMPs relevant to adipose tissue and obesity in chemerin antibody-treated adipocytes, including Mmps 2, 9, 10, 11, 12, 13, and 14. qPCR analysis revealed a 50% decrease in both Mmp2 and Mmp11, but no change in the expression of other Mmps examined (Figure 3.5D). Additionally, a 50% decrease in

the expression of the endogenous MMP inhibitor reversion-inducing-cysteine-rich protein with Kazal motifs (Reck), which was identified to be down-regulated following chemerin antibody treatment in the microarray analysis (Table 3.5), was observed following 100 µg/mL chemerin antibody treatment (Figure 3.5D).

MMP3 is secreted in an inactive form and is activated by removal of the prodomain by extracellular enzymes such as serine proteases (Klein and Bischoff 2011a). In order to investigate MMP3 activity in conditioned adipocyte media, we used two different MMP activity assays that involve the cleavage of either general MMP or MMP3/12-specific substrates to fluorescent molecules. We observed a 1.5-fold increase in both general MMP and MMP3/12 activity in 24 h-conditioned media obtained from adipocytes treated with 100 µg/mL of neutralizing chemerin antibody (Figure 3.5E). This indicates that a modest level of MMP3 is activated in adipocyte-conditioned media following neutralization of chemerin signalling.

Neutralization of chemerin signalling in mature adipocytes increases the expression of several chemokines and promotes the recruitment of macrophages via a Ccl2-dependent mechanism

Analysis of the microarray data revealed a large number of chemokines that were up-regulated following chemerin antibody treatment in mature adipocytes (Table 3.4). We confirmed the up-regulation of chemokine (C-C motif) ligand (Ccl) 2, 3, 5, 7, and serum amyloid A (Saa) 2 and 3 expression following antibody treatment using an independent set of primers. qPCR analysis revealed that all of the investigated genes were up-regulated following 24 h chemerin antibody treatment in a dose-dependent manner (Figure 3.6A). We observed the greatest induction in Saa2 and Saa3 expression (50- and 200-fold, respectively), followed by Ccl3, Ccl2, Ccl7, and Ccl5. In contrast to the other chemokines examined, induction of Ccl3 and Ccl5 expression was not maintained following a 48 h treatment of adipocytes with chemerin antibody (Figure 3.6A).

CCL2 is a key mediator of macrophage recruitment to white adipose tissue in obesity (Kanda et al. 2006). Analysis of conditioned media isolated from adipocytes that were treated with 30 or 100 µg/mL of neutralizing chemerin antibody revealed a

substantial increase in secreted CCL2 protein levels (Figure 3.6B). In order to examine whether the observed increase in chemokine secretion influences the chemotaxis of macrophages, we investigated the ability of the murine macrophage RAW264.7 cell line to migrate towards 24 h-conditioned media from adipocytes treated with or without the neutralizing chemerin antibody. We observed a 2-fold increase in the migration of macrophages towards adipocyte-conditioned media compared to control (serum-free media), indicating that a small amount of basal migration occurs towards adipocyte-secreted factors (Figure 3.6C). However, a significantly higher number of macrophages migrated towards conditioned media isolated from adipocytes that were treated with the chemerin antibody. To examine the contribution of CCL2 to this response, we added neutralizing CCL2 antibody to the conditioned media collected from vehicle, IgG, or antibody-treated adipocytes. Neutralization of CCL2 reduced some, but not all, of the increased migration towards conditioned media from chemerin antibody-treated adipocytes (Figure 3.6C). Considered altogether, this indicates that neutralization of chemerin signalling in MSC-derived adipocytes up-regulates the secretion of chemokines that are able to exert paracrine effects on the migration of macrophages, which are mediated, at least in part, through CCL2 signalling.

Up-regulation of Mmp3 and chemokine expression following neutralizing chemerin antibody treatment is mediated through NFkB and CMKLR1 signalling

Previous studies have demonstrated that both Mmp3 and Ccl2 are targets of nuclear factor kappa-B (NFkB) signalling, a signalling pathway that is frequently associated with the regulation of inflammatory gene expression (Ueda et al. 1994; Porter et al. 2012). In order to investigate whether up-regulation of Mmp3 and Ccl2 in MSC-dervied adipocytes following neutralization of chemerin signalling was mediated by an increase in NFkB signalling, we developed a NFkB-luciferase reporter cell line. Treatment of NFkB-luciferase reporter adipocytes with LPS (Figure 3.7A) or TNFα (Figure 3.7B) resulted in a dose-dependent increase in NFkB activity, indicating that MSC-derived adipocytes respond appropriately to known activators of NFkB signalling. A time course revealed that treatment of adipocytes with neutralizing chemerin antibody increased NFkB activity as early as 3 hours following treatment (Figure 3.7C). Further

analysis of NFkB activation following a 6 h chemerin antibody treatment revealed a dose-dependent induction that was significantly increased following 30 and 100 μg/ml antibody treatment (Figure 3.7D). This was consistent with the antibody concentrations that resulted in up-regulation of Mmp3 and Ccl2 expression (Figures 3.5 and 3.6). Co-treatment of adipocytes with chemerin antibody and sub-maximal doses of TNFα and/or LPS revealed a modest additive effect (Figure 3.7E). Interestingly, 3 h (data not shown) or 24 h treatment (Figure 3.7F) of MSC-derived adipocytes with recombinant mouse chemerin (aa 17-156), in both the presence and absence of LPS, had no effect on NFkB activation.

In order to confirm that the chemerin antibody-induced changes in Mmp3 and Ccl2 expression were mediated by an increase in NFkB signalling, we examined the effect of co-treating adipocytes with chemerin antibody and the NFkB inhibitor Bay11-7082. Pre-treatment of adipocytes with Bay11-7082 significantly reduced chemerin antibody-mediated NFkB activation in a dose-dependent manner (Figure 3.8A). Importantly, pre-treatment of adipocytes with Bay11-7082 reduced the induction of Mmp3 and Ccl2 expression following chemerin antibody treatment approximately 3- and 4-fold, respectively (Figure 3.8B,C). This resulted in a significant decrease in MMP3 protein levels compared to chemerin antibody treatment (Figure 3.8D). In addition, pre-treatment of adipocytes with Bay11-7082 before chemerin antibody treatment reduced the increase in macrophage migration towards adipocyte-conditioned media to basal levels (Figure 3.8E). Considered together, this data suggests that neutralization of chemerin signalling increases Mmp3 and chemokine expression through activation of NFkB signalling.

Lastly, we investigated the contribution of CMKLR1 to the observed change in Ccl2 expression. In order to do this, we cloned the mouse Ccl2 promoter, which contains several putative NFkB response elements, and generated a Ccl2 luciferase reporter construct. Expression of the Ccl2 reporter in Cos7 cells expressing pBSK (control) resulted in a stable level of reporter activity, which increased approximately 3-fold following treatment with TNFα (Figure 3.8F). Notably, expression of CMKLR1 reduced expression of the Ccl2 reporter construct ~50%. Similar to pBSK-expressing cells, treatment with TNFα induced Ccl2 reporter activity 3-fold. For both pBSK and

CMKLR1-expressing cells, recombinant chemerin treatment had no effect on Ccl2 reporter activity. This suggests that the observed effects are mediated through CMKLR1 in a TNFα-independent manner.

Neutralization of chemerin signalling in SVF-derived adipocytes increases Mmp3 and chemokine expression and NFkB signalling

In order to examine the effects of chemerin antibody treatment in an independent primary adipocyte model, we generated adipocytes from the stromal vascular fraction (SVF) of subcutaneous WAT. The SVF is a rich source of preadipocytes and *in vitro* differentiation resulted in primary adipocytes that secreted chemerin at similar levels to MSC-derived adipocytes (Figure 3.9A). Conditioned media from SVF-derived adipocytes exhibited bioactivity at CMKLR1 and was neutralized by the addition of chemerin antibody (Figure 3.9B). Similar to MSC-derived adipocytes, treatment of SVF-derived adipocytes with increasing doses of neutralizing chemerin antibody resulted in a dose-dependent increase in Mmp3 expression (Figure 3.9C). Chemerin antibody treatment also increased the expression of several chemokines including Ccl2 and Ccl7 (Figure 3.9C). Interestingly, the induction of chemokine expression was dramatically higher in SVF-derived adipocytes compared to MSC-derived adipocytes (Figure 3.6). Finally, treatment of SVF-derived adipocytes with the neutralizing chemerin antibody resulted in a dose-dependent activation of an NFkB-luciferase reporter construct (Figure 3.9D. In general, the similarities in gene expression and NFkB activation between MSC- and SVF-derived adipocytes following chemerin antibody treatment suggests that the identified mechanisms of chemerin signalling are conserved across the two cell types.

Mmp3 and Ccl2 expression are differentially regulated in white adipose tissue in CMKLR1 KO animals

We next used two alternative approaches to reduce levels of chemerin signalling in MSC-derived adipocytes in order to further confirm the effects observed with chemerin antibody treatment. We first used an inducible chemerin shRNA system in MSC-derived adipocytes to knockdown endogenous chemerin levels. We observed a 40% decrease in chemerin mRNA levels (Figure 3.10A), which was insufficient to alter

Mmp3 or Ccl2 expression (Figure 3.10A). Similarly, treatment of MSC-derived adipocytes with the CMKLR1 inhibitor CCX832 did not have any impact on Mmp3 or Ccl2 expression compared to vehicle or CCX826 control (Figure 3.10B). There was also no change in NFkB activity following treatment with CCX832 (Figure 3.10C). However, analysis of conditioned media from adipocytes treated with CCX832 did not reveal a reduction in levels of CMKLR1 activation in the Tango assay, indicating that inhibitor treatment did not reduce levels of chemerin signalling in mature adipocytes. Together, this data suggests that currently available *in vitro* approaches to decrease endogenous levels of chemerin signalling in mature adipocytes are not robust enough to confirm the effects of the neutralizing chemerin antibody treatment.

As an alternative to modulating chemerin expression in mature adipocytes *in vitro*, we examined Mmp3 and Ccl2 expression in white adipose tissue isolated from wildtype or CMKLR1 knockout (KO) animals at 12 or 30 weeks of age. The body weight of animals included in the study was monitored for 24 weeks starting at 6 weeks of age. While there was no initial difference in body weight between genotypes, CMKLR1 KO mice exhibited significantly less body mass compared to wildtype mice starting at 14 weeks of age. (Figure 3.11A). Dual-energy X-ray absorptiometry (DEXA) analysis revealed that this corresponded with a decrease in fat mass (Figure 3.11B), indicating that the difference in body weight between the two genotypes is due to a difference in adiposity. Analysis of visceral white adipose tissue depots revealed significantly higher expression of Mmp3 and Ccl2 in CMKLR1 KO mice at 30 and 12 weeks of age, respectively (Figure 3.11C).

Recombinant human chemerin or peptide agonists at CMKLR1 and/or GPR1 do not rescue the effect of mouse chemerin antibody treatment

We next attempted to rescue the effects of the neutralizing chemerin antibody by application of commercially available CMKLR1 and/or GPR1 agonists. We first investigated whether the mouse chemerin antibody inhibited the activity of human recombinant chemerin (aa 21-157). As a baseline measure, 10 nM of mouse chemerin was observed to activate both CMKLR1 and GPR1 in Tango assay, and this activation was reduced following the application of the neutralizing chemerin antibody but not

vehicle (PBS) or IgG control (Figure 3.12A). We then co-treated cells with mouse chemerin, neutralizing mouse chemerin antibody, and an increasing concentration of human recombinant chemerin. Interestingly, treatment with 10 or 30 nM of human recombinant chemerin was able to rescue the effect of the chemerin antibody at both CMKLR1 and GPR1 (Figure 3.12A). To further confirm these results, we investigated the impact of the mouse chemerin antibody on human recombinant chemerin in the L1.2 migration assay. Similar to previous studies (Goralski et al. 2007; Rourke et al. 2015), CMKLR1-expressing L1.2 cells migrated towards 1 nM mouse chemerin, and this was reduced to basal levels following addition of the mouse chemerin antibody (Figure 3.12B). Consistent with the results from the Tango assay for CMKLR1 activation, increasing doses of human recombinant chemerin rescued the reduction in migration caused by the addition of chemerin antibody (Figure 3.12B). Together, this indicates that human recombinant chemerin (aa 21-157) is both active and functional in the presence of the neutralizing mouse chemerin antibody. We then tested whether addition of human recombinant chemerin could rescue the changes in gene expression observed in MSC-derived adipocytes following mouse antibody treatment. As expected, the addition of increasing doses of human recombinant chemerin recovered activity at CMKLR1 when adipocyte-conditioned media was transferred to the Tango assay (Figure 3.12C). However, the addition of human recombinant chemerin did not have any influence on the increased expression of Mmp3 or Ccl2 following chemerin antibody treatment (Figure 3.12D).

We then attempted to rescue the effects of the neutralizing chemerin antibody in MSC-derived adipocytes by the addition of synthetic peptides that were previously confirmed to exhibit activity at mouse CMKLR1 or GPR1 (Chapter 2). The addition of hChe9 did not reduce the increase in NFkB activity resulting from chemerin antibody treatment (Figure 3.13A). However, levels of bioactive chemerin in conditioned media isolated from vehicle or IgG-treated adipocytes, which were assessed using the Tango assay for CMKLR1 activation, were only slightly increased following hChe9 treatment. More importantly, hChe9 treatment did not increase levels of CMKLR1 activation in media collected from chemerin antibody-treated cells (Figure 3.13B). Similarly, treatment of adipocytes with Dys10 did not rescue the effect of mouse antibody treatment

on NFkB activity (Figure 3.13C). In contrast to hChe9 treatment, Dys10 treatment significantly increased levels of CMKLR1 activation (Figure 3.13D). This indicates that similar to human recombinant chemerin, Dys10 treatment, while active at CMKLR1 in the Tango assay, does not recover the effect of the neutralizing chemerin antibody treatment on MSC-derived adipocytes. Considered altogether, this suggests that human recombinant chemerin and synthetic peptides are unable to recapitulate the activity of mouse adipocyte-secreted chemerin.

Concentration of conditioned adipocyte media rescues the effect of chemerin antibody treatment

The observation that treatment with both human recombinant chemerin and synthetic peptides did not rescue the effect of the neutralizing chemerin antibody on mouse adipocytes led us to hypothesize that mouse adipocytes secrete a uniquely modified chemerin isoform. This is consistent with Figure 3B, which demonstrates the presence of two bands similar in size that are positive for chemerin immunostaining. In order to test whether adipocyte-secreted chemerin can rescue the effect of the mouse chemerin antibody, we concentrated adipocyte media using a 10 kDa centrifugal filter column (Figure 3.14A). Western blot analysis revealed significantly higher levels of chemerin, including both identified bands, on the upper fraction of the 10 kDa spin column (10T) compared to adipocyte media alone and the bottom fraction (10B) (Figure 3.14B). As a control, concentrating adipocyte media using a 100 kDa centrifugal filter column (100B, 100T) did not result in concentrated levels of chemerin (Figure 3.14B). Consistent with previous results, treatment of adipocytes with the neutralizing chemerin and control media (24 h-conditioned adipocyte media) increased NFkB activity compared to vehicle or IgG control (Figure 3.14C). Treatment with the lower fraction of the 10 kDa spin column, or both fractions from the 100 kDa spin column, had no effect on the induction of NFkB activity compared to control media. However, treatment with concentrated media taken from the upper fraction of the 10 kDa spin column rescued the induction of NFkB activity following chemerin antibody treatment (Figure 3.14C). Analysis of conditioned media isolated from adipocytes treated with the top fraction of the 10 kDa spin column revealed a 3-fold increase in bioactivity at CMKLR1 compared

to control (Figure 3.14D). This was reduced following treatment with the neutralizing chemerin antibody; however, the conditioned media exhibited higher levels of bioactivity compared to control antibody-treated adipocytes. There was also a modest increase in bioactivity in media isolated from adipocytes treated with the bottom fraction of the 100 kDa spin column, although this was neutralized following treatment with the chemerin antibody. The observation that concentrated adipocyte media, which exhibited parallel increases in immunodetectable levels of chemerin and activity at CMKLR1, is able to rescue the effect of the neutralizing chemerin antibody on NFkB activity supports the concept that adipocyte-secreted chemerin is uniquely-modified compared to recombinant human chemerin or synthetic peptides that display activity at the chemerin receptors.

Several different chemerin isoforms are present in adipocyte-conditioned media

We next performed mass spectrometry analysis in order to identify potential differences between adipocyte-secreted chemerin and recombinant chemerin. We first performed LC-MS/MS on recombinant mouse chemerin (aa 21-156) that was digested with trypsin following SDS-PAGE and silver staining. We detected 22 unique peptides that were similar in sequence to mouse chemerin (Figure 3.15A) and ultimately corresponded to 62.35% overall coverage of the mouse chemerin sequence (Table 3.6, Figure 3.15B). Importantly, identification of a peptide corresponding to the sequence IAQAGEDPHGYFLPGQFAFS confirmed the expected C-terminal sequence of recombinant chemerin (Table 3.7).

Silver staining of proteins immunoprecipitated from conditioned adipocyte media using the neutralizing chemerin antibody revealed the presence of only one band that was distinct from proteins immunoprecipitated using an IgG control (Figure 3.15C). This band was similar in size to both recombinant chemerin as well as the only observed band detected by the chemerin antibody in adipocyte-conditioned media (Figure 3.15D). Using the conditions established with recombinant chemerin, in-gel trypsin digestion and LC-MS/MS analysis of the identified band resulted in the detection of 11 unique peptides that corresponded to 55.56% overall coverage of the chemerin sequence, confirming that the identified band is most likely chemerin (Figure 3.15E, Table 3.6, Table 3.7). Unlike recombinant chemerin, LC-MS/MS analysis of adipocyte-secreted chemerin identified

peptides that resulted in coverage of the chemerin sequence to amino acid 155 ('…QFAF') versus 156 ('…QFAFS'; recombinant chemerin), suggesting that there are differences in the C-terminus between recombinant and adipocyte-secreted chemerin.

Chemerin processing at the C-terminus has been shown to generate a variety of chemerin isoforms with differing levels of bioactivity (Rourke et al. 2013; Zabel et al. 2014). As the last 6 amino acids of mouse chemerin contain 3 trypsin cleavage sites (arginine or lysine residues), we digested chemerin with LysC, a more specific enzyme that only cleaves at the carboxyl side of lysine. This was performed in order to generate a longer C-terminal peptide (predicated aa 132-161) to facilitate analysis of the C-terminal sequence of chemerin. LC-MS/MS analysis of LysC-digested recombinant chemerin (aa 17-156) revealed the presence of 12 unique peptides that corresponded to 51.23% coverage of the mouse chemerin sequence (Table 3.6, Figure 3.16A). As predicted, we observed the presence of one unique peptide that corresponded to the expected C-terminal sequence (aa 132-156, '…QFAFS'). In comparison, we observed a higher number of unique peptides (17) and greater sequence coverage (53.09%) following analysis of LysC-digested adipocyte-secreted chemerin. Importantly, we detected a dramatically higher number of peptides that corresponded to the C-terminal chemerin sequence in LC-MS/MS analysis of adipocyte-secreted chemerin, as compared to recombinant chemerin (7 unique peptides versus 1, Table 3.7, Figure 3.16B). The longest peptide (aa 132-161, '…QFAFSRALRT') corresponded to the entire predicted C-terminal sequence of chemerin following complete LysC digestion. The other unique peptides were increasingly truncated by one amino acid, where the shortest peptide detected (aa 132-154, '…QF') was 7 amino acids less than the predicated full peptide. Figure 3.16C demonstrates the acquired MS/MS spectra for peptides ending in amino acids 154 (aa 132-154, '…QF') and 155 (aa 132-154, '…QFA') to highlight the shift in fragmentation pattern with the addition of an additional amino acid and confirm the quality of LC-MS/MS data.

In order to confirm the presence of the various C-terminal peptides in adipocyte-conditioned media, we performed multiple reaction monitoring (MRM). MRM is a sensitive and selective method to monitor a specific collision-induced fragmentation reaction. Multiple reactions are performed sequentially to allow for the detection of

numerous fragment ions (transitions) arising from different peptide precursors. The transitions that we chose to monitor (Table 3.2) were based on the initial LC-MS/MS data. These included fragments derived from peptides that contained the full C-terminal sequence of mouse chemerin (aa 132-162, "…QFAFSRALRTK") and peptides that were sequentially truncated at the C-terminus as previously observed (Figure 3.16), where the shortest peptide monitored was (aa 132-152, "…Q"). We will refer to the peptides as chemerin-x, where x represents the last amino acid in the peptide sequence.

MRM analysis following LysC digestion of proteins precipitated from adipocyte-conditioned media (no IP) demonstrated clearly defined signals for a number of the targeted peptides. Figure 3.17A demonstrates an example of a clear signal, which was defined as the presence of more than 3 individual transitions in a peak, where the peaks exhibited similar retention times across all three samples, and a signal: noise ratio greater than 3. These included fragments derived from peptides corresponding to the C-terminal sequence of chemerin-152, -156, -158, -159, -160, -161, and -162, where as many as 5 different transitions were detected for some peptides (Table 3.8). There were also several peptides for which the product ion spectra revealed more than one peak, as demonstrated in Figure 3.17B. These included peptides derived from chemerin-153, -155, and -157, making it difficult to estimate the presence of these peptides. Additionally, no signal was detected for the peptide derived from chemerin-154.

Importantly, we observed similar results in signal quality and intensity across three independent biological samples. By comparing transition peak height and total peak area, we provide evidence that peptides derived from chemerin-152, -155, -159, and -160 are detected at high levels, peptides derived from chemerin-153, -156, -158, and -162 are detected at moderate levels, and peptides derived from chemerin-157 and -161 are detected at low levels (Table 3.8). In the absence of peptide standards that would allow direct quantification of targeted peptides, our analysis is only semi-quantitative. Additionally, we cannot exclude the presence of undetected peptides. However, based on the available data, we can conclude with confidence that numerous chemerin isoforms are present in adipocyte-conditioned media.

For both recombinant chemerin and adipocyte-conditioned media, we also observed the presence of peptides that are similar in sequence to serum albumin in the

MS/MS spectra (Table 3.6), although this was higher for adipocyte-secreted chemerin (39.04% coverage compared to 14.17% with LysC digestion). In addition, we also observed the presence of 3 unique peptides that were similar to peptide sequences derived from mouse peptidyl-prolyl cis-trans isomerase A, which is similar in size to chemerin at 18 kDa (PPIA), in both trypsin and LysC-digested immunoprecipitated adipocyte media samples. Finally, we observed a small number of peptides corresponding to mouse histone H2B type 1-F and H2A type-1H in LysC-digested, but not trypsin-digested, adipocyte media samples (Table 3.6).

Overexpression of mouse chemerin in MSC-derived adipocytes rescues the effect of the neutralizing chemerin antibody

Finally, in order to determine whether increased levels of adipocyte-secreted chemerin could rescue the effects of the neutralizing chemerin antibody, we overexpressed mouse chemerin-156 (active chemerin, similar sequence to recombinant chemerin), prochemerin, or GFP (control) in MSC-derived adipocytes. In order to do this, we generated MSCs with stable overexpression of GFP, active chemerin, or prochemerin, and differentiated the cells into mature adipocytes (Chapter 2). Consistent with previous results, chemerin antibody treatment of adipocytes with stable overexpression of GFP resulted in a dose-dependent increase in Mmp3 and Ccl2 expression (Figure 3.18A). However, we did not observe any effect of chemerin antibody treatment on the expression of these genes in adipocytes overexpressing either active or prochemerin. This suggests that unlike recombinant chemerin or synthetic peptides, increased levels of endogenously secreted chemerin can rescue the effect of the chemerin antibody treatment. Analysis of adipocyte-conditioned media in the Tango assay for ß-arrestin recruitment to mouse CMKLR1 confirmed 4- and 1.5-fold increased levels of chemerin bioactivity in media isolated from active- and prochemerin-expressing cells, respectively (Figure 3.18B). Interestingly, despite achieving a rescue in Mmp3 and Ccl2 gene expression, the antibody appeared to neutralize bioactive chemerin to similar levels as GFP-expressing cells, suggesting that the chemerin isoform that rescues Mmp3 and Ccl2 expression in the presence of the neutralizing antibody does not induce ß-arrestin recruitment to CMKLR1.

Discussion

During the development of obesity, ECM remodelling and WAT expansion occur in order to prevent ectopic fat deposition in non-adipose tissue organs. While this remodelling is considered healthy in the short-term, in a chronic state of energy excess, this process becomes maladaptive. Common characteristics of pathologic WAT remodelling include the rapid enlargement of existing adipocytes, macrophage infiltration, angiogenesis, ECM overproduction, and the development of chronic inflammation. Our data demonstrates that inhibition of adipocyte-derived chemerin results in a pro-inflammatory phenotype characterized by increased NFkB activity, MMP activity, chemokine expression, and recruitment of immune cells towards adipocyte-secreted factors. We also provide evidence that these effects are mediated through a uniquely modified adipocyte-derived chemerin isoform. Considered altogether, this suggests that mature adipocytes secrete high levels of a chemerin isoform that plays a local protective role against the development of pathogenic adipose tissue remodelling in obesity.

MMPs are a family of approximately 25 enzymes that play a key role in the degradation of ECM components in WAT. Controlled MMP activity is required for proper adipose tissue expansion and dysregulation of MMP function has been implicated in the pathophysiology of obesity and diabetes (Chun et al. 2006; Lijnen et al. 2002; Park and Yoon 2012; Maquoi et al. 2002). In our study, we demonstrated significant up-regulation of Mmp3 expression and secretion from adipocytes following neutralization of endogenous chemerin signalling. Previous studies have demonstrated that Mmp3 expression in also increased in WAT isolated from obese mice compared to lean controls (Chavey et al. 2003; Maquoi et al. 2002; Unoki et al. 2008). Importantly, MMP3 has been shown to play a role in a variety of processes required for adipose tissue remodelling in obesity. For example, MMP3 regulates adipocyte hypertrophy and lipogenesis, and inhibition of MMP3 activity or loss of Mmp3 expression in mice results in increased adipocyte differentiation (Alexander et al. 2001; Meissburger et al. 2011). Collectively, this suggests that MMP3 functions to shift the adipocyte balance to hyperplasia versus hypertrophy, positively influencing the healthy expansion of WAT. Additionally, MMP3 increases expression of pro-inflammatory TNFα from adipocytes

(Unoki et al. 2008), suggesting that Mmp3 expression promotes the negative metabolic consequences of obesity. Consistent with this, we observed increased Mmp3 expression in WAT from CMKLR1 KO mice, which exhibit reduced adiposity, but worsened glucose tolerance, compared to wildtype mice (Ernst et al. 2012). Considered altogether, this suggests that chemerin regulates Mmp3 levels to positively influence adipocyte differentiation and protect against detrimental adipose tissue expansion.

MMP3 is secreted as an inactive zymogen and requires extracellular processing to an active form. Western blot analysis of adipocyte-secreted MMP3 revealed high levels of latent MMP3 (57-66 kDa) compared to the active form (28 or 48 kDa). Despite the ~100-fold increase in gene expression following chemerin antibody treatment, we observed low levels (1.5-fold) of MMP3 activation by mature adipocytes. It is possible that adipocyte secretion of MMP3-activating enzymes is a limiting factor in Mmp3 activation. Alternatively, the presence of endogenous MMP3 inhibitors, such as tissue inhibitors of metalloproteinases (TIMP) 1-4, or the weak MMP3 inhibitor, amyloid precursor protein-derived inhibitory peptide (for review, see (Higashi and Miyazaki 2003; Baranger et al. 2014)), may limit MMP3 activation in adipocyte cultures. Our microarray results highlighted decreased expression of Reck, an endogenous MMP inhibitor that is specific for MMPs 2, 9, and 14 (Miki et al. 2007; Takagi et al. 2009), indicating that regulation of Mmp activity at both the enzyme and inhibitor level occur in our adipocyte model. Further analysis of MMP3 activation as well as the expression of endogenous inhibitors will be valuable to fully understand the regulation of MMP activity by chemerin signalling in mature adipocytes.

The role of chemerin signalling on Mmp3 expression may extend beyond adipocytes. As MMP3 is a secreted protein, increased levels of Mmp3 secretion from adipocytes might exert paracrine effects within WAT. While our data suggest that the adipocyte-secreted MMP3 is largely inactive, the secretion of activating proteases by other cell types in WAT, such as those present in the SVF, could result in MMP3 activation *in vivo*. Consistent with this, Mmp3 expression is altered in SVF isolated from WAT of obese humans (Meissburger et al. 2011; Traurig et al. 2006). Furthermore, chemerin signalling mediates MMP expression in other cell types, including chondrocytes, endothelial cells, MSCs, and gastric cancer cells, with effects on cellular

processes such as inflammation, vascular remodelling, and cell invasiveness (Berg et al. 2010; Kaur et al. 2010; Kumar et al. 2014; Wang et al. 2014). This suggests that increased levels of circulating chemerin in obesity might contribute to the pathogenesis of a number of diseases through effects on Mmp expression and activity.

A growing body of literature supports a role for chemerin in inflammatory diseases, with studies showing both pro- and anti-inflammatory effects of chemerin in different disease contexts. In addition to mediating changes in the size, shape, and structural integrity of WAT, alterations in ECM composition facilitates the infiltration of cells in WAT during obesity. We demonstrated that inhibition of chemerin signalling in both MSC- and SVF-derived adipocytes increases the expression of numerous chemokines and increases the recruitment of macrophages towards adipocyte-derived factors. Specifically, we demonstrated that the migration of macrophages towards adipocyte-secreted factors was largely dependent on CCL2, a chemokine that plays an important role in the accumulation of monocytes in WAT during obesity (Kanda et al. 2006; Sell and Eckel 2007). However, neutralization of CCL2 did not completely restore levels of macrophage migration to basal, suggesting that the regulation of other chemokines by chemerin signalling also plays a functional role in macrophage recruitment.

Although chemerin has a well-established role as a chemoattractant for a number of immune cells including macrophages (Hart and Greaves 2010; Wittamer et al. 2003), our data suggests that the adipocyte-derived chemerin isoform(s) that influences chemokine expression in adipocytes is different to the chemerin isoforms that promote chemotaxis. Consistent with this, chemerin has been shown to play an anti-inflammatory role in an acute lung injury model, resulting in reduced neutrophil infiltration (Luangsay et al. 2009). Furthermore, similar to our results, chemerin has been shown to play a protective role in allergic asthma by suppressing the recruitment of immune cells through inhibition of CCL2 production (Zhao et al. 2014). As such, it will be valuable to assess the influence of these chemokines, as well as the impact of increased chemokine secretion on the recruitment of cell types other than macrophages. *In vivo* data suggests that CMKLR1 knockout mice exhibit reduced CD3+ T cell migration and increased natural killer cell migration to WAT on a high-fat diet (HFD) (Ernst et al. 2012). It is

worth noting that a previous study reported a very minor decrease in macrophage accumulation in WAT in young, healthy chemerin KO mice (Takahashi et al. 2011). Taken together, this suggests that the role of chemerin signalling in immune cell recruitment is likely context-dependent. Therefore further studies that independently assess macrophage recruitment in WAT and investigate the role of chemerin signalling in obese conditions are essential. Finally, as chemerin has been shown to influence macrophage adhesion and polarization (Hart and Greaves 2010; Lin et al. 2014), studies that address whether chemerin signalling affects the inflammatory status and function of immune cells in WAT will provide further insight into the paracrine regulation of immune cells by adipocyte-derived chemerin.

Healthy WAT expansion is associated with the enhanced recruitment of adipocyte precursor cells that are differentiated into new, small adipocytes, with subsequent vascularization, and minimal induction of ECM production and inflammation. Chemerin expression is regulated by adipocyte hypertrophy (Bauer et al. 2011) and previous studies have demonstrated that chemerin signalling promotes adipogenic differentiation and angiogenesis (Bozaoglu et al. 2010; Goralski et al. 2007; Kaur et al. 2010), suggesting that chemerin acts to promote healthy WAT expansion. Our observations that inhibition of chemerin signalling enhances changes commonly observed in pathogenic WAT remodelling further supports the notion that chemerin signalling plays a protective role against maladaptive WAT expansion. Interestingly, our microarray results also identified a number of genes that were down-regulated following neutralization of chemerin signalling that may play additional roles in WAT remodelling (Table 3.5). These include glucose transporter type 4 (Glut4), carboxylesterase 3 (Ces3), and mesoderm specific transcript (Mest), which are involved in glucose uptake, lipid storage, and regulation of adipocyte size, respectively (Takahashi et al. 2005; Dominguez et al. 2014). Further studies that directly investigate the role of these genes and the function of chemerin in WAT remodelling will be valuable for the development of novel therapeutics to prevent pathologic WAT remodelling.

Obesity activates inflammation through the IKKß/NFkB signalling pathway, which is a central mediator of inflammatory and stress responses (Carlsen et al. 2009; Cai et al. 2005; Arkan et al. 2005). We demonstrated that the effects of chemerin

neutralization on Mmp3 secretion and macrophage recruitment were mediated through an NFkB-dependent pathway, identifying a novel mechanism for regulation of NFkB signalling in WAT. Importantly, our data supports an anti-inflammatory role for chemerin signalling in mature adipocytes. Previous reports demonstrate that suppression of IKKß/NFkB-dependent inflammation via genetic deletion of IKKß or pharmacological inhibition improves obesity-induced insulin resistance and glycemic control in humans and animal models (Yuan et al. 2001; Goldfine et al. 2008; Lee and Lee 2014). This suggests that enhancement of chemerin signalling in adipocytes represents a novel therapeutic avenue to prevent or treat the onset of obesity-associated diseases. Previous studies have demonstrated conflicting results on the role of chemerin signalling on NFkB activation, with one study showing increased NFkB activation in skeletal muscle cells (Sell et al. 2009) and another showing suppression of NFkB signalling in vascular endothelial cells (Yamawaki et al. 2012). This suggests that the effects of chemerin signalling on NFkB activity might be cell type dependent and further studies that determine the mechanisms that underlie regulation of NFkB activity are essential to develop more specifically targeted treatments for inflammation via modulation of chemerin signalling. It is also possible that other signalling pathways contribute to the chemerin antibody-mediated effects, as treatment with the NFkB inhibitor did not reduce Mmp3 and chemokine expression to basal levels. To date, our understanding of chemerin signalling in adipocytes is limited to the observations that chemerin stimulation increases extracellular signal-regulated protein kinases (ERK) 1/2 phosphorylation (Goralski et al. 2007; Roh et al. 2007) and tyrosine phosphorylation of insulin receptor substrate (IRS)-1 (Takahashi et al. 2008). Therefore, future studies that investigate additional mechanisms of chemerin signalling in adipocytes will be valuable to fully elucidate the mechanisms through which chemerin signalling regulates inflammation and WAT remodelling.

An intriguing aspect of this study was the observation that treatment with recombinant chemerin or synthetic CMKLR1/GPR1 agonists was not able to rescue the effect of the neutralizing antibody treatment. This was particularly surprising as conditioned media isolated from adipocytes treated with the chemerin antibody and either recombinant human chemerin or Dys10 maintained bioactivity at CMKLR1. While we

cannot rule out the possibility that the chemerin antibody exhibited non-specific effects, we provide strong evidence that this is unlikely. In particular, mass spectrometry analysis of proteins immunoprecipitated from conditioned adipocyte media using the chemerin antibody identified chemerin with high confidence. This was based on the number of unique peptides identified, percent sequence coverage, and the quality of the MS/MS spectra, with similar results achieved following both trypsin and LysC digestion. The only other protein hits were albumin and histone proteins, which are common non-specific matrix-binding contaminants in protein interaction studies (Mellacheruvu et al. 2013), and PPIA, which is the same size as chemerin and therefore not surprising to be found in the same gel fragment. Furthermore, expression of CMKLR1 decreased Ccl2 reporter expression, suggesting that the observed effects are mediated through a chemerin receptor. Finally, both concentration of adipocyte-conditioned media and overexpression of endogenous adipocyte-secreted chemerin rescued the effect of the antibody. Altogether, this indicates that the observed effects are mediated via chemerin signalling, and that adipocyte-secreted chemerin is likely modified in a unique manner compared to commercially available forms and synthetic peptides.

A potential explanation for the observed differences between recombinant chemerin and adipocyte-derived chemerin is extracellular processing at the C-terminus. Previous studies have identified numerous chemerin isoforms in human inflammatory fluids and that adipocytes express enzymes capable of bioactivating chemerin (Parlee et al. 2012; Rourke et al. 2013). However, this is the first study to directly demonstrate the presence of multiple chemerin isoforms in adipocyte-conditioned media. This is consistent with the observation of two bands very similar in size following western blot analysis of conditioned adipocyte media. Our data is limited to a semi-quantitative analysis and future studies with labeled peptides to directly quantify the abundance of chemerin isoforms will be valuable. However, our data suggests that chemerin-152, 155, 159, and 160 are present in high amounts. Previous studies using chemotaxis or intracellular calcium release assays have suggested that chemerin 152 is inactive, chemerin-155 has relatively low bioactivity, and no data exists regarding the bioactivity of chemerin-159 and -160 (Rourke et al. 2013). It is possible that an isoform with low activity with regard to these measures may exhibit strong activity for an alternate

pathway such as NFkB signalling. Future studies that determine whether particular isoforms are responsible for mediating NFkB activity and the expression of target genes such as Mmp3 and Ccl2 in mature adipocytes will be valuable. Interestingly, the chemerin isoform that is most similar to the highly bioactive recombinant chemerin, chemerin-156, was present in very low amounts in adipocyte-conditioned media. Furthermore, addition of recombinant chemerin did not influence NFkB activity. This suggests that a difference in the distribution and/or function of various chemerin isoforms might be responsible for the observed discrepancies between endogenous chemerin and commercial forms.

There are several biological implications of the presence of multiple chemerin isoforms in adipocyte-conditioned media. Firstly, as suggested above, different chemerin isoforms might activate different signalling pathways. In addition, inactive isoforms might act as antagonists at chemerin receptors. This highlights the need for additional assays to measure levels of chemerin bioactivity beyond ß-arrestin recruitment or calcium release. Additionally, future studies that investigate the properties of various chemerin isoforms with respect to adipocyte function, inflammation, and other cellular processes, will be valuable. Importantly, differences in chemerin processing and the distribution of chemerin isoforms might explain differences in reported pro- versus anti-inflammatory properties of chemerin signalling. As the majority of studies examine commercially available chemerin-157, this highlights the need to generate and study function of other isoforms. Furthermore, it will be interesting to examine whether the distribution of chemerin isoforms differs following treatment with other signalling or inflammatory mediators. The production of chemerin-activating enzymes such as elastase and tryptase increase following TNFα treatment of adipocytes, suggesting that chemerin isoform distribution, and consequently, function, might be altered in inflammatory conditions (Parlee et al. 2012). In addition, studies that investigate chemerin isoform distribution in disease states such as obesity will be valuable. Current studies are limited to measuring total chemerin levels by ELISA, or bioactivity using the Tango assay, and our study suggests that isoform distribution and other biological endpoints of chemerin signalling may play important roles in the contribution of chemerin signalling to the development of disease.

Alternatively, we cannot exclude other possible reasons for the observed difference in activity between adipocyte-derived chemerin and recombinant forms. Beyond proteolytic cleavage, we have a very limited understanding of the post-translational modifications that are associated with chemerin processing. We did not observe evidence of common post-translational modifications (PTMs), including oxidation (methionine residues), phosphorylation (serine, threonine, or tyrosine residues), dyhydration (serine), and acetylation (histidine, lysine, or serine residues) (data not shown) on adipocyte-secreted chemerin. However, we cannot rule out the possibility that adipocyte-derived chemerin is modified compared to bacterially expressed recombinant chemerin. Additionally, the presence of PTMs could explain why overexpression of endogenous chemerin-156 but not recombinant chemerin rescued the effects of chemerin antibody treatment on Mmp3 and Ccl2 expression. Future studies that directly investigate the presence of PTMs in chemerin will be important to fully elucidate the role of chemerin signalling in adipocytes and numerous other cell types.

It is important to note that there are several limitations of this study. Firstly, while similar results were obtained with two different primary adipocyte models, these were both relatively healthy adipocytes and cultured in an isolated cell system. The role of chemerin signalling might be altered in inflammatory conditions such as obesity. In addition, chemerin isoform distribution might be altered with disease conditions or in the presence of other cell types in WAT, such as immune cells, fibroblasts, and preadipocytes, which also secrete proteases that can alter chemerin bioactivity. Future studies that address the role of chemerin signalling within WAT, and the impact of chemerin signalling on other cell types within WAT, will be valuable to understand the role of chemerin signalling in a complex environment such as WAT. Furthermore, due to the lack of specific inhibitors for chemerin receptors and inefficiency of knockdown in mature adipocytes (Chapter 2), we are unable to directly assess which receptor(s) are responsible for the observed effects of chemerin signalling in adipocytes. However, we provide strong evidence that the effects are mediated at least in part through CMKLR1, which exhibited a parallel increase in expression similar to chemerin throughout adipocyte differentiation. In addition, CMKLR1 expression decreased Ccl2 reporter activity and WAT isolated from CMKLR1 KO mice exhibited increases in Mmp3 and

Ccl2 expression. However, it is possible that other receptors play a role in mature adipocytes, highlighting a need for better tools to modulate chemerin receptor expression and delineate receptor-specific effects.

In summary, we provide novel evidence that adipocyte-secreted chemerin is modified to multiple isoforms and that inhibition of adiopcyte-derived chemerin results in a pro-inflammatory phenotype characterized by increased NFkB activation, MMP3 activity, and macrophage recruitment towards adipocyte-secreted factors. This suggests that with obesity, increased chemerin levels play a protective role in WAT remodelling. Importantly, as chemerin, Mmps, and chemokines are all secreted factors, these biological events may also influence systemic processes. Future studies that explore the importance of specific adipoycte-derived chemerin isoforms in WAT, and further elucidate the signalling pathways downstream of chemerin receptor activation, will be valuable for the development of novel therapeutics for the prevention and treatment of obesity and associated diseases.

Tables and figures

Table 3.1. Primer sequences used for cloning and qPCR analysis

All sequences indicated are mouse.

Primer	Forward Sequence (5'-3')	Reverse Sequence (5'-3')
Cloning:		
Mcp1-luc cloning	AAAAACGCGTCAGGTCAAGGCCCG GCTTTGTTA	AAAAGCTAGCTGGCTCTCTGCACTT CTGGCTGCT
Mcp1-luc colony PCR	AGAGCCACTCCATTCACACTTGTG	TGGAAGTTGAATCCGCTGAGTAAG
qPCR:		
Adiponectin	AGCCGCTTATATGTATCGCTCA	TGCCGTCATAATGATTCTGTTGG
ADRP	CCCGTATTTGAGATCCGTGTG	CCTTGCAGGCATAGGTATTGG
AP2	GACAGGAAGGTGAAGAGCATC	GTCACGCCTTTCATAACACATTC
Ccl2	AGGTCCCTGTCATGCTTCTG	TCTGGACCCATTCCTTCTTG
Ccl3	GATTCCACGCCAATTCATCG	TTCAGTTCCAGGTCAGTGATG
Ccl5	CAAGTGCTCCAATCTTGCAG	GAAGCGTATACAGGGTCAGAA
Ccl7	TCTCTCACTCTCTTTCTCCACC	GGGATCTTTTGTTTCTTGACATAGC
Ccrl2	CTCTGCTTGTCCTCGTGCTT	GCCCACTGTTGTCCAGGTAG
CD44	TTCATCCCAACGCTATCTGTG	CGAAGGAATTGGGTAGGTCTG
Chemerin	TACAGGTGGCTCTGGAGGAGTTC	CTTCTCCCGTTTGGTTTGATTG
CMKLR1	GCTTTGGCTACTTTGTGGACTT	CAGTGTTCACGGTCTTCTTCATCTTG
CycA	GAGCTGTTTGCAGACAAAGTTC	CCCTGGCACATGAATCCTGG
GPR1	ATTCAGCGCAGGCACCTTTC	CAAGCTGTCGTGGTGTTTGA
Mmp2	ACCAAGAACTTCCGATTATCCC	CAGTACCAGTGTCAGTATCAGC
Mmp3	GATGAACGATGGACAGAGGATG	AAACGGGACAAGTCTGTGG
Mmp9	GATCCCCAGAGCGTCATTC	CCACCTTGTTCACCTCATTTTG
Mmp10	AGAAATGGACACTTGCACCCT	GAAAGGTGGAAGTTAGCTGG
Mmp11	CCTGATGTACTGAATGCCCG	TCCCTTACAAGCTGCCATG
Mmp12	CCCATCTGGTATTCAAGCTGC	TTCACAGATGCAGAGAAGCC
Mmp13	TTGATGCCATTACCAGTCTCC	ACATGGTTGGGAAGTTCTGG
Mmp14	GGATGGACACAGAGAACTTCG	TTTTGGGCTTATCTGGGACAG
PPARγ	TCGCTGATGCACTGCCTATG	GAGAGGTCCACAGAGCTGATT
Reck	TCCTTCCCTCTCAGCCATAG	CCGTAACATCCCAGCACATAG
Saa2	ACTATGATGCTGCCCAAAGG	ATGTCTGTTGGCTTCCTGG
Saa3	TCTTTGCATCTTGATCCTGGG	CGAGCATGGAAGTATTTGTCTG

Table 3.2. MRM acquisition method details

The following mouse chemerin (UniProt Q9DD06) peptide fragments, based on LysC digestion, were monitored.

Precursor (m/z)	Product (m/z)	Dwell time (ms)	Peptide sequence	Fragment	Charge
720.125	782.368	20	IAQAGEDPHGYFLPGQFAFSRALRTK	b8	+4
720.125	919.427	20	IAQAGEDPHGYFLPGQFAFSRALRTK	b9	+4
720.125	976.448	20	IAQAGEDPHGYFLPGQFAFSRALRTK	b10	+4
720.125	1139.512	20	IAQAGEDPHGYFLPGQFAFSRALRTK	b11	+4
720.125	1049.621	20	IAQAGEDPHGYFLPGQFAFSRALRTK	y9	+4
720.125	978.584	20	IAQAGEDPHGYFLPGQFAFSRALRTK	y8	+4
720.125	831.516	20	IAQAGEDPHGYFLPGQFAFSRALRTK	y7	+4
720.125	744.484	20	IAQAGEDPHGYFLPGQFAFSRALRTK	y6	+4
917.133	919.427	20	IAQAGEDPHGYFLPGQFAFSRALRT	b9	+3
917.133	976.448	20	IAQAGEDPHGYFLPGQFAFSRALRT	b10	+3
917.133	1139.512	20	IAQAGEDPHGYFLPGQFAFSRALRT	b11	+3
917.133	1196.653	20	IAQAGEDPHGYFLPGQFAFSRALRT	y10	+3
917.133	1068.595	20	IAQAGEDPHGYFLPGQFAFSRALRT	y9	+3
917.133	921.526	20	IAQAGEDPHGYFLPGQFAFSRALRT	y8	+3
883.450	919.427	20	IAQAGEDPHGYFLPGQFAFSRALR	b9	+3
883.450	976.448	20	IAQAGEDPHGYFLPGQFAFSRALR	b10	+3
883.450	1139.512	20	IAQAGEDPHGYFLPGQFAFSRALR	b11	+3
883.450	1152.627	20	IAQAGEDPHGYFLPGQFAFSRALR	y10	+3
883.450	1095.606	20	IAQAGEDPHGYFLPGQFAFSRALR	y9	+3
883.450	967.547	20	IAQAGEDPHGYFLPGQFAFSRALR	y8	+3
662.840	685.315	20	IAQAGEDPHGYFLPGQFAFSRALR	b7	+4
662.840	782.368	20	IAQAGEDPHGYFLPGQFAFSRALR	b8	+4
662.840	919.427	20	IAQAGEDPHGYFLPGQFAFSRALR	b9	+4
662.840	976.448	20	IAQAGEDPHGYFLPGQFAFSRALR	b10	+4
662.840	1095.606	20	IAQAGEDPHGYFLPGQFAFSRALR	y9	+4
662.840	967.547	20	IAQAGEDPHGYFLPGQFAFSRALR	y8	+4
662.840	820.479	20	IAQAGEDPHGYFLPGQFAFSRALR	y7	+4
662.840	749.442	20	IAQAGEDPHGYFLPGQFAFSRALR	y6	+4
831.417	919.427	20	IAQAGEDPHGYFLPGQFAFSRAL	b9	+3
831.417	976.448	20	IAQAGEDPHGYFLPGQFAFSRAL	b10	+3
831.417	1139.512	20	IAQAGEDPHGYFLPGQFAFSRAL	b11	+3
831.417	1093.579	20	IAQAGEDPHGYFLPGQFAFSRAL	y10	+3
831.417	996.526	20	IAQAGEDPHGYFLPGQFAFSRAL	y9	+3
831.417	939.505	20	IAQAGEDPHGYFLPGQFAFSRAL	y8	+3
623.814	685.315	20	IAQAGEDPHGYFLPGQFAFSRAL	b7	+4
623.814	782.368	20	IAQAGEDPHGYFLPGQFAFSRAL	b8	+4
623.814	919.427	20	IAQAGEDPHGYFLPGQFAFSRAL	b9	+4
623.814	976.448	20	IAQAGEDPHGYFLPGQFAFSRAL	b10	+4
623.814	996.526	20	IAQAGEDPHGYFLPGQFAFSRAL	y9	+4
623.814	939.505	20	IAQAGEDPHGYFLPGQFAFSRAL	y8	+4
623.814	811.446	20	IAQAGEDPHGYFLPGQFAFSRAL	y7	+4
623.814	664.378	20	IAQAGEDPHGYFLPGQFAFSRAL	y6	+4
793.722	919.427	20	IAQAGEDPHGYFLPGQFAFSRA	b9	+3

Precursor (m/z)	Product (m/z)	Dwell time (ms)	Peptide sequence	Fragment	Charge
793.722	976.448	20	IAQAGEDPHGYFLPGQFAFSRA	b10	+3
793.722	1139.512	20	IAQAGEDPHGYFLPGQFAFSRA	b11	+3
793.722	1093.579	20	IAQAGEDPHGYFLPGQFAFSRA	y10	+3
793.722	980.495	20	IAQAGEDPHGYFLPGQFAFSRA	y9	+3
793.722	883.442	20	IAQAGEDPHGYFLPGQFAFSRA	y8	+3
793.722	826.421	20	IAQAGEDPHGYFLPGQFAFSRA	y7	+3
770.043	782.368	20	IAQAGEDPHGYFLPGQFAFSR	b8	+3
770.043	919.427	20	IAQAGEDPHGYFLPGQFAFSR	b9	+3
770.043	976.448	20	IAQAGEDPHGYFLPGQFAFSR	b10	+3
770.043	1139.512	20	IAQAGEDPHGYFLPGQFAFSR	b11	+3
770.043	1169.610	20	IAQAGEDPHGYFLPGQFAFSR	y10	+3
770.043	1022.542	20	IAQAGEDPHGYFLPGQFAFSR	y9	+3
770.043	909.458	20	IAQAGEDPHGYFLPGQFAFSR	y8	+3
770.043	812.405	20	IAQAGEDPHGYFLPGQFAFSR	y7	+3
1076.51	1139.512	20	IAQAGEDPHGYFLPGQFAFS	b11	+2
1076.51	1176.572	20	IAQAGEDPHGYFLPGQFAFS	y10	+2
718.009	782.368	20	IAQAGEDPHGYFLPGQFAFS	b8	+3
718.009	919.427	20	IAQAGEDPHGYFLPGQFAFS	b9	+3
718.009	976.448	20	IAQAGEDPHGYFLPGQFAFS	b10	+3
718.009	1139.512	20	IAQAGEDPHGYFLPGQFAFS	b11	+3
718.009	1176.572	20	IAQAGEDPHGYFLPGQFAFS	y10	+3
718.009	1013.509	20	IAQAGEDPHGYFLPGQFAFS	y9	+3
718.009	866.441	20	IAQAGEDPHGYFLPGQFAFS	y8	+3
718.009	753.357	20	IAQAGEDPHGYFLPGQFAFS	y7	+3
688.999	782.368	20	IAQAGEDPHGYFLPGQFAF	b8	+3
688.999	919.427	20	IAQAGEDPHGYFLPGQFAF	b9	+3
688.999	976.448	20	IAQAGEDPHGYFLPGQFAF	b10	+3
688.999	1139.512	20	IAQAGEDPHGYFLPGQFAF	b11	+3
688.999	1146.562	20	IAQAGEDPHGYFLPGQFAF	y10	+3
688.999	1089.540	20	IAQAGEDPHGYFLPGQFAF	y9	+3
688.999	926.477	20	IAQAGEDPHGYFLPGQFAF	y8	+3
688.999	779.409	20	IAQAGEDPHGYFLPGQFAF	y7	+3
639.976	685.315	20	IAQAGEDPHGYFLPGQFA	b7	+3
639.976	782.368	20	IAQAGEDPHGYFLPGQFA	b8	+3
639.976	919.427	20	IAQAGEDPHGYFLPGQFA	b9	+3
639.976	976.448	20	IAQAGEDPHGYFLPGQFA	b10	+3
639.976	1136.552	20	IAQAGEDPHGYFLPGQFA	y10	+3
639.976	999.493	20	IAQAGEDPHGYFLPGQFA	y9	+3
639.976	942.472	20	IAQAGEDPHGYFLPGQFA	y8	+3
639.976	779.409	20	IAQAGEDPHGYFLPGQFA	y7	+3
923.942	976.448	20	IAQAGEDPHGYFLPGQF	b10	+2
923.942	1139.512	20	IAQAGEDPHGYFLPGQF	b11	+2
923.942	1162.568	20	IAQAGEDPHGYFLPGQF	y10	+2
923.942	1065.515	20	IAQAGEDPHGYFLPGQF	y9	+2
923.942	928.456	20	IAQAGEDPHGYFLPGQF	y8	+2
616.297	685.315	20	IAQAGEDPHGYFLPGQF	b7	+3
616.297	782.368	20	IAQAGEDPHGYFLPGQF	b8	+3
616.297	919.427	20	IAQAGEDPHGYFLPGQF	b9	+3
616.297	976.448	20	IAQAGEDPHGYFLPGQF	b10	+3

Precursor (m/z)	Product (m/z)	Dwell time (ms)	Peptide sequence	Fragment	Charge
616.297	1065.515	20	IAQAGEDPHGYFLPGQF	y9	+3
616.297	928.456	20	IAQAGEDPHGYFLPGQF	y8	+3
616.297	871.435	20	IAQAGEDPHGYFLPGQF	y7	+3
616.297	708.372	20	IAQAGEDPHGYFLPGQF	y6	+3
850.407	919.427	20	IAQAGEDPHGYFLPGQ	b9	+2
850.407	976.448	20	IAQAGEDPHGYFLPGQ	b10	+2
850.407	1139.512	20	IAQAGEDPHGYFLPGQ	b11	+2
850.407	1130.526	20	IAQAGEDPHGYFLPGQ	y10	+2
850.407	1015.500	20	IAQAGEDPHGYFLPGQ	y9	+2
850.407	918.447	20	IAQAGEDPHGYFLPGQ	y8	+2

Table 3.3. Chromatographic separation gradient protocol

Chromatographic separation was performed as indicated where Solvent A was 1% formic acid in water and Solvent B was 0.1% formic acid in acetonitrile.

Time	Flow rate (µL/min)	Solvent A (%)	Solvent B (%)
0	5	97	3
5	5	97	3
6	5	93	7
7	5	65	35
90	5	65	35
95	5	5	95
100	5	5	95
105	5	97	3
120	5	97	3

Figure 3.1. Experimental workflow to identify novel targets of chemerin signalling in mature adipocytes

Mesenchymal stem cells (MSCs) were isolated from the bone marrow of wildtype C57/Bl6 mice and differentiated into adipocytes. Mature MSC-derived adipocytes were treated with 100 μg/mL of neutralizing anti-chemerin antibody or goat IgG control for 24 h in serum-free media. RNA was isolated and Affymetrix microarray analysis performed to identify changes in gene expression following neutralization of endogenous chemerin signalling.

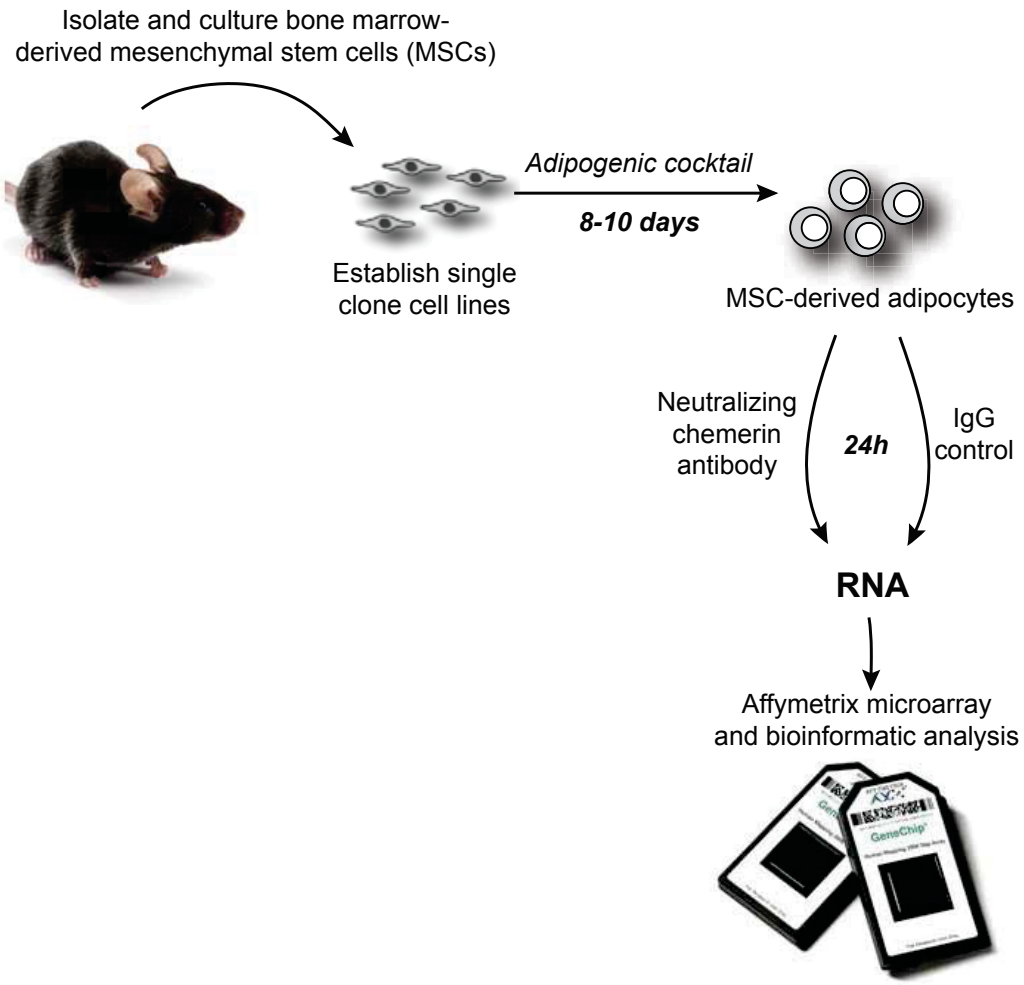
Isolate and culture bone marrow-derived mesenchymal stem cells (MSCs)
Establish single clone cell lines
Adipogenic cocktail
8-10 days
MSC-derived adipocytes
Neutralizing chemerin antibody
24h
IgG control
RNA
Affymetrix microarray and bioinformatic analysis

Figure 3.2. Induction of adipogenic differentiation in MSCs results in the accumulation of lipid, a decrease in the expression of the MSC-marker gene CD44, and an increase in the expression of adipogenic genes

Mesenchymal stem cells (MSCs) isolated from the bone marrow of C57Bl/6 mice were differentiated into adipocytes. Cells were stained with Oil Red O on the indicated day following induction of differentiation (A, 40X magnification) and the amount of Oil Red O stain quantified (B). The expression of the MSC marker gene CD44 (C) and adipogenic genes PPARγ, adiponectin, adipocyte protein (AP)2, and adipocyte differentiation-related protein (ADRP) (D) over adipogenic differentiation was evaluated using qPCR. All values are expressed relative to day 0 where * represents $p<0.05$ compared to day 0 (n=3).

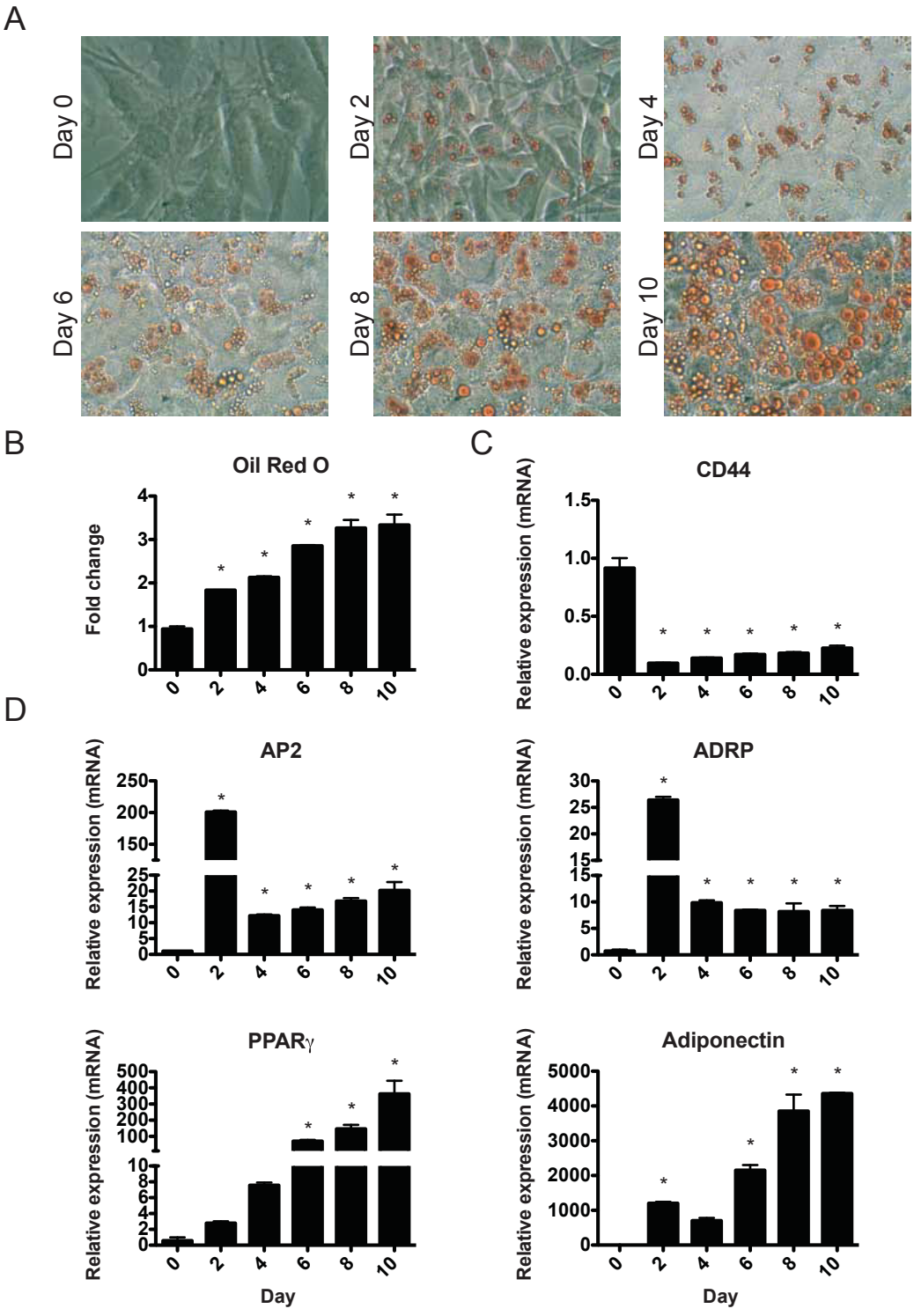
A
Day 0
Day 2
Day 4
Day 6
Day 8
Day 10
B
Oil Red O
Fold change
C
CD44
Relative expression (mRNA)
D
AP2
ADRP
PPARγ
Adiponectin
Relative expression (mRNA)
Day

Figure 3.3. Chemerin and CMKLR1 mRNA, secreted chemerin levels, and bioactivity of conditioned adipocyte media at mouse CMKLR1 and GPR1 increase throughout adipogenic differentiation of MSCs

The expression of chemerin and the three chemerin receptors (CMKLR1, GPR1, and CCRL2) were examined over adipogenic differentiation using qPCR analysis (A). Chemerin secretion from adipocytes was investigated using western blot analysis under both denaturing and non-denaturing conditions. 30 μL of 48 h-conditioned adipocyte media and 10 ng of recombinant mouse chemerin (aa 17-156) was loaded (B). The two blots were scanned at the same intensity. Activation of mouse CMKLR1 and GPR1 following treatment with 50 μL of conditioned adipocyte media was assessed using the cell-based Tango assay (C). All values are normalized to day 0 where * represents $p<0.05$ compared to day 0 (n=3).

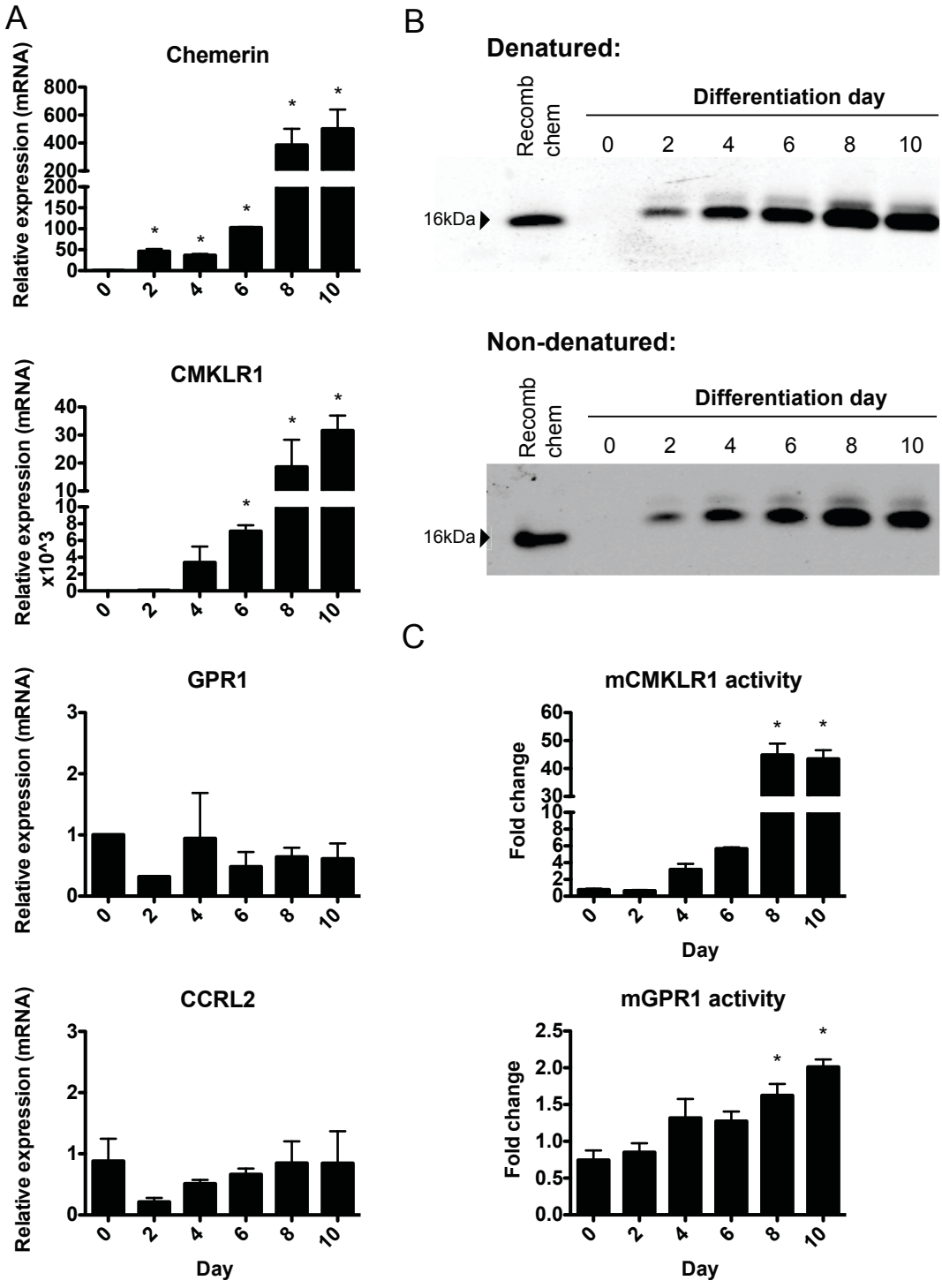
A
Chemerin
Relative expression (mRNA)
CMKLR1
Relative expression (mRNA)
x10^3
GPR1
Relative expression (mRNA)
CCRL2
Relative expression (mRNA)
Day
B
Denatured:
Recomb chem
Differentiation day
0 2 4 6 8 10
16kDa
Non-denatured:
Recomb chem
Differentiation day
0 2 4 6 8 10
16kDa
C
mCMKLR1 activity
Fold change
Day
mGPR1 activity
Fold change
Day

Figure 3.4. Treatment of MSC-derived adipocytes with increasing concentrations of neutralizing chemerin antibody reduces activation of both mouse CMKLR1 and GPR1 and has no effect on cell viability

Mature MSC-derived adipocytes were treated for 24 (A) or 48 (B) h with increasing doses of neutralizing chemerin antibody, vehicle (PBS), or IgG (100 μg/mL) control. Adipocyte-conditioned media was collected and was transferred to the cell-based Tango assay to examine activation of mouse CMKLR1 and GPR1 (A, B; n=3). Cell viability was assessed following 24 or 48 h antibody treatment using the MTT assay (C, n=2). All values are expressed relative to the 24 h vehicle control where * represents $p<0.05$ compared to vehicle treatment within each timepoint.

A 24h incubation on adipocytes:

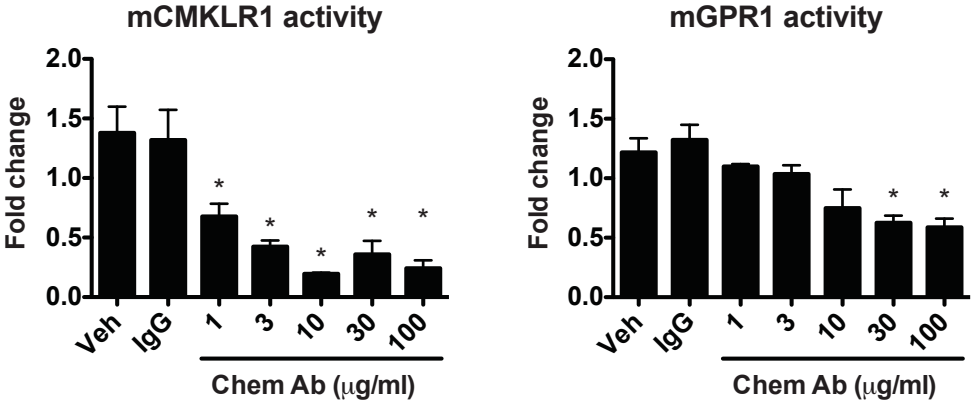

B 48h incubation on adipocytes:

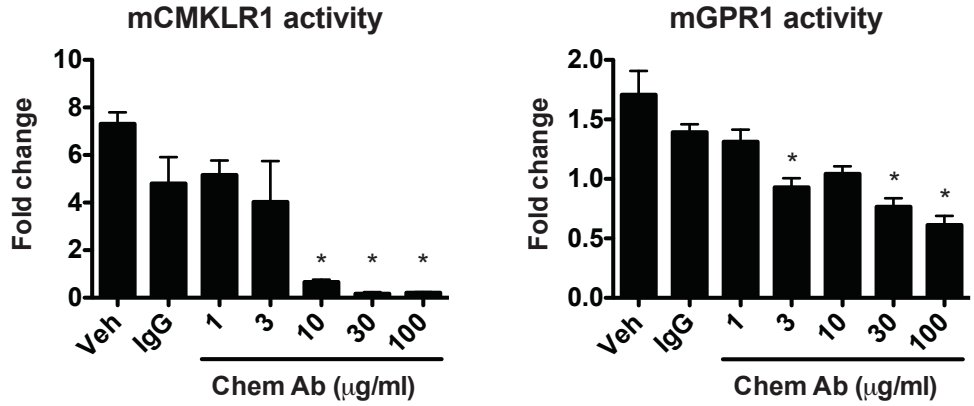

C

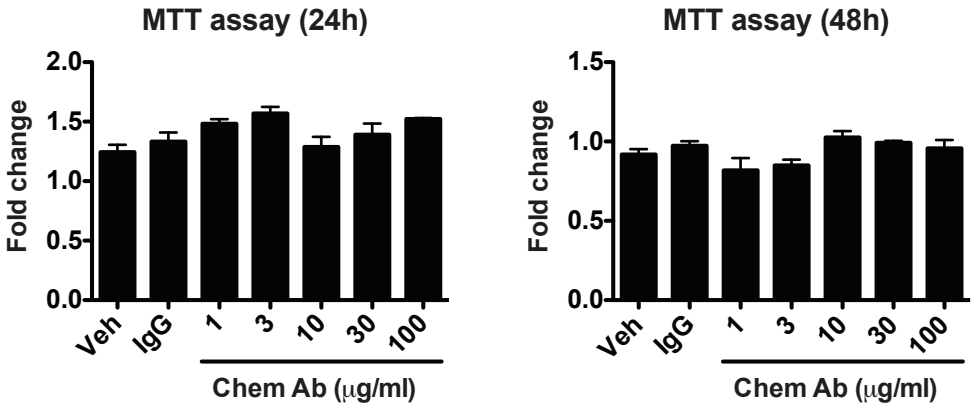

Table 3.4. Genes up-regulated following treatment of MSC-derived adipocytes with neutralizing chemerin antibody

MSC-derived adipocytes were treated with neutralizing chemerin antibody or IgG (control) for 24 h, RNA isolated, and Affymetrix microarray analysis performed. Genes with increased expression following chemerin antibody treatment compared to IgG control (>2.5-fold threshold) are shown.

Accession number	Gene name	Fold change
NM_011315	Saa3: serum amyloid A 3	49.42
NM_011337	Ccl3: chemokine (C-C motif) ligand 3	31.3
NM_010809	Mmp3: matrix metallopeptidase 3	18.87
NM_007807	Cybb: cytochrome b-245, beta polypeptide	16.66
NM_008198	Cfb: complement factor B	16.36
NM_007969	Expi: extracellular proteinase inhibitor	12.32
NM_021394	Zbp1: Z-DNA binding protein 1	9.93
NM_054098	Steap4: STEAP family member 4	7.47
NM_013653	Ccl5: chemokine (C-C motif) ligand 5	7.08
NM_133990	Il13ra1: interleukin 13 receptor, alpha 1	6.99
NM_018734	Gbp3: guanylate binding protein 3	5.56
NM_031168	Il6: interleukin 6	5.42
NM_011314	Saa2: serum amyloid A-2	5.39
NM_011333	Ccl2: chemokine (C-C motif) ligand 2	5.33
NM_021384	Rsad2: radical S-adenosyl methionine domain containing 2	4.87
NM_030720	Gpr84: G protein-coupled receptor 84	4.76
NM_017371	Hpx: hemopexin	4.73
NM_008087	Ptx3: pentraxin related gene	4.73
NM_008489	Lbp: lipopolysaccharide binding protein	4.69
NM_011413	C4a: complement component 4A (Rodgers blood group)	4.51
NM_013654	Ccl7: chemokine (C-C motif) ligand 7	4.47
NM_001045481	Ifi203: interferon activated gene 203	4.36
NM_008880	Piscr2: phospholipid scramblase 2	4.08
NM_023386	Rtp4: receptor transporter protein 4	4.06
NM_008331	Ifit1: interferon-induced protein with tetratricopeptide repeats 1	3.97
NM_021792	Iigp1: interferon inducible GTPase 1	3.88
NM_011414	Slpi: secretory leukocyte peptidase inhibitor	3.87
NM_023044	Slc15a3: solute carrier family 15, member 3	3.76
NM_007609	Casp4: caspase 4, apoptosis-related cystein peptidase	3.68
NM_011854	Oasl2: 2'-5' oligoadenylate synthetase-like 2	3.6
NM_011909	Usp18: ubiquitin specific peptidase 18	3.53
NM_009780	C4b: complement component 4B (Childo blood group)	3.5
NM_008491	Lcn2: lipocalin 2	3.46
NM_016850	Irf7: interferon regulatory factor 7	3.43
NM_173436	Cypt2: cysteine-rich perinuclear theca 2	3.41
NM_029796	Lrg1: leucine-rich alpha-2-glycoprotein 1	3.31
NM_011408	Slfn2: schlafen 2	3.26
NM_010693	Lck: lymphocyte protein tyrosine kinase	3.14

Accession number	Gene name	Fold change
NM_011852	Oas1g: 2'-5' oligoadenylate synthease 1G	3.08
NM_007679	Cebpd: CCAAT/enhancer binding protein (C/EBP), delta	3.05
NM_030150	Dhx58: DEXH (Asp-Glu-X-His) box polypeptide 58	3.00
NM_018738	Igtp: interferon gamma induced GTPase	2.98
NM_010501	Ifit3: interferon-induced protein with tetraticopeptide repeats 3	2.9
NM_008330	Ifi47: interferon gamma inducible protein 47	2.88
NM_173743	Apol9b: apolipoprotein L 9b	2.86
ENSMUST00000094774	Sp110: SP110 nuclear body protein	2.84
NM_001042605	Cd74: CD74 antigen (invariant polypeptide of major histocompatibility complex, class II antigen-associated)	2.83
ENSMUST00000031817	Herc5: hect domain and RLD 5	2.76
NM_133871	Ifi44: interferon-induced protein 44	2.72
NM_008599	Cxcl9: chemokine (C-X-C motif) ligand 9	2.69
NM_172753	Csgalnact1: chondroitin sulfate N-acetylgalactosaminyltransferase 1	2.67
NM_011636	Plscr1: phospholipid scramblase 1	2.66
NM_015783	Isg15: ISG15 ubiquitin-like modifier	2.64
BC151059	Plcxd2: phosphatidylinositol-specific phospholipase C, X domain containing 2	2.64
NM_027835	Ifih1: interferon induced with helicase C domain 1	2.63
NR_003507	Oas1b: 2'-5' oligoadenylate synthetase 1B	2.6
NM_001039530	Parp14: poly (ADP-ribose) polymerase family, member 14	2.59
NM_001037713	Xaf1: XIAP associated factor 1	2.57
NM_028679	Irak3: interleukin-1 receptor-associated kinase 3	2.57
NM_010279	Gfra1: glial cell line derived neurotrophic factor family receptor alpha 1	2.56
NM_010934	Npy1r: neuropeptide Y receptor Y1	2.54
NM_178804	Slit2: slit homolog 2 (Drosophila)	2.54
NM_018746	Itih4: inter alpha-trypsin inhibitor, heavy chain 4	2.5

Table 3.5. Genes down-regulated following treatment of MSC-derived adipocytes with neutralizing chemerin antibody

MSC-derived adipocytes were treated with neutralizing chemerin antibody or IgG (control) for 24 h, RNA isolated, and Affymetrix microarray analysis performed. Genes with reduced expression following chemerin antibody treatment compared to IgG control (<2.5-fold threshold) are shown.

Accession number	Gene name	Fold change
NM_012050	Omd: osteomodulin	-8.95
NM_009504	Vdr: vitamin D receptor	-7.49
NM_008321	Id3: inhibitor of DNA binding 3	-5.47
NM_008590	Mest: mesoderm specific transcript	-4.30
NM_028889	Ehfd1: EF hand domain containing 1	-3.99
NM_016678	Reck: reversion-inducing-cysteine-rich protein with kazal motifs	-3.96
NM_029771	Gper: G protein-coupled estrogen receptor 1	-3.92
NM_133670	Sult1a1: sulfotransferase family 1A, phenol-preferring, member 1	-3.60
NM_130458	Sp7: Sp7 transcript factor 7	-3.53
NM_020025	B3galt2: UDP-Gal:betaGlcNAc beta1,3-galactosyltransferase, polypeptide 2	-3.32
NM_016854	Ppp1r3c: protein phosphatase 1, regulatory (inhibitor) subunit 3C	-3.31
NM_026433	Tmem100: transmembrane protein 100	-3.30
NM_053200	Ces3: carboxylesterase 3	-3.06
NM_009204	Slc2a4: solute carrier family 2 (facilitated glucose transporter), member 4	-3.02
NM_146162	Tmem119: transmembrane protein 119	-2.92
NM_008800	Pde1b: phosphodiesterase 1B, Ca2+ calmodulin dependent	-2.88
NM_010217	Ctgf: connective tissue growth factor	-2.80
NM_007901	S1pr1: sphingosine-1-phosphate receptor 1	-2.71
NM_053191	Pi15: peptidase inhibitor 15	-2.67
NM_008318	Ibsp: integrin binding sialoprotein	-2.67
NM_007409	Adh1: alcohol dehydrogenase 1 (class I)	-2.6
NM_008494	Lfng: LFNG O-fucosylpeptide 3-beta-N-acetylglucosaminyltransferase	-2.57
NM_023850	Chst1: carbohydrate (keratan sulfate Gal-6) sulfotransferase 1	-2.56
ENSMUST00000075637	Ptpn3: protein tyrosine phosphatase, non-receptor type 3	-2.56
NM_175429	Kctd12b: potassium channel tetramerisation domain containing 12b	-2.52
NM_030598	Rcan2: regulator of calcineurin 2	-2.51

Figure 3.5. MMP3 expression, secretion, and activity increase following neutralization of endogenous chemerin signalling

Mature MSC-derived adipocytes were treated with increasing concentrations of neutralizing chemerin antibody, vehicle (PBS), or IgG (100 μg/mL) control for 24 h (A, n=6) or 24 h and 48 h (B, n=3) and Mmp3 expression evaluated using qPCR. Secretion of MMP3 by MSC-derived adipocytes was examined using western blot analysis of 24 h-conditioned adipocyte media (C, n=5). Goat IgG was loaded as control for the presence of heavy chain IgG in antibody-treated media samples. The expression of related MMPs and the endogenous MMP inhibitor Reck was investigated in MSC-derived adipocytes treated for 24 h with neutralizing chemerin antibody (30 or 100 μg/mL), vehicle (PBS), or IgG (100 μg/mL) control (D, n=3). Mmp9 expression was not detected. MMP activity in 24 h adipocyte-conditioned media was assessed using a fluorometric assay using a MMP3/12-specific substrate (E, n=4). All values are expressed relative to the 24 h vehicle control. Statistical significance was evaluated compared to the vehicle control within each timepoint where * represents $p<0.05$.

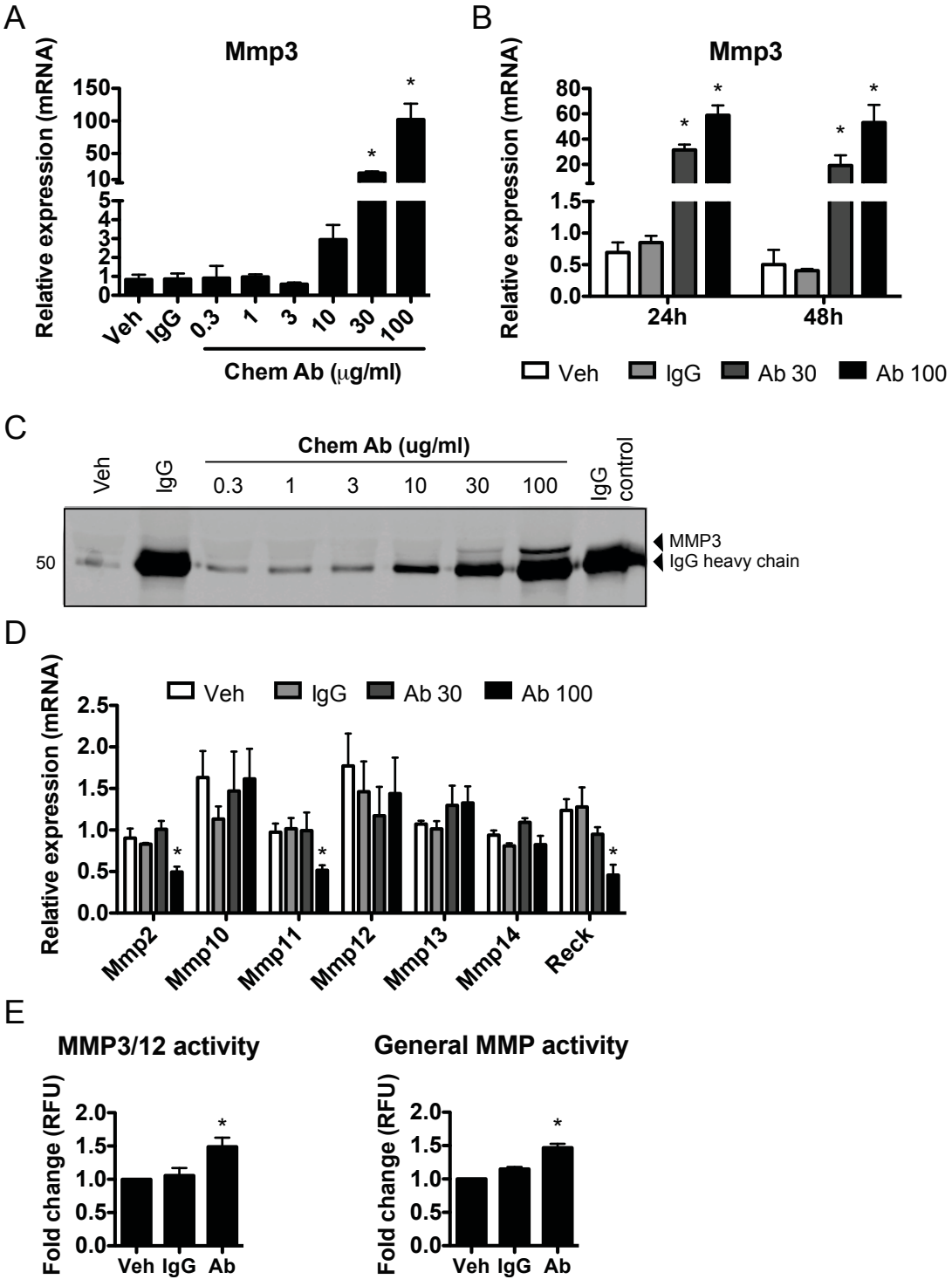
A
Mmp3
Relative expression (mRNA)
Veh
IgG
0.3
1
3
10
30
100
Chem Ab (μg/ml)
B
Mmp3
Relative expression (mRNA)
24h
48h
Veh
IgG
Ab 30
Ab 100
C
Chem Ab (ug/ml)
Veh
IgG
0.3
1
3
10
30
100
IgG control
50
MMP3
IgG heavy chain
D
Veh
IgG
Ab 30
Ab 100
Relative expression (mRNA)
Mmp2
Mmp10
Mmp11
Mmp12
Mmp13
Mmp14
Reck
E
MMP3/12 activity
General MMP activity
Fold change (RFU)
Veh
IgG
Ab

Figure 3.6. Neutralization of endogenous chemerin signalling in MSC-derived adipocytes increases the expression of chemoattractant factors and the migration of murine macrophages towards adipocyte-conditioned media though a Ccl2-dependent mechanism

MSC-derived adipocytes were treated for 24 h or 48 h with vehicle (PBS), IgG (100 μg/mL), or neutralizing chemerin antibody (30 or 100 μg/mL). The expression of various chemoattractant factors was investigated using qPCR analysis. Values are relative to the 24 h vehicle control (A, n=3). CCL2 protein levels in adipocyte-conditioned media following 24 h treatment with vehicle (PBS), IgG (100 μg/mL), or chemerin antibody (1-100 μg/mL) was examined using western blot analysis (B, n=3). The ability of the murine macrophage cell line RAW264.7 to migrate towards control (serum-free media) or 24 h-conditioned adipocyte media following treatment with vehicle (PBS), IgG (100 μg/mL), or chemerin antibody (100 μg/mL) was assessed. Cells that migrated towards adipocyte-conditioned media were labeled with Hoescht, imaged, and counted manually (C, 40x magnification, n=5). The effect of pre-incubating adipocyte-conditioned media with 20 μg/mL of neutralizing CCL2 antibody on macrophage migration was also assessed (C, n=3). Values are expressed relative to the migration control (serum-free media). Statistical significance was determined compared to vehicle control within each timepoint (A) or migration control (C) where * represents $p<0.05$ and # represents $p<0.05$ compared to Ab treatment (C).

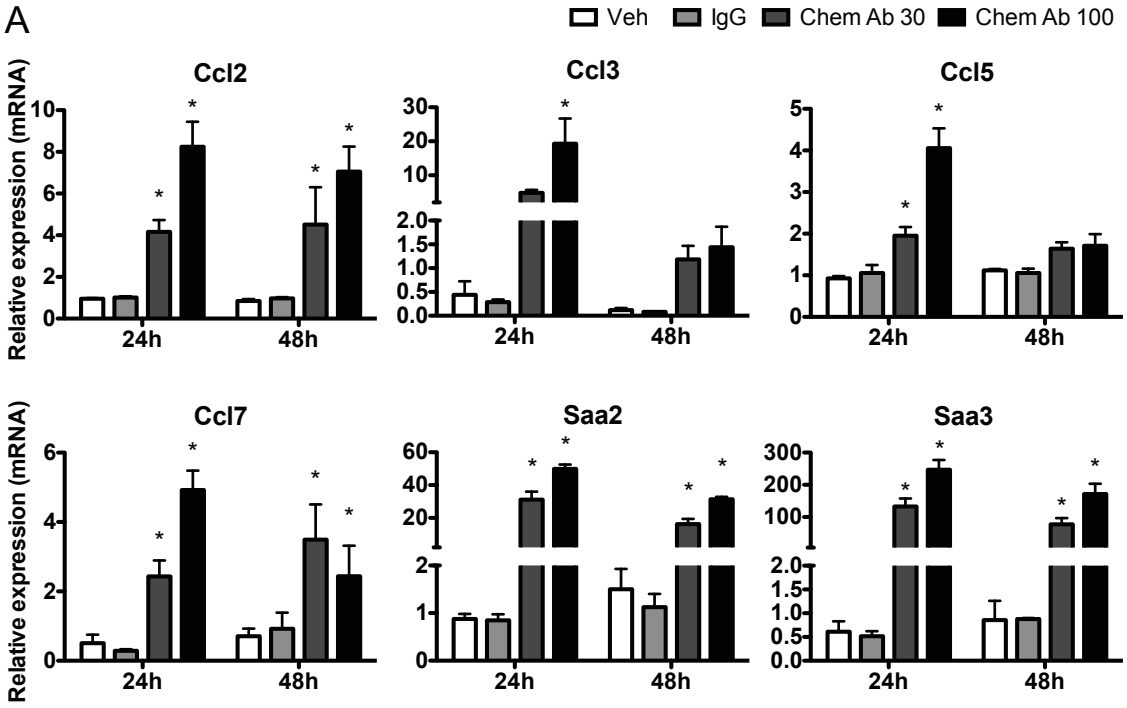
A
Veh
IgG
Chem Ab 30
Chem Ab 100
Ccl2
Ccl3
Ccl5
Ccl7
Saa2
Saa3
Relative expression (mRNA)
24h
48h

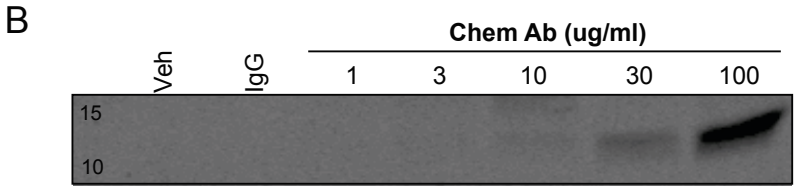
B
Chem Ab (ug/ml)
Veh
IgG
1
3
10
30
100
15
10

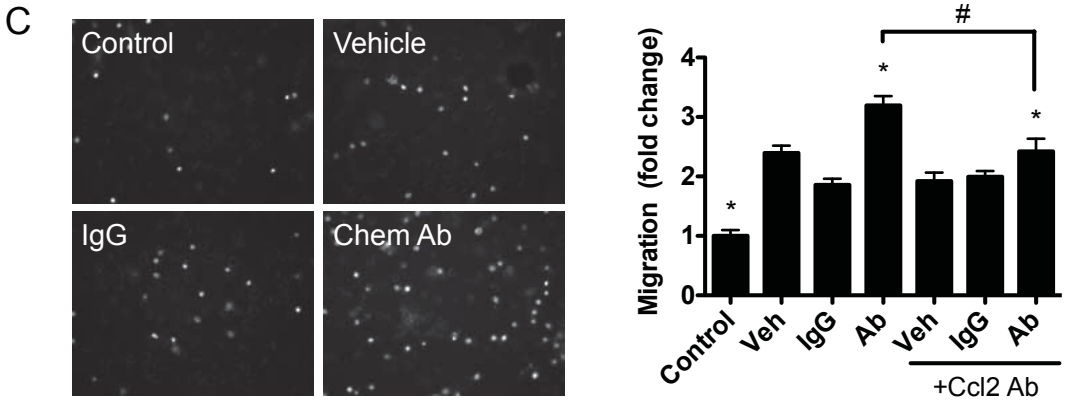
C
Control
Vehicle
IgG
Chem Ab
Migration (fold change)
#
Control
Veh
IgG
Ab
Veh
IgG
Ab
+Ccl2 Ab

Figure 3.7. Neutralization of endogenous chemerin signalling in MSC-derived adipocytes increases NFkB activity

A stable MSC line expressing a NFkB-luciferase reporter gene was generated and cells were subsequently differentiated in mature adipocytes. The ability of NFkB-luciferase MSC-derived adipocytes to respond to 24 h treatment with increasing doses of mouse TNFα (0.1-100 ng/mL, A) or LPS (0.001-100 μg/mL, B) treatment was assessed (n=4). The effect of vehicle (PBS), IgG (100 μg/mL), or neutralizing chemerin antibody (10, 30, or 100 μg/mL) treatment for 1, 3, 6, or 24 h on NFkB activity was investigated (C, n=3). The effect of a 6 h treatment with increasing doses of neutralizing chemerin antibody (0.3-100 μg/mL) on NFkB activity in MSC-derived adipocytes was then assessed (D, n=6). LPS (0.1 μg/mL) was included as a positive control. NFkB activity in MSC-derived adipocytes following 24 h co-treatment with vehicle (PBS), IgG (100 μg/mL), or chemerin antibody (100 μg/mL) and LPS (5 ng/mL) or TNFα (5 ng/mL) (E, n=4) was assessed. The effect of recombinant mouse chemerin (aa 17-156) in the presence (0.01 μg/mL) or absence of LPS (F, n=2) on NFkB activation in MSC-derived adipocytes was also determined. All values are expressed relative to vehicle control where * represents $p<0.05$ compared to vehicle-treated cells (A-D), vehicle-treated within each treatment (control/TNF/LPS/TNF+LPS) (E) or untreated (F).

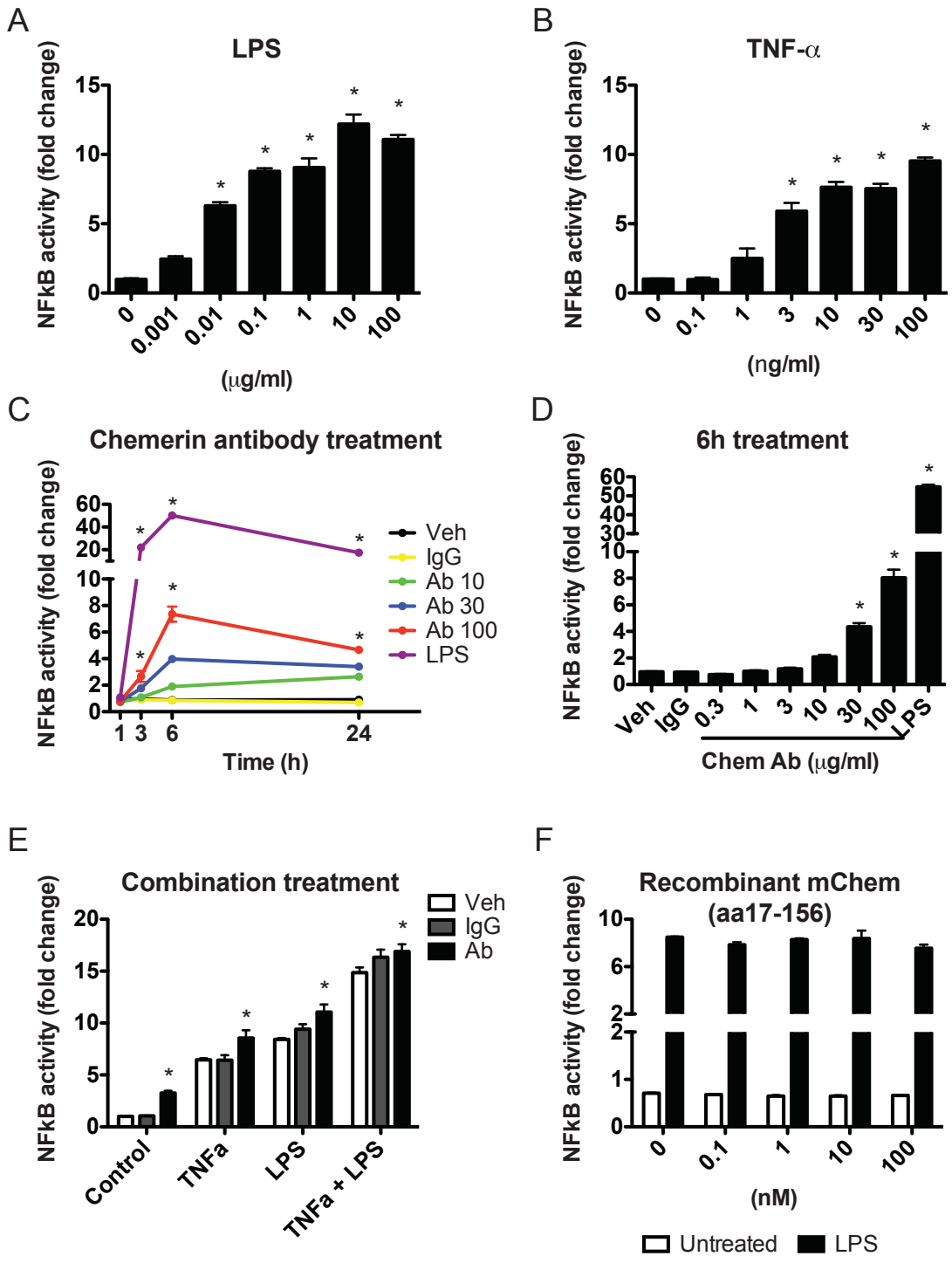
A
LPS
NFkB activity (fold change)
15
10
5
0
0
0.001
0.01
0.1
1
10
100
(μg/ml)
B
TNF-α
NFkB activity (fold change)
15
10
5
0
0
0.1
1
3
10
30
100
(ng/ml)
C
Chemerin antibody treatment
NFkB activity (fold change)
60
40
20
10
8
6
4
2
0
1 3 6
24
Time (h)
Veh
IgG
Ab 10
Ab 30
Ab 100
LPS
D
6h treatment
NFkB activity (fold change)
60
50
40
30
10
8
6
4
2
0
Veh
IgG
0.3
1
3
10
30
100
LPS
Chem Ab (μg/ml)
E
Combination treatment
NFkB activity (fold change)
20
15
10
5
0
Control
TNFa
LPS
TNFa + LPS
Veh
IgG
Ab
F
Recombinant mChem
(aa17-156)
NFkB activity (fold change)
10
6
2
2
1
0
0
0.1
1
10
100
(nM)
Untreated
LPS

Figure 3.8. Inhibition of NFkB signalling in MSC-derived adipocytes reduces the up-regulation of MMP3 expression/secretion and the increased migration of RAW264 macrophages towards adipocyte-conditioned media

MSC-derived adipocytes expressing a NFkB-luciferase reporter were pre-treated for 1 h with increasing doses of the NFkB inhibitor Bay11-7082 or vehicle (DMSO) before the addition of vehicle (PBS), IgG (30 μg/mL), or neutralizing chemerin antibody (30 μg/mL) for 24 h. The effect of Bay-7082 treatment on NFkB activity was assessed (A, n=3). Mmp3 (B, n=4) and Ccl2 (C, n=4) expression in 24 h vehicle, IgG (100 μg/mL), or chemerin antibody (100 μg/mL)-treated adipocytes following 1 h pre-treatment with 10 or 30 μM Bay-7082 was determined using qPCR. Secretion of MMP3 from 24 h vehicle, IgG, or antibody-treated adipocytes was assessed in the presence (100 μM) or absence of Bay-7082 using western blot analysis (D, n=3). Goat IgG was loaded as a control for the presence of IgG heavy chain in antibody-treated adipocyte media samples. The ability of RAW264 macrophages to migrate towards media conditioned by adipocytes treated with vehicle (PBS), IgG (100 μg/mL) or chemerin antibody (100 μg/mL) and Bay-7082 (100 μM) for 24h was assessed (E, n=5). Cos7 cells were co-transfected with a Ccl2 promoter-luciferase reporter construct and mCMKLR1 or empty vector control (pBSK). Cells were treated with PBS, mTNFα (50 ng/mL), and/or mouse chemerin (30 nM, aa 17-156) and reporter activity assessed (F, n=3). Values are expressed relative to vehicle control. In A-E, statistical significance was determined compared to vehicle-treated cells (no inhibitor, no antibody) where * represents $p<0.05$. In F, * represents $p<0.05$ compared to vehicle control within each receptor and # represents $p<0.05$ compared to vehicle pBSK.

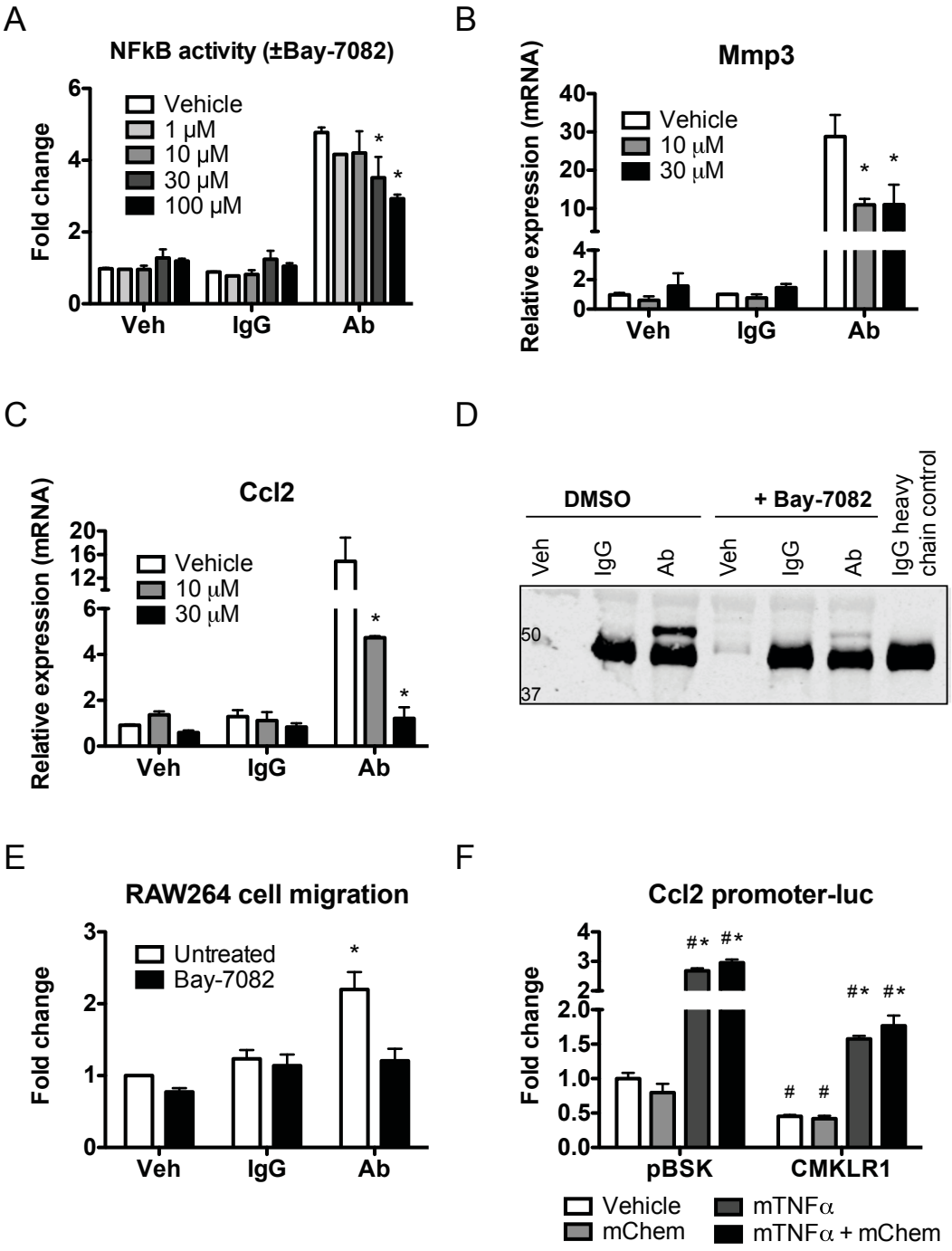
A
NFkB activity (±Bay-7082)
Fold change
Vehicle
1 μM
10 μM
30 μM
100 μM
Veh
IgG
Ab
B
Mmp3
Relative expression (mRNA)
Vehicle
10 μM
30 μM
Veh
IgG
Ab
C
Ccl2
Relative expression (mRNA)
Vehicle
10 μM
30 μM
Veh
IgG
Ab
D
DMSO
+ Bay-7082
Veh
IgG
Ab
Veh
IgG
Ab
IgG heavy chain control
50
37
E
RAW264 cell migration
Fold change
Untreated
Bay-7082
Veh
IgG
Ab
F
Ccl2 promoter-luc
Fold change
pBSK
CMKLR1
Vehicle
mChem
mTNFα
mTNFα + mChem

Figure 3.9. Mmp3 expression, chemokine expression, and NFkB activity increase in SVF-derived adipocytes following neutralization of endogenous chemerin signalling

Preadipocytes isolated from the stromal vascular fraction of subcutaneous white adipose depot of wildtype C57Bl/6 mice were isolated and differentiated into mature adipocytes. Chemerin levels in 24 h-adipocyte conditioned media from MSC- and SVF-derived adipocytes were assessed by western blot analysis under denaturing conditions (A, n=4). SVF-derived adipocytes were treated with vehicle (PBS), IgG (100 μg/mL), or chemerin antibody (30 or 100 μg/mL) for 24h and the ability of the chemerin antibody to inhibit activation of mouse CMKLR1 was assessed by applying the conditioned adipocyte media to the Tango assay (B, n=3). The expression of Mmp3, Ccl2, and Ccl7 in SVF-derived adipocytes treated with vehicle (PBS), IgG (100 μg/mL), or increasing doses of chemerin antibody (1-100 μg/mL) for 24h was determined using qPCR (C, n=4). SVF-derived adipocytes were transduced with NFkB-luciferase reporter and the effect of 2 h vehicle (PBS), IgG (100 μg/mL), or neutralizing chemerin antibody treatment on NFkB activity was assessed (D, n=4). All values are expressed relative to vehicle (PBS) where * represents $p<0.05$ compared to vehicle (PBS) control.

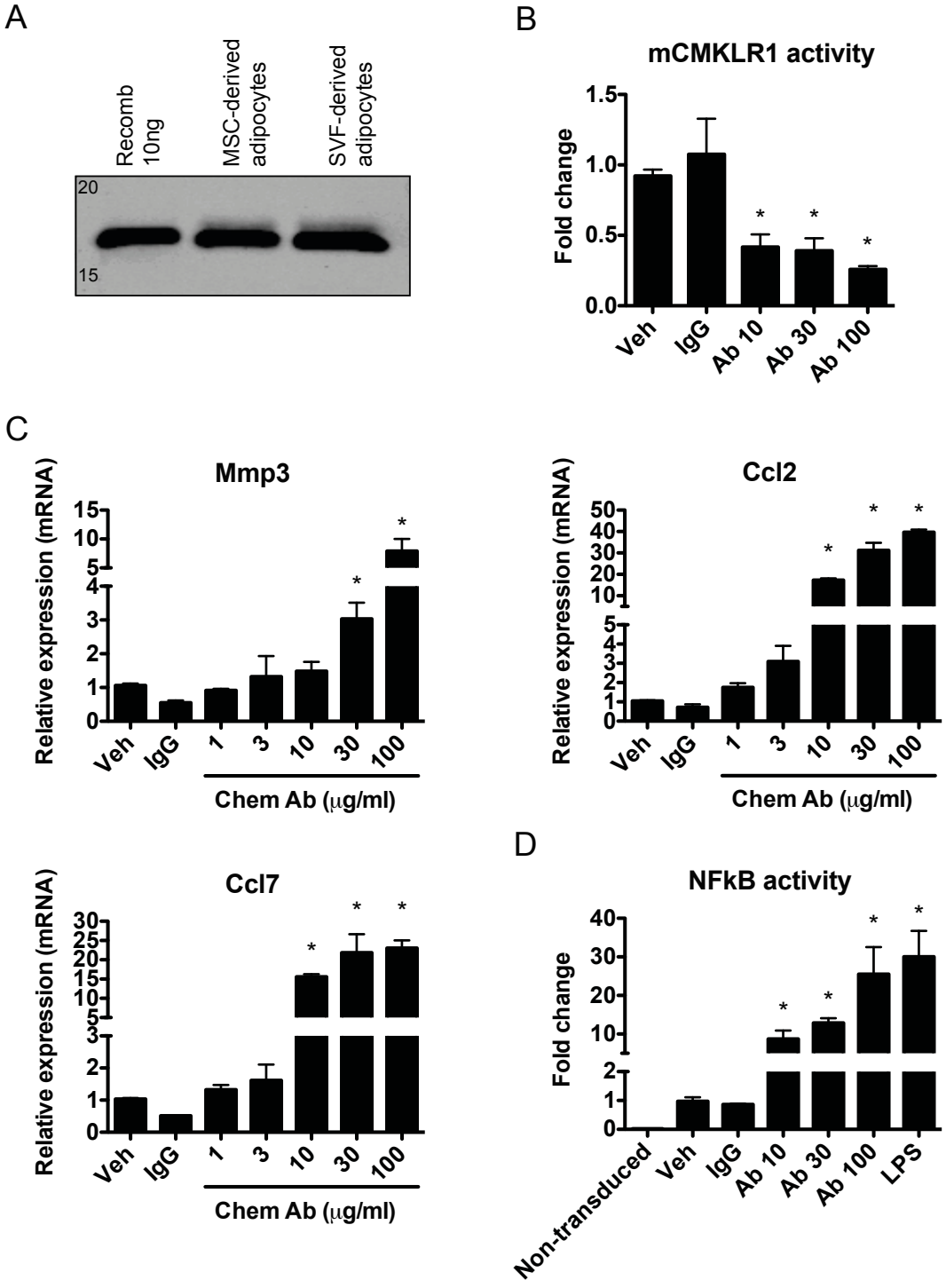
A
Recomb 10ng
MSC-derived adipocytes
SVF-derived adipocytes
20
15
B
mCMKLR1 activity
Fold change
1.5
1.0
0.5
0.0
Veh
IgG
Ab 10
Ab 30
Ab 100
C
Mmp3
Relative expression (mRNA)
Veh
IgG
1
3
10
30
100
Chem Ab (μg/ml)
Ccl2
Relative expression (mRNA)
Chem Ab (μg/ml)
Ccl7
Relative expression (mRNA)
Chem Ab (μg/ml)
D
NFkB activity
Fold change
Non-transduced
Veh
IgG
Ab 10
Ab 30
Ab 100
LPS

Figure 3.10. Techniques to reduce endogenous chemerin/CMKLR1 signalling do not result in sufficient inhibition to reproduce the effects of neutralizing chemerin antibody treatment in mature adipocytes

MSCs expressing cumate-inducible Piggybac chemerin shRNA were differentiated into mature adipocytes and treated with 10x cumate to induce chemerin knockdown. Following 4 days of cumate treatment, RNA was isolated and qPCR analysis used to determine levels of chemerin, Mmp3, and Ccl2 expression (A, n=3). Mature MSC-derived adipocytes were treated with the CMKLR1 inhibitor CCX832, control compound CCX826, or vehicle (DMSO) for 24 h. qPCR analysis was used to determine levels of Mmp3 and Ccl2 expression (B, n=3). NFkB-luciferase-expressing MSC-derived adipocytes were treated with vehicle (DMSO) or increasing concentrations of CCX832 (1-1000 μM). Following 24 h treatment, NFkB activity was determined (C, n=2) where LPS (1 μg/mL) was used as a positive control. The resulting 24 h-conditioned adipocyte media was transferred to the Tango assay to determine levels of mCMKLR1 activation (D, n=2). All values are expressed relative to vehicle control, where * represents $p<0.05$ compared to vehicle control.

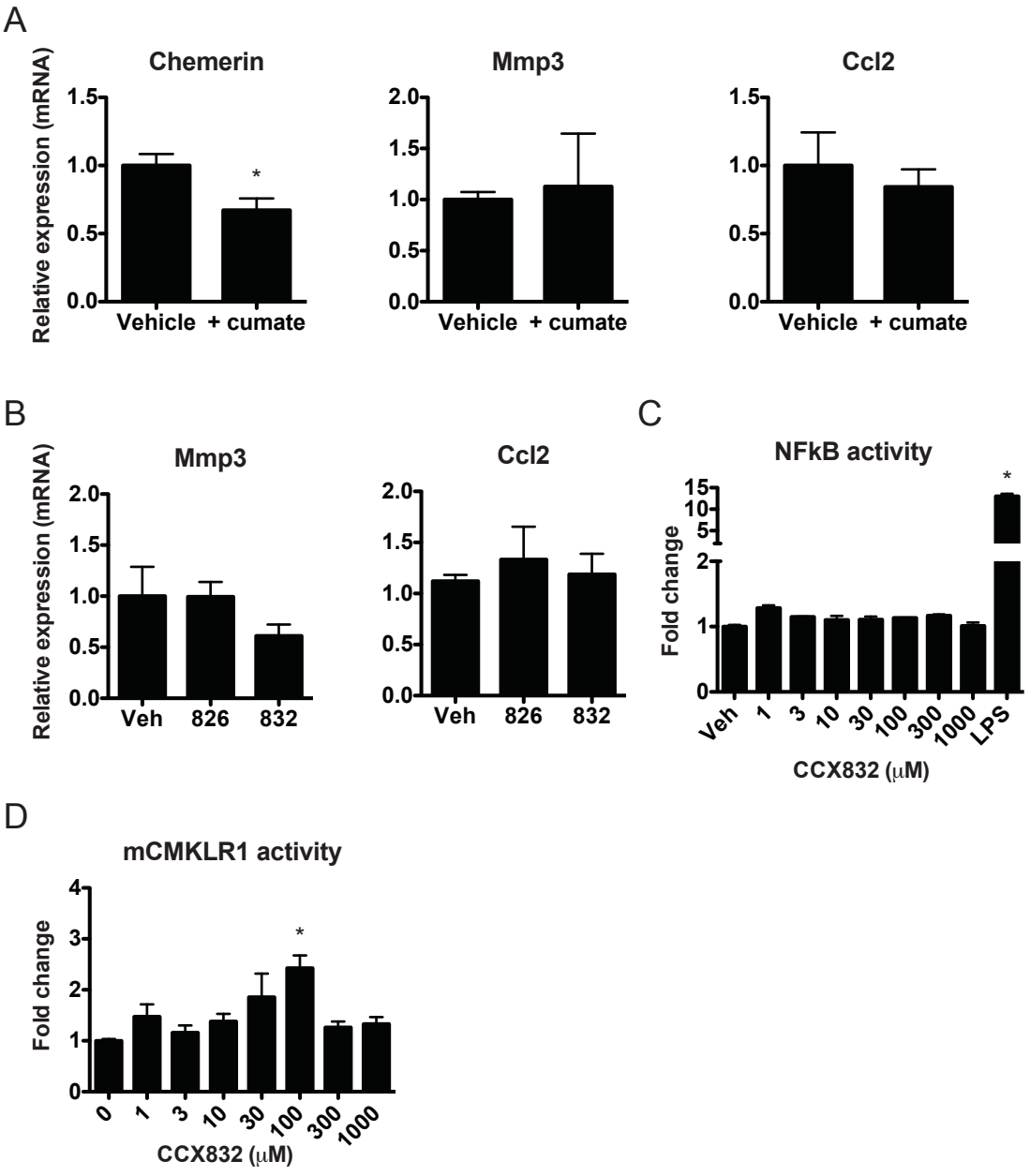
A
Chemerin
Mmp3
Ccl2
Relative expression (mRNA)
1.5
1.0
0.5
0.0
2.0
1.5
1.0
0.5
0.0
1.5
1.0
0.5
0.0
*
Vehicle + cumate
Vehicle + cumate
Vehicle + cumate
B
Mmp3
Ccl2
Relative expression (mRNA)
2.0
1.5
1.0
0.5
0.0
2.0
1.5
1.0
0.5
0.0
Veh 826 832
Veh 826 832
C
NFkB activity
Fold change
15
10
5
2
1
0
*
Veh 1 3 10 30 100 300 1000 LPS
CCX832 (μM)
D
mCMKLR1 activity
Fold change
4
3
2
1
0
*
0 1 3 10 30 100 300 1000
CCX832 (μM)

Figure 3.11. Mmp3 and Ccl2 expression are up-regulated in white adipose tissue isolated from CMKLR1 KO mice

Wildtype and CMKLR1 KO male mice were monitored for 6 or 24 weeks beginning at 6 weeks of age. Body mass was measured weekly (A, n=9-10). DEXA analysis of body composition was performed every four weeks (B, n=8-10). RNA was isolated from visceral white adipose tissue and qPCR analysis performed to investigate expression of Mmp3 and Ccl2 (C, n=5). In C, values are expressed relative to wildtype at the 6-week timepoint. Statistical significance was determined compared to wildtype, where * represents $p<0.05$ compared to wildtype at each timepoint.

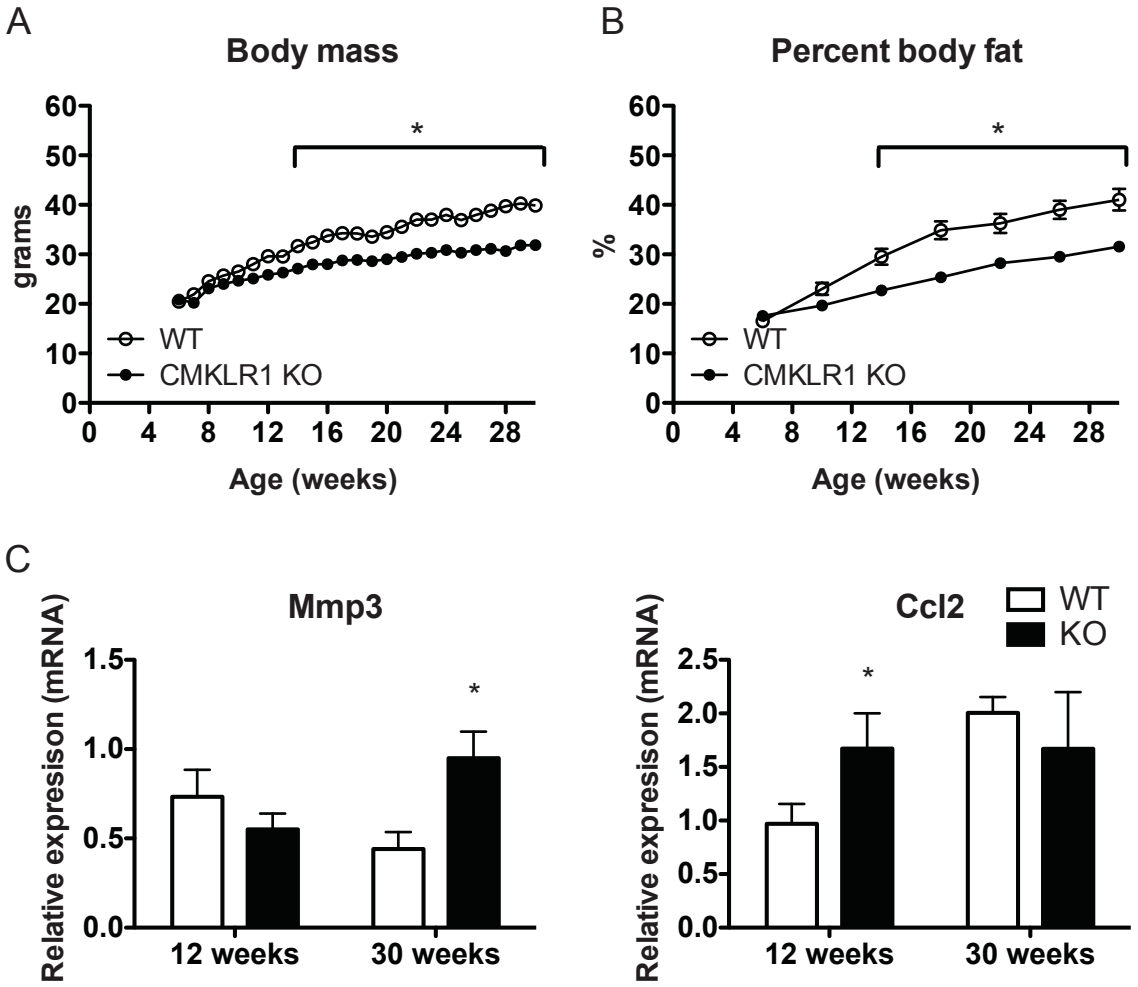
A
Body mass
grams
60
50
40
30
20
10
0
0 4 8 12 16 20 24 28
Age (weeks)
WT
CMKLR1 KO
*
B
Percent body fat
%
60
50
40
30
20
10
0
0 4 8 12 16 20 24 28
Age (weeks)
WT
CMKLR1 KO
*
C
Mmp3
Relative expresison (mRNA)
1.5
1.0
0.5
0.0
12 weeks
30 weeks
*
Ccl2
WT
KO
Relative expresison (mRNA)
2.5
2.0
1.5
1.0
0.5
0.0
*
12 weeks
30 weeks

Figure 3.12. Recombinant human chemerin is not neutralized by mouse chemerin antibody but does not rescue the effect of chemerin antibody treatment in MSC-dervied adipocytes

The ability of mouse neutralizing chemerin antibody to block the activity of human recombinant chemerin (aa 21-157) was determined using the Tango assay. HTLA cells expressing mouse CMKLR1 or GPR1 were treated with vehicle (PBS), IgG (10 μg/mL), or mouse chemerin antibody (10 μg/mL) in combination with 10 nM recombinant mouse chemerin (aa 17-156). Increasing concentrations of human recombinant chemerin (0-30 nM) was added to cells and activation of mouse CMKLR1 or GPR1 was determined (A, n=3). The ability of human recombinant chemerin to function as a chemoattractant in the presence of the mouse chemerin antibody was determined using a CMKLR1-expressing L1.2 cell migration assay. Cells were allowed to migrate towards media containing 1 nM mouse chemerin and vehicle (PBS), IgG (10 μg/mL), mouse chemerin antibody (10 μg/mL), and increasing concentrations of human chemerin (1-30 nM) (B, n=2). MSC-derived adipocytes were treated with vehicle (PBS), IgG (30 μg/mL), or chemerin antibody (30 μg/mL) for 24h in the presence of increasing concentrations of recombinant human chemerin. The resulting conditioned adipocyte media was transferred to the Tango assay to determine levels of chemerin bioactivity at mouse CMKLR1 (C, n=2). qPCR analysis was performed on the treated adipocytes to determine levels of Mmp3 and Ccl2 expression (D, n=4). Values are normalized to vehicle control with 10 nM mouse chemerin (A), no chemerin control (B), or vehicle control (no human chemerin, C-D) where * represents $p<0.05$ compared to vehicle control with 10 nM mouse chemerin (A), no chemerin control (B), or no human chemerin within each antibody treatment group (C-D).

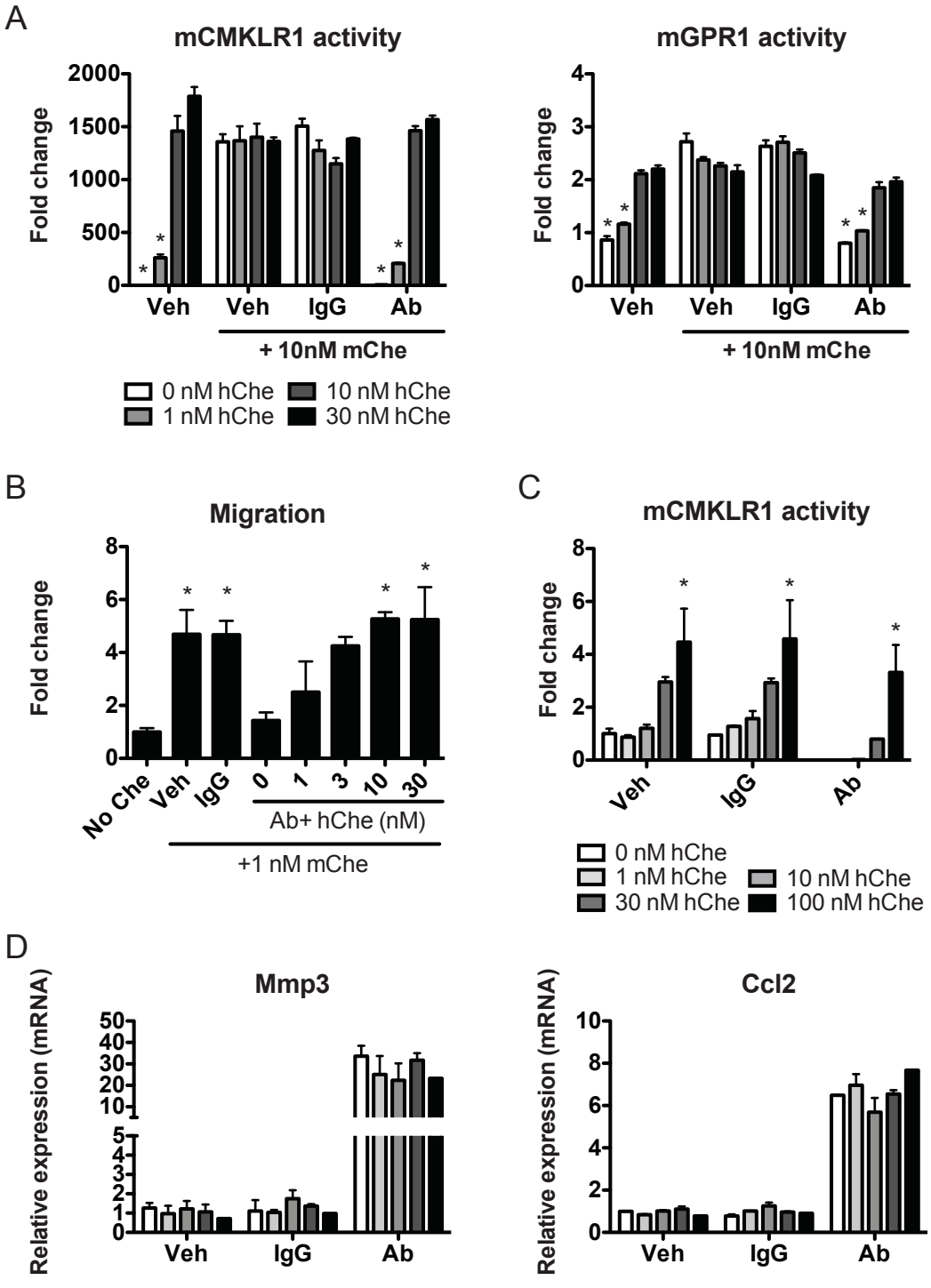
A
mCMKLR1 activity
Fold change
2000
1500
1000
500
0
Veh
Veh
IgG
Ab
+ 10nM mChe
0 nM hChe
10 nM hChe
1 nM hChe
30 nM hChe
mGPR1 activity
Fold change
4
3
2
1
0
Veh
Veh
IgG
Ab
+ 10nM mChe
B
Migration
Fold change
8
6
4
2
0
No Che
Veh
IgG
0
1
3
10
30
Ab+ hChe (nM)
+1 nM mChe
C
mCMKLR1 activity
Fold change
8
6
4
2
0
Veh
IgG
Ab
0 nM hChe
1 nM hChe
10 nM hChe
30 nM hChe
100 nM hChe
D
Mmp3
Relative expression (mRNA)
50
40
30
20
10
5
4
3
2
1
0
Veh
IgG
Ab
Ccl2
Relative expression (mRNA)
10
8
6
4
2
0
Veh
IgG
Ab

Figure 3.13. Treatment of MSC-derived adipocytes with peptide agonists at CMKLR1 does not rescue the effect of neutralizing endogenous chemerin signalling

MSC-derived NFkB-luciferase adipocytes were treated with vehicle (PBS), IgG (10 μg/mL), or neutralizing chemerin antibody (10 μg/mL) for 24 h. The effect of co-treatment with increasing concentrations of hChe9AP (0.01-10 μM) or Dys10 (0-10 μM) on NFkB activity was determined (A, C, n=2). The resulting 24 h-conditioned adipocyte media was transferred to the Tango assay to determine levels of CMKLR1 activation (B, D, n=2). Values are expressed relative to vehicle control (PBS, no peptide treatment) where * represents $p<0.05$ compared to vehicle (PBS) with no peptide treatment.

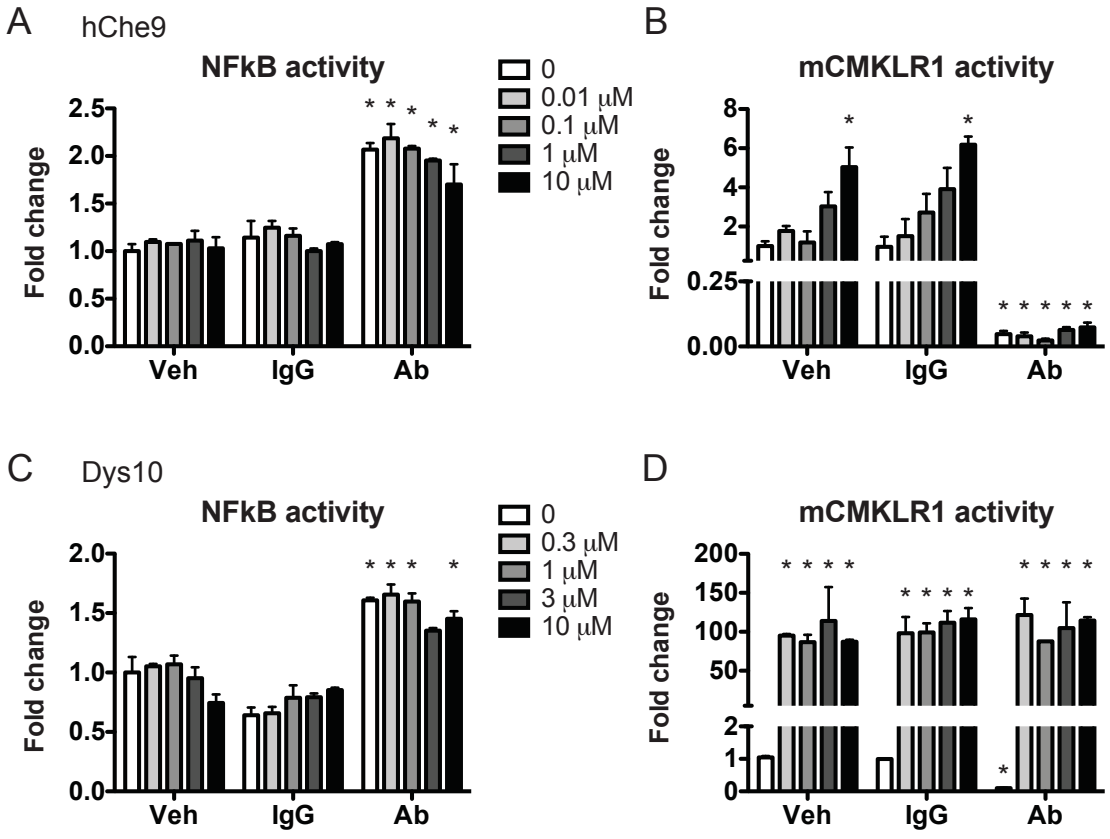
A
hChe9
NFkB activity
Fold change
2.5
2.0
1.5
1.0
0.5
0.0
Veh
IgG
Ab
0
0.01 μM
0.1 μM
1 μM
10 μM
B
mCMKLR1 activity
Fold change
8
6
4
2
0.25
0.00
Veh
IgG
Ab
C
Dys10
NFkB activity
Fold change
2.0
1.5
1.0
0.5
0.0
Veh
IgG
Ab
0
0.3 μM
1 μM
3 μM
10 μM
D
mCMKLR1 activity
Fold change
200
150
100
50
2
1
0
Veh
IgG
Ab

Figure 3.14. Concentration of adipocyte-conditioned media rescues the effect of neutralizing chemerin antibody

24 h MSC-derived adipocyte-conditioned serum-free media was collected and spun in a 10 kDa or 100 kDa spin column to separate adipocyte-secreted proteins based on size (A). Chemerin levels in adipocyte-conditioned media, and the bottom and top fractions of each spin column, were evaluated by Western blot analysis (B, n=4). Recombinant mouse chemerin (aa 17-156) was loaded as a control. MSC-derived NFkB-luciferase adipocytes were treated with vehicle (PBS), IgG (10 μg/mL), or neutralizing chemerin antibody (10 μg/mL) in the presence of control (serum-free media) or isolated fractions from each spin column. Following 24 h, NFkB activity was assessed (C, n=3) and the resulting media was transferred to the Tango assay to examine levels of CMKLR1 activation (D, n=3). Values are expressed relative to vehicle control (no antibody, serum-free media) where * represents $p<0.05$ compared to vehicle control (no antibody, serum-free media) (C, D) and # represents $p<0.05$ compared to antibody-treated adipocytes with serum-free media control (D). B, bottom; T, top.

A

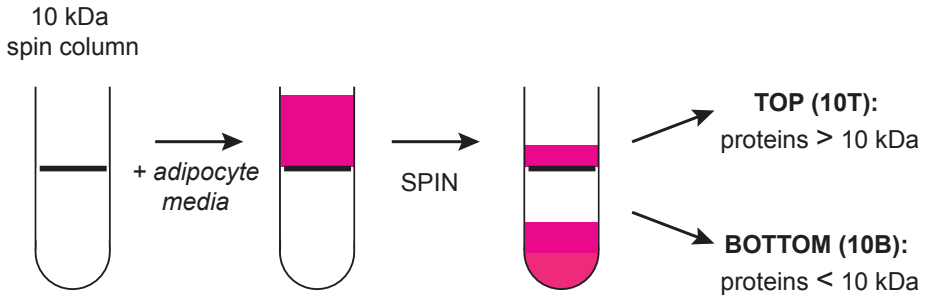
10 kDa
spin column
+ adipocyte
media
SPIN
TOP (10T):
proteins > 10 kDa
BOTTOM (10B):
proteins < 10 kDa

B

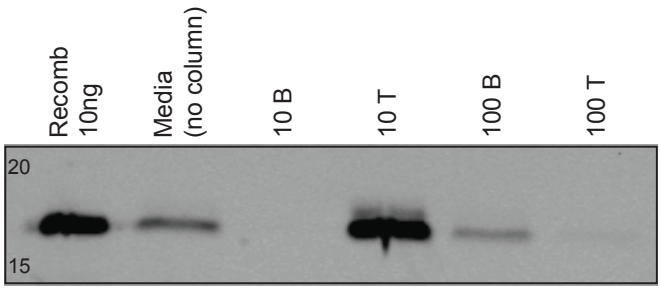
Recomb
10ng
Media
(no column)
10 B
10 T
100 B
100 T
20
15

C

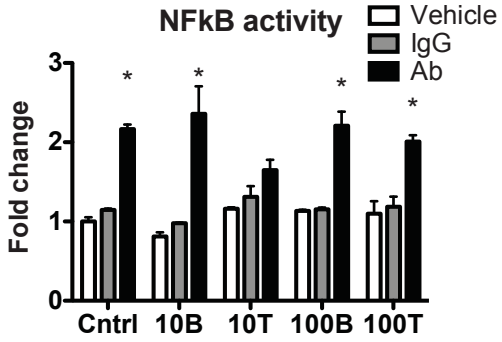
NFkB activity
Vehicle
IgG
Ab
Fold change
3
2
1
0
Cntrl
10B
10T
100B
100T

D

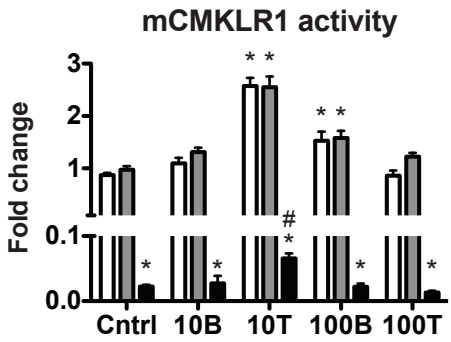
mCMKLR1 activity
Fold change
3
2
1
0.1
0.0
Cntrl
10B
10T
100B
100T

Figure 3.15. Detection of chemerin peptides in adipocyte-secreted media using a tryptic digest and LC-MS/MS analysis

The full mouse chemerin sequence is shown with recombinant mouse chemerin (aa 17-156) indicated in bold (A). Recombinant mouse chemerin was subjected to SDS-PAGE analysis, silver-staining, in-gel digestion with trypsin, and LC-MS/MS. Detected peptides that correspond to the mouse chemerin sequence are highlighted in red and account for 62.35% of total protein coverage (B, n=2). Proteins were immunoprecipitated from adipocyte-conditioned media using the neutralizing chemerin antibody or IgG control and silver staining performed on SDS-PAGE separated proteins (C, n=6). Images are from the same blot but were cropped for presentation. Recombinant chemerin or 24 h-conditioned adipocyte media was assessed by western blot analysis (D, n=10). The silver-stained band corresponding to the predicted size of chemerin (arrow in C) was cut out, digested with trypsin, and subjected to LC-MS/MS analysis. Detected peptides that corresponded to the mouse chemerin sequence are highlighted in red and account for 55.56% of total sequence coverage (E, n=4). Molecular weight markers are indicated in panels C and D.

A

17

MKCLLISLALWLGTVG**TRGTEPELSETQRRSLQVALEEFHKHPPVQLAFQEIGV**
DRAEEVLFSAGTFVRLEFKLQQTNCPKKDWKKPECTIKPNGRRRKCLACIKMDP
KGKILGRIVHCPILKQGPQDPQELQCIKIAQAGEDPHGYFLPGQFAFSRALRTK

156 162

B

Recombinant: 62.35% coverage

17

MKCLLISLALWLGTVGTRGTEPELSETQRRSLQVALEEFHKHPPVQLAFQEIGV
DRAEEVLFSAGTFVRLEFKLQQTNCPKKDWKKPECTIKPNGRRRKCLACIKMDP
KGKILGRIVHCPILKQGPQDPQELQCIKIAQAGEDPHGYFLPGQFAFSRALRTK

156 162

C

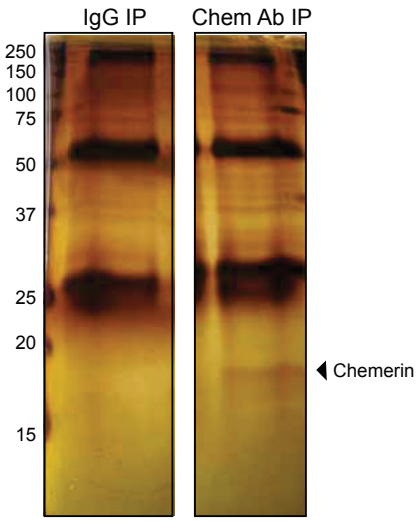

D

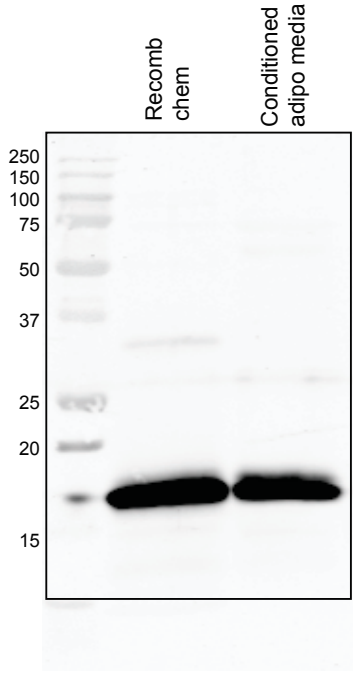

E

Adipocyte-secreted (IP): 55.56% coverage

17

MKCLLISLALWLGTVGTRGTEPELSETQRRSLQVALEEFHKHPPVQLAFQEIGV
DRAEEVLFSAGTFVRLEFKLQQTNCPKKDWKKPECTIKPNGRRRKCLACIKMDP
KGKILGRIVHCPILKQGPQDPQELQCIKIAQAGEDPHGYFLPGQFAFSRALRTK

156 162

Table 3.6. Proteins identified in adipocyte-conditioned media following immunoprecipitation with the neutralizing chemerin antibody

Recombinant mouse chemerin (aa 17-156) or protein(s) immunoprecipitated from adipocyte-conditioned media using the neutralizing chemerin antibody were subjected to SDS-PAGE analysis, silver staining, in-gel digestion with trypsin or LysC, and LC-MS/MS analysis. Proteins for which at least 3 unique peptides were identified are listed.

Accession #	Description	Coverage (%)	Unique peptides (#)	Molecular weight (kDa)
Trypsin Digestion				
Recombinant chemerin				
Q9DD06	Chemerin (Mus musculus)	62.35	22	18.3
cRAP_P02769	Serum albumin (Bos taurus)	5.11	3	69.2
Adipocyte media (chemerin IP)				
Q9DD06	Chemerin (Mus musculus)	55.56	11	18.3
P17742	Peptidyl-prolyl cis-trans isomerase A (Mus musculus)	21.95	3	18.0
LysC Digestion				
Recombinant chemerin				
Q9DD06	Chemerin (Mus musculus)	51.23	12	18.3
cRAP_P02769	Serum albumin (Bos taurus)	14.17	7	69.2
Adipocyte media (chemerin IP)				
cRAP_P02769	Serum albumin (Bos taurus)	39.04	19	69.2
Q9DD06	Chemerin (Mus musculus)	53.09	17	18.3
P10853	Histone H2B type 1-F (Mus musculus)	26.19	4	13.9
Q8CGP6	Histone H2A type 1-H Mus musculus)	63.28	5	13.9
P17742	Peptidyl-prolyl cis-trans isomerase A (Mus musculus)	29.88	3	18.0

Table 3.7. Peptides corresponding to the mouse chemerin sequence identified using LC-MS/MS

Recombinant mouse chemerin (aa 17-156) or chemerin immunoprecipitated from adipocyte-conditioned media were subjected to SDS-PAGE analysis, silver staining, in-gel digestion with trypsin or LysC, and LC-MS/MS analysis. Detected peptides are listed in the order that they occur in the mouse chemerin sequence (Q9DD06, amino to carboxyl terminus).

Enzyme	Recombinant chemerin	Adipocyte-secreted chemerin
Trypsin:	GTEPELSETQR	TEPELSETQR
	PELSETQR	SLQVALEEFHK
	SLQVALEEF	QVALEEFHK
	SLQVALEEFHK	HPPVQLAFQEIGVDR
	LQVALEEFHK	AEEVLFSAGTFVR
	HPPVQLAFQEIGVDR	IVHCPILK
	LAFQEIGVDR	QGPQDPQELQCIK
	AFQEIGVDR	IAQAGEDPHGY
	FQEIGVDR	IAQAGEDPHGYFLPGQF
	AEEVLFSAGTF	IAQAGEDPHGYFLPGQFAF
	AEEVLFSAGTFVR	
	KPECTIKPN	
	IVHCPILK	
	HCPILK	
	QGPQDPQELQ	
	QGPQDPQELQC	
	QGPQDPQELQCIK	
	IAQAGEDPHGY	
	IAQAGEDPHGYFLPGQF	
	IAQAGEDPHGYFLPGQFAF	
	IAQAGEDPHGYFLPGQFAFS	
LysC:	TRGTEPELSETQRRSLQVALEEFHK	GTEPELSETQRRSLQVALEEFHK
	SLQVALEEFHK	TEPELSETQRRSLQVALEEFHK
	QVALEEFHK	PELSETQRRSLQVALEEFHK
	KPECTIK	SLQVALEEFHK
	CLACIK	QVALEEFHK
	ILGRIVHCPILK	KPECTIK
	LGRIVHCPILK	CLACIK
	QGPQDPQELQCIK	ILGRIVHCPILK
	PQELQCIK	LGRIVHCPILK
	IAQAGEDPH	QGPQDPQELQCIK
	IAQAGEDPHGYFLPG	PQELQCIK
	IAQAGEDPHGYFLPGQFAFS	IAQAGEDPHGYFLPGQFA
		IAQAGEDPHGYFLPGQFAF
		IAQAGEDPHGYFLPGQFAFS
		IAQAGEDPHGYFLPGQFAFSR
		IAQAGEDPHGYFLPGQFAFSRA
		IAQAGEDPHGYFLPGQFAFSRAL
		IAQAGEDPHGYFLPGQFAFSRALRT

Figure 3.16. Mass spectrometry analysis of LysC-digested chemerin reveals the presence of multiple chemerin isoforms in adipocyte-conditioned media

Recombinant mouse chemerin or chemerin immunoprecipitated from MSC-derived adipocyte-conditioned media were subjected to LysC digestion and LC-MS/MS analysis. Peptides detected that correspond to the mouse chemerin sequence are highlighted in red to show overall coverage of the mouse chemerin sequence (A, n=3). Further analysis of the identified peptides revealed the presence of a number of peptides corresponding to the C-terminal sequence of chemerin in adipocyte-secreted media but not recombinant chemerin (B). Fragmentation patterns of the peptides IAQAGEDPHGYFLPGQFA (top, MS/MS spectra of $[M+2H]^{2+}$ at m/z 959.46) and IAQAGEDPHGYFLPGQFAF (bottom, MS/MS spectra of $[M+2H]^{2+}$ at m/z 1032.99) (C).

A

Recombinant: 51.23% coverage

17
MKCLLISLALWLGTVGTRGTEPELSETQRRSLQVALEEFHKHPPVQLAFQEIGV
DRAEEVLFSAGTFVRLEFKLQQTNCPKKDWKKPECTIKPNGRRRKCLACIKMDP
KGKILGRIVHCPILKQGPQDPQELQCIKIAQAGEDPHGYFLPGQFAFSRALRTK
156 162

Adipocyte-secreted (IP): 53.09% coverage

17
MKCLLISLALWLGTVGTRGTEPELSETQRRSLQVALEEFHKHPPVQLAFQEIGV
DRAEEVLFSAGTFVRLEFKLQQTNCPKKDWKKPECTIKPNGRRRKCLACIKMDP
KGKILGRIVHCPILKQGPQDPQELQCIKIAQAGEDPHGYFLPGQFAFSRALRTK
156 162

B

Recombinant mChem:	Adipocyte-secreted (IP):
IAQAGEDPHGYFLPGQFAFS	IAQAGEDPHGYFLPGQFA
	IAQAGEDPHGYFLPGQFAF
	IAQAGEDPHGYFLPGQFAFS
	IAQAGEDPHGYFLPGQFAFSR
	IAQAGEDPHGYFLPGQFAFSRA
	IAQAGEDPHGYFLPGQFAFSRAL
	IAQAGEDPHGYFLPGQFAFSRALRT

C

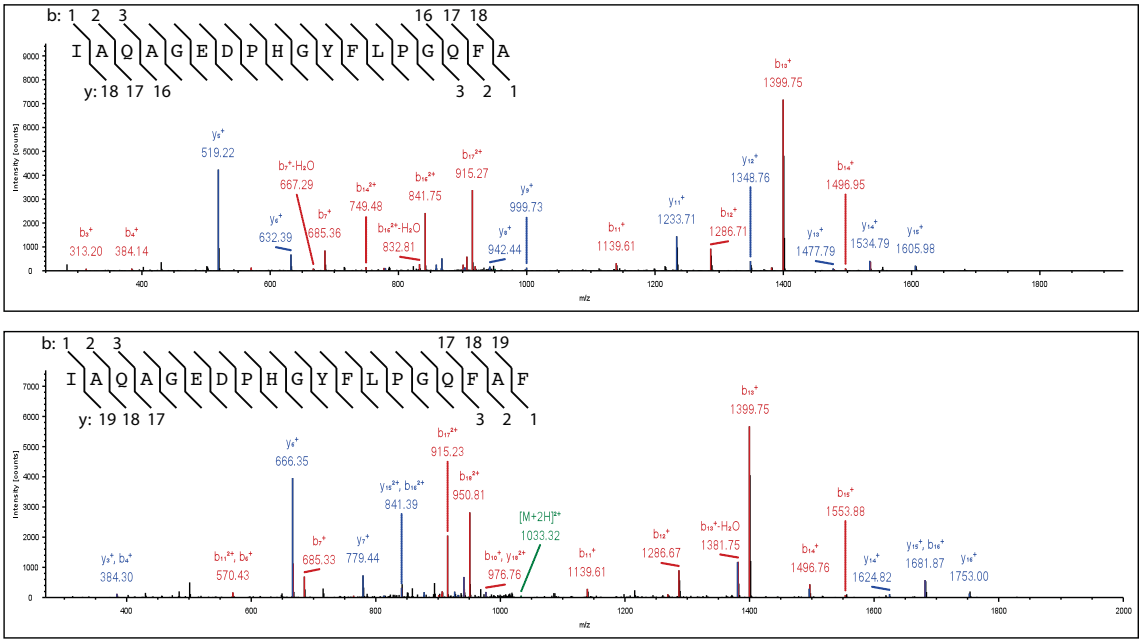

Figure 3.17. Multiple reaction monitoring confirms the presence of numerous chemerin isoforms in adipocyte-conditioned media

MRM was performed on LysC-digested adipocyte-conditioned media. The MRM-extracted ion chromatograms of the acquired transitions corresponding to the peptides IAQAGEDPHGYFLPGQFAFSRALR (A, $[M+4H]^{4+}$ at m/z 662.8397) and IAQAGEDPHGYFLPGQF (B, $[M+3H]^{3+}$ at m/z 616.296) are shown for three independent biological samples (transition intensity versus retention time). Each transition is indicated in a different colour.

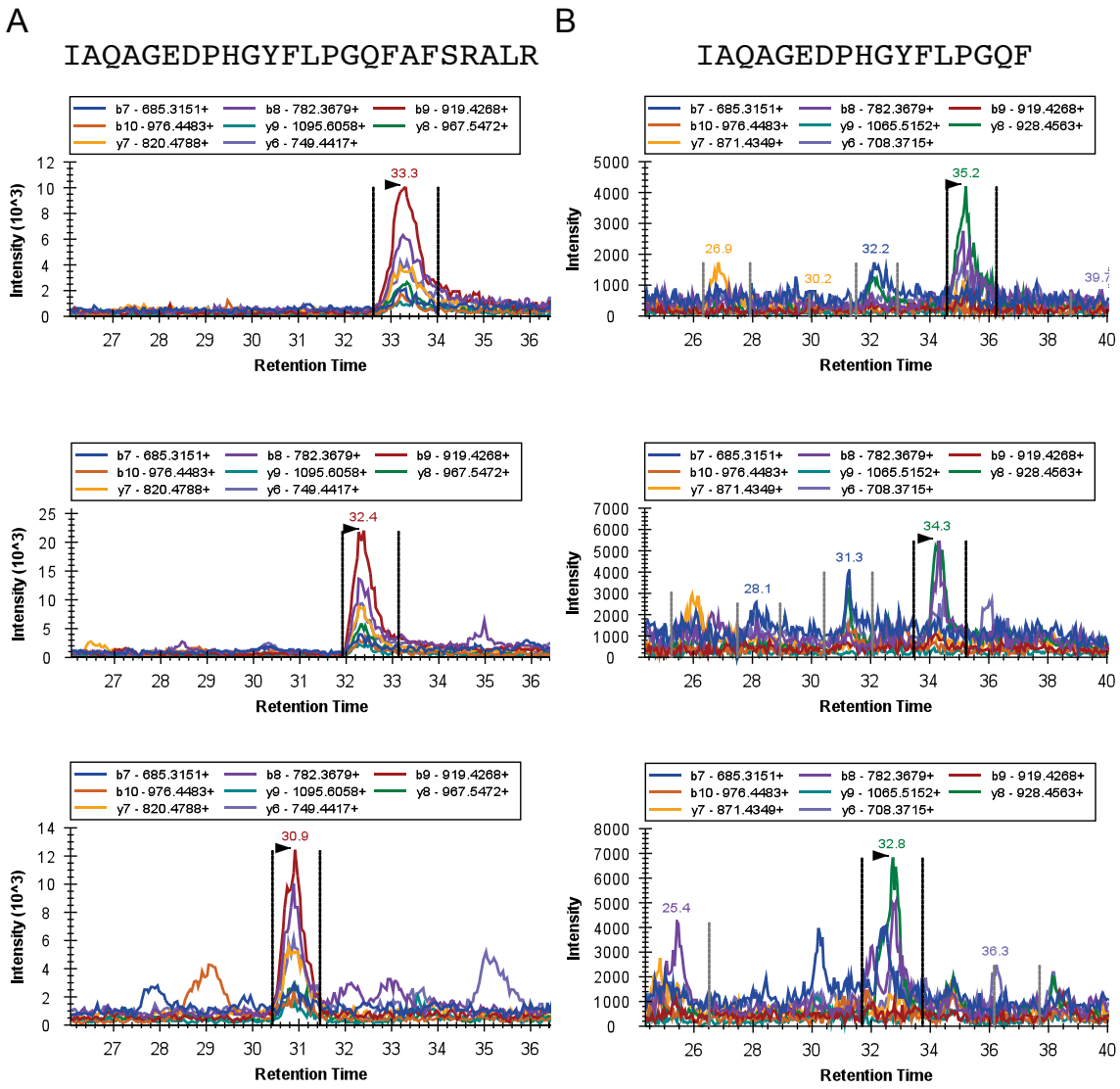
A
IAQAGEDPHGYFLPGQFAFSRALR
b7 - 685.3151+
b8 - 782.3679+
b9 - 919.4268+
b10 - 976.4483+
y9 - 1095.6058+
y8 - 967.5472+
y7 - 820.4788+
y6 - 749.4417+
Intensity (10^3)
Retention Time
33.3
32.4
30.9
B
IAQAGEDPHGYFLPGQF
b7 - 685.3151+
b8 - 782.3679+
b9 - 919.4268+
b10 - 976.4483+
y9 - 1065.5152+
y8 - 928.4563+
y7 - 871.4349+
y6 - 708.3715+
Intensity
Retention Time
35.2
26.9
32.2
30.2
34.3
31.3
28.1
32.8
25.4
36.3

Table 3.8. Multiple reaction monitoring of C-terminal chemerin peptides in adipocyte-conditioned media

MRM was performed on LysC-digested proteins precipitated from adipocyte-conditioned media. Ion chromatograms were analysed using Skyline to determine the number of transitions detected, transition peak height, and total peak area (combined total of all transitions originating from the same precursor). Trends were similar across three independent samples. Peak height and total area values from a representative sample are shown. * represents that clear peaks were only present in 2 of 3 samples.

Peptide sequence	Charge	Transitions (>3)	Peak height	Total area
IAQAGEDPHGYFLPGQFAFSRALRTK	+4	Yes	11843	464361
IAQAGEDPHGYFLPGQFAFSRALRT	+3	Yes	7461	204185
IAQAGEDPHGYFLPGQFAFSRALR	+3	No	--	--
IAQAGEDPHGYFLPGQFAFSRALR	+4	Yes	21501	1979614
IAQAGEDPHGYFLPGQFAFSRAL	+3	Yes	16821	1479543
IAQAGEDPHGYFLPGQFAFSRAL	+4	Yes	23932	3032101
IAQAGEDPHGYFLPGQFAFSRA	+3	Yes	9506	443526
IAQAGEDPHGYFLPGQFAFSR	+3	Unclear	2291	169745
IAQAGEDPHGYFLPGQFAFS	+2	--	--	--
IAQAGEDPHGYFLPGQFAFS	+3	Yes *	5414	677586
IAQAGEDPHGYFLPGQFAF	+3	Unclear	59257	3646091
IAQAGEDPHGYFLPGQFA	+3	No	--	--
IAQAGEDPHGYFLPGQFA	+2	No	--	--
IAQAGEDPHGYFLPGQF	+3	Unclear	5068	460809
IAQAGEDPHGYFLPGQ	+2	Yes	67752	4984258

Figure 3.18. Overexpression of active chemerin and prochemerin rescues the effect of the neutralizing antibody in MSC-derived adipocytes

MSCs with stable integration of pLJM1-GFP, mouse chemerin (active), or mouse chemerin (pro) were differentiated into mature adipocytes. Adipocytes derived from three different MSC colonies for each isoform were treated with vehicle (PBS), IgG (30 μg/mL), or neutralizing chemerin antibody (10 or 30 μg/mL) for 24 h. Mmp3 and Ccl2 expression were determined using qPCR (A, n=3). The resulting 24 h-conditioned adipocyte media was transferred to the Tango assay to determine levels of CMKLR1 activation (B, n=3). Values are expressed relative to vehicle within each colony (A) or GFP (B) where * represents $p<0.05$ compared within each colony (A, B) and # represents $p<0.05$ compared amongst vehicle treatments (B).

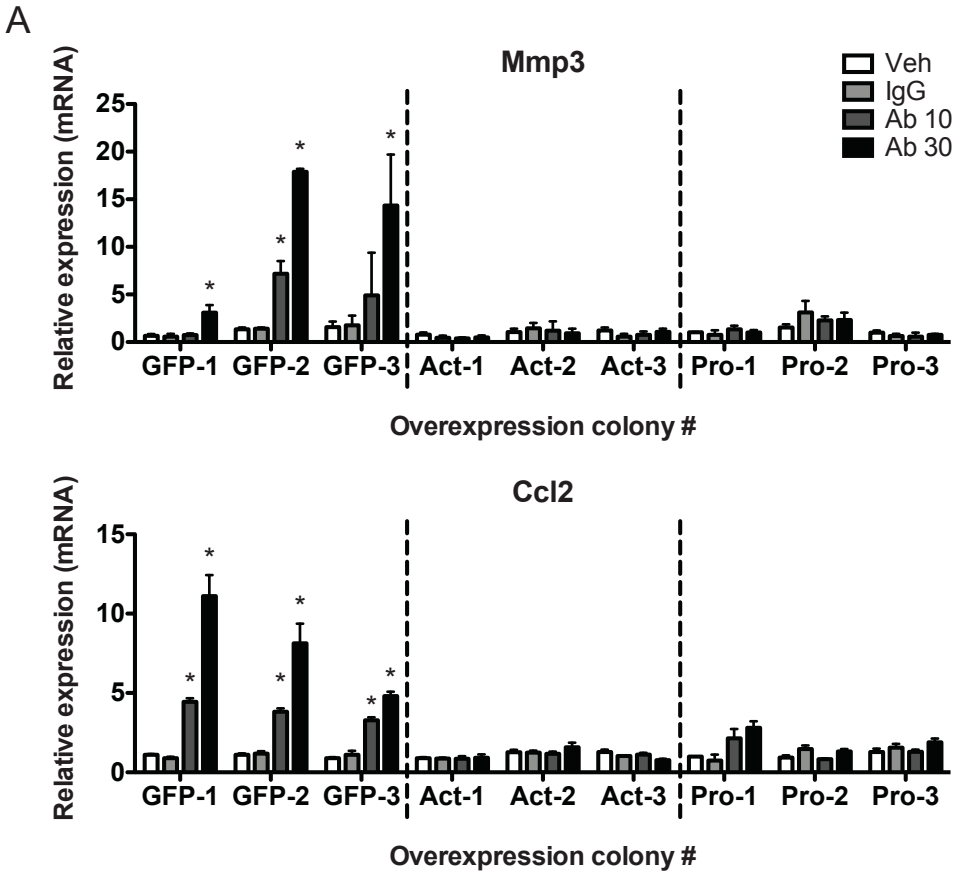
A
Mmp3
Veh
IgG
Ab 10
Ab 30
Relative expression (mRNA)
25
20
15
10
5
0
GFP-1
GFP-2
GFP-3
Act-1
Act-2
Act-3
Pro-1
Pro-2
Pro-3
Overexpression colony #
Ccl2
Relative expression (mRNA)
15
10
5
0
GFP-1
GFP-2
GFP-3
Act-1
Act-2
Act-3
Pro-1
Pro-2
Pro-3
Overexpression colony #

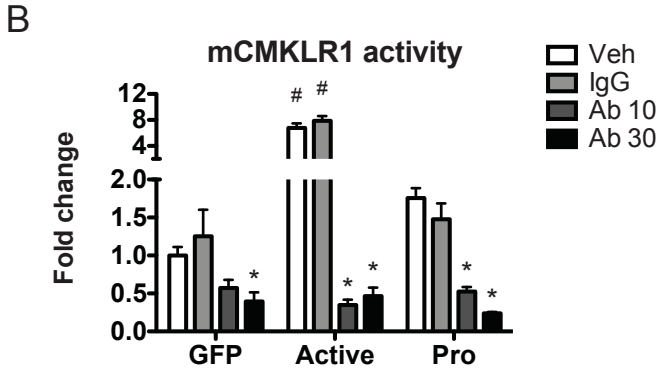
B
mCMKLR1 activity
Veh
IgG
Ab 10
Ab 30
Fold change
12
8
4
2.0
1.5
1.0
0.5
0.0
GFP
Active
Pro

CHAPTER 4: LOCAL CHEMERIN LEVELS ARE POSITIVELY ASSOCIATED WITH DSS-INDUCED COLITIS BUT CONSTITUTIVE LOSS OF CMKLR1 DOES NOT PROTECT AGAINST DEVELOPMENT OF COLITIS

Copyright statement

Contribution statement

Dr. Jillian Rourke performed DEXA scans on mice on day 6 of the study before sacrifice and Dr. Andrew Stadnyk was responsible for assigning the blinded colon inflammation scores. I was responsible for designing and performing all other experiments with guidance from Dr. Christopher Sinal and Dr. Andrew Stadnyk.

Abstract

Inflammatory bowel disease (IBD) is a family of disorders including ulcerative colitis and Crohn's disease that are characterized by chronic and relapsing intestinal inflammation. Increased production of pro-inflammatory mediators, possibly combined with low expression of anti-inflammatory mediators, is thought to promote the development and progression of IBD. In the current study, we demonstrate that expression, secretion, and processing of chemerin, a potent chemoattractant for cells expressing chemokine-like receptor 1 (CMKLR1), increased in the cecum and colon along a gradient positively associated with the severity of inflammation in dextran sodium sulphate (DSS)-induced colitis. We also show that levels of circulating bioactive chemerin increased following DSS treatment. At both 6-8 and 14-16 weeks of age, CMKLR1 knockout mice developed signs of clinical illness more slowly than wildtype and had changes in circulating cytokine levels, increased spleen weight, and increased local chemerin secretion following DSS treatment. However, knockout mice ultimately developed similar levels of clinical illness and local inflammation as wildtype. Finally, contrary to previous reports, intraperitoneal injection of bioactive chemerin had no effect on the severity of DSS-induced colitis. This suggests that local chemerin levels have a greater impact than circulating levels in the pathogenesis of colitis. Considered altogether, bioactive chemerin represents a novel biomarker for IBD severity, although strategies to modulate endogenous chemerin signalling other than chronic CMKLR1 loss are necessary in order to exploit chemerin as a therapeutic target for the treatment of IBD.

Introduction

Inflammatory bowel disease (IBD) is a family of disorders characterized by chronic relapsing inflammation and mucosal damage in the gastrointestinal (GI) tract. IBD is believed to develop in response to a combination of genetic and environmental factors with the two main forms, Crohn's disease (CD) and ulcerative colitis (UC) having distinct pathologies (Ford et al. 2013; Frolkis et al. 2013; Hanauer 2006; Kaser et al. 2010). In both disorders, inflammation involves diffuse leukocyte infiltration and increased levels of pro-inflammatory cytokines, resulting in damage and disruption of the epithelium and the formation of ulcers, crypt abscesses, and in the case of CD, fistulas and strictures (Hanauer 2006; Kaser et al. 2010). IBD is associated with abdominal pain, diarrhea, rectal bleeding, and a significantly compromised quality of life (Ford et al. 2013). Common treatment approaches include anti-inflammatory (e.g. 5-aminosalicylates, glucocorticosteroids), immunosuppressant (e.g. thiopurines), and biologic (e.g. anti-TNF) agents that modulate the function of chemokine and cytokine networks that mediate intestinal inflammation (Bernstein 2015; Ford et al. 2013). However, available treatments are known to produce undesirable effects (e.g. glucocorticoid-stimulated bone loss) and often suffer from high relapse rates (Bernstein 2015; Ford et al. 2013; Podolsky 2002). Thus current research continues to be focused on the signalling networks that underlie the development and progression of IBD in attempts to identify novel therapeutic targets.

Chemerin is an 18-kDa secreted protein that was first isolated from human inflammatory fluids and has since been positively associated with a number of diseases involving chronic inflammation (Wittamer et al. 2003). These include kidney disease, pancreatitis, pre-eclampsia, polycystic ovary syndrome, obesity, and liver disease (for review see (Mariani and Roncucci 2015; Rourke et al. 2013)). Chemerin has also been characterized as an adipokine and secretion of the inactive precursor, prochemerin, from white adipose tissue, in addition to the liver, is thought to be the primary source of circulating chemerin (Goralski et al. 2007). Circulating or locally expressed prochemerin undergoes extracellular processing to generate a variety of bioactive isoforms (for review, see (Rourke et al. 2013)). Bioactive chemerin binds and activates two different G protein coupled receptors (GPCR) – chemokine-like receptor 1 (CMKLR1) and G protein

coupled receptor 1 (GPR1) (Barnea et al. 2008; Meder et al. 2003; Rourke et al. 2013; Wittamer et al. 2003). Chemerin has also been shown to bind to C-C chemokine receptor-like 2 (CCRL2), which is believed to be a non-signalling chemerin receptor (Zabel et al. 2008). All three receptors have been shown to play functional roles in mediating chemerin action in inflammation, immunity, and metabolism ((Rourke et al. 2014), for review see (Rourke et al. 2013; Zabel et al. 2014)). However, the function of chemerin as a potent chemoattractant for leukocytes that express CMKLR1, including macrophages, dendritic cells, and natural killer cells, has received particular attention (Wittamer et al. 2003; Zabel et al. 2005b). Numerous *in vitro* and animal studies have demonstrated that chemerin/CMKLR1 signalling plays an essential role in the recruitment of CMKLR1-expressing cells to sites of localized inflammation or tissue damage (Mariani and Roncucci 2015; Rourke et al. 2013). Importantly, chemerin has been shown to play a role in the recruitment of macrophages to the developing fetal intestine (Maheshwari et al. 2009). With these biological activities in mind, recent studies have focused on whether chemerin plays an active role in IBD.

Clinical studies have demonstrated that circulating total chemerin levels are elevated in patients with both UC and CD and that chemerin expression is higher in colon biopsies from inflamed versus healthy regions in UC patients (Lin et al. 2014; Weigert et al. 2010b). Furthermore, animal studies have shown that injection of bioactive chemerin exacerbates the severity of colitis (Lin et al. 2014). Given that IBD is characterized by increased infiltration of immune cells to the colon, we hypothesized that chemerin signalling plays a pro-inflammatory role in IBD and that a loss of CMKLR1 would protect against development of the disease. We demonstrate that endogenous chemerin expression, secretion, and bioactivity indeed increase with the onset of DSS-induced colitis. In addition, we directly investigate the role of CMKLR1 in an animal model of IBD. We show that while a loss of CMKLR1 does not protect against development of DSS-induced colitis, CMKLR1 KO mice have a slower onset of clinical illness and altered systemic inflammatory parameters.

Methods

Animals

C57BL/6 mice were obtained from the Jackson Laboratory (Bar Harbor, ME). CMKLR1 knockout mice were fully backcrossed onto the C57Bl/6 background and have been previously described (Ernst et al. 2012). All studies were performed with male animals 6-8 weeks of age unless otherwise indicated. For studies involving CMKLR1 heterozygous (HET) and knockout (KO) mice, breedings were between male and female mice heterozygous for CMKLR1 such that littermates of all three genotypes were available and analysed. Mice were maintained under specific pathogen free conditions, at 21°C in a 12 h dark and light cycle with free access to food and water. Animals were sacrificed using an overdose (90 mg/kg) of pentobarbital sodium injected intraperitoneally followed by exsanguination via cardiac puncture. All experimental protocols were approved by the Dalhousie University Committee on Laboratory Animals and in accordance with the Canadian Council on Animal Care guidelines.

Dual-energy X-ray absorptiometry (DEXA)

Mice were anesthetized using isoflurane and body composition was assessed using a GE Lunar Piximus 2 densitometer and LUNAR PIXImus2 software (GE Medical Systems, Milwaukee, WI). The DEXA instrument was calibrated before each use and the head region of each mouse was excluded from analysis.

DSS-induced colitis model

Experimental ulcerative colitis was induced as described previously (Jain et al. 2013). Briefly, facility drinking water was supplemented with 5% or 3.5% w/v DSS (36 000-50 000 MW; MP Biomedicals, Solon, OH, USA) for 5 days *ad libitum*. On day 5, mice were returned to normal drinking water. Healthy control subjects received normal drinking water throughout the study. Water consumption levels were measured daily and no difference between cages was detected (data not shown). Body mass, stool consistency, and presence of blood in the stool (determined using FOB Test, Innovatek Medical Inc., Delta, BC) was monitored daily. Clinical scores (Table 4.1) were assigned based on a scoring system previously described (Stillie and Stadnyk 2009). Mice were

sacrificed on day 6 (e.g. one day after removal of DSS) and the spleen was resected and weighed. The colon was excised, measured, flushed with PBS, and then divided longitudinally into pieces for further analysis as described below.

For experiments involving injection of chemerin, 500 ng of recombinant BSA-free mouse chemerin protein (aa 17-156, R&D, Minneapolis, MN, USA) or PBS (control) was injected intraperitoneally every other day starting on day 0. Recombinant chemerin contained <0.01 endotoxin units per 1 μg protein as assessed by the manufacturer using the limulous amoebocyte lysate (LAL) test.

Explant cultures

Adipose tissue was removed from excised colons and the colon was divided into 5 pieces, rinsed three times with PBS containing penicillin (100 U/mL) and streptomycin (100 μg/mL), and placed in a 24-well plate (Costar, Corning, NY, USA) containing 1mL high glucose (4.5 g/L) DMEM with 10 mM HEPES, 0.5% fetal bovine serum, 2 mM L-glutamine, 50 μM 2-mercaptoethanol, penicillin, and streptomycin. Colon explants were cultured at 37°C with 5% CO_2. After 24 h, explants were collected, pelleted by centrifugation, and the tissue pellet weighed. The supernatant was stored at -80°C in aliquots for further use.

Histology and immunohistochemistry

A longitudinal piece of colon was rolled using the "Swiss roll" method. Rolled colons were fixed in 10% neutral buffered formalin for 24 h and then transferred to 70% ethanol. Colons were then processed for paraffin embedding, 4 μm sections cut from the centre of each roll, and stained with hematoxylin and eosin. Sections were assessed for signs of inflammation by a blinded investigator based on parameters previously described (Stillie and Stadnyk 2009). Briefly, a score was assigned based on the presence of edema (0-1), ulceration (0-3), hyperplasia (0-3), crypt damage (0-5), and inflammatory infiltrate (0-5) (Table 4.2).

For immunohistochemistry, colon sections were deparaffinized, hydrated through a series of ethanol washes (100%, 95%, and 70%), and antigen retrieval performed via incubation with 20 μg/mL proteinase K (Promega, Madison, WI, USA) for 15 min.

Slides were then incubated with 1:25 rat anti-mouse CMKLR1 (AbCam, Boston, MA, USA) overnight at 4°C. The next day, colon sections were washed with PBST, incubated with 3% hydrogen peroxide for 10 min, and then incubated with biotinylated anti-rat secondary (BioLegend, San Diego, CA, USA) for 1 h at room temperature. Slides were washed, incubated with avidin/biotin complex for 30 min (Vector Laboratories, Burlingame, CA, USA) at room temperature, and developed with DAB staining (Vector Laboratories, Burlingame, CA, USA) for 3 min. Slides were then stained with hematoxylin, dehydrated, and mounted with Cytoseal60 (Fisher Scientific, Ottawa, ON). Images were taken using an Axioplan II microscope, Axiocam HRC colour camera, and Zen 2012 Lite software (Zeiss, Toronto, ON). Representative images of three independent experiments are shown.

RNA isolation and quantitative PCR (qPCR)

Immediately after sacrifice, GI tissues were excised and carefully cleared of any attached adipose tissue. White adipose tissue (WAT) samples were isolated from the mesenteric adipose depot. Tissues were cut into pieces and placed into TriZol (Ambion, Carlsbad, CA, USA). Samples were homogenized using PowerGen700 (Fisher Scientific, Ottawa, ON) and RNA was isolated according to manufacturer's instructions until after the addition of 70% ethanol, at which point the sample was transferred to an RNAeasy column (Qiagen, Valencia, CA, USA). RNA was further isolated according to manufacturer's recommendations including the on-column DNA digestion step. RNA was quantified using FLUOstar Omega (BMG LabTech, Cary, NC, USA). Approximately 2 μg of RNA was transcribed to cDNA using EcoDry Premix Double-primed (Clontech, MountainView, CA, USA). cDNA was then diluted to 0.25 μg/μL and qPCR performed using 1 μL of cDNA per reaction, with 0.5 μM primers, and FastStart SYBR green master mix (Roche, Laval, QC). qPCR was performed on LightCycler96 according to manufacturer's recommendations and analysed using LightCycler96 software (Roche, Laval, QC). Relative gene expression was calculated using ΔΔCt method (Livak and Schmittgen 2001) where each sample was normalized to cyclophilin A as the reference gene. Primer sequences were as follows: Chemerin (NM_027851) 5' TACAGGTGGCTCTGGAGGAGTTC, 3' CTTCTCCCGTTTGGTTTGATTG;

CMKLR1 (NM_008153) 5’ GCTTTGGCTACTTTGTGGACTT, 3’ CAGTGTTCACGGTCTTCTTCATCTTG; GPR1 (NM_146250) 5’ ATTCAGCGCAGGCACCTTTC, 3’ CAAGCTGTCGTGGTGTTTGA; CCRL2 (NM_017466) 5’ CTCTGCTTGTCCTCGTGCTT, 3’ GCCCACTGTTGTCCAGGTAG; Cyclophilin A (NM_008907) 5’ GAGCTGTTTGCAGACAAAGTTC, 3’ CCCTGGCACATGAATCCTGG.

Blood collection

For experiments involving daily collection of serum, blood was collected from the saphenous vein of alert mice. For experiments involving serum collection at sacrifice, blood was collected via cardiac puncture after mice had been administered a lethal dose of sodium pentobarbital. For both, blood was allowed to clot at room temperature for 2 h, spun at 2000 g for 20 min, and then the serum collected and stored in aliquots at -80°C until further use.

Analysis of cytokine and chemerin levels

Inflammatory cytokine levels (IL-6, IL-17a, IFN-γ, and TNF) were determined in colon explant supernatant (no dilution) and serum (1:4 dilution) using a Bio-plex multiplex assay according to manufacturer’s instructions (Bio-Rad, Hercules, CA, USA) using a Bio-Plex 200 luminometer (Bio-Rad, Hercules, CA, USA).

Total chemerin levels in serum (1:100 dilution) and explant supernatant (1:20 dilution) were determined by ELISA (R&D, Minneapolis, MN, USA) as per manufacturer’s instructions. For analysis of chemerin levels in colon explant cultures, results were normalized to the weight of colon tissue that was collected.

Bioactive chemerin levels in serum (1:10 dilution) were determined using the Tango assay for mouse CMKLR1 activation as previously described (Barnea et al. 2008; Parlee et al. 2010; Ernst et al. 2010). Briefly, HTLA cells were transfected with mCMKLR1. After 24 h the cells were treated with the sample of interest for 24 h. Cells were then lysed and luminescence detected as a read-out of beta-arrestin recruitment/CMKLR1 activation. Luciferase activity was normalized to β-gal activity as an internal control and the concentration of bioactive chemerin was determined by

plotting against a standard curve generated with recombinant mouse chemerin (aa 17-156, R&D, Minneapolis, MN, USA).

Western blot analysis

For analysis of chemerin levels in colon explant cultures via SDS-PAGE, 10 ng of recombinant mouse chemerin (aa 17-156, R&D, Minneapolis, MN, USA) or 30 µL of culture supernatant was boiled with 6x SDS-PAGE loading buffer containing 2-mercaptoethanol. Proteins were separated on a 15% gel and transferred to nitrocellulose membrane (BioRad laboratories, Mississauga, ON). Blots were blocked with Odyssey blocking buffer (LI-COR, Lincoln, NE, USA) and then incubated with anti-chemerin (R&D, Minneapolis, MN, USA) overnight at 4°C followed by incubation with an IRDye800-conjugated secondary antibody (LI-COR). Immunoreactive bands were detected by scanning at 800 nm using the Odyssey Infrared System (LI-COR Biosciences, Lincoln, NE, USA).

Statistical analysis

All statistical analysis was performed using GraphPad Prism (version 5.0b, La Jolla, CA, USA). All parametric data is shown as mean ± SEM. For comparisons, a Student's t-test (two groups) or one-way ANOVA with a Tukey post-test (3+ groups) was performed, with repeated measures when possible (chemerin levels throughout DSS treatment). A two-way ANOVA with a Bonferonni post-test was used to compare across genotypes and before/after DSS treatment or healthy/DSS-treated animals. Non-parametric data (clinical illness and inflammation scores) are presented as median and were compared using a Kruskal-Wallis test with Dunn's multiple comparison post-test. Within a particular day of treatment, chemerin versus PBS injection groups were compared using a Mann-Whitney test. For all statistical tests, a significant difference was considered $p<0.05$.

Results

Chemerin and CMKLR1 expression increase in the cecum and distal colon following DSS treatment

We first investigated the expression of chemerin and chemerin receptors throughout the mouse gastrointestinal tract. Quantitative PCR (qPCR) analysis demonstrated that chemerin expression was highest in normal mouse stomach, with significantly lower levels in the duodenum, jejunum, and ileum (Figure 4.1A). Basal expression of CMKLR1 or CCRL2 was generally similar across the GI tract with the exception of significantly higher levels of CMKLR1 in mesenteric WAT (Figures 4.1B and 4.1D). However, GPR1 expression was modestly decreased in all tissues except for the distal colon and WAT when compared to stomach (Figure 4.1C). We next examined changes in chemerin and receptor expression within the GI tract following DSS-induced colitis. This model reproducibly induces disease which resembles human UC as it produces a cecum and distal colon-specific mucosal, ulcerating inflammation; however, some features of CD such as transmural inflammation, may also be present (Goyal et al. 2014). Tissues were isolated one day following the removal of DSS from the drinking water in order to minimize any confounding effects of residual DSS on our analyses. qPCR analysis revealed a dramatic increase in chemerin expression in the cecum and distal colon (~6.5-fold) and a modest 1.5-fold increase in mesenteric WAT (Figure 4.1A). Notably, there was no change in chemerin expression in the proximal colon. Similarly, CMKLR1 expression increased ~5-fold in both the cecum and distal colon (Figure 4.1B). There was a modest increase in CMKLR1 expression in the stomach but not in any other tissue examined. While CCRL2 expression increased dramatically in the distal colon and cecum (~12- and ~5-fold, respectively; Figure 4.1D) no changes in GPR1 expression were observed following DSS treatment (Figure 4.1C).

CMKLR1 is highly expressed on leukocytes such as macrophages, dendritic cells, and natural killer cells, as well as intestinal epithelial cell lines (Wittamer et al. 2003; Zabel et al. 2005b; Campbell et al. 2010). In order to investigate whether the increase in CMKLR1 expression in the distal colon was in the cells comprising the colon (e.g. epithelial or muscle cells) or a result of increased cell infiltrate, we performed immunohistochemistry to visualize CMKLR1 expression along the entire length of the

colon. An increase in CMKLR1 expression was observed in colons isolated from animals that received DSS treatment compared to healthy animals, and this was largely on infiltrating immune cells that can be observed in the submucosa (Figure 4.1E). As expected, there was no detection of CMKLR1 in KO animals.

Chemerin secretion from the colon increases in a proximal-distal gradient

Having established that chemerin expression increased in the gastrointestinal tract following DSS treatment, particularly in the distal colon, we next investigated changes in chemerin secretion from the colon. To do this, we generated explant cultures from microdissected regions of the colon from healthy or DSS-treated mice and performed an ELISA to examine total chemerin levels. In healthy animals, chemerin was detected at low levels in the supernatant from middle and distal colon segments but not in the supernatant derived from proximal colon. Consistent with the gene expression data, chemerin expression increased in all three regions following DSS treatment. Specifically, there was a small increase in the proximal segment, a significant increase in the middle segment, and a dramatic increase (from ~8 to 46 ng/g tissue) in the distal segment (Figure 4.2A). Similarly, chemerin was undetectable by Western blot analysis in the supernatant from proximally-derived colon segments but increased along a proximal-distal gradient in both healthy and DSS-treated animals (Figure 4.2B). In all segments of the colon, a band larger in size than the recombinant chemerin control (~16 kDa) was detected in the explant supernatant. This suggests the presence of prochemerin (18 kDa) and indicating a generally absent or very low rate of extracellular processing. However, the detection of an additional band in the distal region from DSS-treated animals which appeared to be similar in size to recombinant chemerin indicates that in addition to increased secretion of chemerin, proteolytic processing of prochemerin occurred selectively in response to DSS-induced inflammation in this colon segment.

Circulating levels of bioactive:total chemerin increase following DSS treatment

We next examined whether circulating chemerin levels change throughout the course of DSS treatment. To do this, blood samples were collected from wildtype mice one day before starting DSS treatment and every day through to sacrifice. Total

chemerin levels as measured by ELISA were decreased starting at day 2 and progressively decreased ~60%, until sacrifice (Figure 4.3A). We then investigated chemerin bioactivity in serum using the cell-based Tango assay, which assesses levels of CMKLR1 activation (Barnea et al. 2008). This demonstrated that chemerin bioactivity in serum did not change over the course of the experiment (Figure 4.B). Notably, this results in an increase in the ratio of circulating bioactive to total chemerin, which is significantly higher on days 5 and 6 of the study (Figure 4.3C). Thus, despite a decrease in total chemerin levels, the relative level of bioactive chemerin in circulation was increased following the induction of DSS-induced colitis.

Signs of DSS-induced illness develop more slowly in CMKLR1-null mice

With the observation that bioactive chemerin levels increased both locally and systemically following the induction of IBD, and that CMKLR1 was the only signalling chemerin receptor to exhibit parallel changes in expression, we investigated the impact of CMKLR1 loss on colitis. To do this, we performed the DSS-induced colitis model with 6-8 week old CMKLR1 wildtype (WT), heterozygous (HET), or knockout (KO) littermate mice and monitored the development of colitis. There was no difference in body weight between any of the three genotypes at the start of the study (day 0). Healthy control animals that received normal drinking water gained weight over the 6 days of the study, with WT mice gaining more weight (5.4%) than HET mice (1.9%) or KO (3.5%) by day 6 (Figure 4.4A). Following treatment with DSS, all three genotypes exhibited significant weight loss on days 5 and 6 when compared to day 0. Dual-energy X-ray absorptiometry (DEXA) analysis on day 6 revealed that all genotypes lost a similar amount of lean and fat mass (~2.8 g and 0.4 g, respectively; Figure 4.4B), with no difference in percent body composition before versus after DSS treatment (Figure 4.4C). However, despite weight loss on day 6, KO mice exhibited significantly less weight loss than WT or HET on day 5 of the study (Figure 4.4A).

Mice were assessed daily for signs of clinical illness and a score based on weight loss, stool consistency, and the presence of blood in the stool was assigned. There was no difference in clinical illness score between genotypes on day 0 or for healthy mice throughout the study (data not shown). By day 6, all genotypes received similar clinical

illness scores of ~8. While KO mice were ultimately not protected from developing signs of clinical illness, the onset of illness occurred more slowly in HET and KO mice (Figure 4.4D). Importantly, KO mice exhibited a significantly lower clinical illness score (3.5 versus 7) than WT on day 5.

Local colonic inflammation is similar between CMKLR1 WT and KO mice

In order to assess colon inflammation among the genotypes following DSS-induced colitis, colons were excised and measured at sacrifice. There was no difference in colon length between genotypes in healthy animals (data not shown). Consistent with the similar clinical illness scores observed by day 6, all three genotypes exhibited similar levels of colon shortening (~25%) following DSS treatment (Figure 4.5A). The level of colon inflammation, based on the presence of edema, crypt structure, cell infiltration, ulcer formation and size, and hyperplasia was also assessed. There were no signs of inflammation in healthy mice (data not shown) and no difference in inflammation score between genotype (Figure 4.5B). As an additional marker of local inflammation, levels of pro-inflammatory cytokines that are increased following intestinal inflammation (Neurath 2014) were assessed in the supernatant of colon explants isolated from 6-8 week old animals. As predicted, significant increases in interferon (IFN)-γ, Interleukin (IL)- 6, IL-17a, and tumor necrosis factor (TNF) were observed for animals that received DSS treatment compared to healthy controls. However, for both healthy and DSS-treated animals, there were no differences in the levels of these cytokines between WT and KO animals (Figure 4.5C). Considered altogether, this indicates that local levels of inflammation were similar in WT and KO animals at the conclusion of the treatment period.

Loss of CMKLR1 alters systemic inflammation response to DSS-induced colitis

The secretion of pro-inflammatory cytokines was measured in the serum of 6-8 week old mice before and after DSS treatment in order to assess changes in systemic inflammation (Figure 4.6A). Levels of IFN-γ and IL-6 were similar in WT and KO animals before DSS treatment. Notably, levels of both IL-17a and TNF were decreased in healthy KO animals. Following DSS treatment, significant increases in circulating

IFN-γ, IL-6, IL-17a, and TNF levels were observed in WT animals. Similarly, increased levels of these cytokines were also observed in KO animals; however, the increase in IL-6 levels was not significant and modest compared to that of WT animals (Figure 4.6A). As an additional systemic parameter of inflammation, spleen weight was measured at sacrifice. In healthy animals, spleen weight was equivalent across the three genotypes. While a general increase in spleen weight was observed for all genotypes in response to DSS treatment (Figure 4.6B), this was significant only for KO animals when compared to healthy controls. Thus the constitutive loss of CMKLR1 altered some systemic inflammatory parameters both basally and in response to DSS-induced colitis.

Locally secreted chemerin levels are increased in CMKLR1 KO mice

In order to determine whether there was a difference in circulating chemerin levels between the genotypes following DSS treatment, total serum chemerin levels were evaluated at sacrifice. Consistent with Figure 4.3, all three genotypes exhibited approximately a 50% decrease in total chemerin levels (measured by ELISA) following DSS treatment (Figure 4.7A). Bioactive chemerin levels (measured by Tango bioassay) were similar in healthy and DSS-treated mice regardless of genotype (Figure 4.7B) and thus resulted in a trend for increased bioactive:total chemerin ratio for all genotypes. Importantly, there was no significant difference in circulating total or bioactive chemerin levels between genotypes (Figure 4.7C). However, analysis of total chemerin levels secreted from colon explant cultures revealed a significant increase in local chemerin secretion from colons isolated from KO mice compared to WT or HET (Figure 4.7D).

Older CMKLR1 KO mice exhibit signs of clinical illness more slowly, have decreased fat mass, and increased local chemerin levels following DSS treatment

Previous work has demonstrated that CMKLR1 KO mice exhibit metabolic perturbations at 14 weeks of age that are not present at 6 weeks of age (Ernst et al. 2012). In order to determine whether age was a factor in the development of colitis in CMKLR1 KO mice, we repeated the DSS-induced colitis experiments in an older group of mice (14-16 weeks). In comparison to the study with 6-8 week old mice, healthy animals did not gain weight over the course of the 6-day experiment. However, as with the younger

group of mice, all three genotypes lost an equivalent amount of weight on days 5 and 6 compared to day 0 following DSS treatment (data not shown). DEXA analysis on day 6 revealed that while all genotypes lost both lean and fat mass (~2.5 and ~1 g, respectively; Figure 4.8A), only KO mice exhibited a significant decrease in percent body fat and an increase in percent lean mass compared to before DSS treatment (Figure 4.8B). Consistent with the pattern in clinical illness for young adult mice, when compared to day 1, clinical illness scores were significant as early as day 4 in older WT mice but not until day 5 and 6 for HET and KO mice. However, all three genotypes had equivalent clinical illness scores by day 6 (Figure 4.8C). Similar to the younger group of mice, all three genotypes of 14-16 week old mice exhibited similar levels of local inflammation, with ~25% colon shortening following DSS treatment and an inflammation score of ~10. However, CMKLR1 KO mice had increased spleen weight following DSS treatment (data not shown). Therefore, as with 6-8 week old mice, older KO mice developed clinical illness more slowly, although ultimately reaching a similar level of illness and local colon inflammation as WT mice.

Compared to 6-8 week old animals, 14-16 week old mice had higher levels of total circulating chemerin (15 nM compared to 10 nM). Similar to the younger group, older mice exhibited a decrease in total chemerin levels following DSS treatment. However, unlike the younger group, a significant decrease in bioactive levels was also observed. The resulting effect was a more modest increase in bioactive:total chemerin ratio compared to 6-8 week old animals (Figure 4.8D). There was no difference between genotypes with relevance to circulating chemerin levels. However, there was significantly higher local chemerin secretion from colon explant cultures isolated from 14-16 week old KO mice compared to WT or HET (Figure 4.8E). Thus for both age groups, while there is no difference in circulating chemerin levels between genotype, locally-secreted chemerin levels are increased in KO animals.

Bioactive chemerin injection does not influence the severity of DSS-induced colitis

To determine the impact of increased circulating bioactive chemerin levels on the development and/or progression of DSS-induced colitis, we injected 6-8 week old WT mice with bioactive chemerin (aa 17-156) or PBS control every other day throughout

DSS treatment starting on day 0. Intraperitoneal injection of 500 ng chemerin increased circulating levels by 30% (Figure 4.9A). This increase is circulating chemerin is physiologically relevant as it is similar to the increase in bioactive:total chemerin ratio in mice administered DSS compared to healthy control (Figure 4.7C).

As expected, mice exhibited significant weight loss and had increased clinical illness scores on days 5 and 6 of DSS treatment; however, there was no difference between PBS control and chemerin-injected animals (Figure 4.9B and 4.9C). Consistent with this, both PBS and chemerin-injected animals exhibited similar levels of colon shortening and increases in spleen weight at sacrifice on day 6 (Figure 4.9D and 4.9E). To confirm that chemerin-injected animals were not inhibited from developing more severe colitis than control animals because of relatively high levels of inflammation on the 5% DSS treatment regime, we decreased the amount of DSS in drinking water to 3.5%. This resulted in reduced amounts of weight loss, clinical illness, colon shortening, and spleen weight increase (Figure 4.9B-E). However, there was no difference in any of these parameters between PBS and chemerin-injected animals, demonstrating that increased bioactive circulating chemerin levels do not influence the development of DSS-induced colitis.

Discussion

While the etiology of IBD is largely unknown, it is generally believed that genetic, environmental, and microbial factors combine to trigger inappropriate immune responses that involve over-production of different pro-inflammatory mediators (Hanauer 2006; Kaser et al. 2010; Neurath 2014). These cytokines and chemokines play a crucial role in controlling intestinal inflammation. Our results support a role for chemerin in the complex signalling network that underlies the pathogenesis of this inflammation. In the current study, we demonstrate that chemerin expression, secretion, and bioactivity are highest in regions of the colon that are the most inflamed. While the cellular source of chemerin was not directly investigated in this study, previous studies have demonstrated that chemerin is expressed in both fetal and cultured adult epithelial cells (Maheshwari et al. 2009). We proposed that chemerin is secreted from the inflamed colon and functions as a chemoattractant to recruit CMKLR1-expressing cells to sites of tissue damage. Surprisingly, while loss of CMKLR1 expression delayed the progression of DSS-induced colitis, it did not ultimately confer protection against disease severity.

A key finding from this study is that local chemerin levels appear to be more biologically relevant in the development of IBD than systemic chemerin levels. We demonstrate that the increase in chemerin expression was most dramatic in inflamed tissues in the GI tract (cecum and colon) and that the increase in chemerin secretion correlated with the severity of inflammation in the colon. This is consistent with human data showing that chemerin expression is higher in colon biopsies from UC patients with more severe inflammation, suggesting that local chemerin levels are tightly associated with local colon inflammation (Lin et al. 2014). In contrast, systemic levels of chemerin in UC and CD patients are not clearly related to disease activity in both sexes (Waluga et al. 2014; Weigert et al. 2010b). Similarly, in our study neither the DSS-induced decrease in circulating total chemerin for all mice, nor the overall higher circulating chemerin in older versus younger mice appeared to have any impact on the disease progression or severity. Furthermore, injection of bioactive chemerin had no observable effect on disease severity. These results are consistent with a study demonstrating that chemerin levels in synovial fluid from arthritic joints are positively associated with disease severity while there was no difference between serum chemerin levels in healthy controls and

osteoarthritis patients (Huang et al. 2012). This suggests that local chemerin levels in diseases involving chronic inflammation are a more important determinant of disease activity than systemic levels.

Importantly, this is the only published study to examine levels of chemerin bioactivity in a model of IBD. We report that despite a decrease in total circulating chemerin levels, the ratio of bioactive:total chemerin is increased in circulation with colitis. Furthermore, the presence of an extra band via SDS-PAGE analysis in the most inflamed region of the colon suggests that local processing of chemerin may occur in DSS-induced inflammation. Thus bioactive chemerin represents a novel biomarker that reflects the extent of inflammation. Although the source of chemerin bioactivation is unknown, this could occur via the secretion of chemerin-activating proteases from the colon (e.g. epithelial cells). However, as many enzymes that are known to process prochemerin, such as immune cell-secreted serine and cysteine proteases, are involved in the inflammatory response, it is likely that infiltrating immune cells contribute significantly to the bioactivation of chemerin in the inflamed colon (Rourke et al. 2013). Recently, it was shown that inhibition of serine proteases reduced inflammation induced by DSS administration (Bermudez-Humaran et al. 2015) and therefore targeting enzymes that generate bioactive chemerin may represent a novel method to manipulate endogenous chemerin signalling. As bioactive levels are often overlooked in both clinical and experimental studies, the findings of this study highlight the importance of studying chemerin bioactivity in pathophysiology.

Bioactive chemerin is a potent chemoattractant for cells that express CMKLR1 and the current study demonstrated that the increase in CMKLR1 expression in DSS-induced colitis resulted at least in part from increased cell infiltration into the colon. We hypothesized that mice lacking CMKLR1 would be protected from inflammatory damage and illness associated with DSS-induced colitis. Surprisingly, CMKLR1 KO mice had similar levels of inflammation to wildtype mice at the final time point although CMKLR1 KO mice did have a delayed onset of weight loss and clinical illness. This could result from a slower infiltration of immune cells into the colon in the absence of CMKLR1. However, it is likely that infiltrating leukocytes are ultimately attracted by other and possibly multiple chemoattractants; for example, inhibition of the neutrophil chemokine

receptor, CXCR2, in mice does not absolutely block neutrophil infiltration in this DSS model (Farooq et al. 2009). Similarly, while chemerin contributes to the recruitment of macrophages in the developing fetal intestine, chemerin levels are lower in the mature intestine, indicating that post-natal attraction is initiated by other chemokines (Maheshwari et al. 2009). Future studies that determine the cell type(s) expressing CMKLR1 in the colon following DSS treatment and examination of potential differences in cell infiltration in CMKLR1 KO mice earlier in the study, or whether there are differences in the populations of infiltrating cells in the absence of CMKLR1 could provide insight into the role of chemerin in immune cell recruitment to the inflamed colon. Recently, Lin et al. did not observe any changes in cell infiltration to the colon following intraperitoneal chemerin injection (Lin et al. 2014). However, given the importance of local chemerin levels, a more accurate model to study the effect of chemerin on cell infiltration to the colon would be via local intra-rectal administration or tissue-selective forced overexpression of chemerin versus systemic injection. Lin et al. proposed that chemerin influences IBD pathogenesis by inhibiting M2 macrophage polarization, which is involved in the resolution of IBD (Lin et al. 2014). CMKLR1 has been shown to be functional on M1 but not M2 macrophages and it would be interesting to assess leukocyte content in the spleen to examine whether a defect in M1/M2 macrophage polarization or other cell populations might explain the increased spleen size in CMKLR1 KO mice (Herova et al. 2015).

Lin et al. also reported that injection of 500ng of chemerin every other day exacerbated the severity of DSS-induced colitis using an 8-day protocol in which mice received DSS in the drinking water for only the first 5 days (Lin et al. 2014). While a limitation of DSS-induced colitis models is often variability in the level of inflammation between groups using similar DSS models, in our experience, this resembles a model that examines the effect of chemerin in recovery from acute colitis rather than the induction of colitis. In the current study, we did not observe a difference in the induction of colitis following the injection of bioactive chemerin using the same dosage and timing of injections in similarly aged mice on the same genetic background. Thus it is possible that while chemerin does not play a significant role in the initiation of colitis, it is important for the resolution of inflammation. Previous studies with CMKLR1 KO mice have

suggested both pathogenic (Demoor et al. 2011; Graham et al. 2009) and protective (Luangsay et al. 2009; Cash et al. 2008; Bondue et al. 2011) roles for chemerin signalling in the initiation and resolution of inflammation, respectively. Thus the role of chemerin in IBD is likely context-specific and future studies examining role of chemerin/CMKLR1 signalling in other DSS models (acute, chronic, recovery) will be useful. Additionally, DSS is a model of chemically-induced mucosal injury and has some limitations as a model of IBD. Therefore the use of other IBD models (TNBS, IL-10 KO, infectious *Citrobacter*) may provide further insight to role of chemerin signalling in IBD as well as other inflammatory diseases.

Interestingly, our study demonstrates that total circulating levels decrease throughout the course of DSS treatment. In the current study, mice lost twice as much body weight compared to a previous report (Lin et al. 2014) and DEXA analysis revealed a significant loss in fat mass. As WAT is an important modifiable source of circulating chemerin, this weight loss could explain a decrease in circulating levels. Consistent with this, the older group of mice had decreased bioactive chemerin levels that correlated with a dramatic loss of fat mass. Importantly, chemerin expression increased in mesenteric WAT following DSS treatment, suggesting an additional potential source of local adipose-derived chemerin levels during DSS-induced inflammation. A relationship between obesity, mesenteric adiposity, and IBD has been proposed and high-fat diet-induced obesity has been shown to aggravate the pathology of IBD (Teixeira et al. 2011; Moran et al. 2013). CMKLR1 has previously been reported to affect adiposity and thus chemerin/CMKLR1 signalling may represent a novel link between adiposity and IBD (Ernst et al. 2012). However, it is important to note that normalizing total serum chemerin levels by fat mass did not alter the magnitude of decrease in chemerin levels following DSS treatment (data not shown). Importantly, previous studies have shown that fasting significantly decreases serum chemerin levels (Chamberland et al. 2013). As DSS-treated mice eat less food when ill, the decrease in chemerin levels may be an indirect consequence of DSS treatment on feeding. Alternatively, the impact of DSS administration on other sources of circulating chemerin, such as the liver, is unknown. Future studies that investigate how both local and systemic inflammation influence

circulating chemerin levels will be important in furthering our understanding of chemerin function in IBD as well as other inflammatory diseases.

The phenotype achieved following DSS-induced colitis in CMKLR1 KO mice was relatively modest and it is important to note that this may be a result of constitutive loss of CMKLR1. Compensatory mechanisms may have developed in these mice and studies with acute modulation of CMKLR1 activation via administration of CMKLR1 inhibitors or conditional GI knockout models will be useful in future studies. Furthermore, up-regulation of chemerin secretion from the colon was observed in KO animals and it is possible that chemerin is acting through receptors other than CMKLR1. We were limited by a lack of specific GPR1 and CCRL2 antibodies that function in immunohistochemistry to examine changes in the protein level of these receptors. However, gene expression data demonstrated that while GPR1 expression did not change following DSS treatment, GPR1 expression was relatively high in the distal colon constitutively compared to other mammalian tissues (data not shown, (Rourke et al. 2014)). Alternatively, CCRL2, which is believed to be a non-signalling receptor, increased in the same tissues as chemerin and CMKLR1. CCRL2 has been hypothesized to bind chemerin and present to nearby cells, and has been shown to enhance optimal swelling in IgE-mediated anaphylaxis (Zabel et al. 2008). Thus it is possible that chemerin plays a role in IBD through any combination of CMKLR1, GPR1, and/or CCRL2 signalling and future studies with additional transgenic chemerin and receptor models will be invaluable. Importantly, while we did not directly test the impact of Resolvin E1, the results of this study suggest that CMKLR1 does not mediate the anti-inflammatory effects of Resolvin E1 in the progression of IBD as previously suggested by others (Ishida et al. 2010; Arita et al. 2005b).

In summary, this study shows that local chemerin levels and bioactivity are positively associated with the development of colitis and that chemerin represents a novel biomarker reflecting the severity of IBD. Surprisingly, constitutive loss of CMKLR1 is not sufficient to prevent the induction of colitis although CMKLR1 KO mice develop illness more slowly. In contrast with a previous report (Lin et al. 2014), increased systemic chemerin levels do not appear to influence the severity of experimental colitis, suggesting that local chemerin levels play a more important role in the pathogenesis of

IBD. Future studies that investigate the role of other chemerin receptors and mechanisms of endogenous chemerin signalling in IBD both more acutely and locally will be important in elucidating the potential of chemerin as a therapeutic target for the treatment of IBD.

Tables and figures

Table 4.1. Clinical illness scoring system

Mice were assessed daily for signs of clinical illness.

Score	Weight loss (%)	Stool consistency	Occult/gross bleeding
0	None	Normal	Normal
1	None	Loose	Normal
2	None	Loose	Blood present
3	1-5	Normal	Blood present
4	1-5	Loose	Blood present
5	1-5	Diarrhea	Blood present
6	5-10	Loose	Blood present
7	5-10	Diarrhea	Blood present
8	10-20	Loose	Blood present
9	10-20	Diarrhea	Blood present
10	>20	x	Blood present

Table 4.2. Inflammation scoring system

Colons isolated from animals were fixed in "Swiss rolls", sectioned, and stained with hematoxylin and eosin. Inflammation scores were assigned by a blinded investigator according to the following parameters.

Score	Submucosal edema	Ulceration	Hyper-plasia	Crypt damage	Infiltrate
0	None or spotty	None	None	None	None
1	Long stretches	<3 small focal	Minor	Patchy, small spaces between crypts	Patchy submucosal or spotty mucosal patches
2		>3 small or 1 large (15 crypt widths)	Moderate	Large spaces between crypts, reduced goblet cells	Considerable submucosal with patchy mucosal
3		Multiple large flat	Severe	Single long stretch lacking crypts	Ulcerated areas infiltrated, mucosal + submucosal
4				Multiple stretches lacking crypts	~50% of affected colon including between mucosal ulcers
5				Continuous long stretches occupying >50% of the length of involved colon	>50% transmural infiltration

Figure 4.1. Chemerin and CMKLR1 expression increase in the cecum and distal colon following DSS treatment

RNA from the indicated tissues was isolated at sacrifice from 6-8 week old mice that received normal drinking water (Veh) or 5% DSS treatment (n=5). qPCR analysis was performed to look at changes in chemerin (A), CMKLR1 (B), GPR1 (C), and CCRL2 (D) expression. CMKLR1 expression throughout the colon of healthy and DSS-treated animals was visualized by immunohistochemistry (E, 40X magnification). Φ represents $p<0.05$ compared to stomach for vehicle-treated animals and * represents $p<0.05$, ** $p<0.01$ and ***$p<0.001$ for vehicle versus DSS-treated animals.

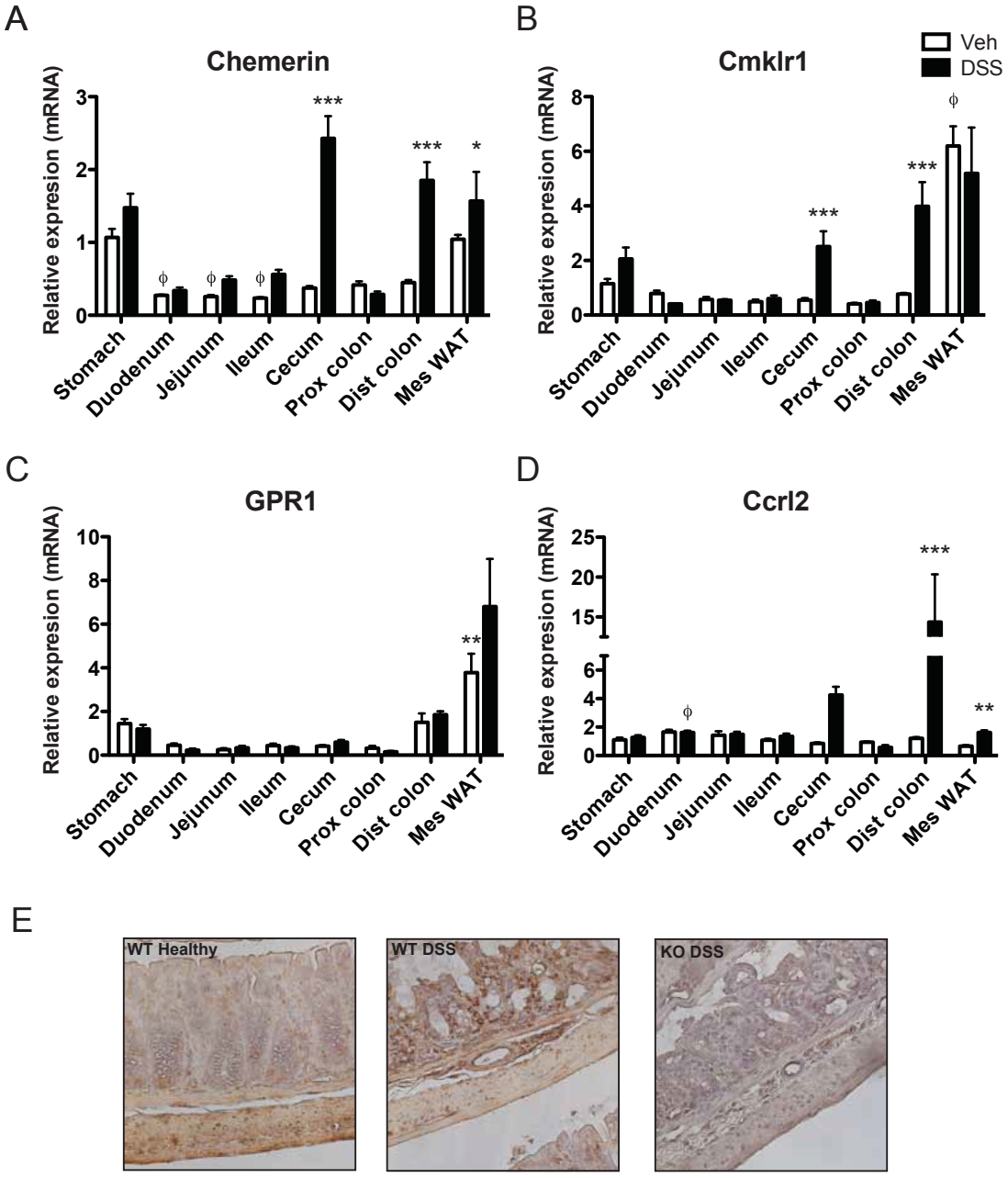
A
Chemerin
Relative expresion (mRNA)
Stomach
Duodenum
Jejunum
Ileum
Cecum
Prox colon
Dist colon
Mes WAT
B
Cmklr1
Veh
DSS
C
GPR1
D
Ccrl2
E
WT Healthy
WT DSS
KO DSS

Figure 4.2. Chemerin secretion increases in a proximal-distal gradient in the colon following DSS treatment

Colons were isolated from 6-8 week old healthy or 5% DSS-treated mice at sacrifice, cut into three segments, and cultured. After 24 h of culture, supernatant from the colon explants was collected and an ELISA performed to determine levels of total secreted chemerin (A). Supernatant from colon explant cultures was also examined via SDS-PAGE with 10 ng of recombinant mouse chemerin (aa 17-156, 16 kDa reference) as a control (B). Representative image is shown. n=6, where *$p<0.05$ and ***$p<0.001$. nd, not detected; P, proximal; M, middle; D, distal.

A

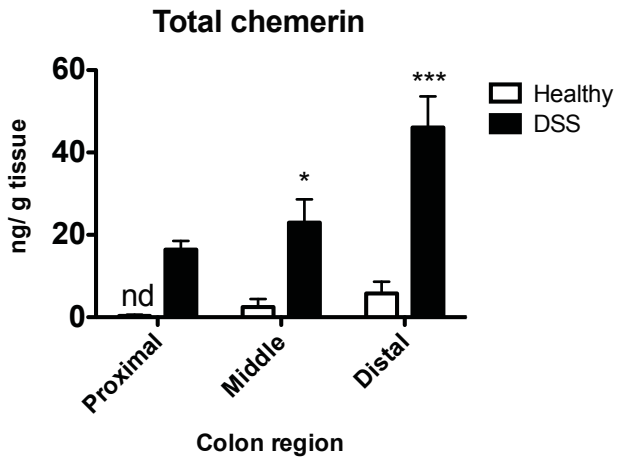
Total chemerin
60
40
20
0
ng/ g tissue
nd
*
***
Healthy
DSS
Proximal
Middle
Distal
Colon region

B

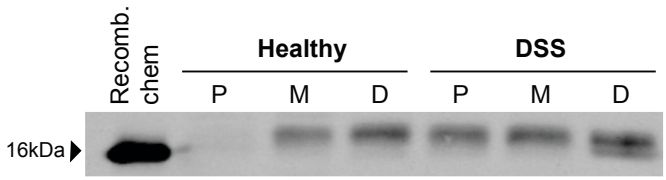
Recomb. chem
Healthy
DSS
P
M
D
P
M
D
16kDa

Figure 4.3. Total circulating chemerin levels decrease, but the ratio of bioactive:total chemerin increases, following DSS treatment

Serum was collected from 6-8 week old mice the day before and on each day of 5% DSS treatment. An ELISA for total chemerin levels (A) and a Tango assay for mCMKLR1 activation (B) were performed. The ratio of bioactive:total chemerin levels was then calculated (C). n=6, where * represents $p<0.05$, **$p<0.01$, ***$p<0.001$ compared to the day before DSS treatment was initiated.

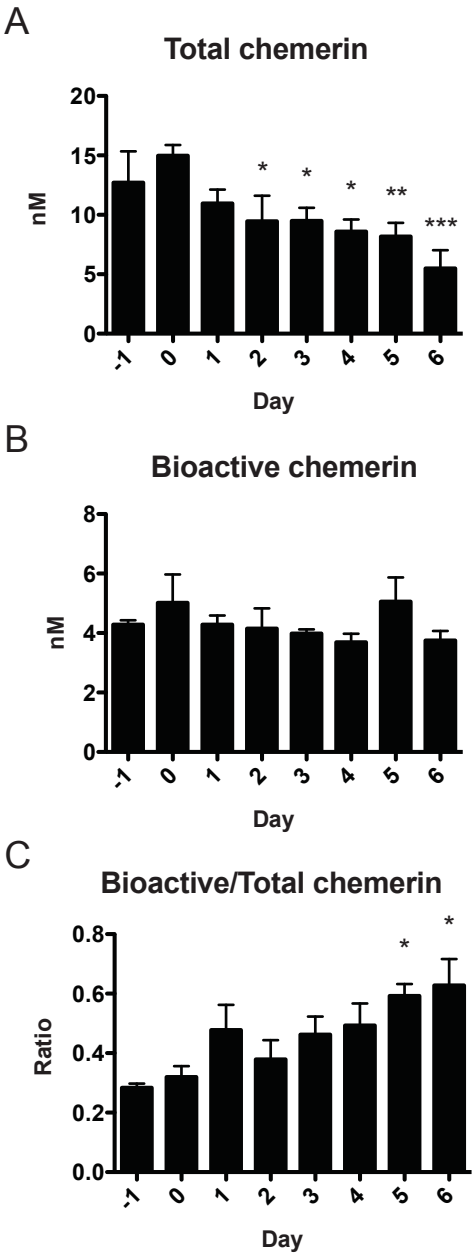
A
Total chemerin
nM
20
15
10
5
0
*
*
*
**
***
-1
0
1
2
3
4
5
6
Day
B
Bioactive chemerin
nM
8
6
4
2
0
-1
0
1
2
3
4
5
6
Day
C
Bioactive/Total chemerin
Ratio
0.8
0.6
0.4
0.2
0.0
*
*
-1
0
1
2
3
4
5
6
Day

Figure 4.4. CMKLR1 KO mice have decreased weight loss on day 5 of treatment and develop signs of clinical illness more slowly than WT mice

Body weight of 6-8 week old mice that received normal drinking water (healthy) or 5% DSS was monitored daily and expressed relative to initial weight on day 0 (A). DEXA analysis was performed before (day -1) and after 5% DSS treatment (day 6, before sacrifice) in 6-8 week old animals. The absolute amounts of fat and lean mass (B) were recorded. These values were then normalized to total body weight to calculate percent body composition (C). Mice were evaluated daily for signs of clinical illness and a score was assigned based on weight loss, stool consistency, and the presence or absence of blood in the stool (D). n=6-9 per genotype, where in A) *** represents $p<0.001$ relative to day 0 and Φ represents $p<0.05$ compared to WT within a treatment group on a particular day. In B-C) * represents $p<0.05$, **$p<0.01$, and ***$p<0.001$ compared to before DSS treatment. In D) * represents $p<0.05$ compared to day 1, Φ<0.05 compared to day 2, and #$p<0.05$ compared to day 3.

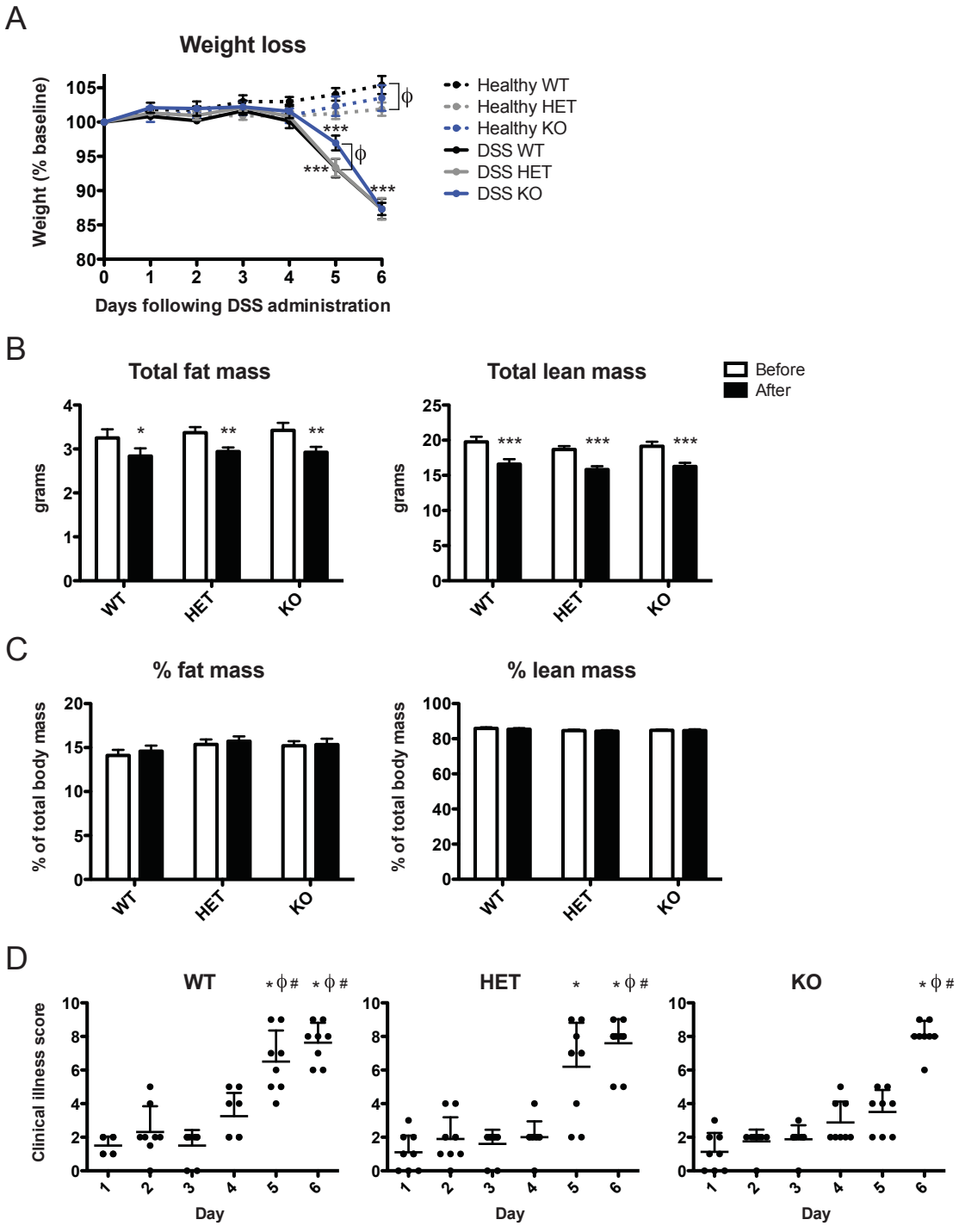
A
Weight loss
Weight (% baseline)
Days following DSS administration
Healthy WT
Healthy HET
Healthy KO
DSS WT
DSS HET
DSS KO
B
Total fat mass
Total lean mass
Before
After
grams
WT
HET
KO
C
% fat mass
% lean mass
% of total body mass
D
WT
HET
KO
Clinical illness score
Day

Figure 4.5. CMKLR1 WT and KO mice have similar levels of local inflammation in the colon following DSS treatment

At sacrifice, the colon was excised from 6-8 week old animals that had received normal drinking water (healthy) or 5% DSS-treatment and measured (A). A blinded investigator scored the level of inflammation in the colon based on the presence of edema, crypt structure, cell infiltration, ulcer formation and size, and hyperplasia, on hematoxylin and eosin stained sections (B). The levels of pro-inflammatory cytokines IFN-γ, IL-6, IL-17A, and TNF secreted from 24 h colon explant cultures isolated at sacrifice was measured using a Multiplex assay (C). n=6-11 per genotype, where * represents $p<0.05$ and *** $p<0.001$ compared to healthy animals of the same genotype.

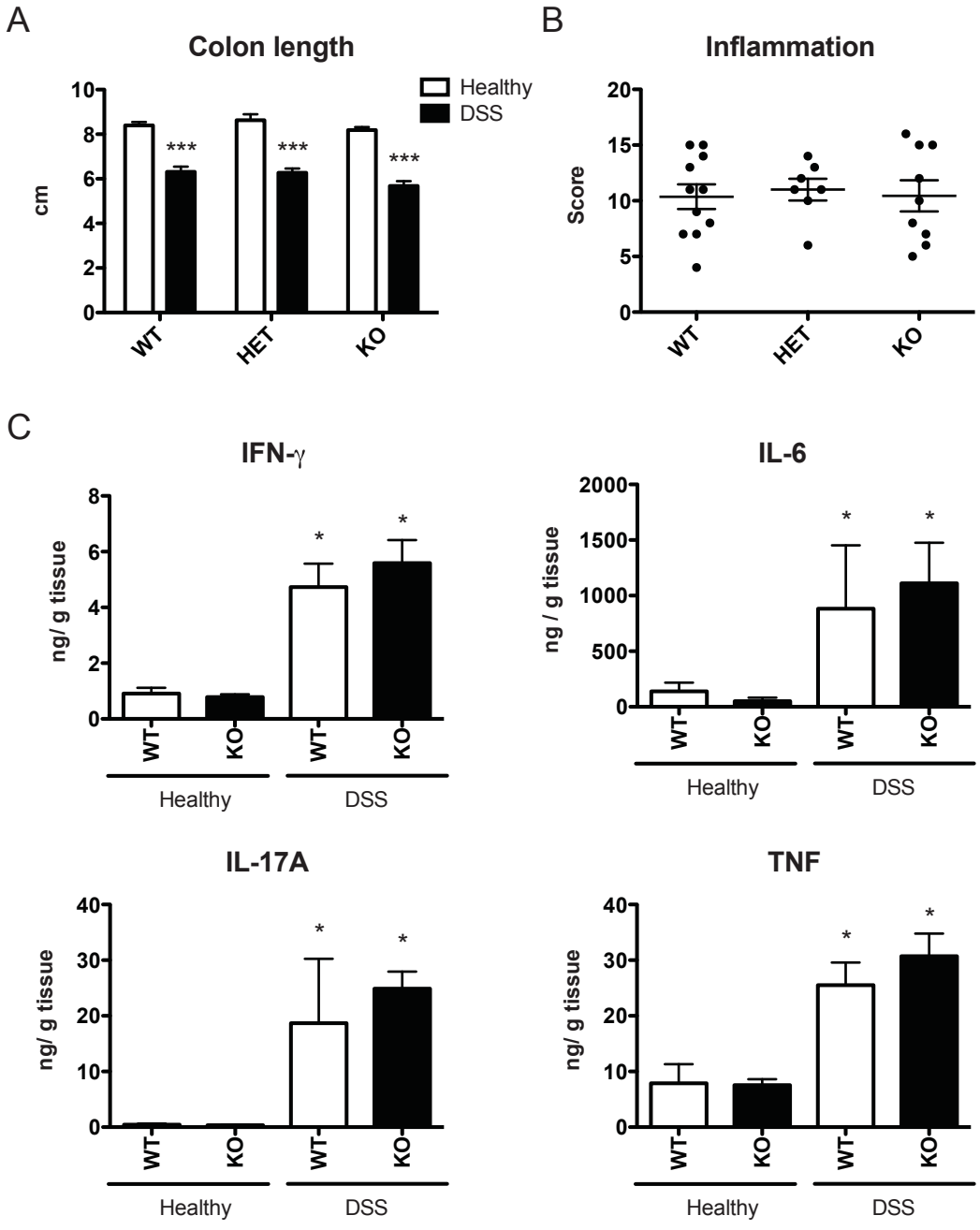
A
Colon length
Healthy
DSS
cm
10
8
6
4
2
0
***
***
***
WT
HET
KO
B
Inflammation
Score
20
15
10
5
0
WT
HET
KO
C
IFN-γ
ng/ g tissue
8
6
4
2
0
*
*
WT
KO
WT
KO
Healthy
DSS
IL-6
ng / g tissue
2000
1500
1000
500
0
*
*
WT
KO
WT
KO
Healthy
DSS
IL-17A
ng/ g tissue
40
30
20
10
0
*
*
WT
KO
WT
KO
Healthy
DSS
TNF
ng/ g tissue
40
30
20
10
0
*
*
WT
KO
WT
KO
Healthy
DSS

Figure 4.6. CMKLR1 KO mice have differences in systemic parameters of inflammation

Circulating levels of the pro-inflammatory cytokines IFN-γ, IL-6, IL-17a, and TNF were measured in the serum of 6-8 week old WT or KO mice before and after 5% DSS treatment using a Multiplex assay (A). Following DSS treatment, the spleens were excised from mice and weighed (B). n=8 (A) and n=6-9 (B) per genotype, where * represents $p<0.05$ and ***$p<0.001$ compared to healthy animals of the same genotype or as indicated.

A

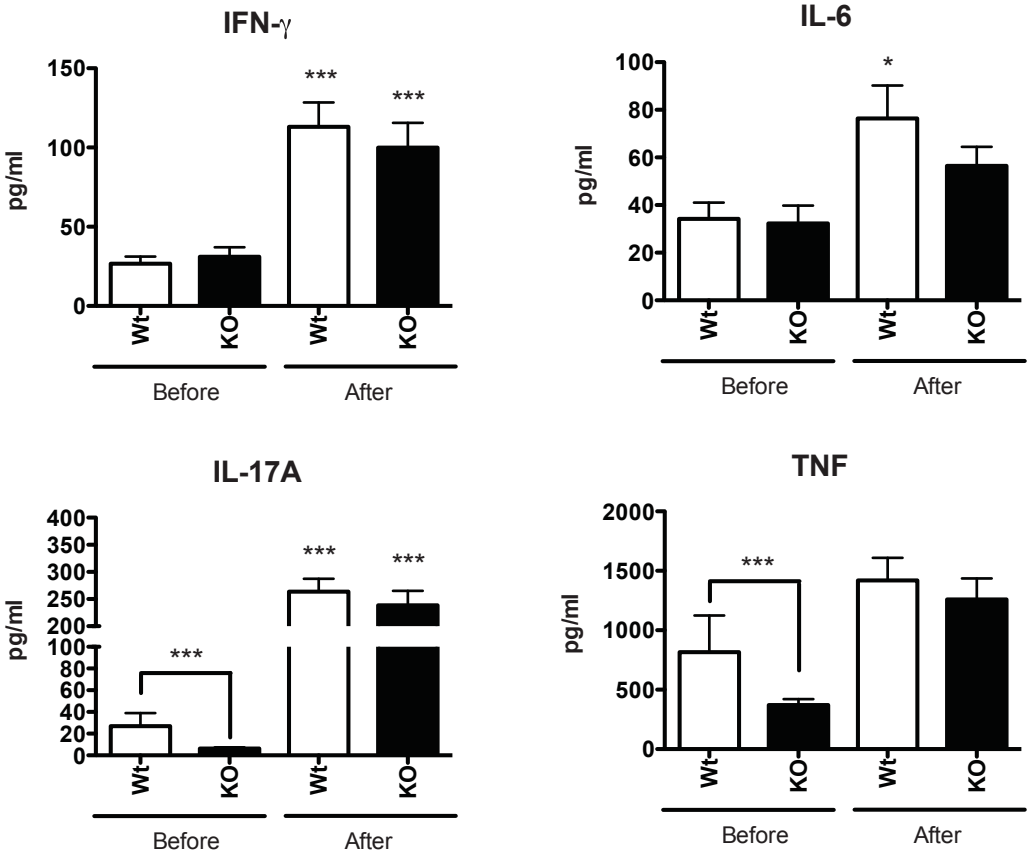
IFN-γ
pg/ml
150
100
50
0
***
***
Wt
KO
Wt
KO
Before
After
IL-6
pg/ml
100
80
60
40
20
0
*
Wt
KO
Wt
KO
Before
After
IL-17A
pg/ml
400
350
300
250
200
100
80
60
40
20
0
***
***
***
Wt
KO
Wt
KO
Before
After
TNF
pg/ml
2000
1500
1000
500
0
***
Wt
KO
Wt
KO
Before
After

B

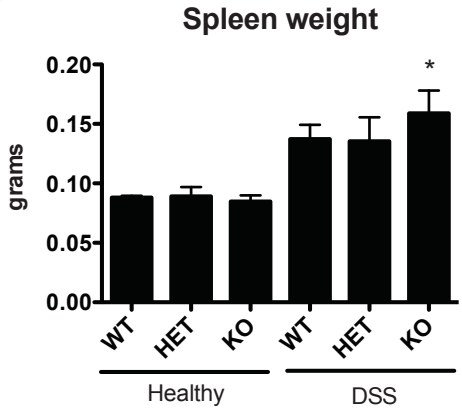
Spleen weight
grams
0.20
0.15
0.10
0.05
0.00
*
WT
HET
KO
WT
HET
KO
Healthy
DSS

Figure 4.7. Changes in circulating chemerin levels are similar between genotypes but CMKLR1 KO mice have increased local secretion of chemerin

Serum was collected via cardiac puncture at sacrifice from 6-8 week old mice that received normal drinking water (healthy) or 5% DSS treatment. Total chemerin levels were measured via ELISA (A) and bioactive chemerin levels were measured using the Tango assay for mouse CMKLR1 activation (B). The ratio of bioactive:total chemerin was then determined (C). Total chemerin levels were also measured in the supernatant from colon explant cultures isolated at sacrifice using an ELISA (D). n=6-9 per genotype, where * represents $p<0.05$ and ***$p<0.001$ compared to healthy controls (A) or WT (B).

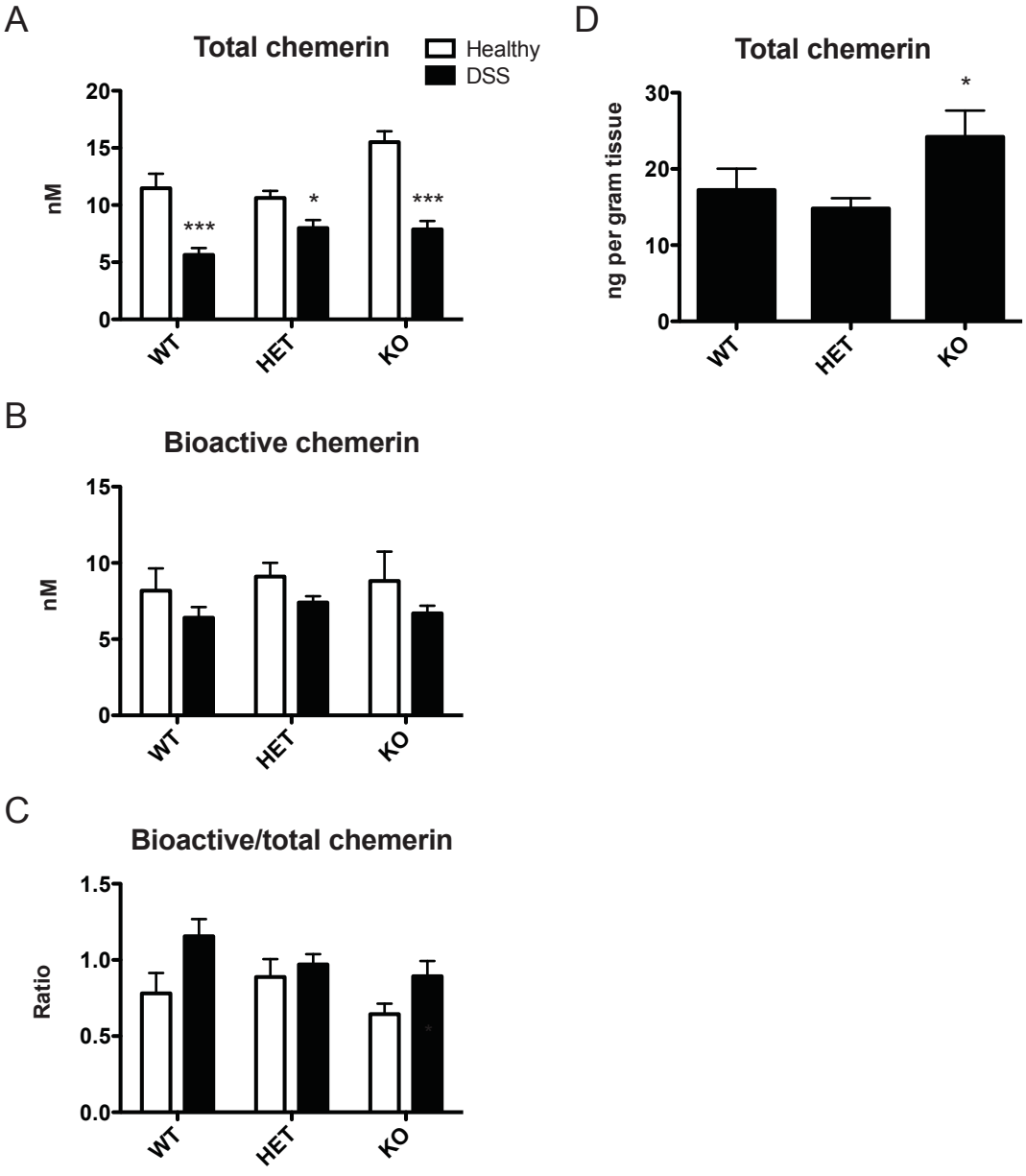
A
Total chemerin
Healthy
DSS
nM
20
15
10
5
0
***
*
***
WT
HET
KO
D
Total chemerin
ng per gram tissue
30
20
10
0
*
WT
HET
KO
B
Bioactive chemerin
nM
15
10
5
0
WT
HET
KO
C
Bioactive/total chemerin
Ratio
1.5
1.0
0.5
0.0
WT
HET
KO

Figure 4.8. 14-16 week old CMKLR1 KO mice lose a greater percentage of fat mass, develop signs of clinical illness more slowly, and have increased local levels of chemerin secretion than WT mice

DEXA analysis was performed before (day -1) and after 5% DSS treatment (day 6, before sacrifice) in 14-16 week old mice that receive normal drinking water (healthy) or 5% DSS. The absolute amounts of fat and lean mass (A) were recorded. These values were then normalized to total body weight to calculate percent body composition (B). Mice were evaluated daily for signs of clinical illness and a score was assigned based on weight loss, stool consistency, and the presence or absence of blood in the stool (C). Serum was collected via cardiac puncture at sacrifice and total chemerin levels were measured via ELISA, bioactive chemerin levels were measured using the Tango assay for mouse CMKLR1 activation, and the ratio of bioactive:total chemerin was determined (D). Total chemerin levels were also measured in the supernatant from colon explant cultures isolated at sacrifice using an ELISA (E). n=6-10 per genotype, where in A-B) * represents $p<0.05$, **$p<0.01$, and ***$p<0.001$ compared to before DSS treatment. For C) * represents $p<0.05$ compared to day 1, $\Phi<0.05$ compared to day 2, and #$p<0.05$ compared to day 3. In D-E) * represents $p<0.05$, **$p<0.01$, and ***$p<0.001$ compared to healthy controls (D) or WT (E).

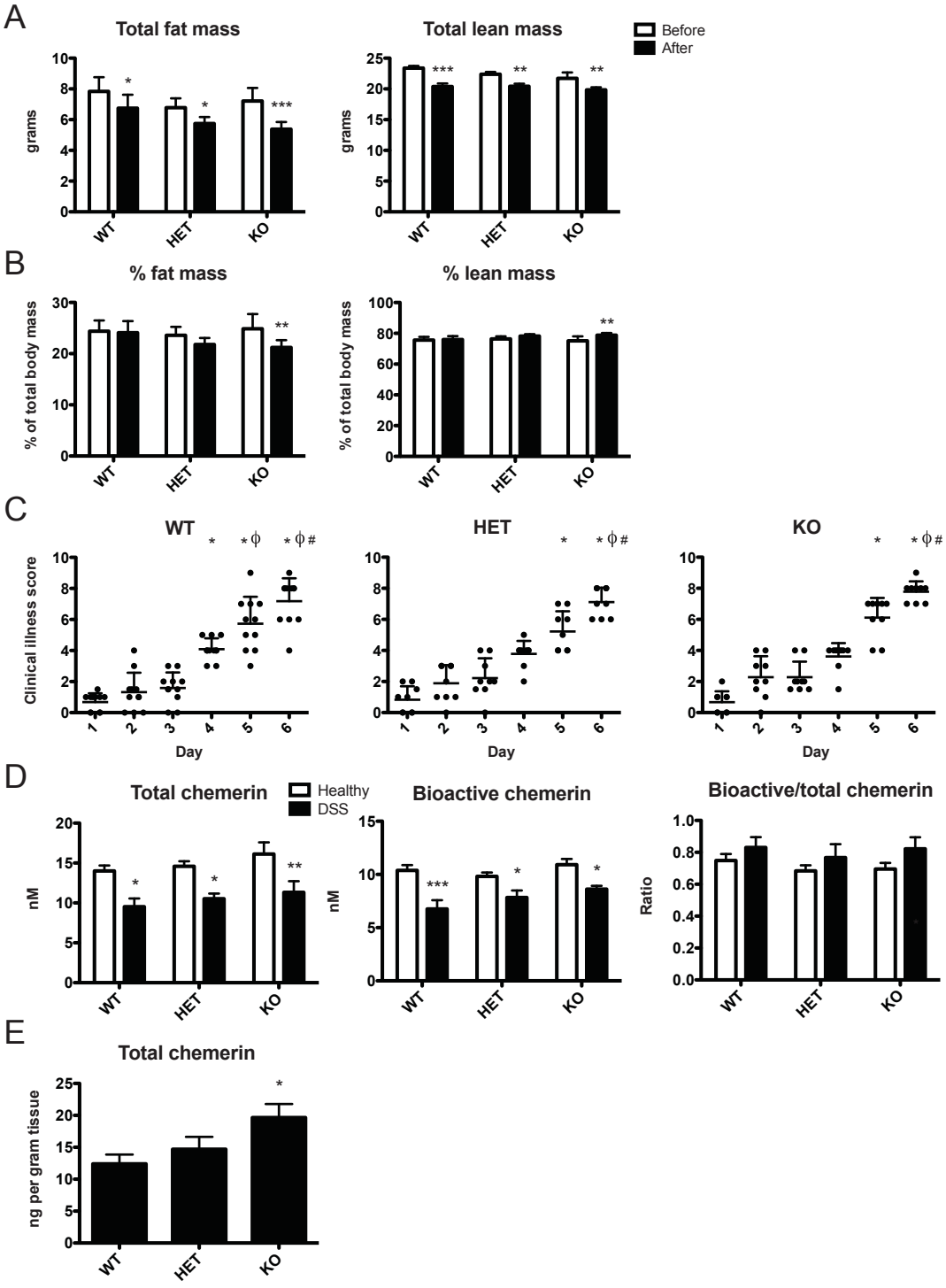
A
Total fat mass
Total lean mass
Before
After
grams
WT
HET
KO
B
% fat mass
% lean mass
% of total body mass
C
WT
HET
KO
Clinical illness score
Day
D
Total chemerin
Healthy
DSS
Bioactive chemerin
Bioactive/total chemerin
nM
Ratio
E
Total chemerin
ng per gram tissue

Figure 4.9. Increased levels of circulating active chemerin do not affect DSS-induced colitis

Recombinant chemerin (aa 17-156) or PBS (control) was administered to 6-8 week old WT animals via intraperitoneal injection every other day. Total chemerin levels in circulation 48 h following injection were measured using an ELISA (A). Body weight was monitored daily for animals receiving 3.5 or 5% DSS and expressed relative to initial starting weight (A). Clinical illness was also scored daily for animals receiving 5% (C) or 3.5% (D) DSS. At sacrifice, the colon was excised and measured (D) and spleen weight recorded (E). n=6-9 per group, where in A) * represents $p<0.05$, in B) * represents $p<0.05$ and ***$p<0.001$ compared to day 0 and in C) * represents $p<0.05$ compared to day 1, $\Phi<0.05$ compared to day 3, and #$p<0.05$ compared to day 3.

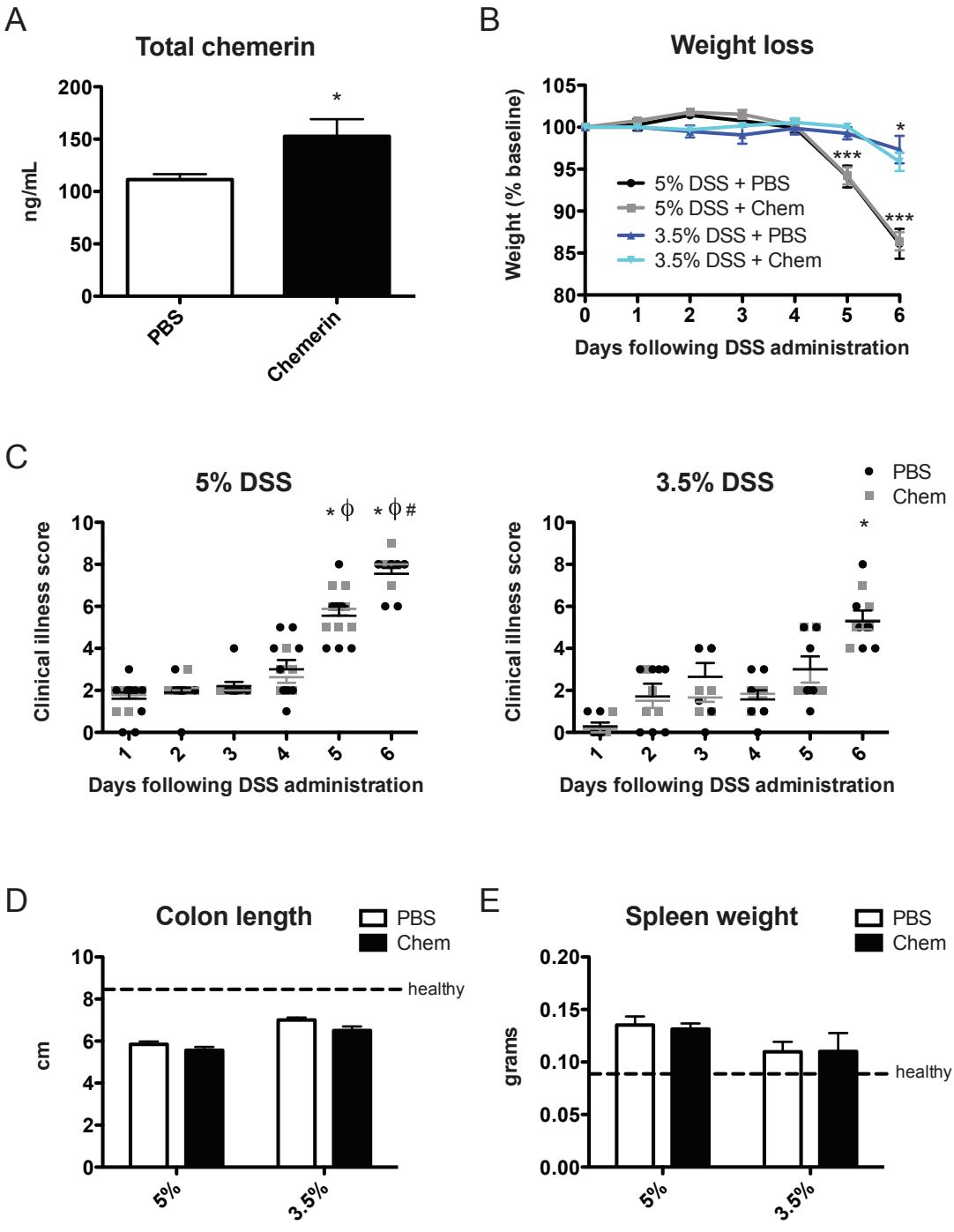
A
Total chemerin
ng/mL
200
150
100
50
0
*
PBS
Chemerin
B
Weight loss
Weight (% baseline)
105
100
95
90
85
80
0
1
2
3
4
5
6
Days following DSS administration
5% DSS + PBS
5% DSS + Chem
3.5% DSS + PBS
3.5% DSS + Chem
*
***
***
C
5% DSS
Clinical illness score
10
8
6
4
2
0
* ϕ
* ϕ #
1
2
3
4
5
6
Days following DSS administration
3.5% DSS
PBS
Chem
*
Clinical illness score
Days following DSS administration
D
Colon length
PBS
Chem
cm
10
8
6
4
2
0
healthy
5%
3.5%
E
Spleen weight
PBS
Chem
grams
0.20
0.15
0.10
0.05
0.00
healthy
5%
3.5%

CHAPTER 5: CMKLR1 LOSS IS ASSOCIATED WITH CHANGES IN THE GUT MICROBIOME CHARACTERIZED BY DECREASED ABUNDANCE OF *AKKERMANSIA* AND *PREVOTELLA* SPECIES

Contribution statement

Ashlee (Yayue) Zheng and Dr. Brian Zabel (Palo Alto Veterans Institute for Research, Palo Alto, CA, USA) collected wildtype (BZ) and chemerin KO fecal samples and genotyped chemerin KO mice. Drs. André Comeau and Morgan Langille (IMR-Integrated Microbiome Resource, Dalhousie University) performed library preparation (16s PCR, quality control, library normalization), 16s sequencing, and assisted with bioinformatic analysis. I was responsible for designing, performing, and analyzing all experiments with guidance from Dr. Christopher Sinal.

Abstract

Chemerin is a chemoattractant for cells that express chemokine-like receptor 1 (CMKLR1) and an adipokine that has been shown to play important roles in metabolism and inflammation. The composition and function of gut microbiota has also been shown to play important roles in the development of metabolic and inflammatory diseases such as obesity, diabetes and inflammatory bowel disease. As previous studies have reported that chemerin exhibits anti-microbial properties, we hypothesized that chemerin signalling mediates metabolic or inflammatory processes via the regulation of gut microbiome composition. In this study, we performed a preliminary assessment of the microbiome composition in fecal samples isolated from healthy young wildtype, chemerin knockout (KO), and CMKLR1 KO mice using Illumina-based sequencing. The KO mice and respective wildtype mice used in this study were housed at different universities. There was no difference in alpha diversity within samples when compared by either facility or genotype. However, we observed a dramatic difference in the presence and abundance of numerous taxa between facilities. There were minor differences in bacterial abundance between wildtype and chemerin KO mice, but significantly more differences in the abundance of several taxa between wildtype and CMKLR1 KO mice. In particular, CMKLR1 KO mice exhibited decreased abundance of *Akkermansia* and *Prevotella*, which correlated with body weight in CMKLR1 KO, but not wildtype mice, and explained a proportion of the separation between genotypes. This suggests that chemerin/CMKLR1 signalling influences metabolic processes through effects on the gut microbiome. Furthermore, the dramatic difference in microbiome composition between facilities might contribute to discrepancies in the metabolic phenotype of CMKLR1 KO mice reported by independent groups. Considered altogether, this assessment of the gut microbiota of young, healthy chemerin and CMKLR1 KO mice provides a foundation for future studies to investigate the relationship between chemerin signalling and the gut microbiome on the development and progression of metabolic and inflammatory disease.

Introduction

The human body is host to a vast number of microbes that include bacteria, fungi, protozoan cells, and viruses, which live in a commensal manner and are collectively termed the microbiota. The healthy human microbiota is comprised of 10^{14} microorganisms that colonize the oral and nasal cavities, the skin surface, and the gastrointestinal (GI) and urogenital tracts (Barlow et al. 2015; Whitman et al. 1998). Together, the microbiota encode 150 times more genes than the human genome (Qin et al. 2010a) and perform a number of functions that are important to human metabolism, energy homeostasis, neuro-hormonal function, and development of the immune system (Barlow et al. 2015). In return, the microbiota benefit from the protective and nutrient-rich environment of the host. Over the past 10-15 years, our understanding of the complexity and contribution of the microbiome to host physiology has increased dramatically. It is now well accepted that the human microbiome plays an important role in both health and disease.

To date, the majority of microbiome research has focused on the composition and function of gut microbiota. The gut microbiome is one of the most diverse, dynamic, and densely colonized microbial communities in the body and the number of microbial cells in the GI tract is 10 times higher than the number of eukaryotic host cells (Costello et al. 2009). Genes encoded by the gut microbiome maintain several essential metabolic functions in the GI tract, including colonic fermentation of dietary fibres, extraction of nutrients, synthesis of vitamins, and bile acid modifications. The composition and activity of gut microbiota also protect against colonization by pathogens and contribute to the maturation of intestinal epithelium, gut motility, and the promotion of gut barrier integrity (Barlow et al. 2015; Hansen et al. 2015; Zhang et al. 2015b). In addition, the gut microbiome plays important roles in a number of systemic processes including the development of immunity, regulation of inflammatory responses, and modulation of GI hormone release (Hansen et al. 2015; Marchesi et al. 2015; Zhang et al. 2015b).

The composition of the gut microbial community co-develops with the host and is strongly influenced by several genetic and environmental factors. These include mode of birth, genotype, age, diet, antibiotic treatment, and exposure to factors such as pathogens and chemicals (Barlow et al. 2015; Cox and Blaser 2015; Marchesi et al. 2015).

Disruption in the normal balance of gut microbial populations, or dysbiosis, results in profound changes in both the activity and function of intestinal microbiota. Increasing evidence from both animal models and human observational studies suggest that gut microbial dysbiosis is associated with a wide range of pathological conditions. These include obesity, diabetes, inflammatory bowel disease (IBD), liver disease, cancer, allergy and autoimmune diseases (Barlow et al. 2015; Marchesi et al. 2015; Zhang et al. 2015b). While many of these associations are correlative, scientists are now beginning to identify direct relationships between gut microbiota composition, activity, and the onset of disease.

Numerous studies have demonstrated that intestinal dysbiosis contributes to the development of metabolic diseases such as obesity and type 2 diabetes (T2D). Early studies demonstrated that "conventionalizing" germ-free mice resulted in a 60% increase in total body fat, despite decreased chow consumption (Backhed et al. 2004). Furthermore, the gut microbiota associated with diet-induced obesity results in a significantly greater increase in adiposity upon transplantation to germ-free recipients compared to that from lean animals (Turnbaugh et al. 2006). Similar results have been observed in humans, where microbiota from an obese twin is rapidly transmissible into mice and negatively influences metabolism compared to microbiota from the lean twin (Ridaura et al. 2013). In general, observational and correlational studies in humans demonstrate that individuals with low bacterial diversity are positively associated with an increased prevalence of obesity, insulin resistance, fatty liver, and low-grade inflammation (Le Chatelier et al. 2013). Several changes in the abundance of particular microbiota have been associated with these differences in body weight and and glucose metabolism (Hansen et al. 2015). These include an increase in the ratio of Firmicutes to Bacteroidetes, which are the two dominant gut phyla in both mouse and human intestinal microbiomes (Keeney et al. 2014; Ley et al. 2006; Turnbaugh et al. 2009). More specifically, an increase in Firmicutes (*Lactobacillus*, *Clostridium*, *Faecalibacterium*), and a decrease in Bacteroidetes (*Bacteroides*, *Prevotella*), Actinobacteria (*Bifidobacterium*), Gammaproteobacteria (*Escherichia*), and Veruccomicrobia (*Akkermansia*) have been observed with obesity (Barlow et al. 2015; Keeney et al. 2014; Okeke et al. 2014). Additionally, T2D patients have been characterized by changes in

Firmicutes (*Roseburia*, *Clostridium*, *Faecalibacterium*) and a decrease in Actinobacteria (*Bifidobacterium*) (Zhang et al. 2015b). Altogether, these changes in bacterial composition are associated with increased capacity for energy harvest, nutrient and lipid absorption, enhanced short chain fatty acid (SCFA) production, lipogenesis, and intestinal permeability (Barlow et al. 2015; Turnbaugh et al. 2006). These enriched microbial functions also affect the oxidative stress response and might directly contribute to the pro-inflammatory state of obese and T2D patients (Tilg and Adolph 2015).

There is also strong evidence that the intestinal microbiome plays a role in the development of IBD. Importantly, IBD does not occur in germ-free animals (Madsen 1999), and disease occurs in the presence of certain bacterial species in genetically susceptible animals (Arrieta et al. 2014; Keeney et al. 2014; Sydora et al. 2005). Additionally, the *Bacteroides fragilis*-expressed molecule polysaccharide A prevents colitis in mice, suggesting that metabolites of bacterial microbiota mediate the balance between health and disease (Mazmanian et al. 2008). Similar to metabolic disease, clinical studies indicate that ulcerative colitis (UC) and Crohn's disease (CD) patients are associated with a significantly less diverse intestinal microbiome. This is generally attributed to an overall reduction in protective species such as Firmicutes (particularly *Faecalibacterium prausnitzii* and *Roseburia hominis*) (Keeney et al. 2014; Zhang et al. 2015b), which have been shown to inversely correlate with disease activity (Machiels et al. 2014). Decreased *Bifidobacterium* and Verrucomicrobia have also been reported (Arrieta et al. 2014; Keeney et al. 2014). In contrast, IBD is associated with increased Enterobacteria species, bacteria of the Clostridiales group, and pathogenic *E. coli* (Arrieta et al. 2014; Keeney et al. 2014; Marchesi et al. 2015; Zhang et al. 2015b). Notably, the IBD metagenome contains 25% fewer genes than the healthy gut, with a correlative decrease in protein expression and functional pathways (Erickson et al. 2012). These pathways are associated with complex carbohydrate degradation, host defense, oxidative stress tolerance, mucin degradation, and epithelial barrier integrity. This results in a shift towards a microbial community that elicits a pro-inflammatory response in patients with IBD (Erickson et al. 2012). Interestingly, similar metabolic shifts are observed in other inflammatory conditions, including obesity and T2D, suggesting a common gut microbial response to chronic inflammation and immune activation.

Chemerin is a potent chemoattractant and adipokine that has been shown to play important roles in both metabolic and inflammatory diseases (for review, see (Rourke et al. 2013; Zabel et al. 2014)). Clinical studies have demonstrated that chemerin levels are positively associated with BMI and deleterious changes in glucose, lipid, and cytokine homeostasis (for review, see (Rourke et al. 2013)). Consistent with this, animal models have demonstrated that chemerin signalling through both chemokine-like receptor 1 (CMKLR1) and G protein coupled receptor 1 (GPR1) influence adiposity and glucose homeostasis (Ernst et al. 2012; Gruben et al. 2014; Rouger et al. 2013; Rourke et al. 2014; Takahashi et al. 2011; Wargent et al. 2015). Additionally, studies investigating the role of chemerin signalling in IBD pathogenesis have demonstrated that local chemerin expression, secretion, and activation increase locally in the colon and are positively associated with severity of inflammation (Dranse et al. 2015; Lin et al. 2014; Weigert et al. 2010b). Together, this data suggests that chemerin serves as a link between obesity, inflammation, and other disorders that have previously been associated with changes in microbiome composition and activity.

In addition to these roles in metabolism and inflammation, two chemerin isoforms (chemerin-157 and chemerin-125) have been shown to exhibit potent antimicrobial activity against the growth of *Escherichia coli* and *Klebsiella pneumoniae* (Kulig et al. 2011). More recently, chemerin was demonstrated to act as an anti-microbial agent in human skin and provide protection against *E. coli*, *Staphylococcus aureus*, *P. aeruginose*, and *Candida albicans* growth, which was directly mediated through an increase in bacterial lysis (Banas et al. 2013). In addition, Staphopain B, a *S. aureus*-derived cysteine protease, has been shown to act as a potent activator of chemerin (Kulig et al. 2007). This suggests that in addition to chemerin modulating microbial growth, the microbiota may also exert an influence on chemerin bioactivity. Based on these overlaps between chemerin signalling, metabolic and inflammatory disease, and known interactions with microbiota, we hypothesized that chemerin signalling plays a role in regulating gut microbiome composition. Ultimately, this might mediate the role of chemerin signalling on the development of metabolic and inflammatory disorders. The objective of this study was to investigate the diversity and relative abundance of microbiota in the lower GI tract in the presence or absence of chemerin signalling. To do

this, we performed Illumina-based sequencing of the hypervariable V6-8 region of the bacterial 16s rRNA gene on DNA extracted from stool samples obtained from healthy wildtype, chemerin knockout (KO), and CMKLR1 KO mice and examined changes in taxa abundance between genotypes.

Methods

Animals

Wildtype (WT) C57Bl/6 mice (Christopher Sinal (CS) colony) and CMKLR1 knockout (KO) mice were maintained in the Carlton Animal Care Facility at Dalhousie University (Halifax, NS, Canada). C57Bl/6 mice (CS) were obtained from the Jackson Laboratory (Bar Harbour, ME). CMKLR1 KO mice were originally created by Deltagen and were fully backcrossed onto the C57Bl/6 (CS) background as previously described (Ernst et al. 2012; Graham et al. 2009). WT C57Bl/6 mice (Brian Zabel (BZ) colony) were obtained from Jackson laboratory. Chemerin KO mice raised on a C57Bl/6 background were maintained in Veterinary Medical Unit at the Veterans Affairs Palo Alto Health Care Systems (VAPAHCS, Palo Alto, CA, USA). Animals were housed in micro-isolator cages under specific pathogen free conditions (*Helicobacter*-, norovirus-, and parvovirus-free) and all mice had free access to food and water in home cages. Mice at Dalhousie University received Prolab RMH 3000 (LabDiet, St. Louis, MO, USA) and mice at Stanford University received Teklad 18% protein rodent diet (Harlan Laboratories, Madison, WI, USA). All WT and KO animals were generated from WT x WT or KO x KO breedings. At weaning (approximately 3 weeks of age), 2 WT and 2 KO female mice were co-housed in a single cage. In total, 18 WT (CS), 18 CMKLR1 KO, 18 WT (BZ) and 18 chemerin KO mice were used in the study. Animal protocols were approved by Dalhousie University Committee on Laboratory animals in accordance with the Canadian Council on Animal Care guidelines and the Institutional Animal Use and Care Committee at the Veterans Affairs Palo Alto Health Care System.

Genotyping

Ear punches were collected from WT (CS) and CMKLR1 KO animals and digested in proteinase K buffer (0.1 M Tris pH 8.0, 5 mM EDTA, 0.2% SDS, 0.2 M NaCl, and 100 µg/mL proteinase K) at 55°C for 120 min. DNA was isolated with isopropanol precipitation, washed in 70% ethanol, and resuspended in distilled water. Samples were genotyped using Taq polymerase (Invitrogen, Burlington, ON) with three primers specific for the CMKLR1 locus (Primer 1: TACAGCTTGGTGTGCTTCCTCGGTC, Primer 2: TGATCTTGCACATGGCCTTCC,

Primer 3: GGGTGGGATTAGATAAATGCCTGCTCT). Each PCR consisted of 30 cycles of 95°C for 30 s, 60°C for 30 s, and 72°C for 30 s with standard PCR conditions (10x PCR buffer (200 mM Tris-HCl pH 8.4, 500 mM KCl), 2.5 mM $MgCl_2$, 0.1 mM dNTPs, and 0.2 μM of each of the three primers). Products were visualized by ethidium bromide staining after electrophoresis on a 2.5% agarose gel using a DyNA Light UV Transilluminator (Mandel, Guelph, ON), ESAS 290 electrophoresis analysis system (Kodak, Rochester, NY, USA), and 1D image analysis software (Kodak, Rochester, NY, USA). Genotyping of WT (BZ) and chemerin KO mice was performed at Stanford University using the standard BZ lab protocol.

Fecal sample collection

Following 3 weeks of co-housing (at approximately 6 weeks of age), fecal samples were collected from each mouse. Mice were placed into an empty sterile cage and left until stool samples were produced (maximum 10 min). 3-4 pellets were collected per animal (approximately 100 mg dry weight per collection period). Samples were transferred with sterile forceps to a clean eppendorf tube and frozen immediately at -80°C until DNA isolation was performed. Fecal samples from WT (BZ) and chemerin KO mice were shipped on dry ice to Dalhousie University. Fecal samples from WT (CS) and CMKLR1 KO mice were also collected at 8 weeks of age. In total, 108 samples were collected. In addition, WT (CS) and CMKLR1 KO mice were weighed using a bench-top balance (Mettler Toledo, Mississauga, ON) at the time of stool collection.

DNA isolation, library preparation, and 16s sequencing

Genomic DNA was isolated from fecal sample samples using PowerFecal DNA Isolation Kit (MO BIO Laboratories, Carlsbad, CA, USA). Approximately 2-3 pellets of stool from each mouse were processed in batches of 24 over 5 consecutive days as per manufacturer's instructions. Isolated DNA was eluted in 100 μL of Solution C6 and stored at -80°C. 16S ribosomal RNA gene fragments were amplified using two different dilutions of each sample (2 μL of undiluted DNA, and 2 μL of 1:10 dilution) using Phusion High-fidelity polymerase (NEB, Whitby, ON) and standard reaction and cycling conditions as recommended by the manufacturer. PCR primer sequences within the 16S

V6-8 region were adapted from those described previously (Comeau et al. 2011) to contain adaptor sequences for Illumina MiSeq and indices to generate a unique barcode for each sample. Primers consisted of Forward: 5'-adaptorL1-index-adaptorR1-ForPrimer-3' and Reverse: 5'-adaptorL2-index-adaptorR2-RevPrimer-3' and generated a usable amplicon size of 438 bp. The duplicate PCR products from each sample were pooled and a sample run on a 2% Sybr Safe 96-well E-gel using the E-base power supply (Invitrogen, Burlington, ON) for verification of PCR quality. PCR products were then purified and library normalization performed using SequalPrep Normalization Plate Kit 96-well (Invitrogen, Burlington, ON). Final pooled library DNA was concentrated using DNA Clean & Concentrator-5 (Zymo Research, Irvine, CA, USA) and DNA was quantified using a Qubit fluorometer (Invitrogen, Burlington, ON). The library was loaded into a MiSeq Sequencer (Illumina, San Diego, CA, USA) at 20 pM. 5% PhiX spike-in was used as a positive control and sequencing was performed using the standard protocol recommended by manufacturer.

Data analysis

Data analysis was performed according to the workflow outlined on https://github.com/mlangill/microbiome_helper#microbiome-helper using the indicated programs (Andrews 2010; Caporaso et al. 2010; Kopylova et al. 2012; Langille 2015; Parks et al. 2014; Zhang et al. 2014b). A selection of raw FASTQ files were evaluated using FASTQC (Andrews 2010) by manual inspection. Parameters assessed by FASTQC include per base sequence quality, per sequence quality scores, per base sequence content, per sequence GC content, per base N content, sequence length distribution, sequence duplication levels, over-represented sequences, adapter content, and Kmer content. Paired-end assembly was then performed using PEAR (Zhang et al. 2014b) and a selection of assembled sequences were inspected using FASTQC. Ns were removed from assembled sequences and files were converted to FASTA format.

Taxonomic analysis and visualization

Sequencing reads were clustered into operational taxonomic units (OTU) with a 97% identity threshold using QIIME (Caporaso et al. 2010). An open OTU picking

protocol was performed using GreenGenes as a reference database of known sequences (DeSantis et al. 2006) and de novo picking was performed for failed sequences with 10% of failed sequences sub-sampled. All samples were normalized to a sequence depth of 15000. All further analysis was first performed for all 108 samples combined, and then individually for all samples within a particular facility using QIIME ((Caporaso et al. 2010) and references within). To visualize diversity within samples, alpha rarefaction plots were generated using a minimum of 1000 sequences and a maximum of 15000 sequences per sample over 15 steps. To examine differences between samples, both unweighted and weighted UniFrac (contains phylogenetic information) beta diversity plots were generated using principal coordinate analysis (PCoA). Additional analysis of Akkermansia and Prevotella abundance (sum of observed sequences within each genus) was performed by dividing the samples into groups (high/low abundance) using the mean abundance of each genus as a threshold.

Statistical analysis

Total weight and weight gain data was graphed using GraphPad Prism (version 5.0b, La Jolla, CA, USA) and assessed using an unpaired Student's t-test. Data (mean ± standard deviation) for alpha rarefaction plots generated through the pipeline described above was graphed using GraphPad Prism. STAMP (Parks et al. 2014) was used to determine statistically significant differences within taxonomic ranks between samples. Two sample comparisons were performed using a two-sided Welch's t-test. Abundance values reported are the minimum, maximum, median, average number, and standard deviation of the number of sequences observed for a particular taxon within a single sample. Box plots of bacterial abundance were created using GraphPad Prism using the Tukey method to plot whiskers and outliers. The line and cross represent the median and mean, respectively, and outliers are represented as dots. Correlations between total weight and abundance values were determined using PAST (Hammer et al. 2001) and significance was calculated using the Pearson's r correlation test or the Spearman rank-order correlation test when data was not normally distributed (as determined by the Shapiro-Wilk normality test). Abundance values were represented as log(abundance) and abundance values of 0 were excluded in the analysis (one sample in the g_Akkermansia

KO comparison). Weight values were missing for 3 WT mice and samples from these animals were excluded from the correlation analysis. For all data, significance was reported as $p<0.05$ and p-values are corrected for testing of multiple groups when necessary.

Results

In order to investigate the impact of a loss of chemerin or CMKLR1 expression on microbiome composition, 16S sequencing was performed on DNA isolated from fecal samples collected from female WT (BZ and CS colonies), chemerin KO, and CMKLR1 KO mice as highlighted in Figure 5.1. There were no apparent differences between WT and KO mice in terms of general health and wellness. Specifically, there was no significant difference in body weight between WT and CMKLR1 KO mice at 6 or 8 weeks of age, and no difference in weight gain over the 2-week period monitored (Figure 5.2). Weight gain in WT (BZ) chemerin KO mice was not measured. In total, 4.8 million sequencing reads were obtained with an average of 41796 sequencing reads per sample (minimum 15540; maximum 70831; median 42038.5; standard deviation 9645.86). There were no major differences in sequence quality between samples and the average Phred score, a measure of the quality of nucleotide identification, for all samples was 33. 98.6% of sequences were assembled, and 1.4% and 0.003% were unassembled or discarded, respectively. Overall, sequences were clustered into a total of 27323 operational taxonomic units (OTUs, sequences with a 3% similarity threshold), of which 16665 could be assigned a phylum name and 3442 a genus name. The remaining sequences were clustered by percentage of identity but assigned to a higher taxonomic rank.

Species richness is similar between facilities and genotypes

We first examined species diversity within samples. To do this, we generated an alpha rarefaction plot for the number of observed OTUs for wildtype (CS and BZ), CMKLR1 KO, and chemerin KO mice (Figure 5.3). This indicates the number of different OTUs identified within each biological sample when sampled at each particular depth. For all four groups of mice, the curve began to plateau at 15000 sequences/sample indicating that the majority of OTUs present within each group had been sampled. Overall there was no significant difference in alpha diversity between both facility and genotype. However, there was a trend for slightly higher diversity in samples collected from VAPAHCS compared to Dalhousie University.

Mice housed in the two different facilities have dramatically altered microbiome profiles

We next investigated differences in the taxonomic composition of the microbiome between the four groups of mice. This was performed using both unweighted (qualitative, based on the presence/absence of OTUs) and weighted (quantitative, considers the abundance of OTUs) UniFrac, which is a metric that compares the distance between biological colonies by incorporating phylogenetic information on the relatedness of the observed organisms. Three-dimensional principal coordinate analysis (PCoA) using both unweighted (Figure 5.4A) and weighted (Figure 5.4B) UniFrac demonstrated significant separation by facility. Principal coordinate 1 (PC1, percent variation explained: 13.69%) of the unweighted UniFrac distinctly separated mice between the two facilities, indicating substantial differences in the presence/absence of OTUs between facilites. However, the weighted UniFrac explained a larger amount of variation between facilities (~63%) after the introduction of PC2 (15.92%) and PC3 (15.16%). This demonstrates that a significant proportion of the difference in microbiome composition between facilities is related to the abundance of overlapping OTUs. Importantly, there was no observable separation between genotypes at either facility using both the unweighted and weighted UniFrac analysis when all four groups of mice were considered together.

To further explore differences in microbiome composition between facilities, we compared the abundance of different OTUs in fecal samples isolated from WT mice at Dalhousie University (CS) and VAPAHCS (BZ). All significant differences between the two facilities at each taxonomic level are highlighted in Table 5.1. There were several differences at the phylum level, including increased levels of Cyanobacteria and Verrucomicrobia, and decreased levels of Actinobacteria, in CS mice compared to BZ. Analysis of the abundance table revealed that significant differences at a single genus level were responsible for the majority of differences at higher taxonomic ranks. For example, the difference in phylum Verrucomicrobia was entirely due to increased abundance of *Akkermansia* in CS mice, and *Bifidobacterium* comprises the majority of differences in the Actinobacteria phylum between facilities. As a result, we focused our analysis on differences at the genus level in order to gain highest resolution when identifying microbial differences between Dalhousie University and VAPAHCS. There

were changes in 22 different identified genera as well as 13 groups that were unclassified at the genus level but associated with known families (Table 5.1). Many of these taxa comprise a very minor proportion of the total microbiome community. For instance, one *Fluviicola* sequence was identified in samples from CS mice and none were observed in samples from BZ mice. Therefore only changes in which the abundance of each genus was greater than 1% of total sequences sampled from at least one facility are shown in Figure 5.5. Levels of *Akkermansia*, *Desulfovibrio*, and *Ruminococcus* were higher in CS mice, and levels of *Bacteroides*, *Bifidobacterium*, *Odoribacter*, *Paracteroides*, *[Prevotella]*, and unclassified bacteria of the *Clostridiaceae* family were decreased compared to BZ mice. Notably, CS mice had significant amounts of *Akkermansia* (~3% of total microbiome) whereas *Akkermansia* was nearly undetectable in BZ mice. In contrast, significant levels of *Bacteroides*, *Bifidobacterium*, *Odoribacter*, *[Prevotella]*, and unclassified members of the Clostridiaceae family comprised ~8.5% of microbiome in BZ mice and were only detected at extremely low levels in CS mice. Altogether, these results confirm our earlier findings that differences in the microbiome composition between the two facilities is due to both the presence/absence of certain bacteria as well as the proportion of overlapping OTUs.

WT (BZ) and chemerin KO mice have very minor differences in Desulfovibrionaceae, Rhodobacteraceae, and Rikenellaceae abundances

In order to determine the impact of a loss of chemerin expression on the mouse gut microbiome, we compared the taxonomic profiles between WT (BZ) and chemerin KO mice, which were both housed at VAPAHCS. Principal coordinate analysis of both unweighted (PC1 6.65%, PC2 5.46%, PC3 5.18%, data not shown) and weighted UniFrac revealed a lack of distinct separation between WT (BZ) and chemerin KO mice (Figure 5.6A). However, weighted UniFrac explained more of the separation between WT (BZ) and chemerin KO mice (PC1 35.91%, PC2 15.39%, PC3 10.68%) suggesting that differences between the two genotypes are related to changes in the relative abundance of OTUs versus their presence or absence. Importantly, there was no effect of cage on the microbiome profile between mice (Figure 5.6B). Further analysis of differences in the abundance of different taxonomic ranks revealed a very modest number of changes

between WT (BZ) and chemerin KO mice (3 significant differences at the genus level). The majority of these comprised a very minor percentage of total sequences sampled and are shown in Table 5.2. The largest differences between WT (BZ) and chemerin KO mice comprised ~0.02-1.5% of total sequences analysed and are shown in Figure 5.7. These include an increase in the abundance of Desulfovibrionaceae and unclassified members of the Rhodobacteraceae family, and a decrease in the abundance of *Rikenella*, in chemerin KO mice compared to WT (BZ). Considered altogether, this data indicates that the microbiome, in terms of relative community abundance, is not substantially altered between healthy WT (BZ) and chemerin KO mice at 6 weeks of age.

CMKLR1 KO mice have an increased abundance of Akkermansia and Prevotella compared to WT (CS)

We next examined differences in gut microbiome profiles between WT (CS) and CKMLR1 KO mice housed at Dalhousie University. Principal coordinate analysis of the unweighted UniFrac revealed no obvious pattern of separation between wildtype and CMKLR1 KO mice, and only explained a relatively minor proportion of the separation between samples (PC1 5.11%, PC2 4.48%, PC3 3.00%, data not shown). However, Principal coordinate analysis of the weighted UniFrac (Figure 5.8A) explained a higher amount of variability between samples (PC1 37.64%, PC2 21.94%, PC3 6.95%). There was a trend for CMKLR1 KO mice to be shifted leftwards on PC3, suggesting that PC3 explains a small amount of separation between genotype. Similar to mice housed at VAPAHCS (Figure 5.6B), there was no obvious separation by cage in both the unweighted (data not shown) and weighted (Figure 5.8B) UniFrac plots. This indicates that there is no effect of cage on the microbiome community in the current study.

Further analysis of OTU abundances revealed a number of significant differences between WT (CS) and CMKLR1 KO mice (Table 5.3). Importantly, the phylum Firmicutes made up a considerable proportion of all sequences in WT mice (~18%) and was significantly higher in CMKLR1 KO mice (~20%) (Figure 5.9). However, it is unclear which bacteria make up this difference as there were no differences in Firmicutes at lower taxa levels. The majority of other significant differences occurred at lower levels, including 8 different taxa at the genus level (Table 5.3). A number of these

differences made up a relatively minor proportion of total sequences (less than 0.2% of total sequences), although there were several differences that comprised >1% of total sequences. These include *Akkermansia*, which comprised ~3-5% of microbiome in WT animals but only ~1% in CMKLR1 KO animals (Figure 5.9). Additionally, *Prevotella* (note this is a different genera from [*Prevotella*] discussed earlier in Figure 5.5, where both are classified in the order Bacteroidales but *Prevotella* is a member of the family Prevotellaceae, whereas *[Prevotella]* is a member of the family [Paraprevotellaceae]) and unclassified members of the Rikenellaceae family decreased ~1.5-fold in CMKLR1 KO animals compared to WT (CS) (Figure 5.9).

Akkermansia and Prevotella abundance are negatively associated with body weight and exhibit similar patterning to WT (CS) and CMKLR1 KO mice

Previous studies have established that *Akkermansia* abundance is negatively correlated with body weight and glucose tolerance in rodent and humans (Everard et al. 2011; Qin et al. 2012; Santacruz et al. 2010). Studies have also shown that a high abundance of *Prevotella* is correlated with obesity and impaired glucose tolerance (Ellekilde et al. 2014; Okeke et al. 2014). Consistent with this, we observed a negative correlation between the weight of each mouse at the time of stool collection (6 or 8 weeks) and *Akkermansia* (Figure 5.10A) or *Prevotella* (Figure 5.10B) abundance within each stool sample. However, this was only significant for CMKLR1 KO mice, and not WT (CS).

Finally, as significant differences in abundance of *Akkermansia* and *Prevotella* were observed in samples from WT (CS) and CMKLR1 KO mice, we investigated whether differences in these genera explained the separation between genotypes observed earlier. To do this, we categorized samples as having a low or high abundance of *Akkermansia* or *Prevotella* based on the average sequence count. Figure 5.11A,B demonstrates that a high abundance of either *Akkermansia* or *Prevotella* separates the samples towards the right on PC3. Interestingly, this pattern is similar to that seen in Figure 5.8 between WT (CS) and CMKLR1 KO animals.

Discussion

Over the past 10-15 years, our knowledge of the role of both commensal gut microbiota and chemerin signalling have been increasingly associated with the development of metabolic and inflammatory disorders. In this study, we investigated the relationship between the two by comparing the diversity and composition of the gut microbiome in fecal samples obtained from mice with normal or reduced levels of chemerin signalling. These findings provide an essential preliminary assessment of the microbiome profile in healthy chemerin and CMKLR1 KO mice. Several key differences in microbiota composition that have implications for the study of metabolic and inflammatory diseases were observed and are discussed in further detail below.

The environment is a significant factor in the composition of gut microbiota

The most striking result from this study was a dramatic difference in gut microbiome composition between Dalhousie University and VAPAHCS. The animals used in this experiment were identical in terms of background strain, vendor source of C57/Bl6 mice, age, sex, breeding strategy, and pattern of co-housing. In addition, DNA isolation from fecal samples and subsequent 16s rRNA sequencing was performed for samples obtained from both facilities at the same time, eliminating any potential differences in sample preparation or sequencing bias. The only notable differences in study design included the type of rodent chow used and the physical location where the mice were housed. However, despite attempts to keep study conditions as similar as possible, there was a trend for increased species richness at VAPAHCS and a large number of differences in bacterial abundance identified between the two facilities. Both unweighted and weighted UniFrac metrics explained a relatively high percentage of variation between the two facilities, indicating that the differences in microbiota composition were due to changes in the presence of particular bacterial species as well as the abundance of common species. These include increased levels of *Bifidobacterium*, *Clostridium*, *Bacteroides*, *Prevotella*, *Odoribacter*, and decreased abundance of *Akkermansia*, *Ruminococcus*, and *Desulfovibrio* in VAPAHC compared to Dalhousie University. It is unclear what factors are responsible for the differences in microbiome profiles between facilities. The rodent chow used at VAPAHCS excludes alfalfa, which

explains a decrease in photosynthesizing Cyanobacteria compared to mice at Dalhousie University. Other dietary factors, such as the percentage of calories from fat (18% versus 14%) might influence the composition of other gut bacteria. Additionally, differences in the cleanliness of the rooms or exposure to pathogens might influence microbial composition. Further identification of the environmental factors that influence microbiome composition will be essential in order to increase reproducibility and recognize potential confounding factors in future studies.

These results are consistent with previous studies that have demonstrated that the microbiome of mice used in biomedical research is greatly influenced by environment. For example, studies have shown that genetically similar mice obtained from different commercial vendors have profound differences in the richness and diversity of fecal microbial populations (Ericsson et al. 2015). Consistent with this, environmental reprogramming of microbiota can ameliorate or accelerate the development of diseases such as obesity and T2D (Ussar et al. 2015). Notably, the abundance of several genera that were identified to be significantly different between Dalhousie University and VAPAHCS (eg. *Bifidobacterium*, *Clostridium*, *Bacteroides*, *Prevotella*, and *Akkermansia*) have been associated with changes in adiposity, T2D, and/or IBD (Barlow et al. 2015; Keeney et al. 2014; Zhang et al. 2015b). This might have important implications for studies that investigate the role of chemerin signalling *in vivo*. For instance, multiple groups have presented conflicting results on the adipose and glucose phenotype of CMKLR1 KO mice. While we previously demonstrated that CMKLR1 KO mice have reduced adiposity but worsened glucose tolerance (Ernst et al. 2012), two other groups published that CMKLR1 KO mice are more susceptible to weight gain but with one group showing worsened, and another showing unchanged, glucose tolerance (Rouger et al. 2013; Wargent et al. 2015). A fourth group has shown no effect of CMKLR1 loss on either weight gain or glucose tolerance (Gruben et al. 2014). Interestingly, the source, and presumably genetics, of the transgenic mouse line used is identical in three of these studies (Ernst et al. 2012; Rouger et al. 2013; Wargent et al. 2015), making the reasons for such discrepancies in the phenotype of CMKLR1 KO mice unclear. Given the profound effect of the environment on microbiome composition, and the known influence of the microbiome on the pathogenesis of disease, it is possible that

differences in microbiome composition confounded the results of these studies. It would be interesting to collect stool samples from CMKLR1 KO mice from each of the different facilities used and compare the microbiome composition between the different mouse colonies. This would be useful not only for studies involving obesity and T2D, but also other diseases that are known to be influenced by the microbiome.

Changes in microbiome composition with a loss of chemerin signalling

As a result of the differences in microbiome composition between Dalhousie University and VAPAHCS, we were limited to comparing chemerin and CMKLR1 KO mice to their respective WT mice within each facility. For both genotypes, there were no changes in alpha diversity compared to wildtype. In contrast to the comparison between the two facilities, there was very little variability between WT and KO mice explained using unweighted UniFrac metrics. An increased amount of variability was explained by the weighted UniFrac, suggesting that differences in microbiome composition between both chemerin and CMKLR1 KO mice compared to their respective WT mice are due to differences in the abundance of common taxa. Within VAPAHCS, there were very few changes in microbiome composition between chemerin KO and WT mice. These included changes in *Rikenella*, *Lactococcus*, and members of the Desulfovibrionaceae and Rhodobacteraceae families. It is unclear what these changes mean in terms of health and/or disease, although changes in these bacteria have been linked with both metabolic and inflammatory diseases (Keeney et al. 2014; Okeke et al. 2014). There were significantly more differences in the abundance of microbiota identified between WT and CMKLR1 KO mice at Dalhousie University, including a relatively high number of differences at the genus level. The largest differences in the abundance of bacteria were in *Akkermansia* and *Prevotella*, which together comprised ~3-8% of the total bacteria isolated from the gut of WT mice and explained ~6% of variability between WT and CMKLR1 KO mice.

It was not possible to directly compare differences between CMKLR1 and chemerin KO mice because of the differences in microbiome composition observed between facilities. However, both chemerin and CMKLR1 KO mice exhibited decreases in the abundance of *Rikenella* compared to WT. A previous study identified that

Rikenella was 1 of 10 genera to be affected by genotype in the feces of obese diabetic *db/db* mice compared to lean controls (Geurts et al. 2011). This suggests a potential link between chemerin signalling and metabolic disease. It was surprising that there were more differences in bacterial abundance identified between CMKLR1 KO and WT mice compared to chemerin KO mice. It is possible that this is an artifact from the differences in environment. For example, *Akkermansia* was nearly undetectable in mice housed at VAPAHCS, so it is difficult to predict whether the abundance of *Akkermansia* would be altered in chemerin KO mice in a manner similar to CMKLR1 KO mice if the genus were present in the bacterial community. Alternatively, ligands other than chemerin, including resolvin E1 and beta-amyloid, have been reported to act as agonists at CMKLR1, although these have yet to be confirmed by independent groups (Arita et al. 2005a; Peng et al. 2015). Therefore, differences in the abundance of microbial populations between chemerin and CMKLR1 KO mice could be explained by signalling through chemerin-independent pathways at CMKLR1. Future studies that house all groups of mice in the same facility will enable the direct comparison of microbiome profiles between chemerin, CMKLR1, and WT mice.

Relationship between the microbiome and CMKLR1 signalling in adiposity

Chemerin signalling has been positively associated with obesity and T2D. In addition to the increased *Rikenella* abundance in chemerin and CMKLR1 KO mice discussed above, the abundance of several bacteria that are known to correlate with adiposity and glucose tolerance were altered between wildtype and CMKLR1 KO mice. These include *Akkermansia*, *Bacteroides*, and *Prevotella*. Recent studies have highlighted a direct role for *Akkermansia*, a mucin-degrading bacteria, in obesity, where treatment of mice with *Akkermansia* has been shown to reduce HFD-induced metabolic disorders including fat mass gain, metabolic endotoxemia, adipose tissue inflammation, and insulin resistance (Everard et al. 2013). This demonstrates that specific bacteria that have been identified to correlate with body weight are able to exert direct metabolic effects on the host. Similar to previous reports (Everard et al. 2011; Qin et al. 2012; Santacruz et al. 2010), we identified a negative relationship between both *Akkermansia* and *Prevotella* abundance and total body weight. Interestingly, this relationship was only

significant for CMKLR1 KO mice. A higher abundance of *Akkermansia* and *Prevotella* populations over a small weight range might explain the lack of significant correlation in WT mice. Alternatively, the influence of a loss of CMKLR1 on the abundance of these microbiota, or the effect of these genera on the body weight of CMKLR1 KO mice, might be differentially regulated. A differential effect of *Akkermansia* or *Prevotella* populations on CMKLR1 KO mice would help to explain previously reported differences in adiposity and glucose tolerance in the absence of CMKLR1 signalling (Ernst et al. 2012; Rouger et al. 2013; Wargent et al. 2015). Future studies that directly address the role of *Akkermansia* and *Prevotella* in CMKLR1 KO mice, including more timepoints to observe mice over a longer period of time, DEXA analysis for body composition, and the effect of a high-fat diet (HFD), will prove useful in further examining the relationship between the gut microbiome on the adiposity and glucose tolerance phenotype of CMKLR1 KO mice.

Relationship between the microbiome and CMKLR1 signalling in IBD

Previous studies have demonstrated a relationship between the abundance of a number of bacterial populations on the development of IBD (Keeney et al. 2014). In general, these studies tend to associate a pro-inflammatory microbial population with an increased risk for the development or increased severity of IBD. Increases in the abundance of *Bacteroides*, *Bifidobacterium*, *Clostridium*, and a decrease in *Akkermansia* levels were observed in samples from VAPAHCS compared to Dalhousie University. These species have been correlated with the prevalence of IBD, suggesting that mice at the two facilities might have altered susceptibility to IBD. Consistent with this, conflicting results have been presented regarding the effect of systemic chemerin injection on the development of IBD (Dranse et al. 2015; Lin et al. 2014). Within Dalhousie University, CMKLR1 KO mice exhibited a decrease in *Akkermansia* and *Prevotella* species. There are a number of studies that associate both of these taxa with the severity of IBD. In particular, it has been suggested that changes in mucin degradation resulting from altered *Akkermansia* abundance influence epithelial cell layer integrity and the pathogenesis of IBD. Consistent with this, *Akkermansia* abundance is reduced in patients with both UC and CD (Png et al. 2010) and administration of

Akkermansia has been shown to protect against the progression of DSS-induced colitis (Kang et al. 2013). In contrast, other groups have shown that *Akkermansia* exacerbates the severity of disease in mouse models of *Salmonella typhimurium*-induced gut inflammation and inflammation-associated colorectal cancer in mice (Ganesh et al. 2013; Zackular et al. 2013). We previously demonstrated that CMKLR1 KO mice develop clinical signs of DSS-induced colitis more slowly than wildtype mice (Dranse et al. 2015), which supports the latter findings. Additionally, a high abundance of *Prevotella* is correlated with the prevalence of UC in humans and increased epithelial inflammation in a colitis mouse model (Lucke et al. 2006; Scher et al. 2013), which is consistent with CMKLR1 KO mice exhibiting slower disease progression. However, it is important to note that we did not observe any changes in key bacteria associated with IBD such as Faecalibacterium. Based on this observation, and the correlative nature of our findings, future studies that directly examine the relationship between chemerin signalling and the microbiome on the pathogenesis of IBD are warranted.

Influence of chemerin as an antibacterial agent on the microbiome

Previous studies have demonstrated that chemerin acts as an antimicrobial agent and prevents the growth of *Escherichia coli*, *Klebsiella pneumoniae*, and *Staphylococcus aureus* (Banas et al. 2013; Kulig et al. 2011). In this study, we did not observe any of these species (data not shown), which is not surprising as these pathogenic species would not normally be present in the healthy gastrointestinal tract. An extremely limited number of unclassified Enterobacteriaceae and *Staphylococcus* sequences (maximum 5 sequences out of 15000 total), for which *E. coli* and *S. aureus* may have been classified under, were identified in samples from Dalhousie University and VAPAHCS. In the absence of these species, we are unable to determine whether the antimicrobial effects of chemerin are occurring in the mouse gut. However, due to the very low number of differences in gut microbiota between chemerin KO and WT mice, it seems unlikely that chemerin is exerting an antimicrobial effect under healthy conditions. This is consistent with the low basal expression of chemerin in the gut (Dranse et al. 2015). It seems more likely that chemerin plays an antimicrobial role to protect against pathogen invasion and exhibits increases in expression and activation in disease states when required. This concept is

supported by evidence that pathogen-derived enzymes such as *S. aureus*-derived Staphopain B are able to elevate levels of bioactive chemerin (Kulig 2007). Future studies that directly examine the susceptibility of chemerin KO animals following infection with pathogenic bacteria, compare the microbiome profiles of chemerin KO animal in challenged conditions, and investigate chemerin isoform distribution in the gastrointestinal tract following changes in microbiota composition, will provide further insight into the role of chemerin as an antibacterial agent.

Limitations

There are several limitations of this study that should be taken into consideration. Firstly, it is important to note that this study was performed using healthy, young mice; however, both CMKLR1 and chemerin KO mice exhibit differences in phenotype under stressed conditions. For example, chemerin KO mice exhibit exacerbated glucose intolerance on a HFD (Takahashi et al. 2011) and CMKLR1 KO mice exhibit differences in adiposity and glucose tolerance when fed a HFD compared to a LFD (Ernst et al. 2012). Additionally, CMKLR1 KO mice develop signs of clinical illness more slowly in an experimentally-induced colitis model (Dranse et al. 2015). As the microbiome is associated with the development of these disorders, it will be interesting to examine whether differences in microbiome composition in chemerin and CMKLR1 KO mice under stressed conditions such as a HFD or chemically-induced colitis influence the development of inflammatory and metabolic diseases. Furthermore, studies that directly investigate the role of chemerin on the growth and/or survival of particular microbiota in diseased states will be interesting. For example, chemerin is secreted at nearly undetectable levels in the colon under basal conditions, but levels of chemerin secretion and activation increase dramatically when inflamed (Dranse et al. 2015). This suggests that the impact of increased chemerin secretion in the colon on the microbiome might be more important in a disease context than in normal physiology.

In addition to health and age, there are several other biological limitations of this study. The majority of studies that have investigated the role of chemerin signalling in obesity, T2D, and inflammatory disorders have been performed with male mice. However, we only examined the microbiome of female mice, and it is possible that

changes in the microbiome are different in male mice. In addition, we co-housed two wildtype and two KO mice at weaning for 3 weeks before fecal sample collection. We did this to eliminate stochastic effects that might result from housing different breeding colonies in isolated cages, but it is possible that co-housing masked differences in microbiota composition between WT and KO mice (Nguyen et al. 2015). Furthermore, we only investigated the microbiome in fecal samples. Changes in microbiota composition and activity have been shown to vary throughout the length of the GI tract (Gu et al. 2013) and analysis of samples from the small intestines and cecum may provide further information on the gut microbiome. Chemerin signalling might also influence the microbiota composition at other anatomical locations, such as the skin, which were not assessed in this study. Finally, we used conventional whole-body knockout animals, and compensation might have occurred in the absence of chemerin/CMKLR1 signalling. Therefore future studies that explore both sexes, alter housing arrangements, include more sampling locations, and investigate more acute methods of manipulating chemerin signalling will be essential to understand the role of the microbiome in chemerin-influenced disease.

A common struggle with bioinformatic studies is the analysis of large datasets and the ability to identify changes that are biologically relevant. In this study, we chose to focus at the genera level in order to gain the highest resolution on bacterial identity without compromising accuracy in classification assignment. Additionally, we focused on populations that comprised >1% of total sequences, under the assumption that dominant species contribute the most to the ecosystem and are the main determinants of local microbiome processes. However, minor community members might also play an important role, and these should be considered in future assessments. There are also some limitations of the technology used. 16s rRNA sequencing with Illumina platforms are useful for sequencing many samples at a high sequencing depth; however, some bacteria, such as rare components of the gut microbiome, might be difficult to detect at the depth of common sequencing (Arrieta et al. 2014). Additionally, it should be noted that the sequencing is only semi-quantitative because the technology relies on endpoint PCR, which is saturating, and the use of primers that differ in efficiency might result in sampling bias. Further studies that use quantitative PCR with primers designed

specifically for certain bacterial species of interest should be used to confirm changes in bacteria abundance. It is also important to note that this study assessed changes in taxonomic classification, but did not assess predictive functional annotation to determine how changes in microbiome composition would influence microbial activity in the gut. Finally, our results are correlative and not causative. Future studies that directly test the influence of microbial species on chemerin-related functions will be essential to determine the direct role of the microbiome in relation to chemerin signalling.

In conclusion, this is the first study that investigates the link between chemerin signalling and microbiome composition. The information gained from these studies will be valuable in the development of studies that directly investigate the relationship between chemerin signalling and the microbiome in the pathogenesis of multiple disease states. Despite attempts to maintain similar experimental conditions between different facilities, these results highlight the impact of the environment on microbiome composition. Importantly, changes in bacteria that are known to influence chemerin-associated diseases were differentially present between facilities, highlighting that the microbiome might be a confounding factor when studying the role of chemerin signalling in obesity and inflammation *in vivo*. Additionally, we demonstrated that differences in the abundance of *Akkermansia* and *Prevotella*, both established to impact adiposity and glucose tolerance, are correlated with body weight and are decreased in CMKLR1 KO mice. This indicates that the microbiome might influence the development of metabolic and inflammatory diseases in relation to chemerin signalling. This has potential implications for the development of novel methods to modify disease risk through lifestyle changes such as dietary intervention, exercise, use of probiotics, or fecal transplantation. Future studies that house mice in the same environment, focus on other methods to modify chemerin signalling, incorporate disease models, and predict functional changes in microbial activity, will be informative to fully elucidate the relationship between chemerin signalling and the microbiome on health and disease.

Tables and figures

Figure 5.1. Experimental design to investigate potential differences in microbiome composition between wildtype, chemerin KO, and CMKLR1 KO mice

Female mice used in this study were housed at VAPAHCS (BZ; Brian Zabel lab) or Dalhousie University (CS; Christopher Sinal lab). All mice were derived from either WTxWT or KOxKO breedings. Weight measurements and fecal samples were collected as indicated. DNA isolation and 16S sequencing was performed on samples from both facilities at the same time at Dalhousie University. Bioinformatic analysis was performed on all 108 samples together as well as independently by facility. WT, wildtype; KO, knockout.

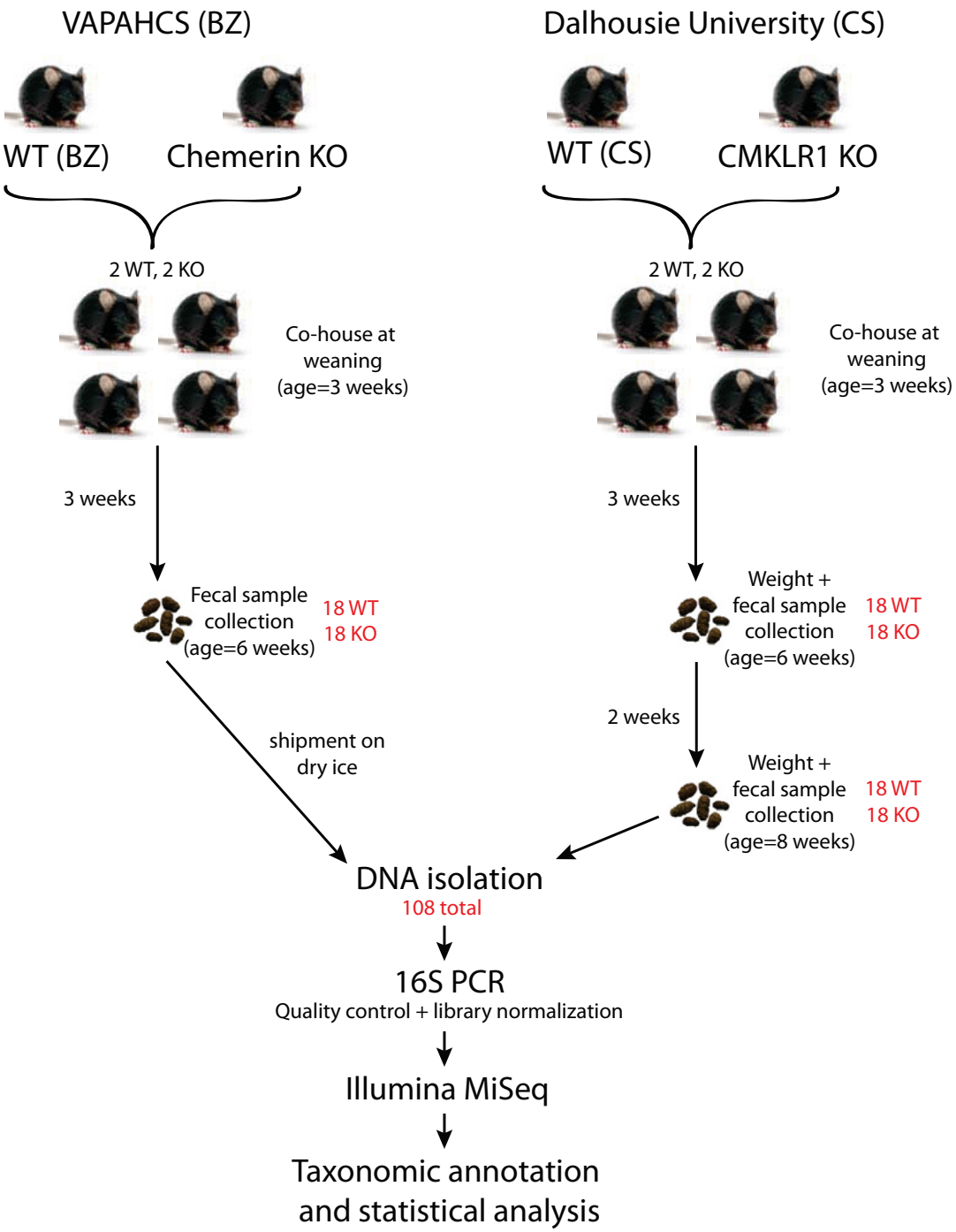
VAPAHCS (BZ)
Dalhousie University (CS)
WT (BZ)
Chemerin KO
WT (CS)
CMKLR1 KO
2 WT, 2 KO
2 WT, 2 KO
Co-house at weaning (age=3 weeks)
Co-house at weaning (age=3 weeks)
3 weeks
3 weeks
Fecal sample collection (age=6 weeks)
18 WT
18 KO
Weight + fecal sample collection (age=6 weeks)
18 WT
18 KO
2 weeks
shipment on dry ice
Weight + fecal sample collection (age=8 weeks)
18 WT
18 KO
DNA isolation
108 total
16S PCR
Quality control + library normalization
Illumina MiSeq
Taxonomic annotation and statistical analysis

Figure 5.2. WT and CMKLR1 KO mice have similar body weights

Body weight was recorded for WT (CS) and CMKLR1 KO mice at both 6 and 8 weeks of age when stool was collected (A). Weight gain was calculated as the difference in weight between weeks 6 and 8 (B).

A

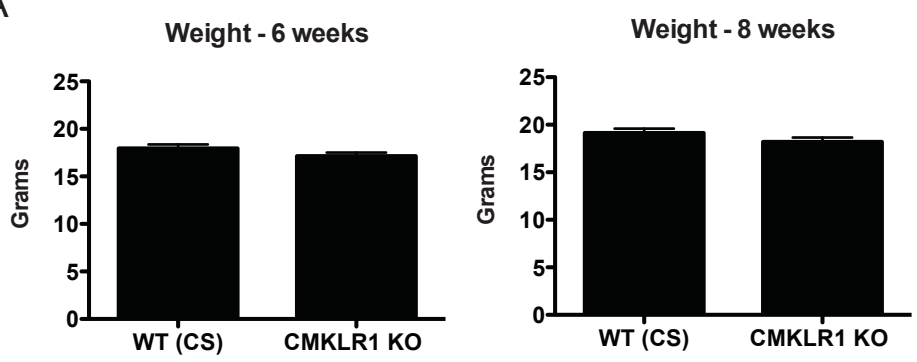
Weight - 6 weeks
Grams
25
20
15
10
5
0
WT (CS)
CMKLR1 KO
Weight - 8 weeks
Grams
25
20
15
10
5
0
WT (CS)
CMKLR1 KO

B

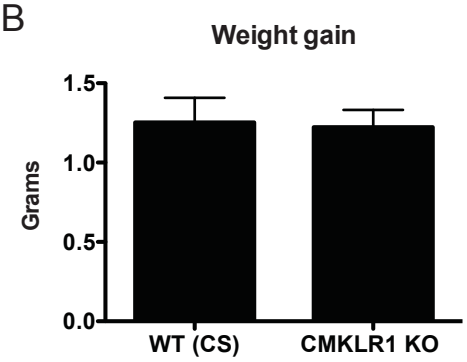
Weight gain
Grams
1.5
1.0
0.5
0.0
WT (CS)
CMKLR1 KO

Figure 5.3. Species richness is similar across both facility and genotype

Alpha rarefaction plot demonstrating the number of observed OTUs (mean ± standard deviation) at the indicated number of 16S sequences sampled per group (minimum 1000, maximum 15000 sequences).

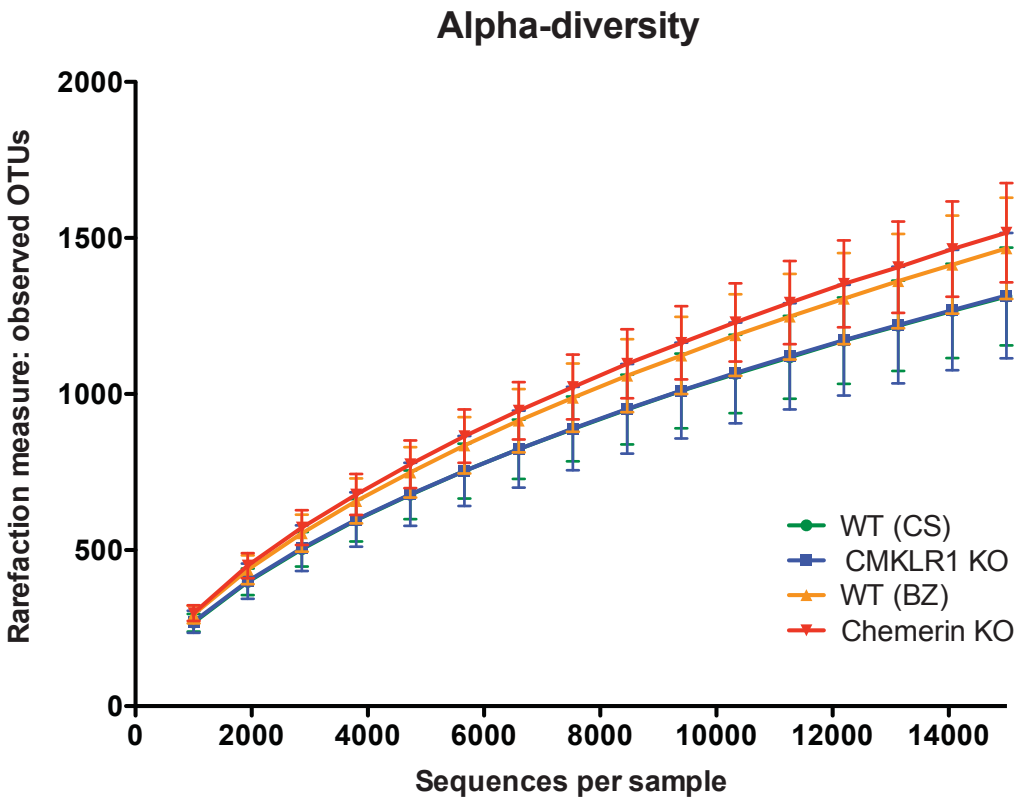
Alpha-diversity
Rarefaction measure: observed OTUs
2000
1500
1000
500
0
0
2000
4000
6000
8000
10000
12000
14000
Sequences per sample
WT (CS)
CMKLR1 KO
WT (BZ)
Chemerin KO

Figure 5.4. Microbiome diversity and abundance is dramatically different between mice housed at VAPAHCS and Dalhousie University, but not between genotypes within a facility

Principal coordinate analysis (PCoA) of 16S sequences sampled from all four groups of mice using both unweighted (A) and weighted (B) UniFrac. Each point represents a different sample.

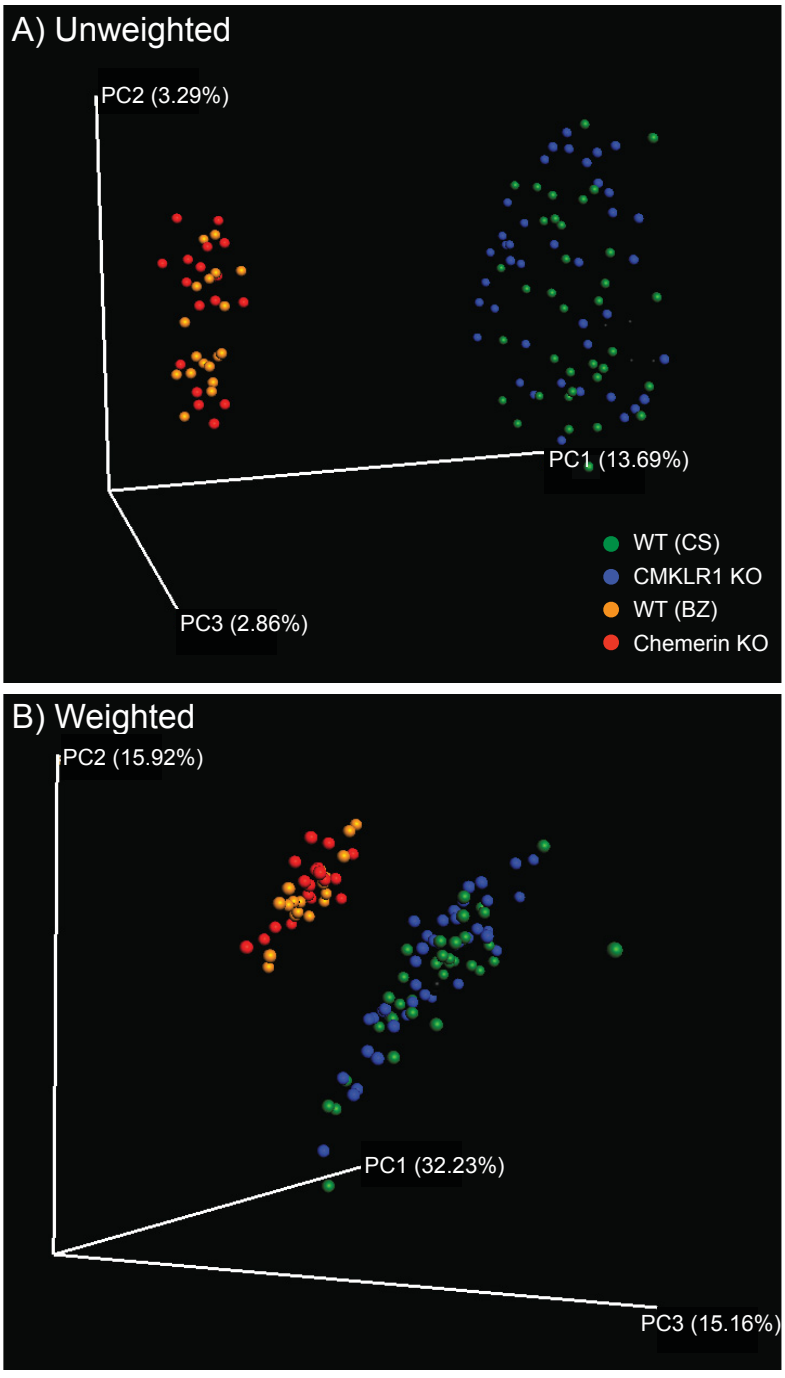
A) Unweighted
PC2 (3.29%)
PC1 (13.69%)
PC3 (2.86%)
WT (CS)
CMKLR1 KO
WT (BZ)
Chemerin KO
B) Weighted
PC2 (15.92%)
PC1 (32.23%)
PC3 (15.16%)

Table 5.1. Significant differences in the abundance of bacteria between wildtype mice housed at VAPAHCS (BZ) and Dalhousie University (CS)

Statistical analysis of 16S sequences isolated from the stool of wildtype mice housed in the two different facilities was performed. Significant differences at each taxonomic rank are indicated. Abundance values are shown for both groups of WT mice and represent the number of sequences identified out of a total of 15 000 sequences analysed per sample. Unclassified represents OTUs that do not have a specific classification but are known to be within the level specified. For simplicity, unclassified ranks are removed from further levels in the table. Taxonomic ranks are represented as k, kingdom; p, phylum; c, class; o, order; f, family; g, genus; and s, species. The minimum (min), maximum (max), median (med), and mean number of observed sequences in a single sample are shown. SD, standard deviation.

Feature	Wildtype (CS)					Wildtype (BZ)					p-value
	Min	Max	Med	Mean	SD	Min	Max	Med	Mean	SD	
Level 2:											
p__Actinobacteria	1	29	10	10.8	6.9	27	139	44	58.7	36.0	2.87E-05
p__Cyanobacteria	1	59	15.5	20.9	17.9	0	8	3.5	3.2	2.4	1.05E-06
p__Verrucomicrobia	10	4027	195	483	747	0	3	0	0.6	0.9	4.39E-04
Unclassified k__Bacteria	0	40	2	5.0	7.9	0	1	0	0.1	0.3	7.20E-04
Level 3:											
c__4C0d-2	1	59	14.5	20.6	17.9	0	8	3	2.9	2.3	1.08E-06
c__Actinobacteria	0	2	0	0.1	0.4	11	122	35	47.3	33.8	1.64E-05
c__Alphaproteobacteria	2	32	14.5	14.3	8.1	1	31	6.5	8.6	7.8	0.017
c__Chloroplast	0	2	0	0.2	0.5	0	0	0	0	0	0.033
c__Erysipelotrichi	1	61	12.5	16.7	14.9	10	214	80	86.2	56.9	7.50E-05
c__Flavobacteriia	0	27	2.5	4.6	6.4	0	2	0	0.3	0.5	2.96E-04
c__Gammaproteobacteria	0	10	1	2.3	2.9	0	3	0	0.5	0.8	1.49E-03
c__Verrucomicrobiae	10	4027	195	484	747	0	3	0	0.7	0.9	4.39E-04
Level 4:											
o__Alteromonadales	0	5	0	0.6	1.2	0	1	0	0.1	0.3	0.036
o__Anaeroplasmatales	0	42	2	8.5	11.4	0	4	0	1.0	1.4	3.96E-04
o__Bacillales	0	3	0	0.3	0.8	0	4	1	1.3	1.3	8.15E-03
o__Bifidobacteriales	0	1	0	0.03	0.2	11	122	35	47.3	33.8	1.62E-05
o__Enterobacteriales	0	3	0	0.4	0.8	0	1	0	0.06	0.2	7.99E-03
o__Erysipelotrichales	1	61	12.5	16.7	14.9	10	214	80	86.2	56.9	7.50E-05
o__Flavobacteriales	0	27	2.5	4.6	6.4	0	2	0	0.3	0.6	2.96E-04
o__RF32	0	20	5.5	7.3	5.6	0	0	0	0	0	3.90E-09
o__Rhodobacterales	0	22	2.5	4.4	5.2	0	3	0.5	0.7	0.9	1.95E-04
o__Rickettsiales	0	9	2	2.4	2.2	0	9	1.5	2.3	2.4	0.021
o__Turicibacterales	0	5	0	0.3	0.9	0	7	2	2.6	2.2	3.43E-04
o__Verrucomicrobiales	10	4027	195	484	747	0	3	0	0.7	0.9	4.39E-04

Feature	Wildtype (CS)					Wildtype (BZ)					p-value
	Min	Max	Med	Mean	SD	Min	Max	Med	Mean	SD	
o__YS2	1	59	14.5	20.6	17.9	0	8	3	2.9	2.3	1.08E-06
Unclassified c__Alphaproteobacteria	0	2	0	0.2	0.5	0	30	4.5	6.6	7.5	2.38E-03
Unclassified c__Bacilli	0	9	0	0.4	1.7	3	14	5.5	6.8	3.2	7.40E-08
Level 5:											
f__Alteromonadaceae	0	3	0	0.3	0.7	0	0	0	0	0	0.027
f__Anaeroplasmataceae	0	42	2	8.5	11.4	0	4	0	1.0	1.4	3.96E-04
f__Bacillaceae	0	1	0	0.1	0.2	0	3	1	1.1	1.2	2.02E-03
f__Bacteroidaceae	0	67	12.5	16.5	18.3	95	462	175	201	90.5	1.09E-07
f__Bifidobacteriaceae	0	1	0	0.03	0.2	11	122	35	47.3	33.8	1.62E-05
f__Clostridiaceae	0	59	8.5	14.6	14.7	1	609	170	207	203	8.55E-04
f__Cryomorphaceae	0	2	0	0.3	0.5	0	0	0	0	0	4.95E-03
f__Enterobacteriaceae	0	3	0	0.4	0.8	0	1	0	0.1	0.2	7.99E-03
f__Erysipelotrichaceae	1	61	12.5	16.7	14.9	10	214	80	86.2	56.9	7.50E-05
f__Flavobacteriaceae	0	27	2	4.0	5.9	0	2	0	0.2	0.5	4.69E-04
f__Halomonadaceae	0	4	0	0.5	1	0	1	0	0.1	0.3	0.039
f__ [Odoribacteraceae]	0	3	0	0.1	0.5	58	385	147	171	86.4	1.93E-07
f__ [Paraprevotellaceae]	0	1	0	0.1	0.3	0	2080	582	657	491	2.75E-05
f__Pelagibacteraceae	0	9	2	2.3	2.2	0	5	1	1.2	1.3	0.027
f__Peptostreptococcaceae	0	1	0	0.03	0.2	0	61	0	12.1	20.4	0.022
f__Porphyromonadaceae	5	220	35	52.3	46.2	45	338	105	113	62.4	1.26e-03
f__Rhodobacteraceae	0	22	2.5	4.3	5.2	0	3	0.5	0.7	0.9	2.11e-04
f__Rikenellaceae	45	1125	222	254	186	93	350	131	149	60.6	3.31e-03
f__S24-7	4965	1.3e4	1.1e4	1.1e4	1607	8390	1.1e4	9994	9831	989	0.036
f__Staphylococcaceae	0	3	0	0.3	0.7	0	0	0	0	0	0.048
f__Turicibacteraceae	0	5	0	0.3	0.9	0	7	2	2.6	2.2	3.43e-04
f__Verrucomicrobiaceae	10	4027	195	484	747	0	3	0	0.7	0.9	4.39e-04
Unclassified o__Bacillales	0	0	0	0	0	0	1	0	0.2	0.4	0.042
Unclassified o__Bacteroidales	0	25	9.5	10.6	5.9	3	18	9.5	10.3	4.7	9.78e-08
Unclassified o__Lactobacillales	0	7	1	1.3	1.5	0	13	7	6.2	3.7	3.05e-05
Unclassified o__RF32	0	20	5.5	7.3	5.6	0	0	0	0	0	3.90e-09
Unclassified o__YS2	1	59	14.5	20.6	17.9	0	8	3	2.9	2.3	1.08e-06
Level 6:											
g__AF12	0	2	0	0.3	0.6	6	54	18	19.2	11.1	1.50e-06
g__Akkermansia	10	4027	195	484	747	0	3	0	0.7	0.9	4.42e-06
g__Allobaculum	0	4	0	0.1	0.7	4	155	74	75.7	47.9	3.82e-06
g__Anaeroplasma	0	42	2	8.5	11.4	0	4	0	1.0	1.4	3.96e-04
g__Bacteroides	0	66	12	16.2	18.1	95	462	174	200	90.5	1.07e-07
g__Bifidobacterium	0	1	0	0.03	0.2	11	120	34	46.6	33.2	1.57e-05
g__Bilophila	0	0	0	0	0	0	19	1	2.7	4.7	0.024
g__Candidatus Arthromitus	0	53	7	11.9	13.7	0	11	0	1.5	6.6	9.77e-05
g__Clostridium	0	10	1	2.2	2.8	0	38	5.5	8.8	10.1	0.014
g__Desulfovibrio	13	301	77.5	114	89.1	0	204	37.5	63.0	59.6	0.017
g__ [Eubacterium]	0	2	0	0.3	0.5	0	0	0	0	0	2.57e-03
g__Fluviicola	0	1	0	0.1	0.3	0	0	0	0	0	0.044

Feature	Wildtype (CS)					Wildtype (BZ)					p-value
	Min	Max	Med	Mean	SD	Min	Max	Med	Mean	SD	
g__Lawsonia	0	6	1.5	1.6	1.4	0	1	0	0.1	0.3	1.36e-07
g__Odoribacter	0	3	0	0.2	0.5	58	385	147	171	86.4	1.93e-07
g__Parabacteroides	5	220	35	52.3	46.2	45	338	105	112	62.4	1.26e-03
g__Polaribacter	0	8	0	1.1	1.9	0	0	0	0	0	1.73e-03
g__ [Prevotella]	0	1	0	0.1	0.3	0	2077	582	657	491	2.73e-05
g__Rikenella	0	0	0	0	0	0	39	10	11.2	12.1	1.14e-03
g__ [Ruminococcus]	17	545	78.5	134	151	16	113	49	49.8	29.6	2.62e-03
g__Staphylococcus	0	3	0	0.3	0.7	0	0	0	0	0	0.048
g__Turicibacter	0	5	0	0.3	0.9	0	7	2	2.6	2.2	3.43e-04
g__Ulvibacter	0	4	0	0.7	1.0	0	1	0	0.1	0.2	1.72e-03
Unclassified f__Bacillaceae	0	1	0	0.1	0.2	0	3	1	1.1	1.2	2.02e-03
Unclassified f__Bacteroidaceae	0	1	0	0.2	0.4	0	0	0	0	0	6.30e-03
Unclassified f__Bifidobacteriaceae	0	0	0	0	0	0	3	0	0.8	1.1	8.75e-03
Unclassified f__Clostridiaceae	0	3	0	0.6	0.8	1	589	164	194	191	4.86e-04
Unclassified f__Coriobacteriaceae	0	7	2	2.0	1.9	0	2	1	0.7	0.8	7.48e-04
Unclassified f__Desulfovibrionaceae	0	0	0	0	0	0	154	2.5	22.9	40.4	0.028
Unclassified f__Enterobacteriaceae	0	2	0	0.4	0.7	0	0	0	0	0	1.73e-03
Unclassified f__Flavobacteriaceae	0	10	1	1.5	2.3	0	1	0	0.1	0.3	8.03e-04
Unclassifiied f__Pelagibacteraceae	0	9	2	2.3	2.2	0	5	1	1.2	1.3	0.027
Unclassified f__Peptostreptococcaceae	0	1	0	0.03	0.2	0	61	0	12.1	20.4	0.022
Unclassified f__Rhodobacteraceae	0	11	1	1.7	2.4	0	3	0	0.4	0.9	1.51e-04
Unclassified f__Rikenellaceae	45	1123	221	252	185	72	260	102	117	47.8	1.70e-04
Unclassified f__S24-7	4965	1.3e4	1.1e4	1.1e4	1608	8390	1.1e4	9317	9832	989	0.036

Figure 5.5. Changes in the abundance of different bacterial genera between wildtype mice housed at Dalhousie or VAPAHCS

Genera that composed more than 1% of sequences sampled and had significant differences in abundance between the two facilities are shown.

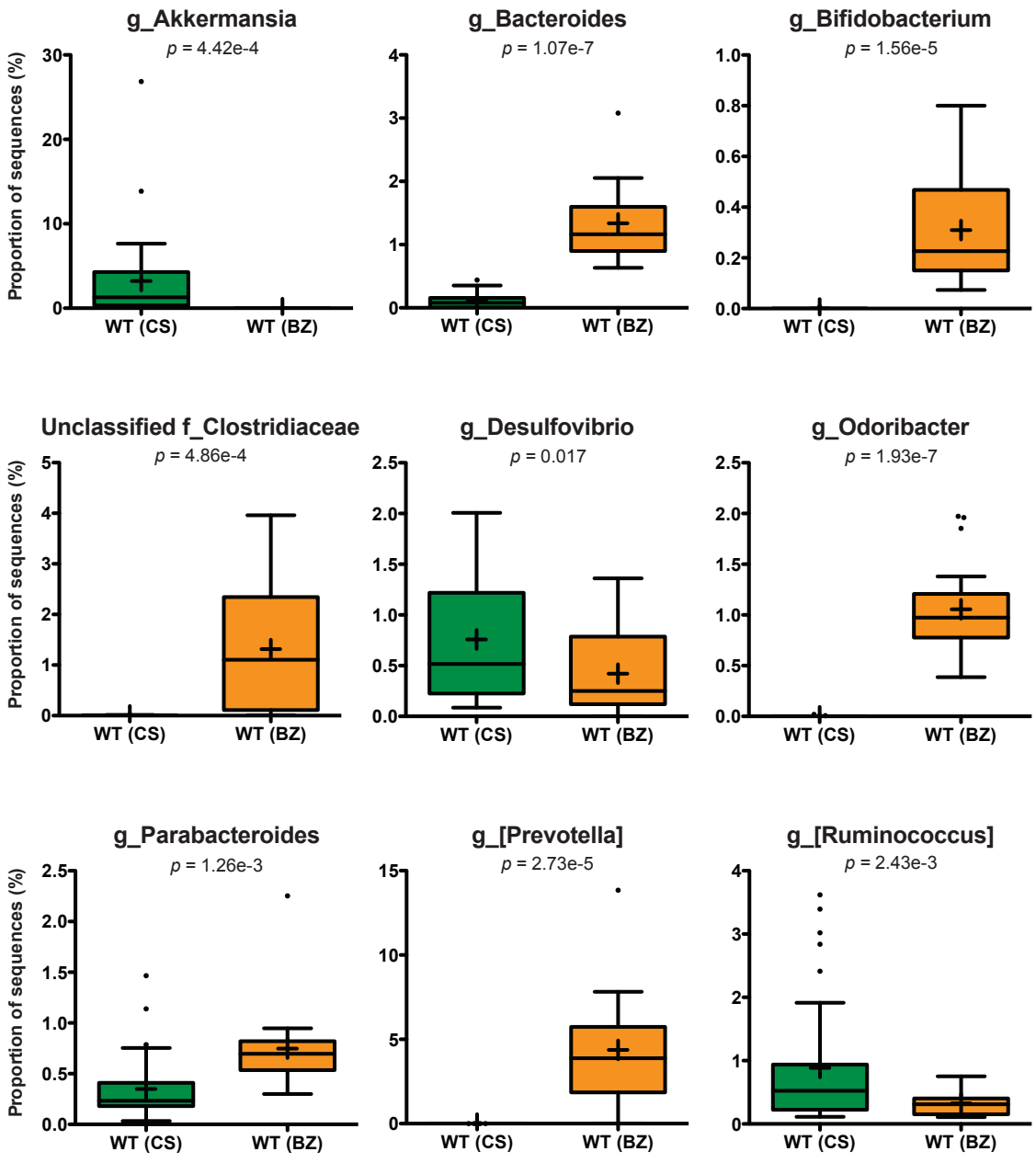
g_Akkermansia
p = 4.42e-4
g_Bacteroides
p = 1.07e-7
g_Bifidobacterium
p = 1.56e-5
Unclassified f_Clostridiaceae
p = 4.86e-4
g_Desulfovibrio
p = 0.017
g_Odoribacter
p = 1.93e-7
g_Parabacteroides
p = 1.26e-3
g_[Prevotella]
p = 2.73e-5
g_[Ruminococcus]
p = 2.43e-3
Proportion of sequences (%)
WT (CS)
WT (BZ)

Figure 5.6. Wildtype and chemerin KO mice exhibit similarities in microbiome composition

Principal coordinate analysis (PCoA) of 16S sequences sampled from WT (BZ) and chemerin KO mice using weighted UniFrac and categorized by genotype (A) or cage (B). Each point represents a different sample. In B, each cage is represented by a different colour.

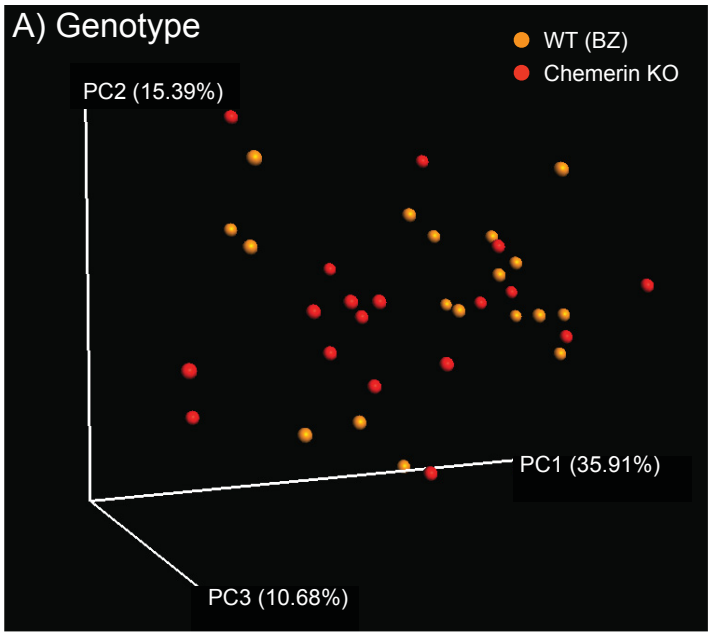
A) Genotype
WT (BZ)
Chemerin KO
PC2 (15.39%)
PC1 (35.91%)
PC3 (10.68%)

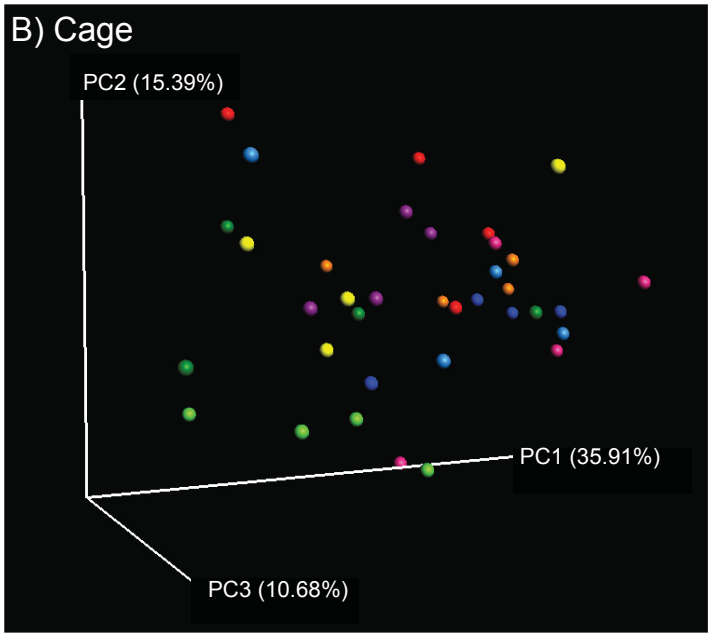
B) Cage
PC2 (15.39%)
PC1 (35.91%)
PC3 (10.68%)

Table 5.2. Significant differences in the abundance of bacteria between wildtype mice (BZ) and chemerin KO mice

Statistical analysis of 16S sequences isolated from the stool of wildtype (BZ) and chemerin KO mice was performed. Significant differences at each taxonomic rank are indicated. Abundance values are shown for both genotypes and represent the number of sequences identified out of a total of 15 000 sequences analysed per sample. Unclassified represents OTUs that do not have a specific classification but are known to be within the level specified. For simplicity, unclassified ranks are removed from further levels in the table. Taxonomic ranks are represented as k, kingdom; p, phylum; c, class; o, order; f, family; g, genus; and s, species. The minimum (min), maximum (max), median (med), and mean number of observed sequences in a single sample are shown. SD, standard deviation.

Feature	Wildtype (BZ)					Chemerin KO					p-value
	Min	Max	Med	Mean	SD	Min	Max	Med	Mean	SD	
Level 2:											
p__Cyanobacteria	0	8	3.5	3.2	2.4	0	4	1	1.4	1.3	0.01
p__Proteobacteria	20	214	102	97.8	58.5	30	402	91	164	109	0.03
Level 3:											
c__4C0d-2	0	8	3	2.9	2.3	0	4	1	1.3	1.2	0.015
c__Deltaproteobacteria	19	212	83	88.8	59.9	22	392	74	152	112	0.043
c__Flavobacteriia	0	2	0	0.3	0.6	0	12	0	2.4	3.3	0.016
Level 4:											
o__Desulfovibrionales	19	212	83	88.7	60.0	22	392	74	152	112	0.044
o__Flavobacteriales	0	2	0	0.3	0.6	0	12	0	2.4	3.3	0.016
o__Rhodobacterales	0	3	0.5	0.7	0.9	0	22	1	4.4	6.5	0.028
o__YS2	0	8	3	2.9	2.3	0	4	1	1.3	1.2	0.015
Level 5:											
f__Cryomorphaceae	0	0	0	0	0	0	1	0	0.2	0.4	0.042
f__Desulfovibrionaceae	19	212	83	88.7	60.0	22	392	74	152	112	0.044
f__Flavobacteriaceae	0	2	0	0.2	0.6	0	11	0	1.8	3.1	0.041
f__Rhodobacteraceae	0	3	0.5	0.7	0.9	0	22	1	4.4	6.5	0.028
Unclassified o__YS2	0	8	3	2.9	2.3	0	4	1	1.3	1.2	0.015
Level 6:											
g__Lactococcus	0	3	0	0.5	0.9	0	0	0	0.00	0.00	0.035
g__Rikenella	0	39	10	11.2	12.1	0	24	1	3.7	6.2	0.028
Unclassified f__Rhodobacteraceae	0	3	0	0.7	0.9	0	20	1	4.3	6.1	0.024

Figure 5.7. Changes in the abundance of different taxonomic ranks between wildtype and chemerin KO mice

Families or genera that had significant differences in abundance between the two genotypes are shown. Unclassified represents OTUs that have not been assigned to a specific genus but are known to be within the family specified.

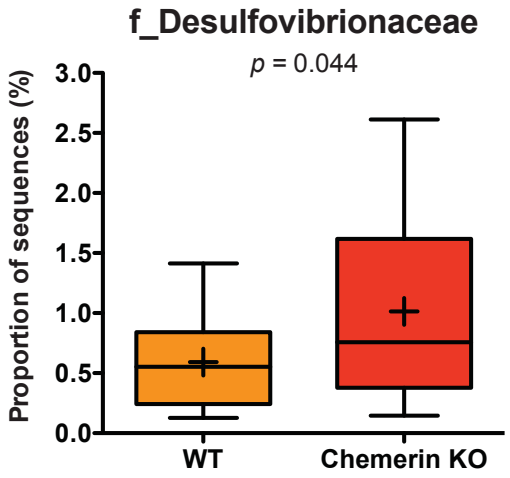
f_Desulfovibrionaceae
p = 0.044
Proportion of sequences (%)
3.0
2.5
2.0
1.5
1.0
0.5
0.0
WT
Chemerin KO

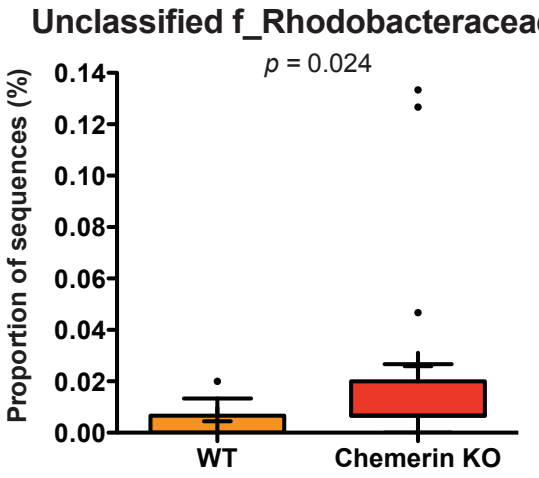
Unclassified f_Rhodobacteraceae
p = 0.024
Proportion of sequences (%)
0.14
0.12
0.10
0.08
0.06
0.04
0.02
0.00
WT
Chemerin KO

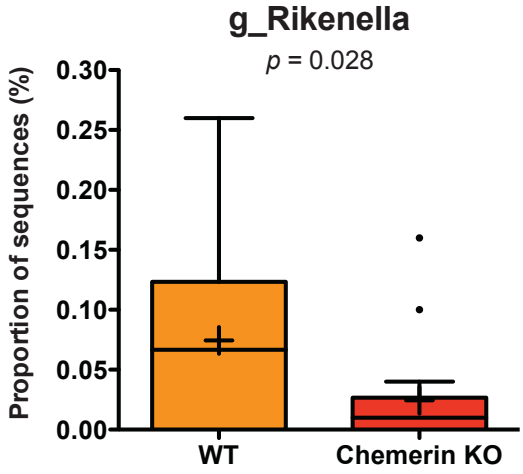
g_Rikenella
p = 0.028
Proportion of sequences (%)
0.30
0.25
0.20
0.15
0.10
0.05
0.00
WT
Chemerin KO

Figure 5.8. Wildtype and CMKLR1 KO mice exhibit a modest separation in bacterial diversity

Principal coordinate analysis (PCoA) of 16S sequences sampled from WT (CS) and CMKLR1 KO mice using weighted UniFrac and categorized by genotype (A) and cage (B). Each point represents a different sample. In B, each cage is represented by a different colour. Two different angles of the same three-dimensional plot are shown to demonstrate separation by genotype on PC3.

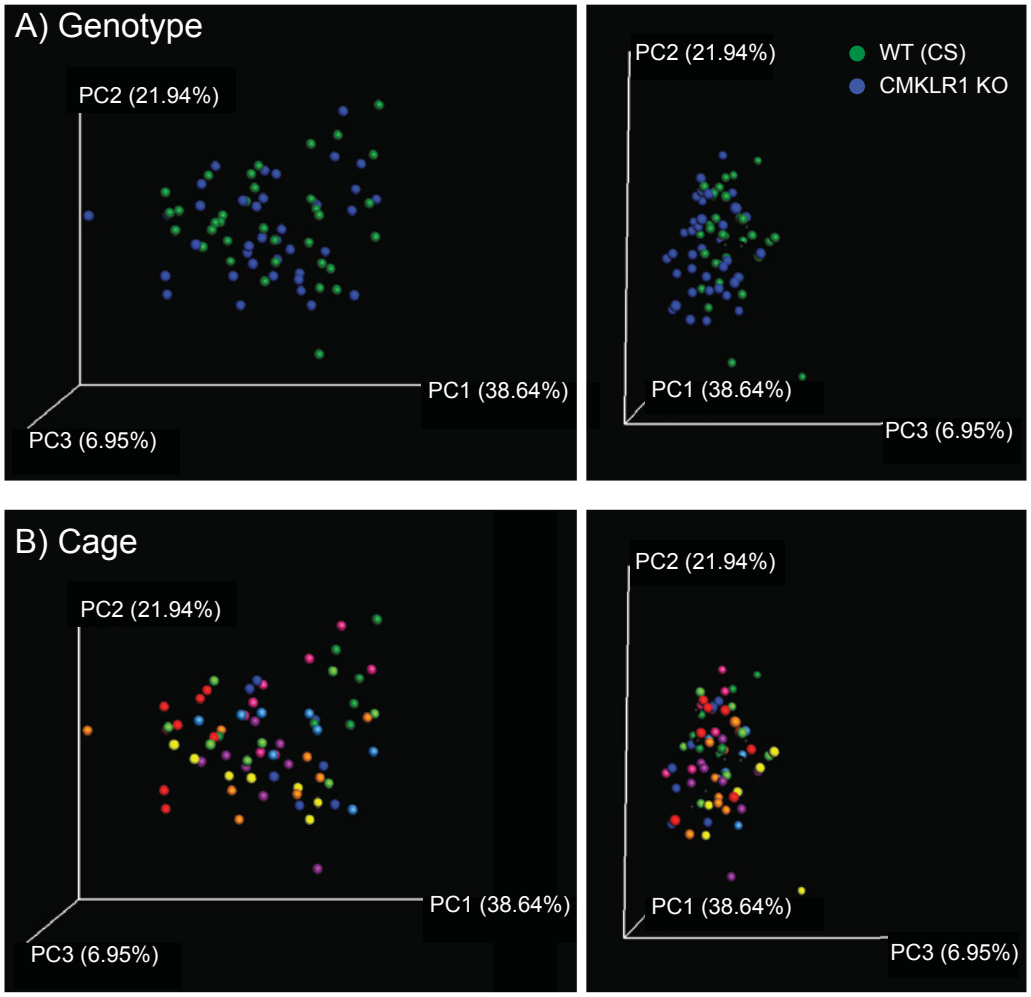
A) Genotype
PC2 (21.94%)
PC1 (38.64%)
PC3 (6.95%)
PC2 (21.94%)
WT (CS)
CMKLR1 KO
PC1 (38.64%)
PC3 (6.95%)
B) Cage
PC2 (21.94%)
PC1 (38.64%)
PC3 (6.95%)
PC2 (21.94%)
PC1 (38.64%)
PC3 (6.95%)

Table 5.3. Significant differences in the abundance of bacteria between wildtype mice (CS) and CMKLR1 KO mice.

Statistical analysis of 16S sequences isolated from wildtype (CS) and CMKLR1 KO mice was performed. Significant differences at each taxonomic rank are indicated. Abundance values are shown for both genotypes and represent the number of sequences identified out of a total of 15 000 sequences analysed per sample. Unclassified represents OTUs that do not have a specific classification but are known to be within the level specified. For simplicity, unclassified ranks are removed from further levels in the table. Taxonomic ranks are represented as k, kingdom; p, phylum; c, class; o, order; f, family; g, genus; and s, species. The minimum (min), maximum (max), median (med), and mean number of observed sequences in a single sample are shown. SD, standard deviation.

	Wildtype (CS)					CMKLR1 KO					
Feature	Min	Max	Med	Mean	SD	Min	Max	Med	Mean	SD	p-value
Level 2:											
p__Cyanobacteria	1	59	15.5	20.9	17.9	1	54	7	12.7	12.6	0.025
p__Firmicutes	1052	5147	245	274	1093	868	5614	324	334	115	0.022
p__Verrucomicrobia	10	4027	195	484	747	0	774	41	148	229	0.013
Unclassified k__Bacteria	0	40	2	5	7.9	0	12	1	2	2.9	0.035
Unclassified unassigned	97	483	200	213	69.3	75	318	175	183	49.0	0.031
Level 3:											
c___4C0d-2	1	59	14.5	20.6	17.9	1	54	7	12.5	12.6	0.027
c___Verrucomicrobiae	10	4027	195	484	747	0	774	41	148	229	0.013
Level 4:											
o__Anaeroplasmatales	0	42	2	8.5	11.3	0	45	1	3.4	7.4	0.026
o__Thiotrichales	0	0	0	0	0	0	1	0	0.1	0.3	0.023
o__Verrucomicrobiales	10	4027	195	484	747	0	774	41	148	229	0.013
o__YS2	1	59	14.5	20.6	17.9	1	54	7	12.5	12.6	0.027
Level 5:											
f__Anaeroplasmataceae	0	42	2	8.5	11.4	0	45	1	3.4	7.4	0.026
f__Bacteroidaceae	0	67	12.5	16.5	18.3	0	42	6	9	10.7	0.036
f__Piscirickettsiaceae	0	0	0	0.00	0.00	0	1	0	0.1	0.3	0.023
f__Prevotellaceae	18	995	376	436	254	10	1050	224	303	252	0.026
f__Rikenellaceae	45	1125	222	254	186	35	485	171	181	92.2	0.039
f__Verrucomicrobiaceae	10	4027	195	484	747	0	774	41	148	229	0.013
Unclassified o__Bacteroidales	0	25	9.5	10.6	6	1	20	4.5	5.6	4.4	9.33e-05
Unclassified o__YS2	1	59	14.5	20.6	17.9	1	54	7	12.5	12.6	0.027
Level 6:											

Feature	Wildtype (CS)					CMKLR1 KO					p-value
	Min	Max	Med	Mean	SD	Min	Max	Med	Mean	SD	
g__Akkermansia	10	4027	195	484	747	0	774	40.5	148	229	0.013
g__Anaeroplasma	0	42	2	8.47	11.3	0	45	1	3.38	7.4	0.026
g__Bacteroides	0	66	12	16.2	18.1	0	42	6	8.9	10.7	0.039
g__Coprococcus	0	121	14	26.3	29.4	1	35	10	11.8	7.62	6.67e-03
g__Prevotella	18	955	376	436	254	10	1050	224	303	252	0.026
Unclassified f__Peptococcaceae	0	3	0	0.5	0.8	0	4	1	1.1	1.2	0.014
Unclassified f__Piscirickettsiaceae	0	0	0	0	0	0	1	0	0.1	0.3	0.023
Unclassified f__Rikenellaceae	45	1125	222	254	185	35	485	171	181	92.2	0.039

Figure 5.9. Changes in the abundance of different bacteria at various taxonomic ranks between wildtype and CMKLR1 knockout mice

Bacterial ranks that composed more than 1% of sequences sampled and had significant differences in abundance between the two genotypes are shown. Unclassified represents OTUs that have not been assigned to a specific genus but are known to be within the family specified.

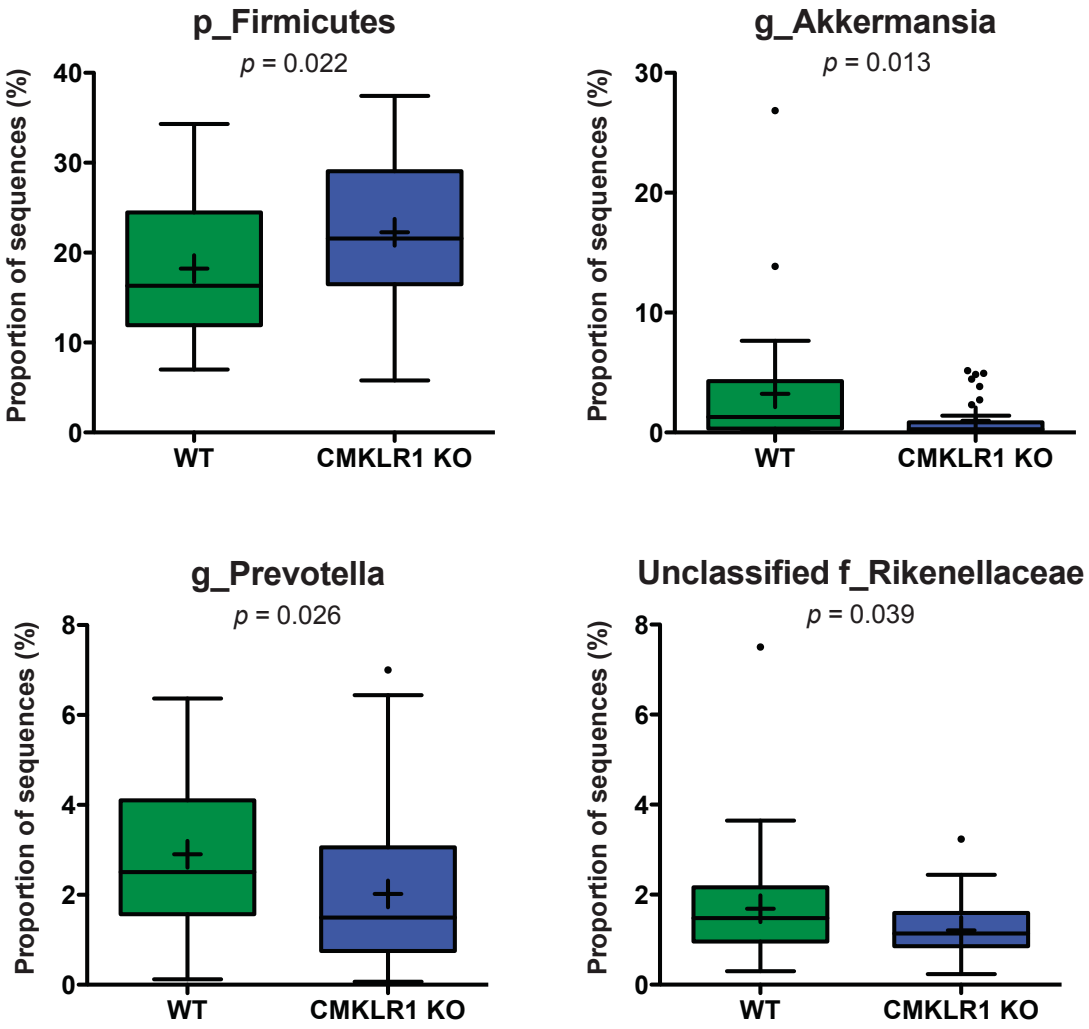
p_Firmicutes
p = 0.022
Proportion of sequences (%)
40
30
20
10
0
WT
CMKLR1 KO
g_Akkermansia
p = 0.013
Proportion of sequences (%)
30
20
10
0
WT
CMKLR1 KO
g_Prevotella
p = 0.026
Proportion of sequences (%)
8
6
4
2
0
WT
CMKLR1 KO
Unclassified f_Rikenellaceae
p = 0.039
Proportion of sequences (%)
8
6
4
2
0
WT
CMKLR1 KO

Figure 5.10. Changes in *Akkermansia* and *Prevotella* abundance are negatively correlated with total body mass in CMKLR1 KO mice

The body weight of each WT (CS) or CMKLR1 KO mouse at the time of fecal sample collection was plotted against the abundance of g__Akkermansia (A) or g__Prevotella (B) within each sample.

A

g__Akkermansia

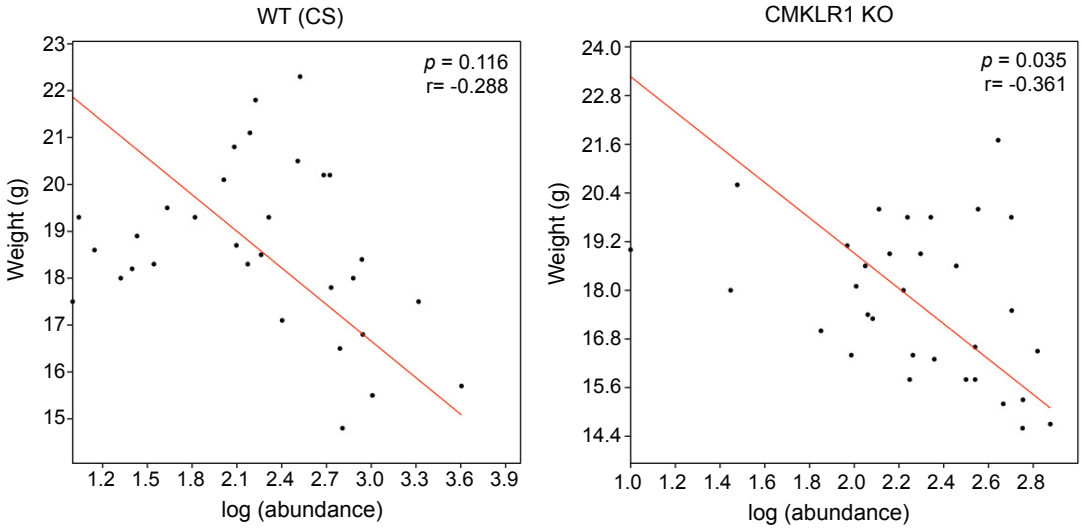

B

g__Prevotella

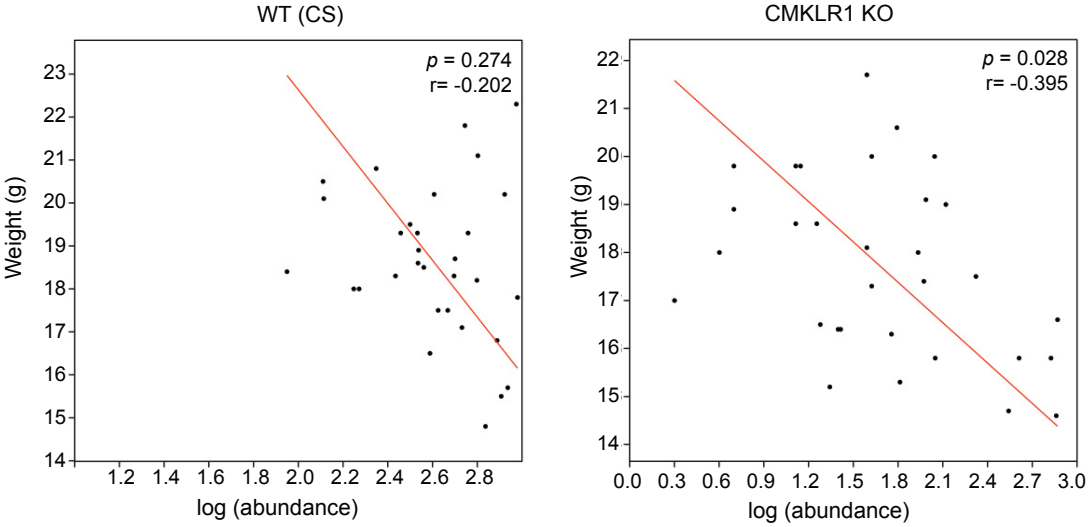

Figure 5.11. Separation along the PC3 axis is explained by differences in *Akkermansia* and *Prevotella* abundance

Principal coordinate analysis (PCoA) of 16S sequences sampled from WT (CS) and CMKLR1 KO mice using weighted Unifrac. Each point represents a different sample. Samples with a high or low abundance of g__Akkermansia (A) or g__Prevotella (B) are indicated with different colours.

A *g__Akkermansia*

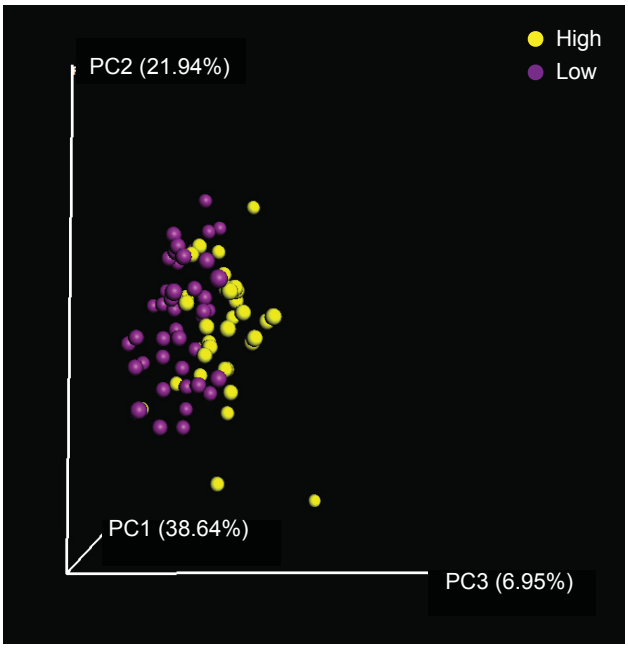

B *g__Prevotella*

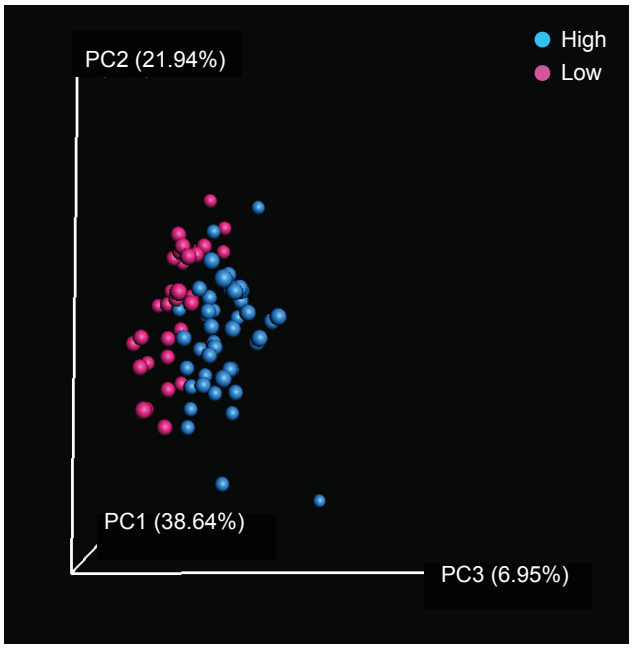

CHAPTER 6: DISCUSSION

Overview

Chemerin is a potent chemoattractant and adipokine that plays important roles in metabolism, inflammation, and immunity. The goal of this thesis was to investigate the role of chemerin signalling in mature adipocytes, on the development of inflammatory bowel disease (IBD), and on the composition of the gut microbiome. The results obtained from these projects provide strong evidence that the role of chemerin signalling is context-specific and that the appropriate promotion or inhibition of chemerin signalling has therapeutic potential for the treatment of obesity and inflammatory disorders. Several key concepts have emerged from this work and are discussed in further detail below, including the importance of context-specific chemerin signalling, the biological function of different chemerin isoforms, and the role of local versus systemic chemerin levels. Furthermore, this chapter evaluates and discusses current limitations in our ability to study the role of chemerin signalling, therapeutic implications of targeting chemerin, and future areas of research that will improve our understanding of chemerin function in health and disease.

Chemerin signalling is context-specific

To date, a large number of clinical studies have reported elevated chemerin levels in a wide range of diseases, including obesity, inflammatory bowel disease (IBD), arthritis, cancer, liver disease, cardiovascular disease (CVD) and type 2 diabetes (T2D) (Rourke et al. 2013; Zabel et al. 2014). Unfortunately, the majority of these studies are correlative and therefore the contribution of chemerin signalling to the pathogenesis of these diseases remains unclear. For many years, chemerin has been considered a pro-inflammatory molecule, largely due to its first known function as a chemoattractant for immune cells that express CMKLR1 and several early studies that demonstrated chemerin signalling played a key role in the recruitment of leukocytes towards sites of tissue injury or inflammation (Wittamer et al. 2003; Zabel et al. 2005b). However, a substantially smaller number of studies have also implicated an anti-inflammatory role for chemerin in inflammation (reviewed in (Rourke et al. 2013; Zabel et al. 2014). The data presented in this thesis suggests that chemerin signalling is associated with both anti-

and pro-inflammatory actions in different physiological contexts: mature adipocytes (Chapter 3) and the development of IBD (Chapter 4), respectively, demonstrating that chemerin exhibits context-specific function. Interestingly, both decreased (Chapters 3 and 5) and increased (Chemerin 4) levels of chemerin signalling were associated with changes in adipose tissue and intestinal homeostasis. There are a number of factors that likely contribute to differences in chemerin function between physiological contexts and these are described in further detail below.

Firstly, the influence of chemerin signalling on processes associated with inflammation is likely cell- and tissue-dependent. A number of studies have demonstrated that chemerin expression is differentially regulated in various cell types. For example, chemerin expression is rapidly up-regulated following treatment with pro-inflammatory stimuli such as TNFα in adipocytes; however, in the same studies, similar treatment conditions did not influence chemerin levels in hepatocytes (Herova et al. 2014) or endothelial cells (Gonzalvo-Feo et al. 2014). Furthermore, chemerin has been shown to activate a wide variety of intracellular signalling pathways, and these are often cell-type specific, which might depend on the availability of second messenger pathways (Rourke et al. 2013). Alternatively, differential expression patterns of chemerin receptors likely contribute to differences in chemerin signalling. Our data demonstrates that chemerin receptor expression is differentially regulated by both development and disease. For example, CMKLR1, but not GPR1 or CCRL2, significantly increased throughout adipogenic differentiation (Chapter 3). Similarly, the three chemerin receptors exhibited differential expression patterns across a panel of tissues isolated from the gastrointestinal tract following the induction of DSS-induced inflammation (Chapter 4). Thus the coordinated expression of chemerin, its receptors, and necessary signalling pathway components in different cells and tissues likely contribute to the context-specific function of chemerin.

Our data also highlights the important finding that chemerin isoforms exhibit differential signalling properties that likely mediate context-specific chemerin function. In chapter 3, we demonstrated that neutralization of chemerin signalling results in a pro-inflammatory phenotype associated with pathogenic adipose tissue remodelling. Interestingly, treatment with the commonly studied chemerin isoform, chemerin-157,

which is typically associated with pro-inflammatory effects, was unable to rescue the effects of the chemerin antibody treatment, despite restoring function in terms of ß-arrestin recruitment to chemerin receptors. This suggests that the adipocyte-secreted chemerin isoform associated with anti-inflammatory properties influences alternate signalling pathways compared to chemerin-157. Furthermore, while we did not directly assess which chemerin isoforms were present in the inflamed colon using our IBD model, western blot analysis of explant cultures isolated from the distal, most inflamed region region of the colon revealed the presence of two bands corresponding to chemerin, suggesting that increased chemerin processing occurs specifically in diseased regions (Chapter 4). This highlights that processing of chemerin to active and/or inactive forms is modified by disease. Considered together with the concept that different chemerin isoforms mediate different signalling pathways, the regulation of chemerin processing and generation of chemerin isoforms in particular disease conditions likely contribute to the context-specific function of chemerin.

Finally, the activities of chemerin signalling are temporally regulated. For instance, chemerin likely undergoes sequential processing during different stages of inflammation, with serine proteases secreted early in the immune response (e.g. by neutrophils (Wittamer et al. 2005)) generating pro-inflammatory chemerin isoforms, and later secreted cysteine proteases (e.g. by macrophages (Cash et al. 2008)) generating less inflammatory isoforms, in order to control the severity of inflammatory responses. In this manner, different chemerin isoforms might contribute to the initiation, maintenance, and resolution of inflammation. We demonstrated that injection of the pro-inflammatory isoform, chemerin-157, did not influence the induction and development of DSS-induced colitis (Chapter 4). In contrast, Lin et al. (2014) reported that chemerin injection exacerbated the severity of colitis in a model that we believe represents recovery from colon inflammation. These results support the notion that chemerin signalling is time-dependent and future studies that further examine the role of chemerin signalling, and isoform distribution, in various acute or chronic inflammation, and recovery models, will be valuable. Similarly, *in vitro* studies have reported discrepancies in findings on the role of chemerin treatment on glucose uptake or lipolysis (Goralski et al. 2007; Kralisch et al. 2009; Roh et al. 2007; Takahashi et al. 2008). The timing and dose of chemerin

treatment were key differences between these studies, suggesting that the length and duration of chemerin signalling might also influence chemerin function.

Given the number of mechanisms that regulate chemerin expression, activity, and function, it is not surprising that we observed contrasting roles for chemerin signalling in our adipocyte and IBD model. Of note, the two models that we studied represent vastly different physiological conditions. In particular, we investigated the impact of blocking endogenous chemerin signalling in healthy adipocytes, which normally secrete high levels of chemerin that is processed to bioactive isoforms. In contrast, the IBD model investigated the role of chemerin signalling in a tissue with low basal chemerin expression and activity that was dramatically up-regulated in inflamed regions following the induction of disease. Thus it is not surprising that modulation of chemerin signalling in these two very different conditions (healthy versus diseased, high versus low basal chemerin expression) was associated with different roles in inflammation. Interestingly, in both cases, disruption of "normal" (for each cell/tissue-type) levels of chemerin signalling was associated with a pro-inflammatory phenotype, suggesting that restoring chemerin levels to "normal", whether that be high (e.g. adipocyte) or low (e.g. colon) levels, is a potential therapeutic method to modulate the development of obesity and inflammatory disorders.

Considered altogether, chemerin plays a context-specific role in inflammation, which is regulated by the expression of chemerin and its receptors, processing to different isoforms, and the timing and duration of chemerin activity. It will be important to further delineate which signalling pathways are activated in different cell types by particular chemerin isoforms, and which receptors mediate the effects of chemerin signalling, in order to fully understand the complexity of chemerin function in both health and disease.

Current limitations in chemerin biology

The observation that chemerin signalling is likely context-specific highlights several limitations in the way that we currently investigate and measure chemerin levels. Several of these limitations were highlighted through the work presented in this thesis and are discussed in further detail below.

Tools to modulate levels of chemerin signalling

Firstly, despite the knowledge that chemerin undergoes complex extracellular processing to a variety of isoforms, the majority of experimental studies are currently performed using only one isoform: chemerin-157. In Chapter 3, I demonstrated that chemerin-157 is unable to rescue the effects of the neutralizing chemerin antibody in mature adipocytes, suggesting that the active chemerin isoform in this model exhibits unique signalling properties. Therefore, future studies should investigate the biological function of other chemerin isoforms and their contribution to previously reported chemerin activities. Chapter 2 described the optimization of two different methods that can be used to generate chemerin isoforms that are not commercially available in order to facilitate the study of these proteins. Importantly, the activity of different chemerin isoforms on a variety of endpoints, including intracellular calcium release, ß-arrestin recruitment to CMKLR1 and GPR1, activation of SRF signalling, NFkB signalling, chemotaxis, and anti-microbial activity, should be investigated in order to determine which isoforms are responsible for mediating the particular functions associated with chemerin signalling. For instance, chemerin-125 exhibits low activity in terms of intracellular calcium mobilization or chemotactic ability but has potent anti-microbial properties (Kulig et al. 2011), suggesting that different isoforms might exert pathway-specific activities. Additionally, evidence suggests that chemerin is more potent at GPR1 than CMKLR1 in terms of ß-arrestin recruitment, but that chemerin stimulates greater levels of calcium mobilization at CMKLR1 compared to GPR1, suggesting receptor-dependent effects (Barnea et al. 2008). Therefore, the activity of chemerin isoforms at different chemerin receptors should be thoroughly investigated in order to fully elucidate the mechanisms of chemerin signalling in terms of both receptor specificity and pathway activation.

Additionally, I demonstrated that the available synthetic peptides do not function at concentrations previously described (Chapter 2) and do not recapitulate all of the activities of full-length recombinant chemerin (Chapter 3). Therefore, it is important to interpret studies that use the chemerin peptides with caution and keep in mind that modulation of chemerin signalling (ie. treatment with inhibitors) might not exhibit the results predicted based on peptide treatments. However, it is important to note that

peptide-specific functions might provide an advantage in the development of therapeutics to modulate specific chemerin functions. Similar to results obtained with the peptides, I demonstrated that the CMKLR1 inhibitor, CCX832, only modestly inhibits receptor function and was unable to reduce levels of chemerin signalling in mature adipocytes (Chapter 2). Importantly, my results suggest that CCX832 exhibits toxicity and/or non-specific effects. As previous studies have reported CMKLR1-dependent functions based on the use of this inhibitor, without demonstrating decreased chemerin signalling, or use of the CCX826 control (Kumar et al. 2015), these results should be interpreted with caution. Additionally, as suggested in Chapter 4, results from experiments using constitutive KO mice might be confounded by the development of compensatory mechanisms. More acute methods to inhibit the activation of CMKLR1 and GPR1 will be essential to further our understanding of chemerin biology. Considered altogether, this work highlights the need for better tools (eg. agonists, inhibitors, conditional KO animals) in order to fully elucidate the role and function of chemerin signalling. We are currently performing high-throughput screening efforts to identify novel modulators of CMKLR1 and/or GPR1 function and have generated CMKLR1/GPR1 double knockout mice, both of which will ultimately facilitate the *in vitro* and *in vivo* study of chemerin signalling.

Evaluation of bioactive versus total chemerin levels

While many reports recognize that standard enzyme-linked immunosorbent assay (ELISA) methodologies for detection of chemerin levels fail to differentiate between active and inactive isoforms, only a few have taken measures to address this deficiency and to date, the majority of studies only report total chemerin levels. In chapter 4, we demonstrated that induction of DSS-induced colitis resulted in a decrease in total chemerin levels but a relative increase in the ratio of bioactive:total chemerin levels. Similarly, analysis of chemerin levels in colon explant cultures revealed the presence of two bands, suggestive of chemerin processing. This indicates that chemerin processing and bioactivity are influenced by disease status and may not be reflected in measurements of total chemerin levels using a standard ELISA. This highlights the importance of studying both bioactive and total chemerin levels in order to fully elucidate the role of

chemerin signalling. There are several established methods to evaluate levels of chemerin bioactivity, several of which are used in this thesis, including the Tango assay for ß-arrestin recruitment, SRF- reporter assay, chemotaxis assays, and aequorin-based calcium assay. Notably, NFkB signalling represents a novel endpoint identified in this thesis (Chapter 3). Importantly, the use of more than one of these assays will be valuable, as specific chemerin isoforms may exhibit differential signalling properties in terms of these endpoints (Chapter 3). It will also be important in future studies to directly investigate the distribution of chemerin isoforms, both in different cell types and tissue, and changes with the onset and/or progression of disease. This can be performed using ELISAs for specific chemerin isoforms (Zhao et al. 2011) or using mass spectrometry protocols optimized in Chapter 3. Studies of this nature will be valuable as some chemerin isoforms may be inactive in signalling assays but act as an antagonist in the presence of active chemerin isoforms. For instance, mChe15 does not exhibit chemotactic properties and does not influence intracellular calcium release, SRF signalling, or ß-arrestin recruitment to CMKLR1 or GPR1 ((Luangsay et al. 2009), Chapter 2), but has been shown to block internalization of CMKLR1 by chemerin agonists (Zhou et al. 2014). Therefore anti-inflammatory properties of C15 can potentially be explained by the inhibition of pro-inflammatory signalling cascades initiated by other chemerin isoforms. Studies that directly investigate the distribution and signalling properties of different chemerin isoforms, in addition to the secretion and activity of chemerin-activating (and in-activating) proteases that regulate the generation of various chemerin isoforms, will be essential. Ultimately, the complementary study of chemerin processing and bioactivity using the described assays will provide valuable insight into function of chemerin in health and disease.

Evaluation of local versus systemic chemerin levels

In addition to measuring total versus bioactive chemerin levels, many clinical studies solely investigate circulating chemerin levels and fail to consider local chemerin levels in the pathogenesis of disease. While systemic chemerin levels are a reasonable biomarker for the presence and severity of diseases such as obesity, CVD, and T2D, measurement of local chemerin levels is likely more reflective of a role for chemerin

signalling in disease progression or activity. For example, we demonstrated that while circulating levels of total chemerin decreased following the induction of DSS-induced colitis, local chemerin levels were significantly increased in the colon (Chapter 4). Similar results, where local chemerin levels were differentially regulated compared to those in circulation, have been obtained with studies investigating local chemerin levels in endometriosis (Jin et al. 2015) and arthritis (Huang et al. 2012). Furthermore, the investigation of chemerin isoform distribution in arthritic joints differed considerably from the distribution of isoforms in circulation (Zhao et al. 2011). This suggests that circulating levels are not necessarily reflective of local disease conditions and that investigation of local chemerin isoform distribution is perhaps a better indicator of the role of chemerin in the progression and activity of disease compared to systemic levels. Furthermore, additional sources of local chemerin levels in disease should be investigated more thoroughly in order to better target chemerin signalling for the treatment of disease. For example, we demonstrated that in addition to increased colon-derived chemerin expression in DSS-induced colitis, chemerin levels were increased in mesenteric WAT that surrounds the intestines, but not in any other adipose tissue depot examined, including subcutaneous, inguinal, gonadal, omental, and peri-renal fat depots (Chapter 4). Similarly, chemerin levels have been reported to increase in periadventitial fat isolated from aortas or coronary arteries taken from patients with atherosclerosis (Kostopoulos et al. 2014), indicating that there may be as of yet undiscovered sources of local chemerin that contribute to the development or progression of disease.

Considered altogether, the development of tools that will aid experimental studies investigating the function of chemerin signalling, and further investigations of local chemerin levels, isoform distribution, and other sources of chemerin, will further our understanding of the role of chemerin signalling in both health and disease.

Therapeutic strategies and clinical utility

Targeting chemerin signalling

Several groups have suggested that targeting chemerin function may be a therapeutic strategy for the prevention and/or treatment of inflammation, insulin

resistance, and obesity-associated co-morbitidies such as T2D and CVD. However, the observation that chemerin acts as both a pro- and anti-inflammatory factor complicates the development of molecules to target chemerin signalling. Importantly, the data presented in this thesis suggests that both enhancement and inhibition of chemerin signalling would provide therapeutic benefit, depending on the context. Several factors will be important for the development and clinical use of chemerin-specific therapeutics. Firstly, the method (agonist versus antagonist), timing, and location of targeting chemerin expression will contribute to the success of novel treatments. For example, Chapter 3 demonstrated that enhancement of chemerin signalling in mature adipocytes likely prevents against maladaptive adipose tissue remodelling and pathogenic adipose tissue expansion. However, in obesity, elevated systemic chemerin levels are associated with disturbances in glucose and lipid homeostasis. Therefore, application of an agonist to promote chemerin signalling in adipose tissue is likely most beneficial in the early stages of adipose tissue expansion. Furthermore, local adipose tissue administration, versus an overall increase in systemic chemerin activity, will be essential to prevent detrimental adverse metabolic effects. We also demonstrated that loss of CMKLR1 signalling delayed the progression of DSS-induced colitis (Chapter 4), suggesting that application of a CMKLR1 inhibitor might be beneficial in the treatment of colon inflammation. Importantly, as chemerin signalling is essential for normal metabolic and immune function, it will be important to focus on restoring the endogenous balance of chemerin levels versus eliminating chemerin signalling entirely. This can be achieved in part by local administration of CMKLR1 or GPR1 inhibitors. Interestingly, a recent study demonstrated that a prototype membrane anchored chemerin agonist was successful in the treatment of inflammation (Doyle et al. 2014). Future studies that investigate whether targeting of methods such as a membrane-anchored chemerin modulator to a specific cell type can contribute to location-specific modulation of chemerin activity will be important in order to achieve local regulation of chemerin activity and minimize detrimental systemic effects.

Importantly, the different pharmacological properties of various chemerin isoforms and peptides can be exploited in order to develop function and receptor-specific therapeutics. For example, the development of peptides that target a specific function

(e.g. mChe15 exhibits anti-inflammatory properties, without affecting ß-arrestin recruitment, SRF signalling, or calcium release; and peptides corresponding to amino acids 66-85 exhibit antimicrobial activity) will contribute to the development of novel therapeutics that target and promote a specific function associated with chemerin signalling, without affecting other essential functions. Importantly, studies that elucidate the functions of specific chemerin isoforms, and the role of the rest of the chemerin protein, will be essential. Additionally, the development of agonists or inhibitors that target a specific chemerin receptor may further regulate the context-specific regulation of chemerin activity in disease conditions.

Alternatively, indirect methods to target chemerin signalling may prove useful in the treatment of metabolic and inflammatory disorders. For example, compounds that modify the expression and/or activity of proteases that process chemerin to bioactive or inactive isoforms might be useful in eliminating dys-regulated chemerin activity. For example, it was recently demonstrated that inhibition of serine proteases reduced inflammation induced by DSS administration (Bermudez-Humaran et al. 2015). Therefore targeting enzymes that modify chemerin bioactivity may represent a novel method to manipulate endogenous chemerin signalling. Furthermore, identification of downstream targets of chemerin signalling also provide novel targets to modify the activity of chemerin signalling. For example, Chapter 3 highlighted that administration of NFkB or Mmp3 inhibitors might prevent pathologic adipose tissue remodelling. Additionally, the research presented in Chapter 5 suggests that modulation of the gut microbiome composition by chemerin, and vice versa, might represent another indirect method to alter inflammatory and metabolic processes.

Importantly, chemerin signalling plays essential roles in the development and function of numerous physiological systems ranging from bone metabolism, food intake, immune function, reproduction, and cancer (Rourke et al. 2013). For example, chemerin has been proposed to both inhibit (Pachynski et al. 2012) and promote (Kumar et al. 2014) tumor growth, suggesting that modulation of chemerin signalling is likely to influence other physiological processes. This highlights the importance of measuring the distribution of chemerin isoforms in disease and further delineating the signalling transduction pathways downstream from CMKLR1 and GPR1 activation in order to

generate novel specific chemerin-targeted treatments that have minimal side effects on other cellular processes.

Chemerin as a biomarker

While pharmacological agents targeting chemerin activity and function are a future prospect, measurement of circulating chemerin levels (total and bioactive) has current potential clinical utility as an early biomarker for metabolic and inflammatory diseases. Numerous studies have reported that elevated chemerin levels act as a non-invasive biomarker for a number of disorders, including colon inflammation (Chapter 4,(Dranse et al. 2015; Lin et al. 2014)), severity of atherosclerotic lesions (Kostopoulos et al. 2014), cardiovascular disease (Aksan et al. 2014; Ji et al. 2014), intra-hepatic lipid content and liver steatosis (Klusek-Oksiuta et al. 2014), cancer (Wang et al. 2014; Zhang et al. 2014a), and glucose intolerance (Fatima et al. 2015). Importantly, chemerin levels are often accurate and reliable indicators of disease severity and survival outcome (Chapter 4, (Aksan et al. 2014; Dranse et al. 2015; Kostopoulos et al. 2014; Lin et al. 2014; Wang et al. 2014; Zhang et al. 2014a)). In addition, decreased chemerin levels have been associated with successful aging (Sanchis-Gomar et al. 2015). Thus while clinical and experimental studies continue to be performed in order to elucidate the biological function and therapeutic potential of targeting chemerin signalling, chemerin levels can currently be used with high confidence as non-invasive biomarker to identify patients at high risk of developing metabolic and inflammatory disease.

Future research questions

The data presented in this thesis supports both pro- and anti-inflamamtory roles for chemerin signalling, suggesting that chemerin regulation and function is context specific. In order to fully understand the role of chemerin signalling in human health and disease, and to modulate levels of chemerin bioactivity for the treatment and/or prevention of metabolic and inflammatory diseases, a number of key research questions remain to be answered. These include:

1. What mechanisms regulate changes in chemerin expression, processing, and activity in disease conditions?
2. Which chemerin isoforms are produced under pathological conditions? How does the distribution of chemerin isoform(s) and overall activity/function change in different disease settings?
3. What are the pharmacological properties of individual chemerin isoforms? Do different isoforms exhibit diversity in activation of specific chemerin receptors and/or intracellular signalling pathways?
4. Is chemerin modified post-translationally?
5. Under what conditions is chemerin pro- versus anti-inflammatory?
6. Does desensitization occur with chronic or high doses of chemerin?
7. Do changes in chemerin activity with metabolic disease impact inflammatory processes, and vice versa?
8. How do medicines commonly prescribed for the treatment of metabolic and inflammatory disorders affect chemerin processing, signalling, and biological function?
9. What is the best approach to modulate chemerin bioactivity in order to prevent and/or treat inflammatory and metabolic disorders without compromising normal chemerin function?

Final remarks

Chemerin is a multi-functional protein that plays essential roles in a variety of metabolic and inflammatory processes. The available evidence indicates that local, context-specific generation of chemerin isoforms regulates the appropriate activation of chemerin signalling pathways and that a disruption in the balance of chemerin signalling influences the development of a variety of metabolic and inflammatory disorders. In particular, the data presented in this thesis demonstrated that disruption of normal levels of chemerin signalling influenced both adipose tissue and intestinal homeostasis. Future work that elucidates the pharmacological properties of specific chemerin isoforms, the distribution of chemerin isoforms in health and disease, and how this affects overall chemerin function, will be essential in order to fully understand the biological role of

chemerin signalling. The development of therapeutics that restore normal levels and function of chemerin signalling will ultimately lead to novel treatments for the prevention and management of inflammatory and metabolic disease.

REFERENCES

Ademoglu, E, Berberoglu, Z, Carlioglu, A, Dellal, F, Gorar, S, Alphan, Z, Uysal, S, and Karakurt, F. 2014. Higher levels of circulating chemerin in both lean and obese patients with polycystic ovary syndrome. *Minerva Ginecol* 66**:** 535-42.

Adrych, K, Stojek, M, Smoczynski, M, Sledzinski, T, Sylwia, SW, and Swierczynski, J. 2012. Increased serum chemerin concentration in patients with chronic pancreatitis. *Dig Liver Dis* 44**:** 393-7.

Aksan, G, Inci, S, Nar, G, Soylu, K, Gedikli, O, Yuksel, S, Ozdemir, M, Nar, R, Meric, M, and Sahin, M. 2014. Association of serum chemerin levels with the severity of coronary artery disease in patients with metabolic syndrome. *Int J Clin Exp Med* 7**:** 5461-8.

Albanesi, C, Scarponi, C, Bosisio, D, Sozzani, S, and Girolomoni, G. 2010. Immune functions and recruitment of plasmacytoid dendritic cells in psoriasis. *Autoimmunity* 43**:** 215-9.

Albanesi, C, Scarponi, C, Pallotta, S, Daniele, R, Bosisio, D, Madonna, S, Fortugno, P, Gonzalvo-Feo, S, Franssen, JD, Parmentier, M, De Pita, O, Girolomoni, G, and Sozzani, S. 2009. Chemerin expression marks early psoriatic skin lesions and correlates with plasmacytoid dendritic cell recruitment. *J Exp Med* 206**:** 249-58.

Alexander, CM, Selvarajan, S, Mudgett, J, and Werb, Z. 2001. Stromelysin-1 regulates adipogenesis during mammary gland involution. *J Cell Biol* 152**:** 693-703.

Alfadda, AA, Sallam, RM, Chishti, MA, Moustafa, AS, Fatma, S, Alomaim, WS, Al-Naami, MY, Bassas, AF, Chrousos, GP, and Jo, H. 2012. Differential patterns of serum concentration and adipose tissue expression of chemerin in obesity: Adipose depot specificity and gender dimorphism. *Mol Cells* 33**:** 591-6.

Andrews, S. 2010. FastQC: a quality control tool for high throughput sequence data. Available online at http://www.bioinformatics.babraham.ac.uk/projects/fastqc/.

Arita, M, Bianchini, F, Aliberti, J, Sher, A, Chiang, N, Hong, S, Yang, R, Petasis, NA, and Serhan, CN. 2005a. Stereochemical assignment, antiinflammatory properties, and receptor for the omega-3 lipid mediator resolvin E1. *J Exp Med* 201**:** 713-22.

Arita, M, Ohira, T, Sun, YP, Elangovan, S, Chiang, N, and Serhan, CN. 2007. Resolvin E1 selectively interacts with leukotriene B4 receptor BLT1 and ChemR23 to regulate inflammation. *J Immunol* 178**:** 3912-7.

Arita, M, Yoshida, M, Hong, S, Tjonahen, E, Glickman, JN, Petasis, NA, Blumberg, RS, and Serhan, CN. 2005b. Resolvin E1, an endogenous lipid mediator derived from omega-3 eicosapentaenoic acid, protects against 2,4,6-trinitrobenzene sulfonic acid-induced colitis. *Proc Natl Acad Sci U S A* 102**:** 7671-6.

Arkan, MC, Hevener, AL, Greten, FR, Maeda, S, Li, ZW, Long, JM, Wynshaw-Boris, A, Poli, G, Olefsky, J, and Karin, M. 2005. IKK-beta links inflammation to obesity-induced insulin resistance. *Nat Med* 11**:** 191-8.

Arrieta, MC, Stiemsma, LT, Amenyogbe, N, Brown, EM, and Finlay, B. 2014. The intestinal microbiome in early life: health and disease. *Front Immunol* 5**:** 427.

Backhed, F, Ding, H, Wang, T, Hooper, LV, Koh, GY, Nagy, A, Semenkovich, CF, and Gordon, JI. 2004. The gut microbiota as an environmental factor that regulates fat storage. *Proc Natl Acad Sci U S A* 101**:** 15718-23.

Banas, M, Zabieglo, K, Kasetty, G, Kapinska-Mrowiecka, M, Borowczyk, J, Drukala, J, Murzyn, K, Zabel, BA, Butcher, EC, Schroeder, JM, Schmidtchen, A, and Cichy, J. 2013. Chemerin is an antimicrobial agent in human epidermis. *PLoS One* 8**:** e58709.

Banas, M, Zegar, A, Kwitniewski, M, Zabieglo, K, Marczynska, J, Kapinska-Mrowiecka, M, Lajevic, M, Zabel, BA, and Cichy, J. 2015. The expression and regulation of chemerin in the epidermis. *PLoS One* 10**:** e0117830.

Baranger, K, Rivera, S, Liechti, FD, Grandgirard, D, Bigas, J, Seco, J, Tarrago, T, Leib, SL, and Khrestchatisky, M. 2014. Endogenous and synthetic MMP inhibitors in CNS physiopathology. *Prog Brain Res* 214**:** 313-51.

Barlow, GM, Yu, A, and Mathur, R. 2015. Role of the Gut Microbiome in Obesity and Diabetes Mellitus. *Nutr Clin Pract*.

Barnea, G, Strapps, W, Herrada, G, Berman, Y, Ong, J, Kloss, B, Axel, R, and Lee, KJ. 2008. The genetic design of signaling cascades to record receptor activation. *Proc Natl Acad Sci U S A* 105**:** 64-9.

Bauer, S, Wanninger, J, Schmidhofer, S, Weigert, J, Neumeier, M, Dorn, C, Hellerbrand, C, Zimara, N, Schaffler, A, Aslanidis, C, and Buechler, C. 2011. Sterol regulatory element-binding protein 2 (SREBP2) activation after excess triglyceride storage induces chemerin in hypertrophic adipocytes. *Endocrinology* 152**:** 26-35.

Becker, M, Rabe, K, Lebherz, C, Zugwurst, J, Goke, B, Parhofer, KG, Lehrke, M, and Broedl, UC. 2010. Expression of human chemerin induces insulin resistance in the skeletal muscle but does not affect weight, lipid levels, and atherosclerosis in LDL receptor knockout mice on high-fat diet. *Diabetes* 59**:** 2898-903.

Berg, V, Sveinbjornsson, B, Bendiksen, S, Brox, J, Meknas, K, and Figenschau, Y. 2010. Human articular chondrocytes express ChemR23 and chemerin; ChemR23 promotes inflammatory signalling upon binding the ligand chemerin(21-157). *Arthritis Res Ther* 12**:** R228.

Bermudez-Humaran, LG, Motta, JP, Aubry, C, Kharrat, P, Rous-Martin, L, Sallenave, JM, Deraison, C, Vergnolle, N, and Langella, P. 2015. Serine protease inhibitors protect better than IL-10 and TGF-beta anti-inflammatory cytokines against mouse colitis when delivered by recombinant lactococci. *Microb Cell Fact* 14**:** 198.

Bernstein, CN. 2015. Treatment of IBD: where we are and where we are going. *Am J Gastroenterol* 110**:** 114-26.

Bluher, M, Rudich, A, Kloting, N, Golan, R, Henkin, Y, Rubin, E, Schwarzfuchs, D, Gepner, Y, Stampfer, MJ, Fiedler, M, Thiery, J, Stumvoll, M, and Shai, I. 2012. Two patterns of adipokine and other biomarker dynamics in a long-term weight loss intervention. *Diabetes Care* 35**:** 342-9.

Bondue, B, De Henau, O, Luangsay, S, Devosse, T, De Nadai, P, Springael, JY, Parmentier, M, and Vosters, O. 2012. The Chemerin/ChemR23 System Does Not Affect the Pro-Inflammatory Response of Mouse and Human Macrophages Ex Vivo. *PLoS One* 7**:** e40043.

Bondue, B, Vosters, O, De Nadai, P, Glineur, S, De Henau, O, Luangsay, S, Van Gool, F, Communi, D, De Vuyst, P, Desmecht, D, and Parmentier, M. 2011. ChemR23 dampens lung inflammation and enhances anti-viral immunity in a mouse model of acute viral pneumonia. *PLoS Pathog* 7**:** e1002358.

Boyuk, B, Guzel, EC, Atalay, H, Guzel, S, Mutlu, LC, and Kucukyalcin, V. 2014. Relationship between plasma chemerin levels and disease severity in COPD patients. *Clin Respir J*.

Bozaoglu, K, Bolton, K, Mcmillan, J, Zimmet, P, Jowett, J, Collier, G, Walder, K, and Segal, D. 2007. Chemerin is a novel adipokine associated with obesity and metabolic syndrome. *Endocrinology* 148**:** 4687-94.

Bozaoglu, K, Curran, JE, Stocker, CJ, Zaibi, MS, Segal, D, Konstantopoulos, N, Morrison, S, Carless, M, Dyer, TD, Cole, SA, Goring, HH, Moses, EK, Walder, K, Cawthorne, MA, Blangero, J, and Jowett, JB. 2010. Chemerin, a novel adipokine in the regulation of angiogenesis. *J Clin Endocrinol Metab* 95**:** 2476-85.

Bozaoglu, K, Segal, D, Shields, KA, Cummings, N, Curran, JE, Comuzzie, AG, Mahaney, MC, Rainwater, DL, Vandeberg, JL, Maccluer, JW, Collier, G, Blangero, J, Walder, K, and Jowett, JB. 2009. Chemerin is associated with metabolic syndrome phenotypes in a Mexican-American population. *J Clin Endocrinol Metab* 94**:** 3085-8.

Brunetti, L, Orlando, G, Ferrante, C, Recinella, L, Leone, S, Chiavaroli, A, Di Nisio, C, Shohreh, R, Manippa, F, Ricciuti, A, and Vacca, M. 2014. Peripheral chemerin administration modulates hypothalamic control of feeding. *Peptides* 51**:** 115-21.

Cai, D, Yuan, M, Frantz, DF, Melendez, PA, Hansen, L, Lee, J, and Shoelson, SE. 2005. Local and systemic insulin resistance resulting from hepatic activation of IKK-beta and NF-kappaB. *Nat Med* 11**:** 183-90.

Campbell, EL, Macmanus, CF, Kominsky, DJ, Keely, S, Glover, LE, Bowers, BE, Scully, M, Bruyninckx, WJ, and Colgan, SP. 2010. Resolvin E1-induced intestinal alkaline phosphatase promotes resolution of inflammation through LPS detoxification. *Proc Natl Acad Sci U S A* 107**:** 14298-303.

Caporaso, JG, Kuczynski, J, Stombaugh, J, Bittinger, K, Bushman, FD, Costello, EK, Fierer, N, Pena, AG, Goodrich, JK, Gordon, JI, Huttley, GA, Kelley, ST, Knights, D, Koenig, JE, Ley, RE, Lozupone, CA, Mcdonald, D, Muegge, BD, Pirrung, M, Reeder, J, Sevinsky, JR, Turnbaugh, PJ, Walters, WA, Widmann, J, Yatsunenko, T, Zaneveld, J, and Knight, R. 2010. QIIME allows analysis of high-throughput community sequencing data. *Nat Methods* 7**:** 335-6.

Carlsen, H, Haugen, F, Zadelaar, S, Kleemann, R, Kooistra, T, Drevon, CA, and Blomhoff, R. 2009. Diet-induced obesity increases NF-kappaB signaling in reporter mice. *Genes Nutr* 4**:** 215-22.

Cash, JL, Bass, MD, Campbell, J, Barnes, M, Kubes, P, and Martin, P. 2014. Resolution mediator chemerin15 reprograms the wound microenvironment to promote repair and reduce scarring. *Curr Biol* 24**:** 1406-14.

Cash, JL, Bena, S, Headland, SE, Mcarthur, S, Brancaleone, V, and Perretti, M. 2013. Chemerin15 inhibits neutrophil-mediated vascular inflammation and myocardial ischemia-reperfusion injury through ChemR23. *EMBO Rep* 14**:** 999-1007.

Cash, JL, Christian, AR, and Greaves, DR. 2010. Chemerin peptides promote phagocytosis in a ChemR23- and Syk-dependent manner. *J Immunol* 184**:** 5315-24.

Cash, JL, Hart, R, Russ, A, Dixon, JP, Colledge, WH, Doran, J, Hendrick, AG, Carlton, MB, and Greaves, DR. 2008. Synthetic chemerin-derived peptides suppress inflammation through ChemR23. *J Exp Med* 205**:** 767-75.

Chakaroun, R, Raschpichler, M, Kloting, N, Oberbach, A, Flehmig, G, Kern, M, Schon, MR, Shang, E, Lohmann, T, Dressler, M, Fasshauer, M, Stumvoll, M, and Bluher, M. 2012. Effects of weight loss and exercise on chemerin serum concentrations and adipose tissue expression in human obesity. *Metabolism* 61**:** 706-14.

Chamberland, JP, Berman, RL, Aronis, KN, and Mantzoros, CS. 2013. Chemerin is expressed mainly in pancreas and liver, is regulated by energy deprivation, and lacks day/night variation in humans. *Eur J Endocrinol* 169**:** 453-62.

Chavey, C, Mari, B, Monthouel, MN, Bonnafous, S, Anglard, P, Van Obberghen, E, and Tartare-Deckert, S. 2003. Matrix metalloproteinases are differentially expressed in adipose tissue during obesity and modulate adipocyte differentiation. *J Biol Chem* 278**:** 11888-96.

Chu, SH, Lee, MK, Ahn, KY, Im, JA, Park, MS, Lee, DC, Jeon, JY, and Lee, JW. 2012. Chemerin and adiponectin contribute reciprocally to metabolic syndrome. *PLoS One* 7**:** e34710.

Chun, TH, Hotary, KB, Sabeh, F, Saltiel, AR, Allen, ED, and Weiss, SJ. 2006. A pericellular collagenase directs the 3-dimensional development of white adipose tissue. *Cell* 125**:** 577-91.

Comeau, AM, Li, WK, Tremblay, JE, Carmack, EC, and Lovejoy, C. 2011. Arctic Ocean microbial community structure before and after the 2007 record sea ice minimum. *PLoS One* 6**:** e27492.

Costello, EK, Lauber, CL, Hamady, M, Fierer, N, Gordon, JI, and Knight, R. 2009. Bacterial community variation in human body habitats across space and time. *Science* 326**:** 1694-7.

Cox, LM, and Blaser, MJ. 2015. Antibiotics in early life and obesity. *Nat Rev Endocrinol* 11**:** 182-90.

De Palma, G, Castellano, G, Del Prete, A, Sozzani, S, Fiore, N, Loverre, A, Parmentier, M, Gesualdo, L, Grandaliano, G, and Schena, FP. 2011. The possible role of ChemR23/Chemerin axis in the recruitment of dendritic cells in lupus nephritis. *Kidney Int* 79**:** 1228-35.

De Poorter, C, Baertsoen, K, Lannoy, V, Parmentier, M, and Springael, JY. 2013. Consequences of ChemR23 heteromerization with the chemokine receptors CXCR4 and CCR7. *PLoS One* 8**:** e58075.

Demoor, T, Bracke, KR, Dupont, LL, Plantinga, M, Bondue, B, Roy, MO, Lannoy, V, Lambrecht, BN, Brusselle, GG, and Joos, GF. 2011. The role of ChemR23 in the induction and resolution of cigarette smoke-induced inflammation. *J Immunol* 186**:** 5457-67.

Deng, Y, Wang, H, Lu, Y, Liu, S, Zhang, Q, Huang, J, Zhu, R, Yang, J, Zhang, R, Zhang, D, Shen, W, Ning, G, and Yang, Y. 2013. Identification of chemerin as a novel FXR target gene down-regulated in the progression of nonalcoholic steatohepatitis. *Endocrinology* 154**:** 1794-801.

Desantis, TZ, Hugenholtz, P, Larsen, N, Rojas, M, Brodie, EL, Keller, K, Huber, T, Dalevi, D, Hu, P, and Andersen, GL. 2006. Greengenes, a chimera-checked 16S rRNA gene database and workbench compatible with ARB. *Appl Environ Microbiol* 72**:** 5069-72.

Dessein, PH, Tsang, L, Woodiwiss, AJ, Norton, GR, and Solomon, A. 2014. Circulating concentrations of the novel adipokine chemerin are associated with cardiovascular disease risk in rheumatoid arthritis. *J Rheumatol* 41**:** 1746-54.

Divoux, A, and Clement, K. 2011. Architecture and the extracellular matrix: the still unappreciated components of the adipose tissue. *Obes Rev* 12**:** e494-503.

Dominguez, E, Galmozzi, A, Chang, JW, Hsu, KL, Pawlak, J, Li, W, Godio, C, Thomas, J, Partida, D, Niessen, S, O'brien, PE, Russell, AP, Watt, MJ, Nomura, DK, Cravatt, BF, and Saez, E. 2014. Integrated phenotypic and activity-based profiling links Ces3 to obesity and diabetes. *Nat Chem Biol* 10**:** 113-21.

Dong, B, Ji, W, and Zhang, Y. 2011. Elevated serum chemerin levels are associated with the presence of coronary artery disease in patients with metabolic syndrome. *Intern Med* 50**:** 1093-7.

Doyle, JR, Krishnaji, ST, Zhu, G, Xu, ZZ, Heller, D, Ji, RR, Levy, BD, Kumar, K, and Kopin, AS. 2014. Development of a membrane-anchored chemerin receptor agonist as a novel modulator of allergic airway inflammation and neuropathic pain. *J Biol Chem* 289**:** 13385-96.

Dranse, HJ, Rourke, JL, Stadnyk, AW, and Sinal, CJ. 2015. Local chemerin levels are positively associated with DSS-induced colitis but constitutive loss of CMKLR1 does not protect against development of colitis. *Physiol Rep* 3.

Du, XY, Zabel, BA, Myles, T, Allen, SJ, Handel, TM, Lee, PP, Butcher, EC, and Leung, LL. 2009. Regulation of chemerin bioactivity by plasma carboxypeptidase N, carboxypeptidase B (activated thrombin-activable fibrinolysis inhibitor), and platelets. *J Biol Chem* 284**:** 751-8.

Eisinger, K, Bauer, S, Schaffler, A, Walter, R, Neumann, E, Buechler, C, Muller-Ladner, U, and Frommer, KW. 2012. Chemerin induces CCL2 and TLR4 in synovial fibroblasts of patients with rheumatoid arthritis and osteoarthritis. *Exp Mol Pathol* 92**:** 90-6.

Ellekilde, M, Krych, L, Hansen, CH, Hufeldt, MR, Dahl, K, Hansen, LH, Sorensen, SJ, Vogensen, FK, Nielsen, DS, and Hansen, AK. 2014. Characterization of the gut microbiota in leptin deficient obese mice - Correlation to inflammatory and diabetic parameters. *Res Vet Sci* 96**:** 241-50.

Erdogan, S, Yilmaz, FM, Yazici, O, Yozgat, A, Sezer, S, Ozdemir, N, Uysal, S, Purnak, T, Sendur, MA, and Ozaslan, E. 2015. Inflammation and chemerin in colorectal cancer. *Tumour Biol*.

Erickson, AR, Cantarel, BL, Lamendella, R, Darzi, Y, Mongodin, EF, Pan, C, Shah, M, Halfvarson, J, Tysk, C, Henrissat, B, Raes, J, Verberkmoes, NC, Fraser, CM, Hettich, RL, and Jansson, JK. 2012. Integrated metagenomics/metaproteomics reveals human host-microbiota signatures of Crohn's disease. *PLoS One* 7**:** e49138.

Ericsson, AC, Davis, JW, Spollen, W, Bivens, N, Givan, S, Hagan, CE, Mcintosh, M, and Franklin, CL. 2015. Effects of vendor and genetic background on the composition of the fecal microbiota of inbred mice. *PLoS One* 10**:** e0116704.

Ernst, MC, Haidl, ID, Zuniga, LA, Dranse, HJ, Rourke, JL, Zabel, BA, Butcher, EC, and Sinal, CJ. 2012. Disruption of the chemokine-like receptor-1 (CMKLR1) gene is associated with reduced adiposity and glucose intolerance. *Endocrinology* 153**:** 672-82.

Ernst, MC, Issa, M, Goralski, KB, and Sinal, CJ. 2010. Chemerin exacerbates glucose intolerance in mouse models of obesity and diabetes. *Endocrinology* 151**:** 1998-2007.

Esteghamati, A, Ghasemiesfe, M, Mousavizadeh, M, Noshad, S, and Nakhjavani, M. 2014. Pioglitazone and metformin are equally effective in reduction of chemerin in patients with type 2 diabetes. *J Diabetes Investig* 5**:** 327-32.

Everard, A, Belzer, C, Geurts, L, Ouwerkerk, JP, Druart, C, Bindels, LB, Guiot, Y, Derrien, M, Muccioli, GG, Delzenne, NM, De Vos, WM, and Cani, PD. 2013. Cross-talk between Akkermansia muciniphila and intestinal epithelium controls diet-induced obesity. *Proc Natl Acad Sci U S A* 110**:** 9066-71.

Everard, A, Lazarevic, V, Derrien, M, Girard, M, Muccioli, GG, Neyrinck, AM, Possemiers, S, Van Holle, A, Francois, P, De Vos, WM, Delzenne, NM, Schrenzel, J, and Cani, PD. 2011. Responses of gut microbiota and glucose and lipid metabolism to prebiotics in genetic obese and diet-induced leptin-resistant mice. *Diabetes* 60**:** 2775-86.

Fanjul-Fernandez, M, Folgueras, AR, Cabrera, S, and Lopez-Otin, C. 2010. Matrix metalloproteinases: evolution, gene regulation and functional analysis in mouse models. *Biochim Biophys Acta* 1803**:** 3-19.

Farooq, SM, Stillie, R, Svensson, M, Svanborg, C, Strieter, RM, and Stadnyk, AW. 2009. Therapeutic effect of blocking CXCR2 on neutrophil recruitment and dextran sodium sulfate-induced colitis. *J Pharmacol Exp Ther* 329**:** 123-9.

Fatima, SS, Butt, Z, Bader, N, Pathan, AZ, Hussain, S, and Iqbal, NT. 2015. Role of multifunctional Chemerin in obesity and preclinical diabetes. *Obes Res Clin Pract* 9**:** 507-12.

Feng, X, Li, P, Zhou, C, Jia, X, and Kang, J. 2012. Elevated levels of serum chemerin in patients with obstructive sleep apnea syndrome. *Biomarkers* 17**:** 248-53.

Ford, AC, Moayyedi, P, and Hanauer, SB. 2013. Ulcerative colitis. *BMJ* 346**:** f432.

Frolkis, A, Dieleman, LA, Barkema, HW, Panaccione, R, Ghosh, S, Fedorak, RN, Madsen, K, and Kaplan, GG. 2013. Environment and the inflammatory bowel diseases. *Can J Gastroenterol* 27**:** e18-24.

Ganesh, BP, Klopfleisch, R, Loh, G, and Blaut, M. 2013. Commensal Akkermansia muciniphila exacerbates gut inflammation in Salmonella Typhimurium-infected gnotobiotic mice. *PLoS One* 8**:** e74963.

Gao, X, Mi, S, Zhang, F, Gong, F, Lai, Y, Gao, F, Zhang, X, Wang, L, and Tao, H. 2011. Association of chemerin mRNA expression in human epicardial adipose tissue with coronary atherosclerosis. *Cardiovasc Diabetol* 10**:** 87.

Geurts, L, Lazarevic, V, Derrien, M, Everard, A, Van Roye, M, Knauf, C, Valet, P, Girard, M, Muccioli, GG, Francois, P, De Vos, WM, Schrenzel, J, Delzenne, NM, and Cani, PD. 2011. Altered gut microbiota and endocannabinoid system tone in obese and diabetic leptin-resistant mice: impact on apelin regulation in adipose tissue. *Front Microbiol* 2**:** 149.

Goldfine, AB, Silver, R, Aldhahi, W, Cai, D, Tatro, E, Lee, J, and Shoelson, SE. 2008. Use of salsalate to target inflammation in the treatment of insulin resistance and type 2 diabetes. *Clin Transl Sci* 1**:** 36-43.

Gonzalvo-Feo, S, Del Prete, A, Pruenster, M, Salvi, V, Wang, L, Sironi, M, Bierschenk, S, Sperandio, M, Vecchi, A, and Sozzani, S. 2014. Endothelial cell-derived chemerin promotes dendritic cell transmigration. *J Immunol* 192**:** 2366-73.

Goralski, KB, Mccarthy, TC, Hanniman, EA, Zabel, BA, Butcher, EC, Parlee, SD, Muruganandan, S, and Sinal, CJ. 2007. Chemerin, a novel adipokine that regulates adipogenesis and adipocyte metabolism. *J Biol Chem* 282**:** 28175-88.

Goralski, KB, and Sinal, CJ. 2009. Elucidation of chemerin and chemokine-like receptor-1 function in adipocytes by adenoviral-mediated shRNA knockdown of gene expression. *Methods Enzymol* 460**:** 289-312.

Goyal, N, Rana, A, Ahlawat, A, Bijjem, KR, and Kumar, P. 2014. Animal models of inflammatory bowel disease: a review. *Inflammopharmacology* 22**:** 219-33.

Graham, KL, Zabel, BA, Loghavi, S, Zuniga, LA, Ho, PP, Sobel, RA, and Butcher, EC. 2009. Chemokine-like receptor-1 expression by central nervous system-infiltrating leukocytes and involvement in a model of autoimmune demyelinating disease. *J Immunol* 183**:** 6717-23.

Graham, KL, Zhang, JV, Lewen, S, Burke, TM, Dang, T, Zoudilova, M, Sobel, RA, Butcher, EC, and Zabel, BA. 2014. A novel CMKLR1 small molecule antagonist suppresses CNS autoimmune inflammatory disease. *PLoS One* 9**:** e112925.

Gruben, N, Aparicio Vergara, M, Kloosterhuis, NJ, Van Der Molen, H, Stoelwinder, S, Youssef, S, De Bruin, A, Delsing, DJ, Kuivenhoven, JA, Van De Sluis, B, Hofker, MH, and Koonen, DP. 2014. Chemokine-like receptor 1 deficiency does not affect the development of insulin resistance and nonalcoholic fatty liver disease in mice. *PLoS One* 9**:** e96345.

Gu, P, Cheng, M, Hui, X, Lu, B, Jiang, W, and Shi, Z. 2015. Elevating circulation chemerin level is associated with endothelial dysfunction and early atherosclerotic changes in essential hypertensive patients. *J Hypertens* 33**:** 1624-32.

Gu, S, Chen, D, Zhang, JN, Lv, X, Wang, K, Duan, LP, Nie, Y, and Wu, XL. 2013. Bacterial community mapping of the mouse gastrointestinal tract. *PLoS One* 8**:** e74957.

Guillabert, A, Wittamer, V, Bondue, B, Godot, V, Imbault, V, Parmentier, M, and Communi, D. 2008. Role of neutrophil proteinase 3 and mast cell chymase in chemerin proteolytic regulation. *J Leukoc Biol* 84**:** 1530-8.

Guzel, EC, Celik, C, Abali, R, Kucukyalcin, V, Celik, E, Guzel, M, and Yilmaz, M. 2014. Omentin and chemerin and their association with obesity in women with polycystic ovary syndrome. *Gynecol Endocrinol* 30**:** 419-22.

Ha, YJ, Kang, EJ, Song, JS, Park, YB, Lee, SK, and Choi, ST. 2014. Plasma chemerin levels in rheumatoid arthritis are correlated with disease activity rather than obesity. *Joint Bone Spine* 81**:** 189-90.

Hah, YJ, Kim, NK, Kim, MK, Kim, HS, Hur, SH, Yoon, HJ, Kim, YN, and Park, KG. 2011. Relationship between Chemerin Levels and Cardiometabolic Parameters and Degree of Coronary Stenosis in Korean Patients with Coronary Artery Disease. *Diabetes Metab J* 35**:** 248-54.

Hammer, O, Harper, DA, and Ryan, PD. 2001. PAST: Paleontological statistics software package for education and data analysis. *Palaeontologia Electronica* 4**:** 9pp.

Hanauer, SB. 2006. Inflammatory bowel disease: epidemiology, pathogenesis, and therapeutic opportunities. *Inflamm Bowel Dis* 12 Suppl 1**:** S3-9.

Hansen, TH, Gobel, RJ, Hansen, T, and Pedersen, O. 2015. The gut microbiome in cardio-metabolic health. *Genome Med* 7**:** 33.

Hart, R, and Greaves, DR. 2010. Chemerin contributes to inflammation by promoting macrophage adhesion to VCAM-1 and fibronectin through clustering of VLA-4 and VLA-5. *J Immunol* 185**:** 3728-39.

Haslam, DW, and James, WP. 2005. Obesity. *Lancet* 366**:** 1197-209.

He, J, Li, JC, Xie, H, Xu, ZH, Sun, YW, and Shan, Q. 2015. Serum Chemerin Levels in relation to Osteoporosis and Bone Mineral Density: A Case-Control Study. *Dis Markers* 2015**:** 786708.

Herova, M, Schmid, M, Gemperle, C, and Hersberger, M. 2015. ChemR23, the Receptor for Chemerin and Resolvin E1, Is Expressed and Functional on M1 but Not on M2 Macrophages. *J Immunol* 194**:** 2330-7.

Herova, M, Schmid, M, Gemperle, C, Loretz, C, and Hersberger, M. 2014. Low dose aspirin is associated with plasma chemerin levels and may reduce adipose tissue inflammation. *Atherosclerosis* 235**:** 256-62.

Higashi, S, and Miyazaki, K. 2003. Identification of a region of beta-amyloid precursor protein essential for its gelatinase A inhibitory activity. *J Biol Chem* 278**:** 14020-8.

Huang, K, Du, G, Li, L, Liang, H, and Zhang, B. 2012. Association of chemerin levels in synovial fluid with the severity of knee osteoarthritis. *Biomarkers* 17**:** 16-20.

Ishida, T, Yoshida, M, Arita, M, Nishitani, Y, Nishiumi, S, Masuda, A, Mizuno, S, Takagawa, T, Morita, Y, Kutsumi, H, Inokuchi, H, Serhan, CN, Blumberg, RS, and Azuma, T. 2010. Resolvin E1, an endogenous lipid mediator derived from eicosapentaenoic acid, prevents dextran sulfate sodium-induced colitis. *Inflamm Bowel Dis* 16**:** 87-95.

Issa, ME, Muruganandan, S, Ernst, MC, Parlee, SD, Zabel, BA, Butcher, EC, Sinal, CJ, and Goralski, KB. 2012. Chemokine-like receptor 1 regulates skeletal muscle cell myogenesis. *Am J Physiol Cell Physiol* 302**:** C1621-31.

Jain, U, Woodruff, TM, and Stadnyk, AW. 2013. The C5a receptor antagonist PMX205 ameliorates experimentally induced colitis associated with increased IL-4 and IL-10. *Br J Pharmacol* 168**:** 488-501.

Ji, Q, Lin, Y, Liang, Z, Yu, K, Liu, Y, Fang, Z, Liu, L, Shi, Y, Zeng, Q, Chang, C, Chai, M, and Zhou, Y. 2014. Chemerin is a novel biomarker of acute coronary syndrome but not of stable angina pectoris. *Cardiovasc Diabetol* 13**:** 145.

Jin, CH, Yi, KW, Ha, YR, Shin, JH, Park, HT, Kim, T, and Hur, JY. 2015. Chemerin Expression in the Peritoneal Fluid, Serum, and Ovarian Endometrioma of Women with Endometriosis. *Am J Reprod Immunol* 74**:** 379-86.

Kanda, H, Tateya, S, Tamori, Y, Kotani, K, Hiasa, K, Kitazawa, R, Kitazawa, S, Miyachi, H, Maeda, S, Egashira, K, and Kasuga, M. 2006. MCP-1 contributes to macrophage infiltration into adipose tissue, insulin resistance, and hepatic steatosis in obesity. *J Clin Invest* 116**:** 1494-505.

Kaneko, K, Miyabe, Y, Takayasu, A, Fukuda, S, Miyabe, C, Ebisawa, M, Yokoyama, W, Watanabe, K, Imai, T, Muramoto, K, Terashima, Y, Sugihara, T, Matsushima, K, Miyasaka, N, and Nanki, T. 2011. Chemerin activates fibroblast-like synoviocytes in patients with rheumatoid arthritis. *Arthritis Res Ther* 13**:** R158.

Kang, CS, Ban, M, Choi, EJ, Moon, HG, Jeon, JS, Kim, DK, Park, SK, Jeon, SG, Roh, TY, Myung, SJ, Gho, YS, Kim, JG, and Kim, YK. 2013. Extracellular vesicles derived from gut microbiota, especially Akkermansia muciniphila, protect the progression of dextran sulfate sodium-induced colitis. *PLoS One* 8**:** e76520.

Kaser, A, Zeissig, S, and Blumberg, RS. 2010. Inflammatory bowel disease. *Annu Rev Immunol* 28**:** 573-621.

Kaur, J, Adya, R, Tan, BK, Chen, J, and Randeva, HS. 2010. Identification of chemerin receptor (ChemR23) in human endothelial cells: chemerin-induced endothelial angiogenesis. *Biochem Biophys Res Commun* 391**:** 1762-8.

Keeney, KM, Yurist-Doutsch, S, Arrieta, MC, and Finlay, BB. 2014. Effects of antibiotics on human microbiota and subsequent disease. *Annu Rev Microbiol* 68**:** 217-35.

Khoo, J, Dhamodaran, S, Chen, DD, Yap, SY, Chen, RY, and Tian, HH. 2015. Exercise-Induced Weight Loss is More Effective Than Dieting for Improving Adipokine Profile, Insulin Resistance and Inflammation in Obese Men. *Int J Sport Nutr Exerc Metab*.

Kim, JY, Xue, K, Cao, M, Wang, Q, Liu, JY, Leader, A, Han, JY, and Tsang, BK. 2013. Chemerin suppresses ovarian follicular development and its potential involvement in follicular arrest in rats treated chronically with dihydrotestosterone. *Endocrinology* 154**:** 2912-23.

Klein, T, and Bischoff, R. 2011a. Active metalloproteases of the A Disintegrin and Metalloprotease (ADAM) family: biological function and structure. *J Proteome Res* 10**:** 17-33.

Klein, T, and Bischoff, R. 2011b. Physiology and pathophysiology of matrix metalloproteases. *Amino Acids* 41**:** 271-90.

Kloting, N, Fasshauer, M, Dietrich, A, Kovacs, P, Schon, MR, Kern, M, Stumvoll, M, and Bluher, M. 2010. Insulin-sensitive obesity. *Am J Physiol Endocrinol Metab* 299**:** E506-15.

Klusek-Oksiuta, M, Bialokoz-Kalinowska, I, Tarasow, E, Wojtkowska, M, Werpachowska, I, and Lebensztejn, DM. 2014. Chemerin as a novel non-invasive serum marker of intrahepatic lipid content in obese children. *Ital J Pediatr* 40**:** 84.

Kopylova, E, Noe, L, and Touzet, H. 2012. SortMeRNA: fast and accurate filtering of ribosomal RNAs in metatranscriptomic data. *Bioinformatics* 28**:** 3211-7.

Kostopoulos, CG, Spiroglou, SG, Varakis, JN, Apostolakis, E, and Papadaki, HH. 2014. Chemerin and CMKLR1 expression in human arteries and periadventitial fat: a possible role for local chemerin in atherosclerosis? *BMC Cardiovasc Disord* 14**:** 56.

Kralisch, S, Weise, S, Sommer, G, Lipfert, J, Lossner, U, Bluher, M, Stumvoll, M, and Fasshauer, M. 2009. Interleukin-1beta induces the novel adipokine chemerin in adipocytes in vitro. *Regul Pept* 154**:** 102-6.

Kukla, M, Zwirska-Korczala, K, Gabriel, A, Waluga, M, Warakomska, I, Szczygiel, B, Berdowska, A, Mazur, W, Wozniak-Grygiel, E, and Kryczka, W. 2010a. Chemerin, vaspin and insulin resistance in chronic hepatitis C. *J Viral Hepat* 17**:** 661-7.

Kukla, M, Zwirska-Korczala, K, Hartleb, M, Waluga, M, Chwist, A, Kajor, M, Ciupinska-Kajor, M, Berdowska, A, Wozniak-Grygiel, E, and Buldak, R. 2010b. Serum chemerin and vaspin in non-alcoholic fatty liver disease. *Scand J Gastroenterol* 45**:** 235-42.

Kulig, P, Kantyka, T, Zabel, BA, Banas, M, Chyra, A, Stefanska, A, Tu, H, Allen, SJ, Handel, TM, Kozik, A, Potempa, J, Butcher, EC, and Cichy, J. 2011. Regulation of chemerin chemoattractant and antibacterial activity by human cysteine cathepsins. *J Immunol* 187**:** 1403-10.

Kulig, P, Zabel, BA, Dubin, G, Allen, SJ, Ohyama, T, Potempa, J, Handel, TM, Butcher, EC, and Cichy, J. 2007. Staphylococcus aureus-derived staphopain B, a potent cysteine protease activator of plasma chemerin. *J Immunol* 178**:** 3713-20.

Kumar, JD, Holmberg, C, Balabanova, S, Borysova, L, Burdyga, T, Beynon, R, Dockray, GJ, and Varro, A. 2015. Mesenchymal Stem Cells Exhibit Regulated Exocytosis in Response to Chemerin and IGF. *PLoS One* 10**:** e0141331.

Kumar, JD, Holmberg, C, Kandola, S, Steele, I, Hegyi, P, Tiszlavicz, L, Jenkins, R, Beynon, RJ, Peeney, D, Giger, OT, Alqahtani, A, Wang, TC, Charvat, TT, Penfold, M, Dockray, GJ, and Varro, A. 2014. Increased expression of chemerin in squamous esophageal cancer myofibroblasts and role in recruitment of mesenchymal stromal cells. *PLoS One* 9**:** e104877.

Kunimoto, H, Kazama, K, Takai, M, Oda, M, Okada, M, and Yamawaki, H. 2015. Chemerin promotes the proliferation and migration of vascular smooth muscle and increases mouse blood pressure. *Am J Physiol Heart Circ Physiol* 309**:** H1017-28.

Lande, R, Gafa, V, Serafini, B, Giacomini, E, Visconti, A, Remoli, ME, Severa, M, Parmentier, M, Ristori, G, Salvetti, M, Aloisi, F, and Coccia, EM. 2008. Plasmacytoid dendritic cells in multiple sclerosis: intracerebral recruitment and impaired maturation in response to interferon-beta. *J Neuropathol Exp Neurol* 67**:** 388-401.

Landgraf, K, Friebe, D, Ullrich, T, Kratzsch, J, Dittrich, K, Herberth, G, Adams, V, Kiess, W, Erbs, S, and Korner, A. 2012. Chemerin as a mediator between obesity and vascular inflammation in children. *J Clin Endocrinol Metab* 97**:** E556-64.

Langille, M. 2015. Microbiome helper: an assortment of scripts to help process and automate varous microbiome and metagenomic bioinformatic tools. Available online at https://github.com/mlangill/microbiome_helper#microbiome-helper.

Le Chatelier, E, Nielsen, T, Qin, J, Prifti, E, Hildebrand, F, Falony, G, Almeida, M, Arumugam, M, Batto, JM, Kennedy, S, Leonard, P, Li, J, Burgdorf, K, Grarup, N, Jorgensen, T, Brandslund, I, Nielsen, HB, Juncker, AS, Bertalan, M, Levenez, F, Pons, N, Rasmussen, S, Sunagawa, S, Tap, J, Tims, S, Zoetendal, EG, Brunak, S, Clement, K, Dore, J, Kleerebezem, M, Kristiansen, K, Renault, P, Sicheritz-Ponten, T, De Vos, WM, Zucker, JD, Raes, J, Hansen, T, Bork, P, Wang, J, Ehrlich, SD, and Pedersen, O. 2013. Richness of human gut microbiome correlates with metabolic markers. *Nature* 500**:** 541-6.

Lee, BC, and Lee, J. 2014. Cellular and molecular players in adipose tissue inflammation in the development of obesity-induced insulin resistance. *Biochim Biophys Acta* 1842**:** 446-62.

Lehrke, M, Becker, A, Greif, M, Stark, R, Laubender, RP, Von Ziegler, F, Lebherz, C, Tittus, J, Reiser, M, Becker, C, Goke, B, Leber, AW, Parhofer, KG, and Broedl, UC. 2009. Chemerin is associated with markers of inflammation and components of the metabolic syndrome but does not predict coronary atherosclerosis. *Eur J Endocrinol* 161**:** 339-44.

Leiherer, A, Muendlein, A, Kinz, E, Vonbank, A, Rein, P, Fraunberger, P, Malin, C, Saely, CH, and Drexel, H. 2015. High plasma chemerin is associated with renal dysfunction and predictive for cardiovascular events - Insights from phenotype and genotype characterization. *Vascul Pharmacol*.

Leroy, X. 2014. Method for identifying modulators of GPCR GPR1 function. US8709734.

Ley, RE, Turnbaugh, PJ, Klein, S, and Gordon, JI. 2006. Microbial ecology: human gut microbes associated with obesity. *Nature* 444**:** 1022-3.

Li, C, and Wong, WH. 2001. Model-based analysis of oligonucleotide arrays: expression index computation and outlier detection. *Proc Natl Acad Sci U S A* 98**:** 31-6.

Li, L, Huang, C, Zhang, X, Wang, J, Ma, P, Liu, Y, Xiao, T, Zabel, BA, and Zhang, JV. 2014. Chemerin-derived peptide C-20 suppressed gonadal steroidogenesis. *Am J Reprod Immunol* 71**:** 265-77.

Lijnen, HR, Maquoi, E, Hansen, LB, Van Hoef, B, Frederix, L, and Collen, D. 2002. Matrix metalloproteinase inhibition impairs adipose tissue development in mice. *Arterioscler Thromb Vasc Biol* 22**:** 374-9.

Lin, Y, Yang, X, Yue, W, Xu, X, Li, B, Zou, L, and He, R. 2014. Chemerin aggravates DSS-induced colitis by suppressing M2 macrophage polarization. *Cell Mol Immunol* 11**:** 355-66.

Livak, KJ, and Schmittgen, TD. 2001. Analysis of relative gene expression data using real-time quantitative PCR and the 2(-Delta Delta C(T)) Method. *Methods* 25**:** 402-8.

Lloyd, JW, Zerfass, KM, Heckstall, EM, and Evans, KA. 2015. Diet-induced increases in chemerin are attenuated by exercise and mediate the effect of diet on insulin and HOMA-IR. *Ther Adv Endocrinol Metab* 6**:** 189-98.

Lu, B, Zhao, M, Jiang, W, Ma, J, Yang, C, Shao, J, and Gu, P. 2015. Independent Association of Circulating Level of Chemerin With Functional and Early Morphological Vascular Changes in Newly Diagnosed Type 2 Diabetic Patients. *Medicine (Baltimore)* 94**:** e1990.

Luangsay, S, Wittamer, V, Bondue, B, De Henau, O, Rouger, L, Brait, M, Franssen, JD, De Nadai, P, Huaux, F, and Parmentier, M. 2009. Mouse ChemR23 is expressed in dendritic cell subsets and macrophages, and mediates an anti-inflammatory activity of chemerin in a lung disease model. *J Immunol* 183**:** 6489-99.

Lucke, K, Miehlke, S, Jacobs, E, and Schuppler, M. 2006. Prevalence of Bacteroides and Prevotella spp. in ulcerative colitis. *J Med Microbiol* 55**:** 617-24.

Lumeng, CN, and Saltiel, AR. 2011. Inflammatory links between obesity and metabolic disease. *J Clin Invest* 121**:** 2111-7.

Machiels, K, Joossens, M, Sabino, J, De Preter, V, Arijs, I, Eeckhaut, V, Ballet, V, Claes, K, Van Immerseel, F, Verbeke, K, Ferrante, M, Verhaegen, J, Rutgeerts, P, and Vermeire, S. 2014. A decrease of the butyrate-producing species Roseburia hominis and Faecalibacterium prausnitzii defines dysbiosis in patients with ulcerative colitis. *Gut* 63**:** 1275-83.

Maclean, B, Tomazela, DM, Shulman, N, Chambers, M, Finney, GL, Frewen, B, Kern, R, Tabb, DL, Liebler, DC, and Maccoss, MJ. 2010. Skyline: an open source document editor for creating and analyzing targeted proteomics experiments. *Bioinformatics* 26**:** 966-8.

Maghsoudi, Z, Kelishadi, R, and Hosseinzadeh-Attar, MJ. 2015. Association of chemerin levels with anthropometric indexes and C-reactive protein in obese and non-obese adolescents. *ARYA Atheroscler* 11**:** 102-8.

Maheshwari, A, Kurundkar, AR, Shaik, SS, Kelly, DR, Hartman, Y, Zhang, W, Dimmitt, R, Saeed, S, Randolph, DA, Aprahamian, C, Datta, G, and Ohls, RK. 2009. Epithelial cells in fetal intestine produce chemerin to recruit macrophages. *Am J Physiol Gastrointest Liver Physiol* 297**:** G1-G10.

Malin, SK, Navaneethan, SD, Mulya, A, Huang, H, and Kirwan, JP. 2014. Exercise-induced lowering of chemerin is associated with reduced cardiometabolic risk and glucose-stimulated insulin secretion in older adults. *J Nutr Health Aging* 18**:** 608-15.

Maquoi, E, Munaut, C, Colige, A, Collen, D, and Lijnen, HR. 2002. Modulation of adipose tissue expression of murine matrix metalloproteinases and their tissue inhibitors with obesity. *Diabetes* 51**:** 1093-101.

Marchesi, JR, Adams, DH, Fava, F, Hermes, GD, Hirschfield, GM, Hold, G, Quraishi, MN, Kinross, J, Smidt, H, Tuohy, KM, Thomas, LV, Zoetendal, EG, and Hart, A. 2015. The gut microbiota and host health: a new clinical frontier. *Gut*.

Mariani, F, and Roncucci, L. 2015. Chemerin/chemR23 axis in inflammation onset and resolution. *Inflamm Res* 64**:** 85-95.

Mariman, EC, and Wang, P. 2010. Adipocyte extracellular matrix composition, dynamics and role in obesity. *Cell Mol Life Sci* 67**:** 1277-92.

Martinez-Santibanez, G, and Lumeng, CN. 2014. Macrophages and the regulation of adipose tissue remodeling. *Annu Rev Nutr* 34**:** 57-76.

Mazmanian, SK, Round, JL, and Kasper, DL. 2008. A microbial symbiosis factor prevents intestinal inflammatory disease. *Nature* 453**:** 620-5.

Meder, W, Wendland, M, Busmann, A, Kutzleb, C, Spodsberg, N, John, H, Richter, R, Schleuder, D, Meyer, M, and Forssmann, WG. 2003. Characterization of human circulating TIG2 as a ligand for the orphan receptor ChemR23. *FEBS Lett* 555**:** 495-9.

Meissburger, B, Ukropec, J, Roeder, E, Beaton, N, Geiger, M, Teupser, D, Civan, B, Langhans, W, Nawroth, PP, Gasperikova, D, Rudofsky, G, and Wolfrum, C. 2011. Adipogenesis and insulin sensitivity in obesity are regulated by retinoid-related orphan receptor gamma. *EMBO Mol Med* 3**:** 637-51.

Mellacheruvu, D, Wright, Z, Couzens, AL, Lambert, JP, St-Denis, NA, Li, T, Miteva, YV, Hauri, S, Sardiu, ME, Low, TY, Halim, VA, Bagshaw, RD, Hubner, NC, Al-Hakim, A, Bouchard, A, Faubert, D, Fermin, D, Dunham, WH, Goudreault, M, Lin, ZY, Badillo, BG, Pawson, T, Durocher, D, Coulombe, B, Aebersold, R, Superti-Furga, G, Colinge, J, Heck, AJ, Choi, H, Gstaiger, M, Mohammed, S, Cristea, IM, Bennett, KL, Washburn, MP, Raught, B, Ewing, RM, Gingras, AC, and Nesvizhskii, AI. 2013. The CRAPome: a contaminant repository for affinity purification-mass spectrometry data. *Nat Methods* 10**:** 730-6.

Miki, T, Takegami, Y, Okawa, K, Muraguchi, T, Noda, M, and Takahashi, C. 2007. The reversion-inducing cysteine-rich protein with Kazal motifs (RECK) interacts with membrane type 1 matrix metalloproteinase and CD13/aminopeptidase N and modulates their endocytic pathways. *J Biol Chem* 282**:** 12341-52.

Min, JL, Nicholson, G, Halgrimsdottir, I, Almstrup, K, Petri, A, Barrett, A, Travers, M, Rayner, NW, Magi, R, Pettersson, FH, Broxholme, J, Neville, MJ, Wills, QF, Cheeseman, J, Allen, M, Holmes, CC, Spector, TD, Fleckner, J, Mccarthy, MI, Karpe, F, Lindgren, CM, and Zondervan, KT. 2012. Coexpression network analysis in abdominal and gluteal adipose tissue reveals regulatory genetic loci for metabolic syndrome and related phenotypes. *PLoS Genet* 8**:** e1002505.

Monnier, J, Lewen, S, O'hara, E, Huang, K, Tu, H, Butcher, EC, and Zabel, BA. 2012. Expression, Regulation, and Function of Atypical Chemerin Receptor CCRL2 on Endothelial Cells. *J Immunol* 189**:** 956-67.

Moran, GW, Dubeau, MF, Kaplan, GG, Panaccione, R, and Ghosh, S. 2013. The increasing weight of Crohn's disease subjects in clinical trials: a hypothesis-generatings time-trend analysis. *Inflamm Bowel Dis* 19**:** 2949-56.

Mullick, A, Xu, Y, Warren, R, Koutroumanis, M, Guilbault, C, Broussau, S, Malenfant, F, Bourget, L, Lamoureux, L, Lo, R, Caron, AW, Pilotte, A, and Massie, B. 2006. The cumate gene-switch: a system for regulated expression in mammalian cells. *BMC Biotechnol* 6**:** 43.

Muruganandan, S, Dranse, HJ, Rourke, JL, Mcmullen, NM, and Sinal, CJ. 2013. Chemerin neutralization blocks hematopoietic stem cell osteoclastogenesis. *Stem Cells* 31**:** 2172-82.

Muruganandan, S, Parlee, SD, Rourke, JL, Ernst, MC, Goralski, KB, and Sinal, CJ. 2011. Chemerin, a novel peroxisome proliferator-activated receptor gamma (PPARgamma) target gene that promotes mesenchymal stem cell adipogenesis. *J Biol Chem* 286**:** 23982-95.

Muruganandan, S, Roman, AA, and Sinal, CJ. 2010. Role of chemerin/CMKLR1 signaling in adipogenesis and osteoblastogenesis of bone marrow stem cells. *J Bone Miner Res* 25**:** 222-34.

Nagpal, S, Patel, S, Jacobe, H, Disepio, D, Ghosn, C, Malhotra, M, Teng, M, Duvic, M, and Chandraratna, RA. 1997. Tazarotene-induced gene 2 (TIG2), a novel retinoid-responsive gene in skin. *J Invest Dermatol* 109**:** 91-5.

Neurath, MF. 2014. Cytokines in inflammatory bowel disease. *Nat Rev Immunol* 14**:** 329-42.

Neves, KB, Nguyen Dinh Cat, A, Lopes, RA, Rios, FJ, Anagnostopoulou, A, Lobato, NS, De Oliveira, AM, Tostes, RC, Montezano, AC, and Touyz, RM. 2015. Chemerin Regulates Crosstalk Between Adipocytes and Vascular Cells Through Nox. *Hypertension* 66**:** 657-66.

Nguyen, TL, Vieira-Silva, S, Liston, A, and Raes, J. 2015. How informative is the mouse for human gut microbiota research? *Dis Model Mech* 8**:** 1-16.

Okeke, F, Roland, BC, and Mullin, GE. 2014. The role of the gut microbiome in the pathogenesis and treatment of obesity. *Glob Adv Health Med* 3**:** 44-57.

Oswiecimska, JM, Ziora, KT, Suwala, A, Swietochowska, E, Gorczyca, P, Ziora-Jakutowicz, K, Machura, E, Szczepanska, M, Ostrowska, Z, Ziora, D, Szalecki, M, Stojewska, M, Matusik, P, and Malecka-Tendera, E. 2014. Chemerin serum levels in girls with anorexia nervosa. *Neuro Endocrinol Lett* 35**:** 490-6.

Ouchi, N, Parker, JL, Lugus, JJ, and Walsh, K. 2011. Adipokines in inflammation and metabolic disease. *Nat Rev Immunol* 11**:** 85-97.

Ouwens, DM, Bekaert, M, Lapauw, B, Nieuwenhove, YV, Lehr, S, Hartwig, S, Calders, P, Kaufman, JM, Sell, H, Eckel, J, and Ruige, JB. 2012. Chemerin as biomarker for insulin sensitivity in males without typical characteristics of metabolic syndrome. *Arch Physiol Biochem*.

Pachynski, RK, Zabel, BA, Kohrt, HE, Tejeda, NM, Monnier, J, Swanson, CD, Holzer, AK, Gentles, AJ, Sperinde, GV, Edalati, A, Hadeiba, HA, Alizadeh, AA, and Butcher, EC. 2012. The chemoattractant chemerin suppresses melanoma by recruiting natural killer cell antitumor defenses. *J Exp Med* 209**:** 1427-35.

Paddison, PJ, Cleary, M, Silva, JM, Chang, K, Sheth, N, Sachidanandam, R, and Hannon, GJ. 2004. Cloning of short hairpin RNAs for gene knockdown in mammalian cells. *Nat Methods* 1**:** 163-7.

Park, D, and Yoon, M. 2012. Compound K, a novel ginsenoside metabolite, inhibits adipocyte differentiation in 3T3-L1 cells: involvement of angiogenesis and MMPs. *Biochem Biophys Res Commun* 422**:** 263-7.

Parks, DH, Tyson, GW, Hugenholtz, P, and Beiko, RG. 2014. STAMP: statistical analysis of taxonomic and functional profiles. *Bioinformatics* 30**:** 3123-4.

Parlee, SD, Ernst, MC, Muruganandan, S, Sinal, CJ, and Goralski, KB. 2010. Serum chemerin levels vary with time of day and are modified by obesity and tumor necrosis factor-{alpha}. *Endocrinology* 151**:** 2590-602.

Parlee, SD, Mcneil, JO, Muruganandan, S, Sinal, CJ, and Goralski, KB. 2012. Elastase and tryptase govern TNFalpha-mediated production of active chemerin by adipocytes. *PLoS One* 7**:** e51072.

Parlee, SD, Wang, Y, Poirier, P, Lapointe, M, Martin, J, Bastien, M, Cianflone, K, and Goralski, KB. 2015. Biliopancreatic diversion with duodenal switch modifies plasma chemerin in early and late post-operative periods. *Obesity (Silver Spring)* 23**:** 1201-8.

Parolini, S, Santoro, A, Marcenaro, E, Luini, W, Massardi, L, Facchetti, F, Communi, D, Parmentier, M, Majorana, A, Sironi, M, Tabellini, G, Moretta, A, and Sozzani, S. 2007. The role of chemerin in the colocalization of NK and dendritic cell subsets into inflamed tissues. *Blood* 109**:** 3625-32.

Peng, L, Yu, Y, Liu, J, Li, S, He, H, Cheng, N, and Ye, RD. 2015. The chemerin receptor CMKLR1 is a functional receptor for amyloid-beta peptide. *J Alzheimers Dis* 43**:** 227-42.

Pfau, D, Bachmann, A, Lossner, U, Kratzsch, J, Bluher, M, Stumvoll, M, and Fasshauer, M. 2010. Serum levels of the adipokine chemerin in relation to renal function. *Diabetes Care* 33**:** 171-3.

Png, CW, Linden, SK, Gilshenan, KS, Zoetendal, EG, Mcsweeney, CS, Sly, LI, Mcguckin, MA, and Florin, TH. 2010. Mucolytic bacteria with increased prevalence in IBD mucosa augment in vitro utilization of mucin by other bacteria. *Am J Gastroenterol* 105**:** 2420-8.

Podolsky, DK. 2002. Inflammatory bowel disease. *N Engl J Med* 347**:** 417-29.

Pohl, R, Rein-Fischboeck, L, Meier, EM, Eisinger, K, Krautbauer, S, and Buechler, C. 2015. Resolvin E1 and chemerin C15 peptide do not improve rodent non-alcoholic steatohepatitis. *Exp Mol Pathol* 98**:** 295-9.

Porter, KM, Epstein, DL, and Liton, PB. 2012. Up-regulated expression of extracellular matrix remodeling genes in phagocytically challenged trabecular meshwork cells. *PLoS One* 7**:** e34792.

Poulos, SP, Hausman, DB, and Hausman, GJ. 2010. The development and endocrine functions of adipose tissue. *Mol Cell Endocrinol* 323**:** 20-34.

Qin, J, Li, R, Raes, J, Arumugam, M, Burgdorf, KS, Manichanh, C, Nielsen, T, Pons, N, Levenez, F, Yamada, T, Mende, DR, Li, J, Xu, J, Li, S, Li, D, Cao, J, Wang, B, Liang, H, Zheng, H, Xie, Y, Tap, J, Lepage, P, Bertalan, M, Batto, JM, Hansen, T, Le Paslier, D, Linneberg, A, Nielsen, HB, Pelletier, E, Renault, P, Sicheritz-Ponten, T, Turner, K, Zhu, H, Yu, C, Li, S, Jian, M, Zhou, Y, Li, Y, Zhang, X, Li, S, Qin, N, Yang, H, Wang, J, Brunak, S, Dore, J, Guarner, F, Kristiansen, K, Pedersen, O, Parkhill, J, Weissenbach, J, Bork, P, Ehrlich, SD, and Wang, J. 2010a. A human gut microbial gene catalogue established by metagenomic sequencing. *Nature* 464**:** 59-65.

Qin, J, Li, Y, Cai, Z, Li, S, Zhu, J, Zhang, F, Liang, S, Zhang, W, Guan, Y, Shen, D, Peng, Y, Zhang, D, Jie, Z, Wu, W, Qin, Y, Xue, W, Li, J, Han, L, Lu, D, Wu, P, Dai, Y, Sun, X, Li, Z, Tang, A, Zhong, S, Li, X, Chen, W, Xu, R, Wang, M, Feng, Q, Gong, M, Yu, J, Zhang, Y, Zhang, M, Hansen, T, Sanchez, G, Raes, J, Falony, G, Okuda, S, Almeida, M, Lechatelier, E, Renault, P, Pons, N, Batto, JM, Zhang, Z, Chen, H, Yang, R, Zheng, W, Li, S, Yang, H, Wang, J, Ehrlich, SD, Nielsen, R, Pedersen, O, Kristiansen, K, and Wang, J. 2012. A metagenome-wide association study of gut microbiota in type 2 diabetes. *Nature* 490**:** 55-60.

Qin, JY, Zhang, L, Clift, KL, Hulur, I, Xiang, AP, Ren, BZ, and Lahn, BT. 2010b. Systematic comparison of constitutive promoters and the doxycycline-inducible promoter. *PLoS One* 5**:** e10611.

Regard, JB, Sato, IT, and Coughlin, SR. 2008. Anatomical profiling of G protein-coupled receptor expression. *Cell* 135**:** 561-71.

Ren, RZ, Zhang, X, Xu, J, Zhang, HQ, Yu, CX, Cao, MF, Gao, L, Guan, QB, and Zhao, JJ. 2012. Chronic ethanol consumption increases the levels of chemerin in the serum and adipose tissue of humans and rats. *Acta Pharmacol Sin* 33**:** 652-9.

Ress, C, Tschoner, A, Engl, J, Klaus, A, Tilg, H, Ebenbichler, CF, Patsch, JR, and Kaser, S. 2010. Effect of bariatric surgery on circulating chemerin levels. *Eur J Clin Invest* 40**:** 277-80.

Reverchon, M, Cornuau, M, Rame, C, Guerif, F, Royere, D, and Dupont, J. 2012. Chemerin inhibits IGF-1-induced progesterone and estradiol secretion in human granulosa cells. *Hum Reprod* 27**:** 1790-800.

Ridaura, VK, Faith, JJ, Rey, FE, Cheng, J, Duncan, AE, Kau, AL, Griffin, NW, Lombard, V, Henrissat, B, Bain, JR, Muehlbauer, MJ, Ilkayeva, O, Semenkovich, CF, Funai, K, Hayashi, DK, Lyle, BJ, Martini, MC, Ursell, LK, Clemente, JC, Van Treuren, W, Walters, WA, Knight, R, Newgard, CB, Heath, AC, and Gordon, JI. 2013. Gut microbiota from twins discordant for obesity modulate metabolism in mice. *Science* 341**:** 1241214.

Roh, SG, Song, SH, Choi, KC, Katoh, K, Wittamer, V, Parmentier, M, and Sasaki, S. 2007. Chemerin--a new adipokine that modulates adipogenesis via its own receptor. *Biochem Biophys Res Commun* 362**:** 1013-8.

Rouger, L, Denis, GR, Luangsay, S, and Parmentier, M. 2013. ChemR23 knockout mice display mild obesity but no deficit in adipocyte differentiation. *J Endocrinol* 219**:** 279-89.

Rourke, JL, Dranse, HJ, and Sinal, CJ. 2013. Towards an integrative approach to understanding the role of chemerin in human health and disease. *Obes Rev* 14**:** 245-62.

Rourke, JL, Dranse, HJ, and Sinal, CJ. 2015. CMKLR1 and GPR1 mediate chemerin signaling through the RhoA/ROCK pathway. *Mol Cell Endocrinol*.

Rourke, JL, Muruganandan, S, Dranse, HJ, Mcmullen, NM, and Sinal, CJ. 2014. Gpr1 is an active chemerin receptor influencing glucose homeostasis in obese mice. *J Endocrinol* 222**:** 201-15.

Rutkowski, P, Sledzinski, T, Zielinska, H, Lizakowski, S, Goyke, E, Szrok-Wojtkiewicz, S, Swierczynski, J, and Rutkowski, B. 2012. Decrease of serum chemerin concentration in patients with end stage renal disease after successful kidney transplantation. *Regul Pept* 173**:** 55-9.

Sanchis-Gomar, F, Pareja-Galeano, H, Santos-Lozano, A, Garatachea, N, Fiuza-Luces, C, Venturini, L, Ricevuti, G, Lucia, A, and Emanuele, E. 2015. A preliminary candidate approach identifies the combination of chemerin, fetuin-A, and fibroblast growth factors 19 and 21 as a potential biomarker panel of successful aging. *Age (Dordr)* 37**:** 9776.

Santacruz, A, Collado, MC, Garcia-Valdes, L, Segura, MT, Martin-Lagos, JA, Anjos, T, Marti-Romero, M, Lopez, RM, Florido, J, Campoy, C, and Sanz, Y. 2010. Gut microbiota composition is associated with body weight, weight gain and biochemical parameters in pregnant women. *Br J Nutr* 104**:** 83-92.

Saremi, A, Shavandi, N, Parastesh, M, and Daneshmand, H. 2010. Twelve-week aerobic training decreases chemerin level and improves cardiometabolic risk factors in overweight and obese men. *Asian J Sports Med* 1**:** 151-8.

Scher, JU, Sczesnak, A, Longman, RS, Segata, N, Ubeda, C, Bielski, C, Rostron, T, Cerundolo, V, Pamer, EG, Abramson, SB, Huttenhower, C, and Littman, DR. 2013. Expansion of intestinal Prevotella copri correlates with enhanced susceptibility to arthritis. *Elife* 2**:** e01202.

Schultz, S, Saalbach, A, Heiker, JT, Meier, R, Zellmann, T, Simon, JC, and Beck-Sickinger, AG. 2013. Proteolytic activation of prochemerin by kallikrein 7 breaks an ionic linkage and results in C-terminal rearrangement. *Biochem J* 452**:** 271-80.

Sell, H, Divoux, A, Poitou, C, Basdevant, A, Bouillot, JL, Bedossa, P, Tordjman, J, Eckel, J, and Clement, K. 2010. Chemerin correlates with markers for fatty liver in morbidly obese patients and strongly decreases after weight loss induced by bariatric surgery. *J Clin Endocrinol Metab* 95**:** 2892-6.

Sell, H, and Eckel, J. 2007. Monocyte chemotactic protein-1 and its role in insulin resistance. *Curr Opin Lipidol* 18**:** 258-62.

Sell, H, Laurencikiene, J, Taube, A, Eckardt, K, Cramer, A, Horrighs, A, Arner, P, and Eckel, J. 2009. Chemerin is a novel adipocyte-derived factor inducing insulin resistance in primary human skeletal muscle cells. *Diabetes* 58**:** 2731-40.

Shevchenko, A, Tomas, H, Havlis, J, Olsen, JV, and Mann, M. 2006. In-gel digestion for mass spectrometric characterization of proteins and proteomes. *Nat Protoc* 1**:** 2856-60.

Shimamura, K, Matsuda, M, Miyamoto, Y, Yoshimoto, R, Seo, T, and Tokita, S. 2009. Identification of a stable chemerin analog with potent activity toward ChemR23. *Peptides* 30**:** 1529-38.

Shin, HY, Lee, DC, Chu, SH, Jeon, JY, Lee, MK, Im, JA, and Lee, JW. 2012. Chemerin levels are positively correlated with abdominal visceral fat accumulation. *Clin Endocrinol (Oxf)* 77**:** 47-50.

Spiroglou, SG, Kostopoulos, CG, Varakis, JN, and Papadaki, HH. 2010. Adipokines in periaortic and epicardial adipose tissue: differential expression and relation to atherosclerosis. *J Atheroscler Thromb* 17**:** 115-30.

Stefanov, T, Bluher, M, Vekova, A, Bonova, I, Tzvetkov, S, Kurktschiev, D, and Temelkova-Kurktschiev, T. 2014. Circulating chemerin decreases in response to a combined strength and endurance training. *Endocrine* 45**:** 382-91.

Stejskal, D, Karpisek, M, Hanulova, Z, and Svestak, M. 2008. Chemerin is an independent marker of the metabolic syndrome in a Caucasian population--a pilot study. *Biomed Pap Med Fac Univ Palacky Olomouc Czech Repub* 152**:** 217-21.

Stepan, H, Philipp, A, Roth, I, Kralisch, S, Jank, A, Schaarschmidt, W, Lossner, U, Kratzsch, J, Bluher, M, Stumvoll, M, and Fasshauer, M. 2011. Serum levels of the adipokine chemerin are increased in preeclampsia during and 6 months after pregnancy. *Regul Pept* 168**:** 69-72.

Stillie, R, and Stadnyk, AW. 2009. Role of TNF receptors, TNFR1 and TNFR2, in dextran sodium sulfate-induced colitis. *Inflamm Bowel Dis* 15**:** 1515-25.

Suganami, T, Tanaka, M, and Ogawa, Y. 2012. Adipose tissue inflammation and ectopic lipid accumulation. *Endocr J* 59**:** 849-57.

Sun, K, Kusminski, CM, and Scherer, PE. 2011. Adipose tissue remodeling and obesity. *J Clin Invest* 121**:** 2094-101.

Sydora, BC, Tavernini, MM, Doyle, JS, and Fedorak, RN. 2005. Association with selected bacteria does not cause enterocolitis in IL-10 gene-deficient mice despite a systemic immune response. *Dig Dis Sci* 50**:** 905-13.

Takagi, S, Simizu, S, and Osada, H. 2009. RECK negatively regulates matrix metalloproteinase-9 transcription. *Cancer Res* 69**:** 1502-8.

Takahashi, M, Kamei, Y, and Ezaki, O. 2005. Mest/Peg1 imprinted gene enlarges adipocytes and is a marker of adipocyte size. *Am J Physiol Endocrinol Metab* 288**:** E117-24.

Takahashi, M, Okimura, Y, Iguchi, G, Nishizawa, H, Yamamoto, M, Suda, K, Kitazawa, R, Fujimoto, W, Takahashi, K, Zolotaryov, FN, Hong, KS, Kiyonari, H, Abe, T, Kaji, H, Kitazawa, S, Kasuga, M, Chihara, K, and Takahashi, Y. 2011. Chemerin regulates beta-cell function in mice. *Sci Rep* 1**:** 123.

Takahashi, M, Takahashi, Y, Takahashi, K, Zolotaryov, FN, Hong, KS, Kitazawa, R, Iida, K, Okimura, Y, Kaji, H, Kitazawa, S, Kasuga, M, and Chihara, K. 2008. Chemerin enhances insulin signaling and potentiates insulin-stimulated glucose uptake in 3T3-L1 adipocytes. *FEBS Lett* 582**:** 573-8.

Tan, BK, Chen, J, Farhatullah, S, Adya, R, Kaur, J, Heutling, D, Lewandowski, KC, O'hare, JP, Lehnert, H, and Randeva, HS. 2009. Insulin and metformin regulate circulating and adipose tissue chemerin. *Diabetes* 58**:** 1971-7.

Teixeira, LG, Leonel, AJ, Aguilar, EC, Batista, NV, Alves, AC, Coimbra, CC, Ferreira, AV, De Faria, AM, Cara, DC, and Alvarez Leite, JI. 2011. The combination of high-fat diet-induced obesity and chronic ulcerative colitis reciprocally exacerbates adipose tissue and colon inflammation. *Lipids Health Dis* 10**:** 204.

Terra, X, Auguet, T, Guiu-Jurado, E, Berlanga, A, Orellana-Gavalda, JM, Hernandez, M, Sabench, F, Porras, JA, Llutart, J, Martinez, S, Aguilar, C, Del Castillo, D, and Richart, C. 2013. Long-term changes in leptin, chemerin and ghrelin levels following different bariatric surgery procedures: Roux-en-Y gastric bypass and sleeve gastrectomy. *Obes Surg* 23**:** 1790-8.

Terrinoni, A, Candi, E, Oddi, S, Gobello, T, Camaione, DB, Mazzanti, C, Zambruno, G, Knight, R, and Melino, G. 2000. A glutamine insertion in the 1A alpha helical domain of the keratin 4 gene in a familial case of white sponge nevus. *J Invest Dermatol* 114**:** 388-91.

Tilg, H, and Adolph, TE. 2015. Influence of the human intestinal microbiome on obesity and metabolic dysfunction. *Curr Opin Pediatr* 27**:** 496-501.

Tonjes, A, Fasshauer, M, Kratzsch, J, Stumvoll, M, and Bluher, M. 2010. Adipokine pattern in subjects with impaired fasting glucose and impaired glucose tolerance in comparison to normal glucose tolerance and diabetes. *PLoS One* 5**:** e13911.

Traurig, MT, Permana, PA, Nair, S, Kobes, S, Bogardus, C, and Baier, LJ. 2006. Differential expression of matrix metalloproteinase 3 (MMP3) in preadipocytes/stromal vascular cells from nonobese nondiabetic versus obese nondiabetic Pima Indians. *Diabetes* 55**:** 3160-5.

Turnbaugh, PJ, Hamady, M, Yatsunenko, T, Cantarel, BL, Duncan, A, Ley, RE, Sogin, ML, Jones, WJ, Roe, BA, Affourtit, JP, Egholm, M, Henrissat, B, Heath, AC, Knight, R, and Gordon, JI. 2009. A core gut microbiome in obese and lean twins. *Nature* 457**:** 480-4.

Turnbaugh, PJ, Ley, RE, Mahowald, MA, Magrini, V, Mardis, ER, and Gordon, JI. 2006. An obesity-associated gut microbiome with increased capacity for energy harvest. *Nature* 444**:** 1027-31.

Ueda, A, Okuda, K, Ohno, S, Shirai, A, Igarashi, T, Matsunaga, K, Fukushima, J, Kawamoto, S, Ishigatsubo, Y, and Okubo, T. 1994. NF-kappa B and Sp1 regulate transcription of the human monocyte chemoattractant protein-1 gene. *J Immunol* 153**:** 2052-63.

Unoki, H, Bujo, H, Jiang, M, Kawamura, T, Murakami, K, and Saito, Y. 2008. Macrophages regulate tumor necrosis factor-alpha expression in adipocytes through the secretion of matrix metalloproteinase-3. *Int J Obes (Lond)* 32**:** 902-11.

Ussar, S, Griffin, NW, Bezy, O, Fujisaka, S, Vienberg, S, Softic, S, Deng, L, Bry, L, Gordon, JI, and Kahn, CR. 2015. Interactions between Gut Microbiota, Host Genetics and Diet Modulate the Predisposition to Obesity and Metabolic Syndrome. *Cell Metab* 22**:** 516-30.

Vermi, W, Lonardi, S, Morassi, M, Rossini, C, Tardanico, R, Venturini, M, Sala, R, Tincani, A, Poliani, PL, Calzavara-Pinton, PG, Cerroni, L, Santoro, A, and Facchetti, F. 2009. Cutaneous distribution of plasmacytoid dendritic cells in lupus erythematosus. Selective tropism at the site of epithelial apoptotic damage. *Immunobiology* 214**:** 877-86.

Vermi, W, Riboldi, E, Wittamer, V, Gentili, F, Luini, W, Marrelli, S, Vecchi, A, Franssen, JD, Communi, D, Massardi, L, Sironi, M, Mantovani, A, Parmentier, M, Facchetti, F, and Sozzani, S. 2005. Role of ChemR23 in directing the migration of myeloid and plasmacytoid dendritic cells to lymphoid organs and inflamed skin. *J Exp Med* 201**:** 509-15.

Visse, R, and Nagase, H. 2003. Matrix metalloproteinases and tissue inhibitors of metalloproteinases: structure, function, and biochemistry. *Circ Res* 92**:** 827-39.

Waluga, M, Hartleb, M, Boryczka, G, Kukla, M, and Zwirska-Korczala, K. 2014. Serum adipokines in inflammatory bowel disease. *World J Gastroenterol* 20**:** 6912-7.

Wang, C, Wu, WK, Liu, X, To, KF, Chen, GG, Yu, J, and Ng, EK. 2014. Increased serum chemerin level promotes cellular invasiveness in gastric cancer: a clinical and experimental study. *Peptides* 51**:** 131-8.

Wang, D, Yuan, GY, Wang, XZ, Jia, J, Di, LL, Yang, L, Chen, X, Qian, FF, and Chen, JJ. 2013a. Plasma chemerin level in metabolic syndrome. *Genet Mol Res* 12**:** 5986-91.

Wang, L, Yang, T, Ding, Y, Zhong, Y, Yu, L, and Peng, M. 2015. Chemerin plays a protective role by regulating human umbilical vein endothelial cell-induced nitric oxide signaling in preeclampsia. *Endocrine* 48**:** 299-308.

Wang, Q, Kim, JY, Xue, K, Liu, JY, Leader, A, and Tsang, BK. 2012. Chemerin, a novel regulator of follicular steroidogenesis and its potential involvement in polycystic ovarian syndrome. *Endocrinology* 153**:** 5600-11.

Wang, Q, Leader, A, and Tsang, BK. 2013b. Inhibitory roles of prohibitin and chemerin in FSH-induced rat granulosa cell steroidogenesis. *Endocrinology* 154**:** 956-67.

Wargent, ET, Zaibi, MS, O'dowd, JF, Cawthorne, MA, Wang, SJ, Arch, JR, and Stocker, CJ. 2015. Evidence from studies in rodents and in isolated adipocytes that agonists of the chemerin receptor CMKLR1 may be beneficial in the treatment of type 2 diabetes. *PeerJ* 3**:** e753.

Watts, SW, Dorrance, AM, Penfold, ME, Rourke, JL, Sinal, CJ, Seitz, B, Sullivan, TJ, Charvat, TT, Thompson, JM, Burnett, R, and Fink, GD. 2013. Chemerin connects fat to arterial contraction. *Arterioscler Thromb Vasc Biol* 33**:** 1320-8.

Weigert, J, Neumeier, M, Wanninger, J, Filarsky, M, Bauer, S, Wiest, R, Farkas, S, Scherer, MN, Schaffler, A, Aslanidis, C, Scholmerich, J, and Buechler, C. 2010a. Systemic chemerin is related to inflammation rather than obesity in type 2 diabetes. *Clin Endocrinol (Oxf)* 72**:** 342-8.

Weigert, J, Obermeier, F, Neumeier, M, Wanninger, J, Filarsky, M, Bauer, S, Aslanidis, C, Rogler, G, Ott, C, Schaffler, A, Scholmerich, J, and Buechler, C. 2010b. Circulating levels of chemerin and adiponectin are higher in ulcerative colitis and chemerin is elevated in Crohn's disease. *Inflamm Bowel Dis* 16**:** 630-7.

Whitman, WB, Coleman, DC, and Wiebe, WJ. 1998. Prokaryotes: the unseen majority. *Proc Natl Acad Sci U S A* 95**:** 6578-83.

World Health Organization (WHO). Obesity and Overweight Fact sheet No311. 2015. [Online]. [Accessed November 2015].

Wilson, PW. 2004. Estimating cardiovascular disease risk and the metabolic syndrome: a Framingham view. *Endocrinol Metab Clin North Am* 33**:** 467-81, v.

Wittamer, V, Bondue, B, Guillabert, A, Vassart, G, Parmentier, M, and Communi, D. 2005. Neutrophil-mediated maturation of chemerin: a link between innate and adaptive immunity. *J Immunol* 175**:** 487-93.

Wittamer, V, Franssen, JD, Vulcano, M, Mirjolet, JF, Le Poul, E, Migeotte, I, Brezillon, S, Tyldesley, R, Blanpain, C, Detheux, M, Mantovani, A, Sozzani, S, Vassart, G, Parmentier, M, and Communi, D. 2003. Specific recruitment of antigen-presenting cells by chemerin, a novel processed ligand from human inflammatory fluids. *J Exp Med* 198**:** 977-85.

Wittamer, V, Gregoire, F, Robberecht, P, Vassart, G, Communi, D, and Parmentier, M. 2004. The C-terminal nonapeptide of mature chemerin activates the chemerin receptor with low nanomolar potency. *J Biol Chem* 279**:** 9956-62.

Xiang, D, Zhang, J, Chen, Y, Guo, Y, Schalow, A, Zhang, Z, Hu, X, Yu, H, Zhao, M, Zhu, S, Lu, H, Wu, M, Yu, Y, Moldenhauer, A, and Han, W. 2010. Expressions and purification of a mature form of recombinant human Chemerin in Escherichia coli. *Protein Expr Purif* 69**:** 153-8.

Xiaotao, L, Xiaoxia, Z, Yue, X, and Liye, W. 2012. Serum chemerin levels are associated with the presence and extent of coronary artery disease. *Coron Artery Dis* 23**:** 412-6.

Yamaguchi, Y, Du, XY, Zhao, L, Morser, J, and Leung, LL. 2011. Proteolytic cleavage of chemerin protein is necessary for activation to the active form, Chem157S, which functions as a signaling molecule in glioblastoma. *J Biol Chem* 286**:** 39510-9.

Yamamoto, T, Qureshi, AR, Anderstam, B, Heimburger, O, Barany, P, Lindholm, B, Stenvinkel, P, and Axelsson, J. 2010. Clinical importance of an elevated circulating chemerin level in incident dialysis patients. *Nephrol Dial Transplant* 25**:** 4017-23.

Yamawaki, H, Kameshima, S, Usui, T, Okada, M, and Hara, Y. 2012. A novel adipocytokine, chemerin exerts anti-inflammatory roles in human vascular endothelial cells. *Biochem Biophys Res Commun* 423**:** 152-7.

Yan, Q, Zhang, Y, Hong, J, Gu, W, Dai, M, Shi, J, Zhai, Y, Wang, W, Li, X, and Ning, G. 2012. The association of serum chemerin level with risk of coronary artery disease in Chinese adults. *Endocrine* 41**:** 281-8.

Yang, M, Yang, G, Dong, J, Liu, Y, Zong, H, Liu, H, Boden, G, and Li, L. 2010. Elevated plasma levels of chemerin in newly diagnosed type 2 diabetes mellitus with hypertension. *J Investig Med* 58**:** 883-6.

Yang, S, Wang, Q, Huang, W, Song, Y, Feng, G, Zhou, L, and Tan, J. 2015. Are serum chemerin levels different between obese and non-obese polycystic ovary syndrome women? *Gynecol Endocrinol***:** 1-4.

Yen, K, Lee, C, Mehta, H, and Cohen, P. 2013. The emerging role of the mitochondrial-derived peptide humanin in stress resistance. *J Mol Endocrinol* 50**:** R11-9.

Yilmaz, Y, Kurt, R, Gurdal, A, Alahdab, YO, Yonal, O, Senates, E, Polat, N, Eren, F, Imeryuz, N, and Oflaz, H. 2011a. Circulating vaspin levels and epicardial adipose tissue thickness are associated with impaired coronary flow reserve in patients with nonalcoholic fatty liver disease. *Atherosclerosis* 217**:** 125-9.

Yilmaz, Y, Yonal, O, Kurt, R, Alahdab, YO, Eren, F, Ozdogan, O, Celikel, CA, Imeryuz, N, Kalayci, C, and Avsar, E. 2011b. Serum levels of omentin, chemerin and adipsin in patients with biopsy-proven nonalcoholic fatty liver disease. *Scand J Gastroenterol* 46**:** 91-7.

Yoo, HJ, Choi, HY, Yang, SJ, Kim, HY, Seo, JA, Kim, SG, Kim, NH, Choi, KM, Choi, DS, and Baik, SH. 2012. Circulating chemerin level is independently correlated with arterial stiffness. *J Atheroscler Thromb* 19**:** 59-66; discussion 67-8.

Yuan, M, Konstantopoulos, N, Lee, J, Hansen, L, Li, ZW, Karin, M, and Shoelson, SE. 2001. Reversal of obesity- and diet-induced insulin resistance with salicylates or targeted disruption of Ikkbeta. *Science* 293**:** 1673-7.

Zabel, BA, Allen, SJ, Kulig, P, Allen, JA, Cichy, J, Handel, TM, and Butcher, EC. 2005a. Chemerin activation by serine proteases of the coagulation, fibrinolytic, and inflammatory cascades. *J Biol Chem* 280**:** 34661-6.

Zabel, BA, Kwitniewski, M, Banas, M, Zabieglo, K, Murzyn, K, and Cichy, J. 2014. Chemerin regulation and role in host defense. *Am J Clin Exp Immunol* 3**:** 1-19.

Zabel, BA, Nakae, S, Zuniga, L, Kim, JY, Ohyama, T, Alt, C, Pan, J, Suto, H, Soler, D, Allen, SJ, Handel, TM, Song, CH, Galli, SJ, and Butcher, EC. 2008. Mast cell-expressed orphan receptor CCRL2 binds chemerin and is required for optimal induction of IgE-mediated passive cutaneous anaphylaxis. *J Exp Med* 205**:** 2207-20.

Zabel, BA, Silverio, AM, and Butcher, EC. 2005b. Chemokine-like receptor 1 expression and chemerin-directed chemotaxis distinguish plasmacytoid from myeloid dendritic cells in human blood. *J Immunol* 174**:** 244-51.

Zackular, JP, Baxter, NT, Iverson, KD, Sadler, WD, Petrosino, JF, Chen, GY, and Schloss, PD. 2013. The gut microbiome modulates colon tumorigenesis. *MBio* 4**:** e00692-13.

Zapf, JW, Weir, MS, Emerick, V, Villafranca, JE, and Dunlap, RB. 1993. Substitution of glutamine for glutamic acid-58 in Escherichia coli thymidylate synthase results in pronounced decreases in catalytic activity and ligand binding. *Biochemistry* 32**:** 9274-81.

Zhang, J, Jin, HC, Zhu, AK, Ying, RC, Wei, W, and Zhang, FJ. 2014a. Prognostic significance of plasma chemerin levels in patients with gastric cancer. *Peptides* 61**:** 7-11.

Zhang, J, Kobert, K, Flouri, T, and Stamatakis, A. 2014b. PEAR: a fast and accurate Illumina Paired-End reAd mergeR. *Bioinformatics* 30**:** 614-20.

Zhang, O, Ji, Q, Lin, Y, Wang, Z, Huang, Y, Lu, W, Liu, X, Zhang, J, Liu, Y, and Zhou, YJ. 2015a. Circulating chemerin levels elevated in dilated cardiomyopathy patients with overt heart failure. *Clin Chim Acta* 448**:** 27-32.

Zhang, R, Liu, S, Guo, B, Chang, L, and Li, Y. 2014c. Chemerin induces insulin resistance in rat cardiomyocytes in part through the ERK1/2 signaling pathway. *Pharmacology* 94**:** 259-64.

Zhang, YJ, Li, S, Gan, RY, Zhou, T, Xu, DP, and Li, HB. 2015b. Impacts of gut bacteria on human health and diseases. *Int J Mol Sci* 16**:** 7493-519.

Zhao, D, Bi, G, Feng, J, Huang, R, and Chen, X. 2015. Association of Serum Chemerin Levels with Acute Ischemic Stroke and Carotid Artery Atherosclerosis in a Chinese Population. *Med Sci Monit* 21**:** 3121-8.

Zhao, L, Yamaguchi, Y, Sharif, S, Du, XY, Song, JJ, Lee, DM, Recht, LD, Robinson, WH, Morser, J, and Leung, LL. 2011. Chemerin158K protein is the dominant chemerin isoform in synovial and cerebrospinal fluids but not in plasma. *J Biol Chem* 286**:** 39520-7.

Zhao, L, Yang, W, Yang, X, Lin, Y, Lv, J, Dou, X, Luo, Q, Dong, J, Chen, Z, Chu, Y, and He, R. 2014. Chemerin suppresses murine allergic asthma by inhibiting CCL2 production and subsequent airway recruitment of inflammatory dendritic cells. *Allergy* 69**:** 763-74.

Zhou, JX, Liao, D, Zhang, S, Cheng, N, He, HQ, and Ye, RD. 2014. Chemerin C9 peptide induces receptor internalization through a clathrin-independent pathway. *Acta Pharmacol Sin* 35**:** 653-63.

APPENDIX A: COPYRIGHT PERMISSION LETTERS

JOHN WILEY AND SONS LICENSE TERMS AND CONDITIONS

Nov 01, 2015

This Agreement between Helen Dranse ("You") and John Wiley and Sons ("John Wiley and Sons") consists of your license details and the terms and conditions provided by John Wiley and Sons and Copyright Clearance Center.

License Number	3740470310503
License date	Nov 01, 2015
Licensed Content Publisher	John Wiley and Sons
Licensed Content Publication	Obesity Reviews
Licensed Content Title	Towards an integrative approach to understanding the role of chemerin in human health and disease
Licensed Content Author	J. L. Rourke,H. J. Dranse,C. J. Sinal
Licensed Content Date	Dec 6, 2012
Pages	18
Type of use	Dissertation/Thesis
Requestor type	Author of this Wiley article
Format	Print and electronic
Portion	Full article
Will you be translating?	No
Title of your thesis / dissertation	Chemerin signalling in adipose tissue and intestinal homeostasis
Expected completion date	Jan 2016
Expected size (number of pages)	300
Requestor Location	Helen Dranse 6057 Coburg Road Apt6 Halifax, NS B3H 1Z1 Canada Attn: Helen Dranse
Billing Type	Invoice
Billing Address	Helen Dranse 6057 Coburg Road Apt6 Halifax, NS B3H 1Z1 Canada Attn: Helen Dranse
Total	0.00 CAD
Terms and Conditions	

ELSEVIER LICENSE
TERMS AND CONDITIONS

Nov 01, 2015

This is a License Agreement between Helen Dranse ("You") and Elsevier ("Elsevier") provided by Copyright Clearance Center ("CCC"). The license consists of your order details, the terms and conditions provided by Elsevier, and the payment terms and conditions.

All payments must be made in full to CCC. For payment instructions, please see information listed at the bottom of this form.

Supplier	Elsevier Limited The Boulevard,Langford Lane Kidlington,Oxford,OX5 1GB,UK
Registered Company Number	1982084
Customer name	Helen Dranse
Customer address	6057 Coburg Road Apt6 Halifax, NS B3H 1Z1
License number	3740470140419
License date	Nov 01, 2015
Licensed content publisher	Elsevier
Licensed content publication	Molecular and Cellular Endocrinology
Licensed content title	CMKLR1 and GPR1 mediate chemerin signaling through the RhoA/ROCK pathway
Licensed content author	Jillian L. Rourke,Helen J. Dranse,Christopher J. Sinal
Licensed content date	Available online 9 September 2015
Licensed content volume number	n/a
Licensed content issue number	n/a
Number of pages	1
Start Page	0
End Page	0
Type of Use	reuse in a thesis/dissertation
Portion	figures/tables/illustrations
Number of figures/tables/illustrations	2
Format	both print and electronic
Are you the author of this Elsevier article?	Yes
Will you be translating?	No
Original figure numbers	Figure 2C, methods

Copyright Clearance Center

Confirmation Number: 11479816
Order Date: 11/01/2015

Customer Information

Customer: Helen Dranse
Account Number: 3000957383
Organization: Helen Dranse
Email: helendranse@dal.ca
Phone: +1 (902) 818-1543
Payment Method: Invoice

This is not an invoice

Order Details

Endocrinology

Billing Status: **N/A**

Order detail ID: 68831646
ISSN: 1945-7170
Publication Type: e-Journal
Volume:
Issue:
Start page:
Publisher: ENDOCRINE SOCIETY
Author/Editor: Endocrine Society ; HighWire Press

Permission Status: **Granted**
Permission type: Republish or display content
Type of use: Republish in a thesis/dissertation
Order License Id: 3740480056499

Requestor type	Author of requested content
Format	Print, Electronic
Portion	chart/graph/table/figure
Number of charts/graphs/tables/figures	1
Title or numeric reference of the portion(s)	Figure 1 body mass (2 panels)
Title of the article or chapter the portion is from	Disruption of the chemokine-like receptor-1 (CMKLR1) gene is associated with reduced adiposity and glucose intolerance
Editor of portion(s)	N/A
Author of portion(s)	Ernst MC, Haidl ID, Zuniga LA, Dranse HJ, Rourke JL, Zabel BA, Butcher EC, Sinal CJ
Volume of serial or monograph	153
Issue, if republishing an article from a serial	2
Page range of portion	N/A
Publication date of portion	Feb 2012
Rights for	Main product
Duration of use	Current edition and up to 5 years
Creation of copies for	

Creation of copies for the disabled	no
With minor editing privileges	yes
For distribution to	Canada
In the following language(s)	Original language of publication
With incidental promotional use	no
Lifetime unit quantity of new product	Up to 499
Made available in the following markets	academia
The requesting person/organization	Helen Dranse, co-author
Order reference number	
Author/Editor	Ernst, MC, Haidl ID, Zuniga LA, Dranse HJ, Rourke JL, Zabel BA, Butcher ED, Sinal CJ
The standard identifier	Chemerin signalling in adipose tissue and intestinal homeostasis
Title	Disruption of the chemokine-like receptor-1 (CMKLR1) gene is associated with reduced adiposity and glucose intolerance
Publisher	Endocrine Society
Expected publication date	Jan 2016
Estimated size (pages)	300

Note: This item was invoiced separately through our **RightsLink service.** More info **$ 0.00**

Total order items: 1 **Order Total: $0.00**

Permissions

Table of Contents

Manage Table of content Alerts

Navigate

Alerts
All Issues
Current Issue
Feedback
Submit

More Information

Journal Scope
Author Guidelines
Press
Advertisers
Privacy Policy
Terms and Conditions
Ethics Policy
PubMed Central Policy
Permissions
Article Publication Charges
Institutional and Funder Payments
Publishing with Physiological Reports
Contact the Journal

Sister Journals

AJP - Cell Physiology
AJP - Endocrinology and Metabolism
AJP - Gastrointestinal and Liver Physiology
AJP - Heart and Circulatory Physiology
AJP - Lung Cellular and Molecular Physiology
AJP - Regulatory, Integrative and Comparative Physiology
AJP - Renal Physiology
Experimental Physiology
Journal of Applied Physiology
Journal of Neurophysiology
The Journal of Physiology
Physiological Genomics